Development of Fully Functional Microfluidic Based Platforms for Rapid On-site Water Quality Analysis

Monika Czugała (M.Sc. Eng.)

Thesis submitted in partial fullfilment of the requirements for the degree of

Doctor of Philosophy

September 2013

Research Supervisor: Prof. Dermot Diamond
Co-Supervisor: Dr. Fernando Benito-Lopez
National Centre for Sensor Research / School of Chemical Sciences
Dublin City University

For my parents,

Lucy and Mark

"Nothing in life is to be feared, it is only to be understood. Now is the time to understand more, so that we may fear less."

Marie Curie - Skłodowska

General Declaration

I hereby certify that this material, which I now submit for assessment on the programme of study leading to the award of Doctor of Philosophy is entirely my own work, and that I have exercised reasonable care to ensure that the work is original, and does not, to the best of my knowledge, breach any law of copyright, and has not been taken from the work of others save and to the extent that such work has been cited and acknowledged within the text of my work.

Signed: _____ Date: _____

(Monika Czugala, ID: 10117776)

Acknowledgements

First of all, I would like to thank to Prof. Dermot Diamond for giving me the opportunity to work in his group and for the great support and encouragement during my PhD. It has been a personally developing experience where I was given a chance not only to broaden my knowledge but also build my character. I have also learnt that '*there are no problems, there are only challenges'*.

I also would like to thank to Fernando for contributing with his knowledge and experience to the realisation of my research project. For being enthusiastic and inspiring, which was invaluable throughout the good and bad moments of my Ph.D.

I am also grateful to Prof. Ducrée from Biomedical Diagnostics Institute for the fruitful collaboration and for giving me the possibility to use the lab facilities. A big thank you goes to Robert, for sharing his amazing knowledge about centrifugal microfluidics and enjoyable discussions.

Thanks to Dr. A. Llobera and Dr. X. Muñoz-Berbel for their scientific help, for taking care of me during my research visit to CNM, Spain, and for being great friends.

Thanks to all the members of Adaptive Sensor Group, Michele, Larisa, Bartosz, Simon G., Vincenzo, for the fruitful scientific discussions. A special thanks go to the engineers, who helped me a lot along the Ph.D. and were always available to manufacture the mechanical parts, build circuits for me, and answer all my questions about electronics – Damien, Fiachra, Cormac, Tom, Eoghan. Without you guys this would not have been possible. Thanks to

Claudio, John, Simon C., Giusy, Deirdre, Mercedes and all the people within Clarity and NCSR that helped me, in different ways.

Thanks to Cecilia and my friends back in Poland, for believing in me and asking me every visit when I will get Nobel prize - Edzia, Jacus, Tomus. Special thanks go to my Sis, who has been my great support for years, and who is always there for me. You, my dear friends, make me believe that somehow the time stops, and that some things stay the same, no matter what happens and where we are.

I would like to thank my parents who raised me with a love of science for great unconditional support at each and every step throughout my whole education process. For believing in me and making me believe that I can aim high to achieve more.

And most of all special thanks go to the person who joined me in this adventure, my best friend and partner, Kevin. For being patient and encouraging, and whose faithful scientific and private support during the Ph.D. was invaluable. Thank you.

List of Publications

Journal Publications

1. M. Czugala, C. O'Connell, Llobera, F. Sánchez, X. Munoz-Berbel, D. Diamond and F. Benito-Lopez, *Evaluation of photochromic properties of acrylated spiropyran incorporated within photoresponsive ionogel microvalves*, Langmuir. (in preparation)
2. M. Czugala, R. Gorkin III, D. Kutzburch, R. Burger, F. Benito-Lopez, D. Diamond, *Well-chip development kit for miniaturization of colorimetric and fluorescence-based immunoassays*, Lab Chip. (submitted September 2013)
3. C. E. Nwankire, M. Czugala, R. Burger, K. J. Fraser, T. O'Connell, T. Glennon, D. Diamond and J. Ducrée, *A portable centrifugal analyser for liver function screening*, Lab Chip. (submitted September 2013)
4. M. Czugala, C. O'Connell, C. Blin, P. Fischer, K. J. Fraser, F. Benito-Lopez and D. Diamond, *Photopatterning and actuation behaviour of photoresponsive phosphonium-based ionogel microstructures,* Langmuir. (submitted May 2013)
5. M. Czugala, C. Fay, Noel O'Connor, B. Corcoran, F. Benito-Lopez and D. Diamond, *Portable integrated microfluidic platform for the monitoring and detection of nitrite*, Talanta, 2013, 997-1004.
6. M. Czugala, D. Maher, F. Collins, R. Burger, F. Hopfgartner, Y. Yang, J. Zhaou, J. Ducrée, A. Smeaton, K. J. Fraser, D. Diamond and F. Benito-

Lopez, *CMAS: fully integrated portable Centrifugal Microfluidic Analysis System for on-site colorimetric analysis*, RSC Advances, 2013, 3, 15928-15938.

7. M. Czugala, R. Gorkin, T. Phelan, J. Gaughran, V. F. Curto, J. Ducrée, D. Diamond and F. Benito-Lopez, *Optical sensing system based on wireless paired emitter detector diode device and ionogels for lab-on-a-disc water quality analysis,* Lab Chip, 2012, 12, 5069-5078.
8. *M. Czugala*, B. Ziolkowski, D. Diamond, *Integrating stimulus responsive materials and microfluidics – The key to next generation chemical sensors*, J. Int. Mat. Syst. Struct., 2012, doi: 10.1177/1045389X12459591.

Conference Publications

1. M. Czugala, C. O'Connell, A. McKeon, C. Blin, A. Llobera, C. Fernández Sánchez, X. Munoz-Berbel, P. Fischer, D. Diamond and F. Benito-Lopez, *Photo-patterning of ionogel microstructures for on-chip microvalve application controlled by fiber optics,* 17th International Conference on Solid-State Sensors, Actuators and Microsystems (Transducers 2013), 16-20th June, 2013, Barcelona, Spain.
2. M. Czugala**,** D. Maher, R. Burger, K. J. Fraser, J. Ducrée, D. Diamond and F. Benito-Lopez, *Portable Lab-on-a-disc system integrating photo-switchable micro-valves for in-situ aquatic environmental monitoring*, 16th International Conference on Miniaturized Systems for Chemistry and Life Sciences Conference (MicroTAS), 28th Oct. – 1st Nov., 2012, Okinawa, Japan.
3. M. Czugala, R. Gorkin, T. Phelan, J. Ducrée, D. Diamond, and F. Benito-Lopez, *Novel Optical Sensing System based on Wireless Paired Emitter-Detector Device for Lab on a Disc Water Quality Analysis,* 15th

International Conference on Miniaturized Systems for Chemistry and Life Sciences Conference (MicroTAS), 2-6th Oct., 2011, Seattle, USA.

4. M. Czugala, B. Ziolkowski, R. Byrne, D. Diamond, F. Benito-Lopez, *Materials science: The key to revolutionary breakthroughs in microfluidic devices*, Proc. SPIE 8107, 2011, doi: 10.1117/12.895330.
5. R. Gorkin, M. Czugala, C. Rovira-Borras, J. Ducrée, D. Diamond, F. Benito-Lopez, *A Wireless Paired Emitter Detector Diode Device as optical Sensor for Lab-on-a-Disc Applications*, The 16th International Conference on Solid-State Sensors, Actuators and Microsystems (Transducers), 5-9th June, 2011, Beijing, China.

Oral Presentations

1. M. Czugala, C. O'Connell, A. McKeon, C. Blin, A. Llobera, C. Fernández Sánchez, X. Munoz-Berbel, P. Fischer, D. Diamond and F. Benito-Lopez, *Photo-patterning of ionogel microstructures for on-chip microvalve application controlled by fiber optics,* 17th International Conference on Solid-State Sensors, Actuators and Microsystems (Transducers), 16-20th June, 2013, Barcelona, Spain.
2. M. Czugala, D. Maher, R. Burger, K. J. Fraser, J. Ducrée, D. Diamond and F. Benito-Lopez, *Fully integrated portable Centrifugal Microfluidic Analysis System for on-site colorimetric water analysis (CMAS*), ATWARM International Conference 2013: Water - The Greatest Global Challenge, 14-16th May 2013, Dublin, Ireland.
3. M. Czugala, D. Maher, R. Burger, K. J. Fraser, J. Ducrée, D. Diamond and F. Benito-Lopez, *Portable lab-on-a-disc system for in-situ aquatic environmental monitoring,* QUESTOR Meeting, 13-14th Nov., 2012, Belfast, United Kingdom.
4. M. Czugala, A. Llobera, X. Munoz-Berbel, D. Diamond and F. Benito-Lopez, *Generation of Fully Functioning Biomimetic Analytical Platforms*

for Water Quality. Biannual ATWARM Meeting, 13-14th Nov., 2012, Belfast, United Kingdom.

5. M. Czugala, D. Maher, R. Burger, K. J. Fraser, J. Ducrée, D. Diamond and F. Benito-Lopez, *Portable lab-on-a-disc system integrating photo-switchable micro-valves for in-situ aquatic environmental monitoring,* 16th International Conference on Miniaturized Systems for Chemistry and Life Sciences (MicroTAS) Conference, 30th Oct. – 2nd Nov., 2012, Okinawa, Japan.
6. F. Benito-Lopez, L. Florea, V. F. Curto, M. Czugala, D. Diamond, *Functional Materials: Smart Solutions to Generate Useful Micro-fluidic Devices*, 2nd International Symposium on Functional Nanomaterials 2012, 6-7th Sept., Dublin, Ireland (Invited talk).
7. M. Czugala, D. Maher, R. Burger, R. Gorkin, J. Ducrée, D. Diamond, F. Benito-Lopez and K. Fraser, *Micro-Fluidic Centrifugal Platforms for In-Situ Aquatic Environmental Analysis*, Sino-European Symposium on Environment and Health (SESEH), 20-25th Aug. 2012, Galway Ireland.
8. M. Czugala, R. Gorkin, D. Maher, K. Fraser, J. Ducrée, D. Diamond, F. Benito-Lopez, *Portable Lab-On-A-Disc Wireless System For In-Situ Multiparameter Water Quality Analysis,* International Conference on Environmental Science and Technology, 25-29th June, 2012, Houston, Texas, USA.
9. M. Czugala, F. Benito-Lopez and D. Diamond, *Portable Lab-on-a-Disc System for In-situ Aquatic Environmental Monitoring,* Biannual ATWARM Meeting, 1-2nd May 2012, Cranfield, United Kingdom.
10. M. Czugala, F. Benito-Lopez, D. Diamond, *Next Generation Autonomous Analytical Platforms for Remote Environmental Monitoring: Generation of Fully Functioning Biomimetic Analytical Platforms for Water Quality*, Biannual ATWARM Meeting, 29th Nov. - 1st Dec. 2011, Belfast, United Kingdom.

11. M. Czugala, D. Diamond, F. Benito-Lopez, *Novel optical sensing system based on wireless paired emitter detector device for lab on a disc water quality analysis*, 10th Oct. 2011, University of California, Berkeley, USA (Invited Talk).
12. M. Czugala, R. Gorkin, T. Phelan, J. Ducrée, D. Diamond, and F. Benito-Lopez, *Novel Optical Sensing System based on Wireless Paired Emitter-Detector Device for Lab on a Disc Water Quality Analysis,* 15th International Conference on Miniaturized Systems for Chemistry and Life Sciences, (MicroTAS) Conference, 2-6th Oct., 2011, Seattle, USA.
13. M. Czugala, D. Diamond, F. Benito-Lopez, *Towards the Generation of Fully Functioning Biomimetic Analytical Platforms for Water Quality Analysis Using Ionogel*, Centro Nacional de Microelectrónica (CNM), Universitat Autonoma de Barcelona, 16th Sept. 2011, Barcelona, Spain. (Invited Talk)
14. M. Czugala, B. Ziolkowski, R. Byrne, D. Diamond, F. Benito-Lopez, Materials Science: The Key to Revolutionary Breakthroughs in Microfluidic Devices, SPIE-2011, Nanoscience + Engineering, 21–25th Aug., 2011, San Diego, California, USA.
15. F. Benito-Lopez, L. Florea, V. F. Curto, M. Czugala, K. J. Fraser, S. Coyle, R. Byrne, D. Diamond, *New Functional Materials for Fluid Control and Sensing in Microfluidic Devices,* 14th July, 2011, University of California, Berkeley, USA. (Invited Talk)
16. L. Florea, V. F. Curto, M. Czugala, R. Byrne, S. Coyle, D. Diamond, F. Benito-Lopez, New Functional Materials for Fluid Control and Sensing in Microfluidic Devices, 10th June 2011, University of Granada, Spain. (Invited Talk)
17. M. Czugala, F. Benito-Lopez, D. Diamond, *Next Generation Autonomous Analytical Platforms for Remote Environmental Monitoring: Generation*

of Fully Functioning Biomimetic Analytical Platforms for Water Quality, Biannual ATWARM Meeting, 10-12th May 2011, Essen, Germany.

18. M. Czugala, F. Benito-Lopez, D. Diamond, *Next Generation Autonomous Analytical Platforms for Remote Environmental Monitoring: Generation of Fully Functioning Biomimetic Analytical Platforms for Water Quality*, Biannual ATWARM Meeting, 16-18th Nov. 2010, University, Belfast, United Kingdom.

Poster Presentations

1. M. Czugala, D. Maher, R. Burger, K. J. Fraser, J. Ducrée, D. Diamond and F. Benito-Lopez, *Fully integrated portable Centrifugal Microfluidic Analysis System for on-site colorimetric water analysis (CMAS),* ATWARM International Conference 2013: Water - The Greatest Global Challenge, 14-16th May 2013, Dublin, Ireland.
2. M. Czugala, A. Llobera, X. Munoz-Berbel, D. Diamond and F. Benito-Lopez, *Generation of Fully Functioning Biomimetic Analytical Platforms for Water Quality.* Biannual ATWARM Meeting, 13–14th Nov, 2012, Belfast, United Kingdom.
3. M. Czugala, C. Fay, P. Ortiz, A. Llobera, D. Diamond and F. Benito Lopez, *Photo-actuated Ionogel Microvalves for Real-Time Water Quality Analysis in a Micro-fluidic Device*, 2nd International Symposium on Functional Nanomaterials 2012, 6-7th September 2012, Dublin, Ireland.
4. C. O'Connell, M. Czugala, F. Benito Lopez, D. Diamond, *Micro-bioreactors Controlled with Photonic Ionogel Actuators*, 2nd International Symposium on Functional Nanomaterials, 6-7th September 2012, Dublin, Ireland.

5. C. O'Connell, M. Czugala, F. Benito Lopez, D. Diamond, *Micro-bioreactors Controlled with Photonic Ionogel Actuators*, The Technology Touchdown Symposium, 30-31st August 2012, Dublin, Ireland.
6. M. Czugala, F. Benito Lopez, D. Diamond, *Generation of Fully Functioning Biomimetic Analytical Platforms for Water Quality*, Biannual ATWARM Meeting, 1-2nd May 2012, Cranfield, United Kingdom.
7. M. Czugala, C. Fay, D. Diamond, F. Benito-Lopez, *Point-of-care System for Aquatic Environmental Monitoring*, Clarity Site Review 25th April 2012, Dublin, Ireland.
8. M. Czugala, P. Ortiz, C. Fay, A. Llobera, F. Benito-Lopez, D. Diamond, *Photo-actuated Ionogel Microvalves for Real-time Water Quality Analysis in a Micro-fluidic Device*, Lab on a Chip European Congress, 28-29th March 2012, Edinburgh, United Kingdom.
9. M. Czugala, C. Fay, D. Diamond, F. Benito-Lopez, *Photo-actuated Ionogel Microvalves for Real-time Water Quality Analysis in a Micro-fluidic Device*, QUESTOR@DCU Workshop, 2nd March 2012, Dublin, Ireland.
10. M. Czugala, D. Diamond, F. Benito-Lopez, *Next generation autonomous analytical platforms for remote environmental monitoring: generation of fully functioning biomimetic analytical platforms for water quality.* Biannual ATWARM Meeting, 29th Nov. - 1st Dec. 2011, Belfast, United Kingdom.
11. M. Czugala, D. Diamond, F. Benito-Lopez, *Next generation autonomous analytical platforms for remote environmental monitoring: Generation of Fully Functioning Biomimetic Analytical Platforms for Water Quality*, Marie Curie Researchers Symposium, SCIENCE – Passion, Mission, Responsibilities, Polish Presidency of the EU Council, 25-27th September 2011, Warsaw, Poland.
12. M. Czugala, D. Diamond, F. Benito-Lopez, *Next generation autonomous analytical platforms for remote environmental monitoring: Generation of*

Fully Functioning Biomimetic Analytical Platforms for Water Quality, Biannual ATWARM Meeting, 10–12th May 2011, Essen, Germany.

13. M. Czugala, R. Gorkin, C. Rovira-Borras, J. Ducrée, D. Diamond and F. Benito-Lopez, *Microfluidic System with a Wireless Paired Emitter Detector Diode Device as optical Sensor for Water Quality Monitoring*, QUESTOR@DCU Workshop, 4th March 2011, Dublin, Ireland.
14. M. Czugala, R. Gorkin, C. Rovira-Borras, J. Ducrée, D. Diamond and F. Benito-Lopez, *Microfluidic System with a Wireless Paired Emitter Detector Diode Device as optical Sensor for Water Quality Monitoring*, 6th Conference on Analytical Sciences (CASi), 21-22nd Feb, 2011, Dublin, Ireland.
15. M. Czugala, D. Diamond and F. Benito-Lopez, *Next generation autonomous analytical platforms for remote environmental monitoring: Generation of Fully Functioning Biomimetic Analytical Platforms for Water Quality*, Biannual ATWARM Meeting, 16–18th Nov 2010, Belfast, United Kingdom.

Awards

1. Travel grant to attend the 16th International Conference on Miniaturized Systems for Chemistry and Life Sciences (MicroTAS) in Okinawa, Japan.
2. Travel grant to attend the 15th International Conference on Miniaturized Systems for Chemistry and Life Sciences (MicroTAS) from the Chemical and Biological Microsystems Society in Seattle, Washington, USA.
3. GICSERV Program Fellowship: 7th call, from the Consejo Superior de Investigaciones Científicas (CSIC, Spanish government) in collaboration with Dr. Andreu Llobera at Centro Nacional de Microelectrónica (CNM), Barcelona, Spain. Project title: *Photonic ionogel-based tunable micromixers.*

Patent

1. M. Czugala, D. Maher, K. J. Fraser, D. Diamond and F. Benito-Lopez, *A Colorimetric Centrifugal Microfluidic Analysis System*, United Kingdom 1207239.3, Filed 25th April, 2012.

Aims of the Thesis

The aim of this thesis is to develop a fully functioning biomimetic analytical platform for environmental monitoring designed to take advantage of the latest developments in computing platforms, materials chemistry, wireless communications and microfabrication. The ultimate goal is to combine optical sensing, microfluidics technology and stimuli responsive polymeric materials to perform *in-situ* water analysis. The platform is a generic analytical device, capable of monitoring target environmental and health parameters based on colorimetric assays *in-situ*. In particular this thesis focuses on:

1. Characterisation of the actuation behaviour of photoresponsive ionogel microvalves.

2. Integration of soft sensors and actuators into microfluidic platforms and demonstration of their application to environmental monitoring.

3. Development of portable, wireless platforms for water quality analysis. The platforms are desired to be reliable, sensitive, low cost and require low power consumption.

4. Validation of the developed platforms by comparing the obtained results with standard bench-top instruments.

Selected Publications and Author Contribution

This thesis includes five original manuscripts published in peer-reviewed journals, one patent application and one submitted manuscript. The core theme of the thesis is the development of fully integrated microfluidics based platforms for water quality analysis. The ideas, development and writing up of all the manuscripts and the patent in the thesis were the principal responsibility of myself, the candidate, working within the School of Chemical Sciences under the supervision of Prof. Dermot Diamond and Dr. Fernando Benito-Lopez. The inclusion of co-authors reflects the fact that part of the work came from active collaborations between researchers and acknowledges input into team-based research. In the case of chapters 2 to 7 my contribution to the work involved the following:

Thesis chapter	Publication title	Publication status*	Nature and extent of candidate's contribution
2	Integrating stimulus responsive materials and microfluidics – The key to next generation chemical sensors	Published, Journal of Intelligent Material Systems and Structures, 2012.	First author, manuscript development and writing up.
3	Photopatterning and actuation behaviour of photoresponsive phosphonium-based ionogel microstructures	Submitted, Langmuir, 2013.	First author, initiation, key ideas, experimental design, data collection and analysis, manuscript development and writing up.
4	Portable Integrated Microfluidic Platform for the monitoring and detection of nitrite	Published, Talanta, 2013.	First author, initiation, key ideas, experimental design, data collection and analysis, manuscript development and writing up.
5	A wireless paired emitter detector diode device as optical sensor for lab-on-a-disc applications	Published, Proceedings Transducers 2011.	Co-author, initiation, key ideas, experimental design, data collection and analysis, manuscript development and writing up.
6	Optical sensing system based on wireless paired emitter detector diode device and ionogels for lab-on-a-disc water quality analysis	Published, Lab on a Chip, 2012.	First author, initiation, key ideas, experimental design, data collection and analysis, manuscript development and writing up.
7	CMAS: fully integrated portable Centrifugal Microfluidic Analysis System for on-site colorimetric analysis	Published, RSC Advances, 2013.	First author, initiation, key ideas, experimental design, data collection and analysis, manuscript development and writing up.

* I have renumbered sections of submitted or published papers in order to generate a consistent presentation within the thesis.

Signed: _____ Date: _____

Monika Czugala

Signed: _____ Date: _____

Prof. Dermot Diamond

Signed:  Date: _____

Dr. Fernando Benito Lopez

Thesis Outline

A detailed overview of each chapter is given below:

Chapter 1

This chapter gives an overview of the themes common to most of the papers included in this thesis and sets the following chapters in the context of existing literature. Important topics including: water quality analysis, microfluidics, optical sensors and stimuli responsive materials are discussed in order to inform the reader on the concepts that will be further used in the experimental chapters (Chapter 3 to 7). Moreover, this chapter presents the context in which the experimental chapters contribute to the scientific advancement of the research area.

Chapter 2

This chapter reviews the current state-of-the-art of stimulus responsive materials for liquid handling on microfluidic platforms. The chapter highlights that photoswitchable soft actuators based on spiropyran can be controlled in a unique, unprecedented way by simply using light irradiation, and indicates aspects where there is a need for further innovation in the field.

Chapter 3

This chapter presents the fabrication of photopatterned microstructures produced using an in-house photolithography system built with the assistance of Dr. Peer Fischer from Fraunhofer Institute, Freiburg, Germany. The materials

were based on photoresponsive phosphonium based ionogels functionalised with the spiropyran and the swelling and shrinking behaviour of the ionogel microstructures described. The influence of surface-area-to-volume ratio of the microstructures on the swelling kinetics is presented and discussed.

Chapter 4

In this chapter, a portable, microfluidic analytical platform for the monitoring of nitrite anions in water using the Griess method is presented. The innovative approaches consist of the combination of biomimetic photoswitchable ionogel microvalves for fluid manipulation and detection of the colour intensity of the Griess reagent nitrite complex using a low cost paired emitter detector diode (PEDD). This work has been done in collaboration with the Engineering Department at the NCSR, in particular with Mr. Cormac Fay, who developed the PEDD and communication system.

Chapter 5

This chapter demonstrates the application of a portable wireless PEDD sensing configuration for lab-on-a-disc based colorimetric analysis. This is the first time that a PEDD detector has been combined with centrifugal microfluidics. The performance of the sensitive detector for the measurement of concentrations of coloured solutions, as a proof of principle, is described. This work has been done in collaboration with the Biomedical Diagnostics Institute, in particular with Dr. Robert Gorkin, who fabricated the CDs.

Chapter 6

In this chapter the first use of the PEDD as an optical sensor for water quality monitoring in a lab-on-a-disc device is presented. The centrifugal disc was based on an ionogel sensing area and applied for pH (quantitative) and turbidity (qualitative) monitoring of water samples. This work has been done in

collaboration with the engineering department at the NCSR, in particular with Mr. Thomas Phelan, who developed the PEDD and communication system.

Chapter 7

This chapter illustrates, for the first time, a wireless system capable of *in-situ* reagent-based colorimetric analysis. The Centrifugal Microfluidic Analysis System (CMAS) incorporates an easily reconfigurable detector board, which allows a wide range of centrifugal microfluidic layouts to be implemented. The stand-alone capabilities of the system, combined with the portability and wireless communication through a dedicated Android App on a 7" Tablet, provides the flexibility crucial for on-site water monitoring. The centrifugal disc was designed for nitrite detection within water samples, as a proof of principle. This work has been done in collaboration with the engineering department at the NCSR, in particular with Dr. Damien Maher and Dr. Fiachra Collins, who developed the PEDD and the communication system and the School of Computing, in particular with Mr. Frank Hopfgartner and Ms. Yang Yang for the development of the Android application for CMAS.

Chapter 8

This chapter presents the conclusions of this thesis, summarises the work carried out and outlines the challenges and opportunities lying ahead.

Thesis Outline

Abstract

Environmental monitoring has grown substantially in recent years in response to increasing concerns over the contamination of natural, industrial, and urban areas with potentially harmful chemical agents. Traditional monitoring of water contamination is based upon manual *in-situ* 'grab' sampling followed by laboratory testing. Advantages of this strategy include high precision and accuracy of the measurements, however because of the expense involved in maintaining these facilities there are inherent restrictions in terms of spatial and temporal sampling. In contrast, *in-situ* measurements generated with portable instruments present a much more scalable model, enabling denser monitoring. The challenge is to develop inexpensive and reliable devices that can be used *in-situ*, with the capability to make the resulting data available remotely via web-databases, so that water quality can be monitored independently of location. Miniaturisation of analytical devices through the advent of microfluidics has brought wide opportunities for water analysis applications. The vision is to miniaturise processes typically performed in a central clinical lab into small, simple to use devices – so called lab-on-a-chip (LOC) systems. Microfludic systems are especially promising for point-of-care applications due to the low cost, low reagent consumption and portability, and the focus of this thesis is to provide novel microfluidic platforms towards an integrated system for water quality analysis.

A main outcome of my work was the development and validation of innovative integrated systems that were designed and developed for quantitative

analysis of turbidity and qualitative analysis of pH and nitrites in water samples. The microfluidic manifolds were designed and fabricated using rapid prototyping techniques such as soft lithography and CO_2 laser cutting. For fluid propulsion, various methods were employed: back pressure, capillary forces (typical microfluidic manifolds) and centrifugal force (centrifugal discs). In the latter, fluid propulsion was performed by the forces induced due to the rotation of the disc, thus eliminating the need for external pumps since only a spindle motor is necessary to rotate the disc. Centrifugal discs systems are especially promising for point-of-care applications, and as a final output the fully integrated portable wireless system for *in-situ* colorimetric analysis was demonstrated. In all systems a low cost but highly sensitive paired emitter-detector diode (PEDD) method was employed to perform colorimetric measurements. Moreover, due to the wireless communication, acquisition parameters were controlled remotely and the results were downloaded from distant locations and displayed in real time. The autonomous capabilities of the system, combined with the portability and wireless communication, provide the basis for a flexible new approach for on-site water monitoring. In addition, their small size and low weight offered the advantage of portability. The suitability of the low-power analysers for the precise and continuous measurement of samples was established, since the analysers exhibited low limits of detection. Freshwater samples were analysed and the results were compared to those generated with a conventional bench-top instruments showing good agreement.

Additionally, stimuli-responsive materials based on *N*-isopropylacrylamide (NIPAAm) phosphonium ionogels were characterised and incorporated within microfluidic platforms as sensors and actuators. The phase change NIPAAm ionogel functionalised with spirobenzopyran chromophores was characterised and applied for fluid control within microfluidic manifold. Microvalve actuation was performed by the localised white light irradiation, thus allowing for non-contact manipulation of the liquids inside of the

microchannels. This is the first time that photoresponsive ionogel microvalves were incorporated within portable, wireless integrated microfluidic analytical platform. Moreover, phosphonium based ionogels incorporating pH sensing dye were used for pH sensing of water samples.

This work presents the core technology for an integrated microfluidic platforms for fundamental research as well as for point-of-use applications. The key outputs of my work are:

1. Design, fabrication and characterisation of novel microfluidic manifolds.
2. Stimuli-responsive ionogel materials were successfully employed within microfluidic devices for sensing and actuating applications.
3. Portable, wireless, integrated systems based on microfluidic platforms were developed and their successful application for analysis of pH, turbidity and nitrites was demonstrated.

List of Abbreviations

ABS	Acrylonitrile butadiene styrene co-polymer
ACN	Acetonitrile
ADC	Analog to digital converter
AMF	Alternating magnetic field
BCP	Bromocresol Purple
CAD	Computer Aided Design
CCD	Charge coupled device
CD	Centrifugal disc
CMAS	Centrifugal Microfluidic Analysis System
DCM	Dichloromethane
DMAP	4-(Dimethylamino)pyridine
DMF	Dimethylformamide
DMPA	2,2-5 dimethoxy-2-phenyl acetophenone
EOF	Electroosmotic flow
EPA	Environmental Protection Agency
EtOH	Ethanol
FIA	Flow injection analysis
FIA	Fluorescence immunoassays
GO-GMA	Glycidyl methacrylate functionalised graphene-oxide
GPS	Global Positioning System
HCl	Hydrochloric acid
H_3PO_4	Phosphoric acid
IL	Ionic liquid
IR	Infrared
ISNBP	Indolinespiro nitro-benzopyran
ISBP	Indolinespirobenzopyran
LED	Light-emitting diode
LCST	Lower critical solution temperature
LOC	Lab-on-a-chip
LUMO	Lowest unoccupied molecular orbital
MBAAm	*N,N'*-methylene-bis(acrylamide)

MC	Merocyanine
MC-H^+	Protonated merocyanine
MeOH	Methanol
MPTMS	3-(Trimethoxysilyl) propyl methacrylate
NaOH	Sodium Hydroxide
$NaNO_2$	Sodium nitrite
NED	*N*-(1-naphthyl)ethylenediamine dihydrochloride
NIPAAm	*N*-isopropylacrylamide
PCB	Printed circuit board
PDMS	Polydimethylsiloxane
PEDD	Paired emitter detector diode
PGMEA	Propylene glycol methyl ether acetate
PMMA	Poly(methylmethacrylate)
POC	Point-of-care
PSA	Pressure-sensitive adhesive
P(SPNIPAAm)	Copolymer of an acrylated SP and poly(*N*-isopropylacrylamide)
R^2	Coefficient of correlation
ROMP	Ring opening metathesis polymerisation
RSD	Relative standard deviation
SA/V	Surface area-to-volume
SEM	Scanning electron microscopy
SP	Spiropyran
SP-COOH	1'-(3-carboxypropyl)-3',3'-dimethyl-6-nitrospiro[2H-1]-benzopyran- 2,2' -indoline
THF	Tetrahydrofuran
$[P_{4,4,4,14}][Cl]$	Tetrabutyl-phosphonium chloride
$[P_{6,6,6,14}][Cl]$	Trihexyltetradecyl-phosphonium chloride
$[P_{4,4,4,14}][dca]$	Tetrabutyl-phosphonium dicyanoamide
$[P_{6,6,6,14}][dca]$	Trihexyltetradecyl-phosphonium dicyanoamide
$[P_{6,6,6,14}][NTf_2]$,	Trihexyltetradecyl-phosphonium bis(trifluoromethanesulfonyl)-amide
μTAS	Micro-Total Analysis Systems
UV	Ultraviolet
Vis	Visible
WHO	World Health Organisation
WNS	Wireless network systems

Chapter 1

Introduction

1.1 Importance of water quality

Globally, water is an essential resource for living systems, industrial processes, agricultural production and domestic use and its quality degree influences the entire human activity from economics to health. In spite of the significant efforts made to improve water quality, according to data collected by the World Health Organisation (WHO), more than one in six people worldwide, 894 million people, do not have access to safe drinking water.[1] Furthermore, 2.6 billion people in the world are short of even the most basic forms of sanitation. Lack of sanitation is the world's largest cause of infection.[2] Together, the water and sanitation crises have claimed more lives than any war has claimed through guns.[2]

The WHO mentioned in its 2012 report 'UN-Water Global Analysis and Assessment of Sanitation and Drinking-Water' that its main objective is to monitor the inputs required to extend and sustain water, sanitation and hygiene systems and services.[3] Therefore, there is a prevailing global necessity for the identification of disruptive water quality monitoring systems to trigger early warning of contamination of water supplies as well as systems capable of continuous monitoring of water quality. A Flash Eurobarometer survey report entitled 'Attitudes of Europeans towards water-related issues' published in 2012[4] shows that Europeans care about water quality. The survey was requested by Directorate-General for the Environment. Three key findings of the survey are that:

- The majority of Europeans are concerned about water quality; nearly 7 out of 10 respondents believe that water quality is a serious issue in their country (68%).
- The most widespread view among Europeans is that the quality of groundwater, rivers, lakes and coastal waters has either improved (23 %)

or remained the same (25 %) over the past ten years, while 44% believe it has deteriorated.

- Europeans consider chemical pollution to be the main threat to the water environment (84 %).

1.1.1 Water quality monitoring

In Ireland, the investigation of water pollution incidents and identification of pollution sources is responsibility of Environmental Protection Agency (EPA). The EPA ensures that Ireland's environment is protected, and monitors changes in environmental trends to detect early warning signs of neglect or deterioration. Water monitoring can be conducted for many purposes, the five major purposes are to:

1. Characterise waters and identify changes or trends in water quality over time.
2. Identify specific existing or emerging water quality problems.
3. Gather information to design specific pollution prevention or remediation programs.
4. Determine whether program goals such as compliance with pollution regulations or implementation of effective pollution control actions are being met.
5. Respond to emergencies, such as spills and floods.

The EU Water Framework Directive (WFD 2000/60/EC)[5] is dictating more stringent monitoring of aquatic environments. Although sensor technology is rapidly evolving and some parameters can currently be measured online (such as pH, conductivity and dissolved oxygen), most of the water analysis are carried out in centralised laboratories and are based on the application of conventional monitoring techniques to field-collected samples.[6]

Advantages of employing this strategy include high precision and accuracy of the measurements, however because of the expense involved in maintaining these facilities there are inherent restrictions in terms of the number of locations and sampling frequency.[7] The use of recent technological breakthroughs may hold the key to address these issues. Indeed, as the list of emerging pollutants included in the EU WFD increases every year, the task of developing a low cost continuous monitoring system with highly selective sensors for each pollutant is becoming increasingly difficult.

1.1.2 Towards point-of-use water analysis

In both process studies and routine monitoring, *in-situ* chemical measurement capabilities offer a variety of substantial advantages relative to shipboard and laboratory analysis. Prompt *in-situ* analysis without human intervention considerably reduces sample contamination possibilities, improves rates of sample throughput, and increases observational endurance. Quite importantly, prompt analysis creates opportunities for adaptive sampling of dynamic chemical gradients, either autonomously (*e.g.,* through sensor control of sampling platforms) or through human-directed responses (*e.g.*, surface-tethered control of depth). *In-situ* water analysis generally provides, as well, substantial reductions in overall measurement costs. In summary, there are several motivations to develop point-of-use systems:

- De-centralised testing (*i.e.* no need for central laboratories).
- Applications in resource poor regions such as developing countries where infrastructure is poor and sample transport to centralised facilities is not feasible.
- Short sample-to-answer times, allowing faster treatment of water.
- Low sample and reagent consumption.

- Improved reliability due to automation.
- Overall cost reduction.

Today state of the art *in-situ* water quality monitoring instruments are based on the two main domains:

- Hand held monitors – semi-manual data collection.
- Remote autonomous analysers – self-powered communication enabled systems.

Globally, hand held monitors are more common, mainly due to their lower cost and low effort to operate and to maintain. There is a wide range of commercially available portable devices that provide rapid indication of water quality parameters. Some techniques are relatively cheap (< $100 USD), but they do not possess data logging capabilities and allow for only one spot test (*e.g.* Hanna instruments nitrite ULR Checker (HI 764),[8] and API® test kits).[9] Conversely, more sophisticated probes allow multi-parameter measurements with integrated wireless data transmission, but their application is quite limited due to the high cost of hardware and maintenance (Hach® Hydrolab DS5[10] and YSI® V2 Multiparameter Water Quality Sondes,[11] costs typically $20K or greater). Very often currently marketed remote monitors are custom made systems based on integration of off-the-shelf systems. They are bulky in size (medium cabinet size), costly (€10K - €20K) and based on monolithic data systems built for one client. This in turn, means that the majority of collected data cannot be displayed on-line and is rarely shared with the science community.

Today, there are not many on-line water quality data about chemical species available in the public domain, the internet, or available on-line to the research community. The importance of on-line available information is critical in terms of health and public security on one hand and for better research on the other.[7] Beside the data availability, the actual state-of the-art

remote monitoring systems prevent the ability to interact with the sensor performance and data remotely.[12] With today's evolving smart-city and "Big Data" concepts, the need for data interoperability is growing fast; and systems that can communicate with other systems will play important role. The innovation aspect in water monitoring is the design of end-to-end continuous, real time solutions from sensor to database. The developed technology will be implemented into a self-powered, communication-enabled instrument that will perform all calculations and data representation in the cloud. This is also an important step forward, retrieving and presenting spatial information of various environmental parameters which, until now is a very complicated task, especially when there is a requirement for real time data streaming and analysing. Nowadays, commonly used sensing technologies are based on gathering samples for laboratory examinations and then re-positioning the data on a selected map. In this sense, a radical step - forward in the state-of-the-art is required: moving from written logbook data to a cloud based network of sensors. Thus, these innovative sensors incorporating advances in mobile communications and the internet shall open a new era of environmental monitoring potentially linking the molecular with the digital world.

1.1.3 Growth prospects for the water management industry

The scale of the commercial opportunity in environmental monitoring was highlighted by a recent report that identified industrial and environmental testing applications as the market sector with the highest growth for sensors incorporating microfluidics, rising by an average of 23 % p.a. from 2012 to 2016, to *ca.* $4 billion.[13] According to market analysts, the

global water market was valued at $515 billion in 2010 and is estimated to be as large as $1 trillion by 2020.[14] In Europe, the water sector has a turnover of about €100 billion p.a., involving 9,000 active small and medium enterprises (SMEs) and 600,000 direct jobs in water utilities alone, which represents about one third of the world water market.[15] A 1% increase of the rate of growth of the water industry in Europe could create between 10,000 and 20,000 jobs. A recent EC publication reported that there are more than 54,000 surface water monitoring stations in Europe; 24,000 for surveillance monitoring and 40,000 for operational monitoring, with around 10,000 common for both. In addition, there are an estimated 51,000 groundwater monitoring stations.[16] Globally, over 250,000 water utility companies are estimated to be in service operating; 84% of utilities operated under public ownership with the rest under private ownership.[17] The data shows that the water market holds enormous economic potential for the future. According to a landmark report[14] recently issued by the 2030 Water Resources Group, formed to contribute new insights to the increasingly critical issue of water resource scarcity, by 2030 under an average economic growth scenario and if no efficiency gains are assumed, global water requirements would grow from 4,500 billion m^3 today to 6,900 billion m^3. The report also estimates that by 2030, India, China, Brazil, and South Africa collectively will account for 30% of world GDP and 42% of projected global water demand. It is clear therefore, that there are significant opportunities in these countries for low cost monitoring technologies, that could be exported from Europe.

1.2 Microfluidics

Initially introduced by Manz *et al.*,[18] microfluidics has been the focus of a tremendous level of research activity over the past 20 years and significant

scientific advances have been made in the area. Microfluidic devices, defined as miniaturised reaction vessels fabricated by using methods of microtechnology and precision engineering, consist of three-dimensional structures (microchannels) with diameters typically in the range of 10-500 μm,[19] which are used to manipulate reagent solutions. The fabrication of microfluidic systems has been reviewed elsewhere.[20, 21] A wide variety of materials and techniques have been used for the fabrication of microfluidic analytical systems. Some of the most commonly used materials include silicon, glass, and polymers such as poly(dimethylsiloxane) (PDMS), poly(methyl methacrylate) (PMMA) and polycarbonate (PC). Depending on the material, application, size and aspect ratio of features required, fabrication techniques including photolithography, soft lithography, micro-milling, injection moulding and embossing have been used to form microfluidic chips with a range of components such as microchannels, mixers, separators, integrated detectors, valves and pumps.

One obvious advantage of microfluidics is that miniaturised components and processes use smaller volumes of fluid, thus leading to reduced reagent consumption. This decreases costs and permits small quantities of precious samples to be stretched further (for example, divided up into a much larger number of screening assays).[22] Quantities of waste products are also reduced. Moreover, the low thermal mass and large surface area to volume ratio of small components facilitates rapid heat transfer, enabling quick temperature changes and precise temperature control. In exothermic reactions, this feature can help to eliminate the buildup of heat or "hot spots" that could otherwise lead to undesired side reactions or even explosions.[23] The large surface to volume ratio is also an advantage in processes involving support-bound catalysts or enzymes, and in solid-phase synthesis. At the small length scales of microfluidic devices, diffusive mixing is

fast, often increasing the speed and accuracy of reactions.

The scale of integration is another advantage of μTAS where distinct fluidic operations can be integrated in miniaturised systems by exploiting appropriate fabrication technologies. A single integrated microfluidic device can perform significant biological or chemical processing from beginning to end, including the sampling, pre-processing, and measurement involved in an assay. Performing all fluid handling operations within a single microfluidic device saves time, reduces risk of sample loss or contamination, and can eliminate the need for bulky, expensive laboratory robots. Furthermore, the operation of the microfluidic device can be fully automated, thus increasing throughput, improving ease of use, repeatability and reducing the element of human error. Automation is especially useful in applications requiring remote operation, such as devices performing continuous monitoring of chemical or environmental processes in inaccessible locations.[24]

Furthermore, microfluidic devices allow for increasing the throughput by exploiting parallelism. Single microfluidic devices have been demonstrated that perform hundreds or thousands of identical assays or reactions utilising synchronization and control-sharing so that their operation is not significantly more complex than that of a non-parallel chip. Being planar and on the same scale as semiconductor integrated circuits, microfluidic devices are ideally able to be integrated with electronic or optical components such as sensors, actuators, and control logic. Numerous actuators, such as valves, pumps, heating elements, and electrodes for electrophoresis or electrokinetic flow, have also been demonstrated (see Chapter 2).

Small integrated microfluidic devices also offer the feature of portability, enabling mobile applications in chemical analysis, point-of-care medicine, or *in-situ* water analysis. The ability to perform integrated diagnostic tests where they are needed rather than in a centralised lab could

reduce costs, improve turn-around time, and reduce the risk of sample mix-up. If manufactured cheaply, devices could be disposable, eliminating cross-contamination between tests.

In addition, due to the numerous advantages offered by the microscaled channels, the concept of microfluidic "lab-on-a-chip" (LOC) has triggered significant effort in the development of materials and their employment in miniaturised devices. In particular, switchable materials offer intriguing possibilities and the potential to integrate sophisticated functions in a simple overall design. Stimuli responsive materials, in particular, thanks to their increasing ease of fabrication and simple control, will be increasingly integrated with microfluidic manifolds, and could significantly advance the development of fully integrated microfluidic systems (discussed in further detail in Chapter 2).

1.2.1 Microfluidics in aquatic environmental monitoring

μTAS provides a route for the generation of micro-dimensioned analytical instruments that can be operated in remote locations, enabling *in-situ* water analysis to become a reality.[25] It has been previously described that there are clear advantages of using microfluidic devices in the integration of sample processing in order to meet the increasing needs of modern environmental monitoring.[26] The small amounts of sample and reagents typically required, reduced measurement times, improved sensitivity, higher selectivity, and greater repeatability make "lab-on-a-chip" based systems attractive options for generating fully integrated μTAS platforms.[27, 28] Several implementations of microfluidics in environmental monitoring have been reported.[29] Schaap *et al.*[30] developed an opto-fluidic lab-on-a-chip that

functions as a compact robust tool for the fast screening, real-time monitoring, and initial classification of algae. Diamond *et al.*[31-33] presented a microfluidic sensor for long-term monitoring of phosphate levels that incorporates sampling, reagent and waste storage, detection, and wireless communication into a compact and portable device. An interesting approach for environmental monitoring was presented by Curtis *et al.*[34] based on a portable cell-based impedance sensor for toxicity testing of drinking water. In addition, Zou *et al.*[35] presented an on-site water analyser capable of automatically performing long-term continuous sampling for heavy metals measurement using a continuous flow sensing method with an array of disposable polymer chips.

However, despite this effort, apart from important applications in high throughput screening, sample preparation for large analytical instruments and biomedical diagnostics, examples of microfluidic based analytical instruments targeting remote environmental sensing remain frustratingly elusive. In a recent editorial in *Lab on a Chip* Whitesides[36] referred to this issue, stating that this decade must be the decade of 'lab-on-chip' applications, appealing for much broader application of the concept beyond the clinical arena. Simultaneously, in a recent *Analytical Chemistry* editorial Murray highlighted that developing low cost analytical platforms for environmental monitoring is the fundamental challenge now facing the analytical chemistry community.[37] Therefore, with such motivation and urge, the time has never been more right to address this challenge.

1.2.2 Centrifugal microfluidics

Centrifugal discs (CDs) offer many intrinsic advantages compared with typical pump-driven systems. Rotational actuation is simply implemented by

controlling the frequency of a spindle motor to rotate the substrate. As the spinning frequency can easily be controlled over more than three orders of magnitude, the range of forces covers approximately six orders of magnitude, which is far superior to common, pressure-driven lab-on-a-chip systems. The volumetric flow rate is dependent on the speed at which the disc spins, the geometry, dimensions, and surface functionality of the fluidic channels, the distance the liquid is from the centre of the disc, and fluid properties, such as density, and viscosity. A wide range of flow rates can be achieved with a high degree of accuracy and precision, simply by using combinations of different spin speeds and channel geometries.[38]

Another advantage of the centrifugal technology is the far-ranging independence of the fluid actuation from parameters such as conductivity and pH.[27] Furthermore, due to the inertia of the disc, the spinning motion is self-stabilising, thus eliminating jittering known from reciprocating or syringe pumps. This system-intrinsic robustness of centrifugal liquid handling proves to be a major benefit for environmental diagnostic applications where one of the challenges is the wide variety of fluidic properties. The rotational actuation, which is driven by a basic, low-cost spindle motor, also obviates the need for external, pressure-generating pumps and their world-to-chip interfacing. The use of CDs has undeniable advantage in regards to portability, which is a key issue for *in-situ* water monitoring systems. Moreover, the modular nature of the CD completely separates the instrument-based driving and detection units from liquid samples and reagents, which are exclusively handled by the microstructured, typically disposable disc. The latter aspects are beneficial for analytical applications since all fluidic handling operations can be isolated within a totally encapsulated system, thus minimising risks of sample contamination and fluidic leakage into electronics and optics areas.

In addition, by employing centrifugal microfluidic technology, multiple experiments can be automated, enabling parallel processing and integration towards sample-to-answer systems. Fluidic processing steps, such as metering of sample fluids and the mixing of reagents can be automated simply by the incorporation of different spinning profiles. Centrifugal pumping also provides forces across the entire length of a fluid element, allowing smooth and controlled flow. All of these centrifugal microfluidic technologies and functions make the CD-based analytical approach a powerful tool for complete automation, reducing time and error due to handling.

Several implementations of centrifugal discs for environmental monitoring have been reported; [29] Salin *et al.* developed discs for the detection of aqueous sulfide,[39] nitrate, nitrite[40] and chromium VI[29] employing centrifugal microanalysis. More recently, Hwang *et al.*[41] published a microfluidic centrifugal disc that is capable of simultaneous determination of several nutrients in water samples (nitrite, nitrate, ammonium, orthophosphate, and silicate). Among the commercially available systems based on the centrifugal microfluidic platforms, the LaMotte WaterLink Spin[42, 43] system deserves particular attention. As presented in Fig. 1.1, the system is based on an analyser and single-use disc containing all the required reagents, to perform tests within 1 min. While the system allows for multi-parameter measurements, it is a bench-top system and provides no *in-situ* water testing.

Figure 1.1. LaMotte Waterlink Spin system for swimming pool water analysis (http://www.lamotte.com/waterlink_spin.html).

1.2.2.1 Centrifugal hydrodynamics

The fluid manipulation within centrifugal discs primarily relies on the three rotationally induced (pseudo) forces acting in the plane of rotation of the disc.[44, 45] A particle or fluid volume density, ρ, on a planar substrate rotating at a distance, r, from a central axis experiences the radially directed centrifugal force density (Fig. 1.2):

$$f_{CE} = \rho r \omega^2 \tag{1.1}$$

which scales with the square of the (angular) rotational frequency, ω. Secondary effects, which are induced by the spinning frame of reference (*i.e.*, the disc), are the Euler force density:

$$f_E = \rho r \; d\omega \; / \; dt \tag{1.2}$$

which is directed against a change in fluid velocity and results in swirling currents propelled by rotational acceleration, and the Coriolis force density:

$$f_C = 2\rho\omega\boldsymbol{v} \tag{1.3}$$

which deflects objects perpendicular to their direction of motion at the

velocity, v, in the plane of rotation.

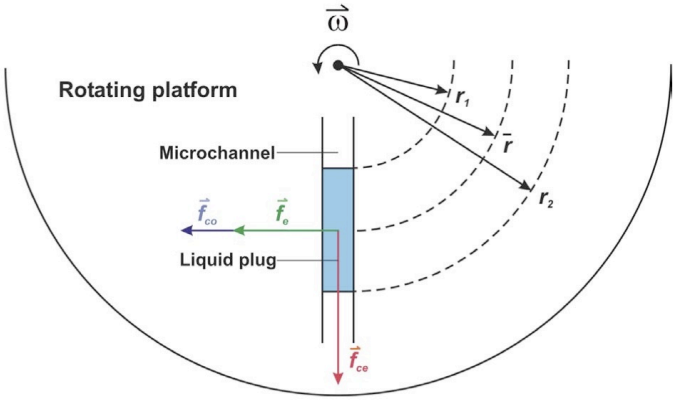

Figure 1.2. Schematic presentation of the forces on a centrifugal microfluidic platform.[45]

1.3 Optical and colorimetric sensors

An optical sensor is a device that converts light energy into electronic signals. These electronic signals can, in turn, be interpreted by a processor unit. When a change in signal occurs, it will result in either an increase or decrease of the electrical output. Research and development in optical sensors has been driven by the fact that optical sensors have inherent advantages over traditional sensing methods. For example, they exhibit good sensitivity, have a wide dynamic range, and have multiplexing capabilities.[47]

The origins of colorimetric sensing stretches back to the 16th century when chemists extracted dyes from lichens and mosses, to create early versions of a universal indicator.[48] These indicator dyes contained substances which change colour depending on the hydrogen ion concentration in a sample, showing if it is acidic or alkaline. The use of litmus or indicator paper means that when measuring pH, the need for precise amounts of sample and reagent were removed. It also removed the possibility of destroying a sample

by getting this measurement wrong. This advancement in the technology made testing quicker, cheaper and easier.

In recent years, these colorimetric reagents have been extensively explored and have been immobilised in various polymers, both natural and synthetic. Polymers like gelatin, albumin, and cellulose have been used, depending on the characteristics and requirements of the sensors.[49] These optically responsive materials are being integrated with various other components to create new types of optical sensors. Such sensors have been applied to measure various kinds of chemical samples, such as gases,[50] electrolytes[51] and neutral biomolecules.[52] This colorimetric form of optical sensing also presents advantages over more traditional sensing methods. For example it is fully non-destructive, does not consume any of the sample, is repeatable, low cost, easy to use and reliable.[49]

1.3.1 Light emitting diodes as optical detection systems

In order to bring analytical measurements into the emerging 'networked world', appropriate analytical devices are required that possess the characteristics of reliability, low power consumption, low cost and compatibility with wireless communications systems. The miniaturisation of analytical instruments using microfluidics is one strategy to move this concept forward, however, the successful performance of the instrument can not be achieved without an optical detector. One potential technique to perform optical measurements within microfluidic-based platforms is the use of light emitting diodes (LEDs). The advancement in LED sources and photodetector technologies provides compact, low power and low cost detectors for incorporating colorimetric analytical methods into remotely deployable

devices.[25]

LEDs were first used for chemical analysis three decades ago.[53] They offer a number of advantages compared to existing light sources in optoelectronic applications, including increased lifetime, low cost, reduced power consumption, higher brightness, rugged construction, efficiency, flexibility, better spectral purity and suitable driving force.[54] Commonly, optical system configurations combine LEDs as a light source with a charge coupled device (CCD),[55] a light wave multimeter[56] and a photodiode.[57] For reference, the first configuration of optical sensing system using LED as a light detector was presented by Mims III *et al.*[58, 59] Using a simple circuit that contained an operational amplifier to measure the photocurrent obtained by a reversed biased LED, the LED sensor was applied to the detection of sunlight. The novel use of an LED as both light source and detector (paired emitter detector diode, PEDD) for chemical analysis was developed by Lau *et al.*[60] In normal light emitting mode, if an LED is connected between two digital I/O pins in series with a resistor, when a voltage is supplied through the LED's anode, through a resistor to ground, the LED will light up. To operate as a light detector, the LED is reverse biased (*i.e.*, when the LED's cathode is connected to a pin in logic high state (output mode), the LEDs internal capacitance is charged). When the state of the I/O is reversed, it causes its junction capacitance to discharge; this discharge happens at a rate proportional to the light intensity falling upon the reverse biased LED.[60] In order to perform a light intensity measurement, the I/O pin is checked over a fixed number of processor counts. A microprocessor count is done across the I/O pins to see how long the voltage takes to decay to logic zero, from the moment the capacitance starts to decay (Fig. 1.3). The voltage threshold point is dependent on the type of circuitry components being used. If the time required for this discharge is accurately measured, this in turn provides a

measure of the diode photocurrent, meaning we have indirectly measured the incoming light from the emitter LED. This method of operation has been used extensively in modern optical sensor research, and is explained in more detail by O'Toole *et al.*[61] The PEDD optical technique is very versatile and can be configured in a variety of ways to measure absorbance or reflectance. Diamond and co-workers further described the developments of PEDD based sensors with regard to configuration and application.[62, 63]

A distinct advantage of using the paired emitter detector-diode optical sensor in comparison with widely used LED-photodiode system is that the LED-LED combination is a less expensive in both the cost of components (0.4 euro cents per sensor) and the low cost of the signal transduction circuitry.[60] The measuring technique employed by the PEDD device does not require an A/D converter as the output seen by the microprocessor is a direct pulse-duration-modulated digital signal. Additional advantages of the PEDD device is the size, low power consumption (can operate in microwatts range), can detect low absolute light levels (*ca.* 0.0001 lx), responds to a broad spectral range (280 to $>$ 900 nm) and can achieve excellent S/N performance due to its inherent integrating mode of operation.

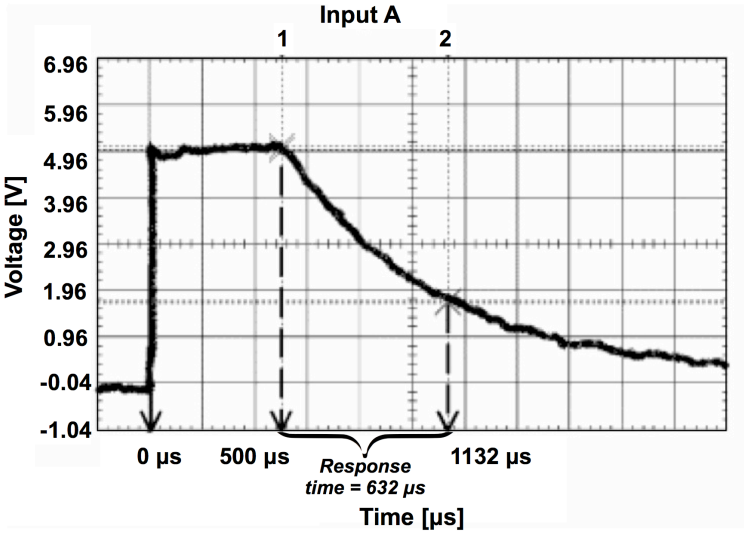

Figure 1.3. Typical discharge curve for an LED charged up to 5 V and then discharged to a threshold of 1.7 V under artificial lighting.[61]

There are many examples of the implementation of colorimetric analysis in chemical sensing and the utilisation of LEDs as light emitters and detectors. An interesting approach to the photometric measurements based on PEDD for pH detection, enzymatic detection of urea, and evaluation of urease and alkaline phosphatase activities was presented by Koncki *et al.*[64] Integration of colorimetric methods for nutrients such as phosphate,[65] ammonia[50] and nitrite[66] into microfluidic manifolds with PEDD-based optical detection systems has been also presented. For example, a very interesting example was published by O'Toole *et al.*,[65] who applied a paired emitter-detector diode for the detection of phosphate using the malachite green spectrophotometric method.

1.4 Stimuli responsive materials

1.4.1 Ionic liquids as building blocks for stimuli responsive materials

According to current convention, ionic liquids are salts that melt below

100 °C and are comprised entirely of cations and anions. ILs typically contain a large bulky asymmetric cation together with a smaller π-delocalised anion which exhibit mere electrostatic interactions.[67] Variation of important physico-chemical properties can be achieved by the appropriate choice of the cation/anion combination, where the number of potential anion–cation combinations possible reputedly equates to one trillion (10^{12}) different ILs.[68] This sort of variation in physical properties gave rise to Seddon's description of ILs as 'designer solvents'.[69] In contrast to conventional organic liquids/solvents, important physical properties of ILs such as viscosity, density, melting point and conductivity can be tuned to some degree to suit a particular need.[68] A sub-class of ILs known as room temperature ionic liquids (RTILs) that is, ILs with melting point below ca. 25 °C, has attracted special interest. These ILs have many interesting properties such as ionic and electronic conductivity, rather high thermal stability, negligible vapour pressure, and in some cases high solvation power. This last property enables ILs to dissolve substances, *eg.* monomers (*N*-isopropylacrylamide) and crosslinkers (*N,N'*-metylenbis acrylamide) that are difficult to dissolve in conventional molecular solvents.[68] ILs are used in diverse research applications such as electrolytes in electrochemical devices,[70] including rechargeable lithium cells[71] and actuators.[72]

1.4.2 Ionogels

Ionogels are hybrid materials in which the chemistry of an IL encapsulated within a polymer support matrix is facilitated in the solid state. By endowing a polymer gel with an IL important characteristics such as thermal stability and ionic conductivity can be improved. An excellent review by Bideau *et al.*[73] presents ionogels as a new class of hybrid materials, in

which the properties of the IL are hybridised with those of various components, which may be organic (*e.g.* bio-polymer),[74] inorganic (*e.g.* carbon nanotubes, silica)[75] or hybrid organic-inorganic (*e.g.* polymer and inorganic fillers).[76] An ionogel has properties arising from both the polymeric network stabilising the ionogel and the functionalities of the immobilised IL.[68] Due to very low vapour pressure ionogels exhibit high resistance to cracking and drying, which renders them attractive as soft actuators. In contrast, the conventional materials often show rapid degradation of performance due to their loss of solvent by evaporation.[77]

1.4.3 Stimulus responsive ionogels

A stimulus responsive polymeric network formed with an IL as the liquid component, rather than a conventional molecular solvent, can be termed a 'stimulus responsive ionogel'. Nádherná *et al.*[78] described the use of an ionogel based on poly(ethyleneglycol) and 1-butyl-3-methylimidazolium hexafluorophosphate [C_4mim][PF_6] as an amperometric sensor for nitrogen dioxide. Using the ionogel as the electrolyte, the authors reported a detection limit as low as 0.3 ppm. Magnetic ionogels have been prepared by Xie *et al.*[79] by filling PMMA with magnetic IL 1-butyl-3-methylimidazolium tetrachloroferrate (III) or [Bmim][$FeCl_4$]. Benito-Lopez *et al.*[80] presented photoresponsive microvalves based on an ionogel of which there were two distinct components: (1) the polymer gel, a co-polymer based on (poly(*N*-isopropylacrylamide) (pNIPAAM) and SP, and (2) phosphonium ILs. Ionogels have been employed also within optodes, mainly as the plasticiser to produce the film. Zhu *et al.*[81] used phosphonium based ionogels with a conventional chromoionophore for the detection of important inorganic acids such as HCl and H_2SO_4. The authors detailed enhanced selectivity toward hydrophilic

anions for the ionogels *versus* conventional plasticisers, which they have attributed to the increased dielectric constant of the ionogel. Kavanagh *et al.* [82] presented ionogels as optodes with significant template simplification (as a result of the particular IL used), whilst the ionogel/optode produced three distinct colors in the presence of Cu^{2+} and Co^{2+} ions.

1.5 References

1. World Health Organization, Progress on Drinking Water and Sanitation **2008**. http://www.who.int/water_sanitation_health/monitoring/jmp_report_7_10_lores.pdf.
2. Water.org, Water Facts - Sanitation. http://water.org/learn-about-the-water-crisis/facts/.
3. World Health Organisation, UN-Water Global Analysis and Assessment of Sanitation and Drinking-Water, **2012**. http://www.unwater.org/downloads/UN-Water_GLAAS_2012_Report.pdf.
4. Flash Eurobarometer 344, Attitudes of Europeans towards water-related issues; **2012**.
5. The European Parliament and the Council of the EU, Directive 2000/60/EC of the European Parliament and of the Council establishing a framework for Community action in the field of water policy. In *2000/60/EC* EU, **2000**.
6. Lucey, J., Water Quality in Ireland 2007-2008:Key Indicators of the Aquatic Environment. *Environmental Protection Agency Website (Online)* **2009**.
7. Diamond, D., Peer Reviewed: Internet-Scale Sensing. *Analytical Chemistry* **2004,** *76* (15), 278 A-286 A.
8. Hanna Instruments: http://www.hannainst.com/usa/prods2.cfm?id=045001&ProdCode=HI764. (accessed March 18, 2013).
9. API Test kits: http://www.apifishcare.co.uk/product.php?sectionid=1&catid=4&subcatid=0&id=82. (accessed March 18, 2013).
10. Hach: http://www.hachhydromet.com/web/ott_hach.nsf/id/pa_ds5-multiparameter-sonde.html. (accessed March 18, 2013).

11. YSI: http://www.ysi.com/productsdetail.php?6920-V2-3. (accessed March 18, 2013).
12. Diamond, D.; Coyle, S.; Scarmagnani, S.; Hayes, J., Wireless Sensor Networks and Chemo-/Biosensing. *Chemical Reviews* **2008,** *108* (2), 652-679.
13. Mounier, E., BioMems and Microfluidics are poised for growth. *MEMS Trends* **2012**, 3.
14. 2030 Water Resources Group, Chartering Our Water Future: Economic frameworks to inform decision-making, **2009**.
15. Water Joint Progrmamming Initiative, Water Challenges for a Changing World, **2012**. http://world-water-forum-2012-europa.eu/IMG/pdf/WWF6_Solutions_Water_JPI.pdf.
16. United Nations Environment Programme Global Environment Monitoring System (GEMS)/Water Programme, *Water Quality for Ecosystem and Human Health*, **2008**.
17. Eccles, R. G., Amy C. Edmondson, George Serafeim, Sarah E. Farrell, *A Note on Water, HBS No, N9-412-050*. Boston, **2012**.
18. Manz, A.; Graber, N.; Widmer, H. M., Miniaturized total chemical analysis systems: A novel concept for chemical sensing. *Sensors and Actuators B: Chemical* **1990,** *1* (1-6), 244-248.
19. Czugala, M.; Ziolkowski, B.; Byrne, R.; Diamond, D.; Benito-Lopez, F., Materials science: the key to revolutionary breakthroughs in micro-fluidic devices. *Proceedings SPIE 8107, Nano-Opto-Mechanical Systems (NOMS)* **2011**, 81070C-81070C.
20. Becker, H.; Gartner, C., Polymer microfabrication technologies for microfluidic systems. *Analytical and Bioanalytical Chemistry* **2008,** *390* (1), 89-111.
21. Abgrall, P.; Gue A. M., Lab-on-chip technologies: making a microfluidic network and coupling it into a complete microsystem - a review. *Journal of Micromechanics and Microengineering* **2007,** *17* (5), R15-R49.
22. Travis, D.; Boone, Z.; Fan, H.; Herbert, H.; Hooper; Ricco, A. J.; Hongdong, T.; Williams, S. J.; Plastic advances microfluidic devices. *Analytical Chemistry* **2002**, *74* (3), 78A– 86A.
23. DeWitt, S. H., Microreactors for chemical synthesis. *Current Opinion in Chemical Biology* **1999**, *3* (3), 350–356.
24. Diamond, D., Peer Reviewed: Internet-Scale Sensing. *Analytical Chemistry* **2004**, *76* (15), 278A-286A.
25. Sequeira, M.; Diamond, D.; Daridon, A.; Lichtenberg, J.; Verpoorte, S.; de Rooij, N. F., Progress in the realisation of an autonomous environmental monitoring device for ammonia. *TrAC Trends in*

Analytical Chemistry **2002,** *21* (12), 816-827.

26. Duford, D. A.; Peng, D. D.; Salin, E. D., Magnetically Driven Solid Sample Preparation for Centrifugal Microfluidic Devices. *Analytical Chemistry* **2009,** *81* (11), 4581-4584.
27. Gorkin, R.; Park, J.; Siegrist, J.; Amasia, M.; Lee, B. S.; Park, J.-M.; Kim, J.; Kim, H.; Madou, M.; Cho, Y.-K., Centrifugal microfluidics for biomedical applications. *Lab on a Chip* **2010,** *10* (14), 1758-1773.
28. Watts, A. S.; Urbas, A. A.; Moschou, E.; Gavalas, V. G.; Zoval, J. V.; Madou, M.; Bachas, L. G., Centrifugal Microfluidics with Integrated Sensing Microdome Optodes for Multiion Detection. *Analytical Chemistry* **2007,** *79* (21), 8046-8054.
29. LaCroix-Fralish, A.; Clare, J.; Skinner, C. D.; Salin, E. D., A centrifugal microanalysis system for the determination of nitrite and hexavalent chromium. *CORD Conference Proceedings* **2009,** *80* (2), 670-675.
30. Schaap, A.; Bellouard, Y.; Rohrlack, T., Optofluidic lab-on-a-chip for rapid algae population screening. *Biomedical Optics Express* **2011,** *2* (3), 658-664.
31. Cleary, J.; Slater, C.; McGraw, C.; Diamond, D., An autonomous microfluidic sensor for phosphate: On-Site analysis of treated wastewater. *IEEE Sensors Journal* **2008,** *8* (5), 508-515.
32. Bowden, M.; Diamond, D., The determination of phosphorus in a microfluidic manifold demonstrating long-term reagent lifetime and chemical stability utilizing a colorimetric method. *Sensors and Actuators B: Chemical* **2003,** *90* (1-3), 170-174.
33. Bowden, M.; Sequiera, M.; Krog, J. P.; Gravesen, P.; Diamond, D., Analysis of river water samples utilizing a prototype industrial sensing system for phosphorus based on micro-system technology. *Journal of Environmental Monitoring* **2002,** *4* (5), 767-771.
34. Curtis, T. M.; Widder, M. W.; Brennan, L. M.; Schwager, S. J.; van der Schalie, W. H.; Fey, J.; Salazar, N., A portable cell-based impedance sensor for toxicity testing of drinking water. *Lab on a Chip* **2009,** *9* (15), 2176-2183.
35. Zou, Z.; Jang, A.; MacKnight, E. T.; Wu, P.-M.; Do, J.; Shim, J.S .; Bishop, P. L.; Ahn, C. H., An on-site heavy metal analyzer with polymer lab-on-a-chips for continuous sampling and monitoring. *IEEE Sensors* **2009,** *9* (5), 586-594.
36. Whtiesides, G., Solving problems. *Lab on a Chip* **2010,** *10* (18), 2317-2318.
37. Niessner, R., Measuring the invisible. *Analytical Chemistry* **2010,** *82* (19), 7863-7863.

38. Siegrist, J.; Gorkin, R.; Bastien, M.; Stewart, G.; Peytavi, R.; Kido, H.; Bergeron, M.; Madou, M., Validation of a centrifugal microfluidic sample lysis and homogenization platform for nucleic acid extraction with clinical samples. *Lab on a Chip* **2010,** *10* (3), 363-371.
39. Kong, M. C. R.; Salin, E. D., Spectrophotometric determination of aqueous sulfide on a pneumatically enhanced ccntrifugal microfluidic platform. *Analytical Chemistry* **2012,** *84* (22), 10038-10043.
40. Yongqing, X.; Templeton, E.J.; Salin, E. D., Rapid simultaneous determination of nitrate and nitrite on a centrifugal microfluidic device. *Talanta* **2010,** *82*, 1612-1615.
41. Hwang, H.; Kim, Y.; Cho, J.; Lee, J.-y.; Choi, M.-S.; Cho, Y.-K., Lab-on-a-Disc for Simultaneous Determination of Nutrients in Water. *Analytical Chemistry* **2013,** *85* (5), 2954-2960.
42. LaMotte http://www.lamotte.com/component/option,com_pages/lang,en/mid,/page,261. (accessed 15/04/2012).
43. LaMotte http://www.youtube.com/watch?v=eUc3_uybYqE&feature=relmfu. (accessed 15/04/2012).
44. Madou, M.; Zoval, J.; Jia, G.; Kido, H.; Kim, J.; Kim, N., Lab on CD. *Annual Review on Biomedical Engineeing* **2006,** *8*, 601-628.
45. Ducrée. J.; Haeberle, S.; Lutz, S.; Pausch, S.; von Stetten, F.; Zengerle, R., The centrifugal microfluidic Bio-Disk platform. *Journal of Micromechanics and Microengineering* **2007,** *17* (7), S103.
46. Lutz, S. Centrifugal microfluidic systems for protein and nucleic acid analysis. Albert-Ludwigs-Universität Freiburg, Freiburg, **2011**.
47. Paschotte, R., Encyclopedia of Laser Physics and Technology. Willey-VCH: Weinheim, **2008**.
48. Nash III, T. H., Lichen Biology. Cambridge University Press: Cambridge, **1996**.
49. Agayn, V.; Walt David, R., Fiber-optic sensors based on degradable polymers. In *Diagnostic Biosensor Polymers*, American Chemical Society **1994**, *556*, 21-33.
50. Shepherd, R. L.; Yerazunis, W. S.; Lau, K. T.; Diamond, D., Low-cost surface-mount LED gas sensor. *IEEE Sensors Journal,* **2006,** *6* (4), 861-866.
51. Gunnlaugsson, T.; Glynn, M.; Tocci, G. M.; Kruger, P. E.; Pfeffer, F. M., Anion recognition and sensing in organic and aqueous media using luminescent and colorimetric sensors. *Coordination Chemistry Reviews* **2006,** *250* (23-24), 3094-3117.

52. Higuchi, A.; Yang, S.-T.; Siao, Y.-D.; Hsieh, P.-V.; Fukushima, H.; Chang, Y.; Chen, W.-Y., Preparation of fractioned DNA aptamer - complex through ultrafiltration and the colorimetric sensing of thrombin. *Journal of Membrane Science* **2009,** *328* (1-2), 97-103.
53. Dasgupta, P. K.; Eom, I.-Y.; Morris, K. J.; Li, J., Light emitting diode-based detectors: Absorbance, fluorescence and spectroelectrochemical measurements in a planar flow-through cell. *Analytica Chimica Acta* **2003,** *500* (1-2), 337-364.
54. Kovacs, A.; Barna, P. B.; Labar, J. L., The nucleation and growth of intermetallic Al-Pt phases in co-deposited thin films. *Thin Solid Films* **2003,** *433* (1-2), 78-81.
55. Carter, J. C.; Alvis, R. M.; Brown, S. B.; Langry, K. C.; Wilson, T. S. ; McBride, M. T.; Myrick, M. L. ; Cox, W. R.; Grove, M. E.; Colston, B. W., Fabricating optical fiber imaging sensors using inkjet printing technology: A pH sensor proof-of-concept, *Biosensors and Bioelectronics* **2006***, 21* (7), 1359-1364.
56. Weigl, B. H.; Wolfbeis, O. S., Sensitivity studies on optical carbon dioxide sensors based on ion pairing, *Sensors and Actuators, B: Chemical* **1995**, *28* (2), 151-156.
57. Crowley, K.; Pacquit, A.; Hayes, J.; Lau, K. T.; Diamond, D., A gas-phase colorimetric sensor for the detection of amine spoilage products in packaged fish, *IEEE Sensors Journal* **2005**, *2*, 754-757.
58. Mims III, F.M., Sun photometer with light emitting diode as spectrally selective detectors, *Applied Optics* **1992**, *31* (32), 6965-6967.
59. Mims III, F.M.; How to monitor ultraviolet radiation from the sun, *Scientific American* **1993**, *263*, 106-109.
60. Lau, K. T.; Baldwin, S.; Shepherd, R. L.; Dietz, P. H.; Yerzunis, W. S.; Diamond, D., Novel fused-LEDs devices as optical sensors for colorimetric analysis. *Talanta* **2004,** *63* (1), 167-173.
61. O'Toole, M.; Diamond, D., Absorbance based light emitting diode optical sensors and sensing devices. *Sensors* **2008,** *8*, 2453-2479.
62. Lau, K. T.; Shepherd, R.; Diamond, D., Solid state pH sensor based on light emitting diodes (LED) as detector platform. *Sensors* **2006,** *6* (8), 848-859.
63. Lau, K.-T.; Baldwin, S.; O'Toole, M.; Shepherd, R.; Yerazunis, W.; Izuo, S.; Ueyama, S.; Diamond, D., A low-cost optical sensing device based on paired emitter-detector light emitting diodes. *Analytica Chimica Acta* **2005,** *557*, 111-116.
64. Pokrzywnicka, M.; Koncki, R.; Tymecki, L., A Very simple photometer based on paired-emitter-detector diodes. *Analytical Chemistry* **2009,** *54* (3), 427-435.

65. O'Toole, M.; Lau, K. T.; Shepherd, R.; Slater, C.; Diamond, D., Determination of phosphate using a highly sensitive paired emitter-detector diode photometric detector. *Analytica Chimica Acta* **2007,** *597*, 290-294.
66. O' Toole, M; Shepherd, R.; Lau, K. T.; Diamond, D., Detection of Nitrite by flow injection analysis using a novel Paired Emitter-Detector Diode (PEDD) as a photometric detector. *Proceedings SPIE* **2007,** *6755, 67550P*
67. Zhao, C.; Burrell, G.; Torriero, A. A. J.; Separovic, F.; Dunlop, N. F.; MacFarlane, D. R.; Bond, A. M., Electrochemistry of room temperature protic ionic liquids. *The Journal of Physical Chemistry B* **2008,** *112* (23), 6923-6936.
68. Fraser, K. J.; MacFarlane, D. R., Phosphonium-based ionic liquids: An overview. *Australian Journal of Chemistry* **2009,** *62* (4), 309-321.
69. Seddon, K., Ionic liquids: Designer solvents for green synthesis. *Chemical Engineering* **2002,** *730*, 33-35.
70. Pernak, J.; Stefaniak, F.; Węglewski, J., Phosphonium acesulfamate based ionic liquids. *European Journal of Organic Chemistry* **2005,** *2005* (4), 650-652.
71. Sakaebe, H.; Matsumoto, H., *N*-Methyl-*N*-propylpiperidinium bis(trifluoromethanesulfonyl)imide (PP13-TFSI) - novel electrolyte base for Li battery. *Electrochemistry Communications* **2003,** *5* (7), 594-598.
72. Ding, J.; Zhou, D.; Spinks, G.; Wallace, G.; Forsyth, S.; Forsyth, M.; MacFarlane, D., Use of ionic liquids as electrolytes in electromechanical actuator aystems based on inherently conducting polymers. *Chemistry of Materials* **2003,** *15* (12), 2392-2398.
73. Le Bideau, J.; Viau, L.; Vioux, A., Ionogels, ionic liquid based hybrid materials. *Chemical Society Reviews* **2011,** *40* (2), 907-925.
74. Mohmeyer, N.; Kuang, D.; Wang, P.; Schmidt, H.-W.; Zakeeruddin, S. M.; Gratzel, M., An efficient organogelator for ionic liquids to prepare stable quasi-solid-state dye-sensitized solar cells. *Journal of Materials Chemistry* **2006,** *16* (29), 2978-2983.
75. Viau, L.; Tourne-Peteilh, C.; Devoisselle, J.-M.; Vioux, A., Ionogels as drug delivery system: one-step sol-gel synthesis using imidazolium ibuprofenate ionic liquid. *Chemical Communications* **2010,** *46* (2), 228-230.
76. Gayet, F.; Viau, L.; Leroux, F.; Mabille, F.; Monge, S.; Robin, J.-J.; Vioux, A., Unique combination of mechanical strength, thermal stability, and high ion conduction in PMMA-silica nanocomposites containing high loadings of ionic liquid. *Chemistry of Materials* **2009,** *21* (23), 5575-5577.

77. Ueki, T.; Watanabe, M., Macromolecules in ionic liquids: Progress, challenges, and opportunities. *Macromolecules* **2008,** *41* (11), 3739-3749.
78. Nadherna, M.; Opekar, F.; Reiter, J., Ionic liquid, polymer electrolyte for amperometric solid-state NO_2 sensor. *Electrochimica Acta* **2011,** *56* (16), 5650-5655.
79. Xie, Z.-L.; Jelicic, A.; Wang, F.-P.; Rabu, P.; Friedrich, A.; Beuermann, S.; Taubert, A., Transparent, flexible, and paramagnetic ionogels based on PMMA and the iron-based ionic liquid 1-butyl-3-methylimidazolium tetrachloroferrate(III) [Bmim][$FeCl_4$]. *Journal of Materials Chemistry* **2010,** *20* (42), 9543-9549.
80. Benito-Lopez, F.; Byrne, R.; Răduţă, A. M.; Vrana, N. E.; McGuinness, G.; Diamond, D., Ionogel-based light-actuated valves for controlling liquid flow in micro-fluidic manifolds. *Lab on a Chip* **2010,** *10* (2), 195-201.
81. Zhu, J.; Zhai, J.; Li, X.; Qin, Y., Applications of hydrophobic room temperature ionic liquids in ion-selective optodes. *Sensors and Actuators B: Chemical* **2011,** *159* (1), 256-260.
82. Kavanagh, A.; Byrne, R.; Diamond, D.; Radu, A., A two-component polymeric optode membrane based on a multifunctional ionic liquid. *Analyst* **2011,** *136* (2), 348-353.

Chapter 2

Integrating stimulus responsive materials and microfluidics – The key to next generation chemical sensors

M. Czugala,[1] B. Ziolkowski,[1] D. Diamond

Journal of Intelligent Material Systems and Structures, 2012
doi: 10.1177/1045389X12459591

CLARITY: Centre for Sensor Web Technologies, National Centre for Sensor Research, Dublin City University, Dublin 9, Ireland

[1]Both authors contributed equally to this work.

Abstract

New generations of chemical sensors require both innovative (evolutionary) engineering concepts and (revolutionary) breakthroughs in fundamental materials chemistry, such as the emergence of new types of stimuli responsive materials. Intensive research in those fields in recent years have brought interesting new concepts and designs for microfluidic flow control and sample handling that integrate high quality engineering with new materials. This chapter reviews recent developments in this fascinating area of science, with particular emphasis on photoswitchable soft actuators and their incorporation into microfluidic devices that are increasingly biomimetic in nature.

2.1 Introduction

In a utopian future, water quality will be monitored through large numbers of densely deployed sensors that are capable of detecting key quality parameters with exquisite selectivity and sensitivity, and of functioning reliably in an autonomous manner for long periods of time (years). The information generated by these sensor networks will be analysed and filtered, and key events flagged in real time to key stakeholders (agency enforcement officers, water treatment specialists, and the general public). However, in reality, issues like biofouling and surface degradation mean that sensor characteristics change rapidly in real samples, and consequently, chemical sensors must be regularly recalibrated to ensure the information they send is reliable. This results in complex and very costly devices that must integrate fluidics, standards, and waste storage, as well as sampling and analytical procedures. Consequently, monitoring programmes are dominated by manual grab sampling at a relatively small number of locations, with a frequency often restricted to 3 or 4 times per year. Scale up in terms of sampling frequency and number of locations is dictated by cost, and therefore the key to significant movement towards the utopian vision is to drive down the cost base of environmental monitoring.

Analysis of the component cost base of autonomous analysers built by our group (Gen1[1] and Gen2), together with a speculated cost analysis of a future platform based on fully integrated polymer actuator valves and pumps are presented in Fig. 2.1. These show clearly for Gen1 and Gen 2, that the single greatest contribution to the cost base is the fluidic handling category. In the first generation (Gen1) design, this amounted to over 80 % of the total

1 These are 1st and 2nd Generation versions of fluidic based colorimetric chemical analysers targeting analytes such as phosphate, nitrate, pH, COD etc.

cost of *ca.* €2,000, and while this dropped in the second generation design through good engineering and careful choice of components, it was still almost 2/3 of the total component cost of *ca.* €180. These are figures based on platforms that have been produced within Adaptive Sensor Group at Dublin City University. A 'concept' integrated analyser with integrated polymer actuator pumps has been made by our group, and the estimated total cost is in the region of €20 - 50 per unit, of which *ca.* 50 % of costs related to fluid handling components. The figures here are more speculative, but there is no doubt that if the fluid handling components could be fully integrated into the fluidic system, for example using highly automated in-situ photopolymerisation of the key liquid handling components, the unit cost would be considerably lower.

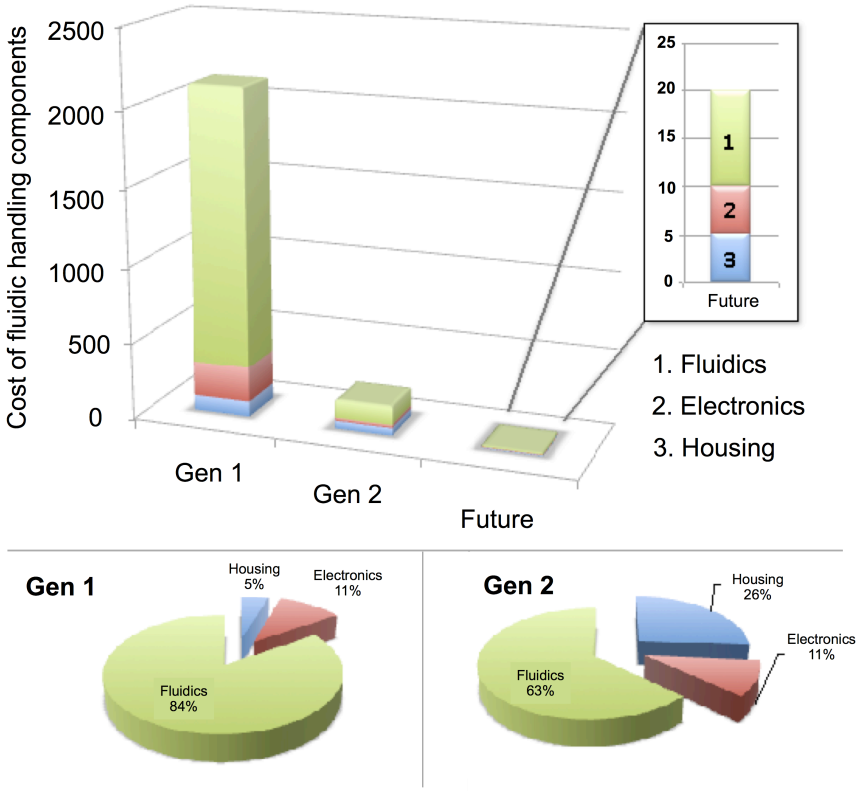

Figure 2.1. Analysis of component costs (€) for first-generation (Gen1), second-generation (Gen2) and future 'concept' analyser. Total component cost by category (top) drops from *ca.* €2000, to below €200 and to *ca.* €20 per

unit, respectively.

Furthermore, if the control stimulus for valve actuation/fluidic control does not require physical contact (*e.g.* light, heat, magnetism, *etc.*) then manufacturing would be further simplified, as the fluid handling layer could be produced as an entirely stand-alone unit. Therefore in this chapter, strategies for making and integrating polymer actuators in microfluidic systems will be reviewed, and speculate on how the field may progress over the coming years.

2.2 Polymer actuator valves in microfluidic systems

Valves are one of the most important components within microfluidic systems, since they provide directional control of flow and facilitate essential actions, such as sample/standard selection and addition of reagents. Some key requirements of an ideal microvalve are;

- Zero flow resistance in the open position.
- Zero leakage in the closed position.
- Infinite tolerance to high pressure in the closed position.
- Instant response to switching between the open and closed positions.
- Simple routes to fabrication and integration *in-situ* within the microfluidic system.
- Prepared from readily available and processable materials.

Many different types of microvalves have been demonstrated, and while none of these can be described as totally satisfactory, they do present significant advances in the realisation of some of these ideal characteristics.[1] In most conventional systems a diaphragm is coupled to an actuator, powered

from an external source, which deflects the diaphragm via a magnetic field, voltage or heating.

2.2.1 Magnetically actuated valves

Flow regulation in microfluidic devices by magnetic forces has many advantages, such as capability of generating large angular displacement as well as possibility of using very strong magnetic force to drive actuation. Satarkar *et al.*[2] developed the nanocomposite hydrogel valve, in which magnetic nanoparticles were dispersed in temperature-responsive *N*-isopropylacrylamide (NIPAAm) polymer matrix (Fig. 2.2). The swelling and collapse of the hydrogel nanocomposite can be remotely controlled by application of an alternating magnetic field (AMF) at a frequency 293 kHz. A disadvantage of this hydrogel microvalve is that its response is reported as sluggish, but this can be improved by moving to smaller valve dimensions, as gel processes are typically diffusion driven, and smaller feature sizes reduce the diffusion pathlength. Similar oscillating magnetic field actuated valves were prepared by Ghosh *et al.*[3]

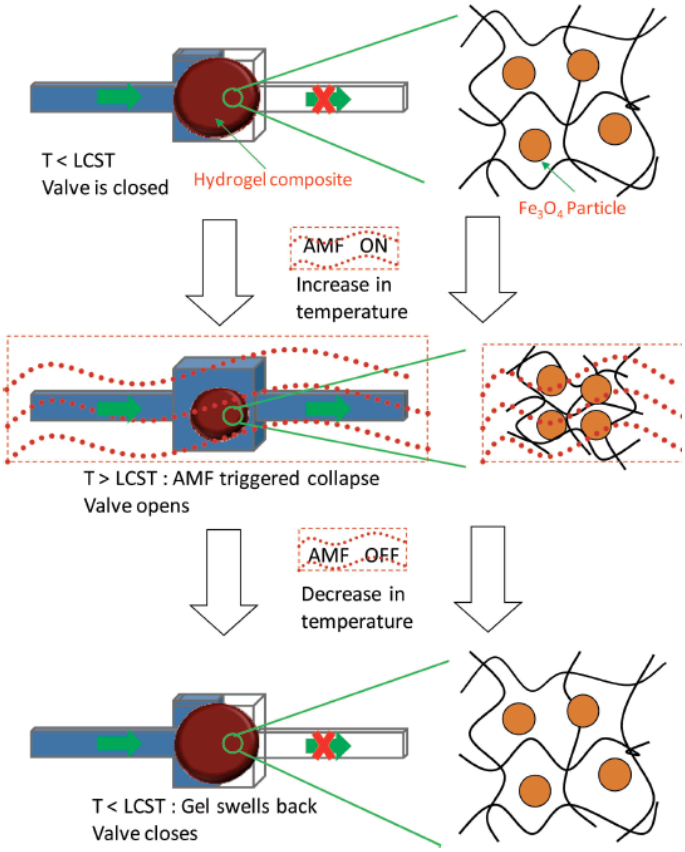

Figure 2.2. Scheme presenting the hydrogel nanocomposite valves performance with an AMF. The application of the AMF results in the collapse of the hydrogel, leading to the opening of the valve. Source: Reproduced from Satarkar *et al.* (2009) by permission of The Royal Society of Chemistry.

2.2.2 Pneumatic valves

Pneumatic microvalves represent another type of fluid handling, however, they require external laboratory infrastructure – gas cylinders, computers, ground electricity, for their operation which makes it difficult to incorporate them into autonomous monitoring instruments. The development of PMMA/PDMS pneumatic valves and pumps for disposable microfluidics was reported by Zhang *et al.*[4] Pneumatic microstructures were fabricated by sandwiching a PDMS membrane between PMMA fluidic channel and manifold wafers, as in Fig. 2.3. Valve control was obtained by applying pressure on the pneumatic layer sited in a displacement chamber using a

computer regulated solenoid. Apart from providing up to 15.4 mL s^{-1} at 60 kPa fluid pressure, the valve seals reliably against forward fluid pressures as high as 60 kPa. A PMMA diaphragm pump was presented based by connecting three valves in series. Simultaneously, the fluid flow rate could be accurately controlled from nL to mL per second, simply by changing the valve actuation time, the displacement chamber volume, and the applied pressure.

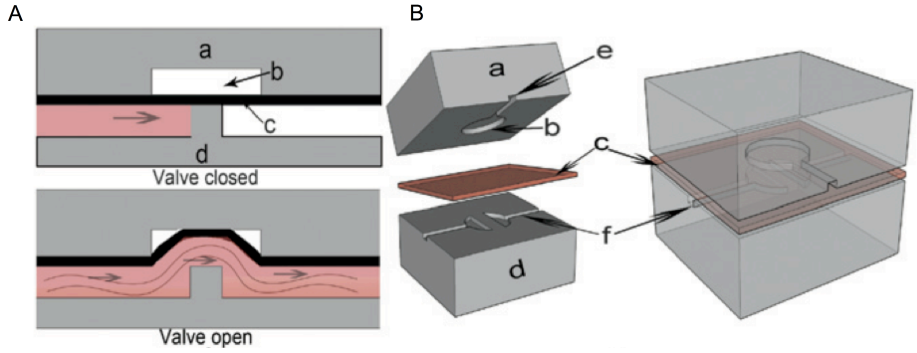

Figure 2.3. A) Cross-sectional views of a three-layer monolithic PMMA/PDMS membrane valve and B) exploded and assembled illustrations of a single PMMA/PDMS membrane valve. (a) PMMA pneumatic wafer, (b) displacement chamber, (c) PDMS membrane, (d) PMMA fluidic wafer, (e) pneumatic channel and (f) fluidic channel. Source: Reproduced from Zhang *et al.* (2009) by permission of The Royal Society of Chemistry.

Go and Shoji[5] presented a three-dimensional in-plane hemisphere PDMS microvalve without dead volume and leakage flow. A closing time of 0.1 s and an opening time of 0.5 s were obtained by applying a pneumatic pressure of 10 kPa to the PDMS membrane. Even though a faster response for closing was possible, it took a longer time to release the membrane for opening.

2.2.3 Electrothermal valves

In contrast to many other technologies, electrothermally actuated phase change microvalves developed by Kaigala *et al.*[6] can be readily scalable to smaller dimensions, allowing the fabrication of a portable and inexpensive genetic analysis platform. This easily integrated, reusable microvalve technology that can be easily incorporated within standard lab-on-a-chip technologies is based on the polyethylene glycol polymer (PEG) that exhibits a large volumetric change between its solid and liquid phases**.** The volumetric expansion, thermally controlled by applying thin film resistive elements that are patterned with standard microfabrication techniques, switches a flexible PDMS membrane between opened or closed state between two discontinuous channels (Fig. 2.4). The switching time for opening/closing, was on the order of minutes, and the microvalve was reported to be leakage-free to a pressure of 30 psi at a temperature of 50 °C in the PEG reservoir.

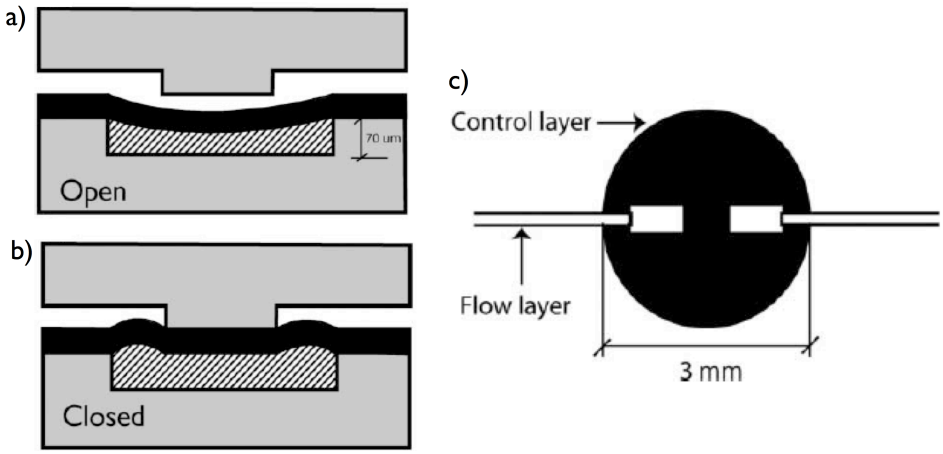

Figure 2.4. (a and b) Cross-sectional and (c) top views of the microvalve structure. The features in the control layer are 70 μm deep while those in the fluidic layer are 90 μm deep. (a) Open state of valve and (b) closed state of valve. Source: Reproduced from Kaigala *et al.* (2008) by permission of The Royal Society of Chemistry.

Selvaganapathy *et al.*[7] realised normally open electrothermally actuated inline microvalve for liquid regulation. The actuation mechanism was based on a thermally activated phase change in the Paraffin layer resulting in a high volumetric expansion. The microvalve was surface micromachined on top of preformed flexible microfluidic channels using a low temperature fabrication process. As the Paraffin was heated beyond its melting point using the microheaters underneath them, it undergoes a volume expansion, which deflects the flexible diaphragm of the piston, closing the microchannel beneath it. Actuation was achieved at power as low as 35 mW with the response times of 15 ms. Similar valves opened by melting a polymer with heat provided from a laser were demonstrated by Garcia-Cordero *et al.*[8] These valves were fully integrated into a microfluidic platform and are characterised by very low cost. The disadvantage is that they can be used only once.

2.2.4 Soft polymer valves

Most conventional microvalves coupled to piezoelectric, thermopneumatic, electrostatic or electromagnetic actuators require high power consumption, which is highly unfavourable for autonomously deployed instruments. Soft polymer actuators offer an alternative approach that is more biomimetic in nature and in principle can require relatively low energy for actuation. For example, hydrogels swell and contract significantly due to water movement into/out of the gel. These volume changes are associated with phase transition behaviour triggered by small alterations of certain external stimuli. These materials can respond to a variety of external stimuli, such as pH, temperature, or light. Among these hydrogels, pH responsive materials have been the focus of particular attention. By converting chemical energy into mechanical work, pH sensitive hydrogels can exhibit both sensing

and actuating functions simultaneously. For example, for the pH-sensitive hydrogel poly(2-hydroxyethyl methylacrylate-co-acrylic acid), poly(HEMA-co-AA), the movement of water is initiated by the ionisation of the polymer backbone.[9] Beebe *et al.*[10] reported a channel with two strips of poly(HEMA-co-AA) deposited along the walls using the laminar flow characteristics to enable polymer precursors to be restricted only to the channel wall region. Under conditions of high pH, swelling of the hydrogel structures occurred and blocked the channel. As the pH in the sensing channel was changed from 11 to 2, the hydrogel contracted to open the flow in the adjacent channel. Although swelling and shrinkage of the hydrogel in response to pH change are reversible and repeatable, reopening of the channel from the closed state (at which point the hydrogel is fully expanded) may limit the use of this design in some applications. In general it is found that the dynamics of reswelling in hydrogels are much slower than contraction, due to the inherent asymmetry of diffusion in these materials.[11, 12]

Since diffusion is the rate-limiting factor governing the swelling process of hydrogels, the response time can be improved by reducing the size of hydrogel microstructures. In order to fabricate stable hydrogel actuators with fast response times, hydrogel films were photopolymerised using a photomask around prefabricated posts.[13] At pH 11, the films expanded, closing the channel, whereas flushing the channel with solution at pH 2 resulted in the valves opening, with response time of 12 s. Based on the valve mechanism described above, a pH-dependent flow sorter was also demonstrated (Fig. 2.5).[10] The entrance to each branch of 'T' channel was gated with hydrogel microstructure that expanded in one branch of the channels at high pH and contracts in low pH, whereas a hydrogel of different composition in another branch exhibited an inverse behaviour. In this way, the microfluidic device

directed the flow to the appropriate branch, depending on the pH of the solution.

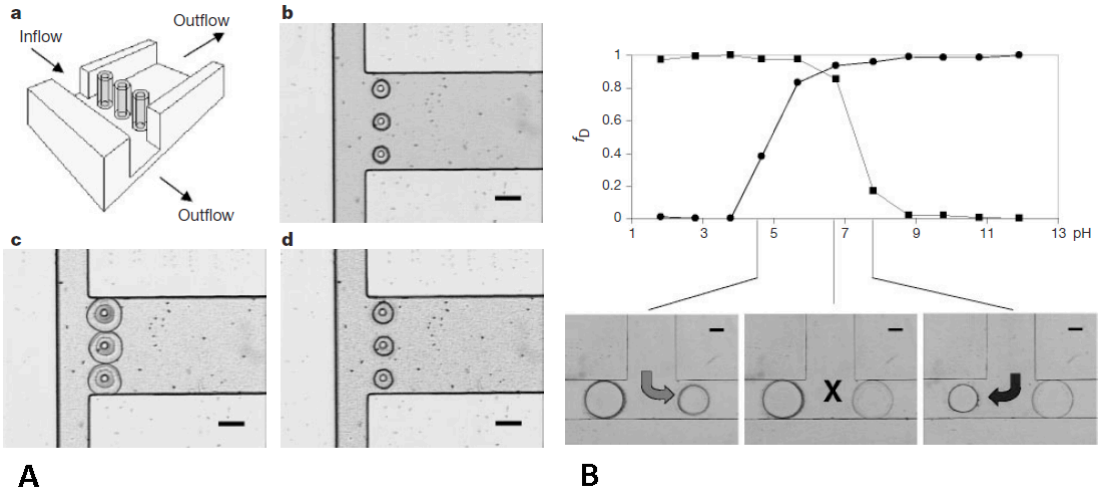

Figure 2.5. (a) Prefabricated posts in a microchannel serve as supports for hydrogel films, improving stability during volume changes: (i) a diagram of the hydrogel films around the posts, (ii) the actual device after polymerisation of the hydrogel, (iii) the hydrogel films block the side channel branch in their expanded state and (iv) the contracted hydrogels allow fluid to flow down the side branch. (b) The volume response of two different hydrogels with respect to the pH of the surrounding fluid. Top, the fractional change in diameter (f_D) of the hydrogels with respect to pH. Bottom, images showing a device that directs a fluid stream on the basis of its pH. The hydrogel gating the right branch (circles) expands in base and contracts in acid. The hydrogel gating the left branch (squares) behaves in the opposite manner (expands in acid and contracts in base). The fluid enters from the centre channel at a rate of 0.05 mL min^{-1}. At a pH of 7.8, the flow is directed down the left branch. At a pH of 4.7, the flow is directed down the right branch. Both hydrogels expand to shut off the flow when the pH is changed to 6.7. Scale bars, 300 μm. Source: Reprinted with permission from Beebe *et al.* (2000). Copyright: 2000 Nature.

Yu *et al.*[14,15] presented a biomimetic bistrip valve capable of directional flow control in response to changes in the local fluid environment. The valve structure is similar to the venous valve, consisting of a pair of pH sensitive poly(HEMA-co-AA) hydrogel strips overlapped by the pair of pH-insensitive strips (Fig. 2.6). When exposed to high pH, dissimilar expansion to adjacent

hydrogel strips caused the valve to bend during swelling, thus forming a normally closed check valve allowing only forward flow of pressure above the threshold value. If low pH solution enters the channel, the pH sensitive strips shrink, allowing both forward and backward flow. In comparison to traditional microfluidic valves where actuation occurs very rapidly, here the activation and deactivation times are quite slow, at 6 and 3 minutes respectively. However, this slow operating valve can be successfully applied in drug delivery and bioassay devices, where timescales for events can be of the order of hours.

However, in order to handle biological cells and proteins, manipulation of fluids with neutral pH is desired. In order to minimise the complexity of fully polymeric integrated fluidic circuits (IFC), all electronically controllable components should ideally be made with one type of hydrogel. This can be achieved with poly(*N*-isopropylacrylamide) (PNIPAAm), one of the best-known temperature-sensitive multifunctional hydrogels. At a temperature above the lower critical solution temperature (LCST) of 32 ˚C PNIPAAm chains undergo rapid and reversible entropy driven phase transition from extended hydrated coils to collapsed hydrophobic globules that precipitate in water.[16, 17] The temperature-sensitive PNIPAAm hydrogel, which is typically controlled by electronic heating elements, has been used widely for fabrication of not only the standard elements of liquid handling, such as microvalves[18 19 20] and micropumps,[21] but also specific active components such as chemostat valves[18] and chemical sensors.[22]

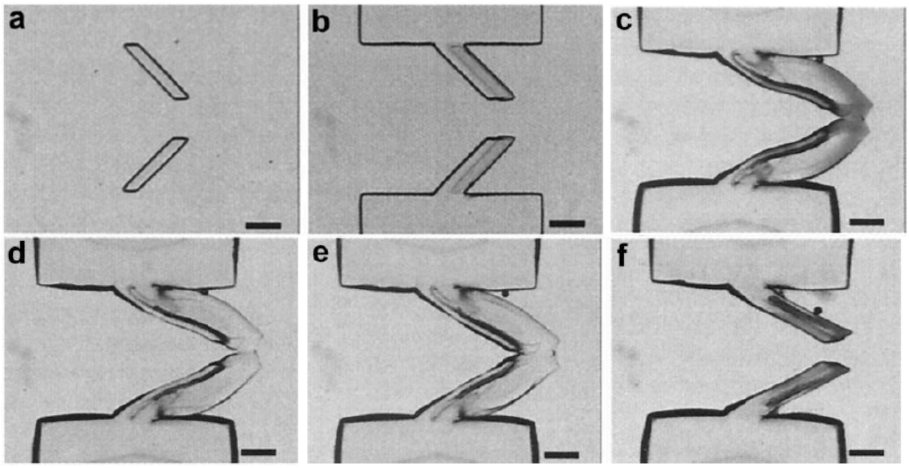

Figure 2.6. Fabrication and operation of a biomimetic valve based on a bistrip hydrogel. (a) Bistrip hydrogel is patterned by simultaneous photopolymerisation. (b) The anchor of the valve is formed using a non-responsive hydrogel. (c) When exposed to basic solution, the bistrip hydrogels expand and curve to form a normally closed valve. (d) The bistrip valve is pushed open to allow the flow in one direction (from left to right). (e) The flow is restricted in the opposite direction. (f) When exposed to acidic solutions, the valve is deactivated, returning to the permanently open state. Scale bars represent 500 μm. Source: Reproduced from Beebe *et al.* (2000). Copyright by the National Academy of Sciences.

Although robust valves with fast response to external stimuli and successful performance of repeated "open-close" cycles have been reported,[19] their transition temperature (slightly above 30 ^{o}C causes shrinkage and valve opening) is too low for some applications, such as on-chip PCR, for which the valves must remain closed at much higher temperatures. Frechet *et al.*[23] realised thermally actuated valves by crosslinking NIPAAm with *N*-ethylacrylamide (NEAAm), for which the LCST can be adjusted within a wide temperature range to meet the specific requirements of some applications. In order to avoid valve displacement during operation, the microchannels were vinylised to enable covalent attachment of the photopolymerised gels. As a result, a 5 mm long poly(NIPAAm-co-NEAAm) (1:1 molar ratio) valve holds pressure up to 18 MPa without noticeable

dislocation, leakage or structural damage in closed mode. Although the authors demonstrated the versatility of the valve and its ability to perform well under conditions typical of numerous microfluidic processes, displaying actuation times in the range of 1 - 4 s, there is still the need for thermoelectrical elements to implement temperature control. What is more, application of heat induced phase transition is not suitable for samples containing heat sensitive materials, such as protein and cells.

2.3 Micropumps in fluidic systems

In contrary to widely researched and tested microvalves, there are not many publications related to hydrogel-based electronically controllable micropumps. Richter *et al.*[21] presented diffusion micropump (Fig. 2.7a), which peristaltic operation provides a continuous and relatively homogeneous pumping. The flow rate obtained for this device is 2.8 ± 0.4 μl min^{-1}, with the maximum flow rate of pumping stroke determined by the shrinking kinetics of the hydrogel. This process is strongly dependent on the heating power of the heating meanders in addition to the properties of the elastic PDMS membrane. The higher the pressure of the membrane (directly proportional to its increasing thickness), the faster actuator shrinks. On the other hand, the increase of membrane thickness significantly influences the reload time of the pump and decreases the maximum swelling volume of hydrogel.

However, this kind of micropump is unsuitable for some applications. For example, some solvents can destroy the hydrogel structure, particles cannot pass the actuation chamber, since the monolithic PNIPAAm actuator is placed directly in the pump chamber, or the pumping pressure can be not sufficient enough. Another pump described by this group based on displacement (Fig. 2.7b), provides higher performance (flow rate of 4.5 μL

min^{-1} and a back pressure of 1.28 kPa) based on a hydrogel actuator separated from the process medium by a movable membrane. Inexpensive design, simple control and soft lithographic fabrication make these hydrogel pumps a significant advance towards the realisation of disposable microfluidic components.

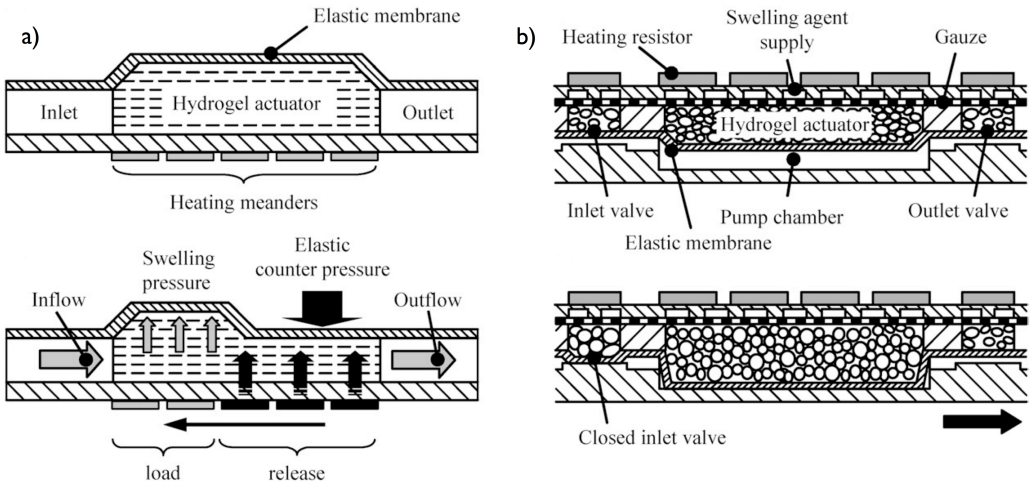

Figure 2.7. (a) Schematic set-up and operating principle of diffusion micropump and (b) displacement micropump. Source: Reproduced from Richter *et al.* (2009) by permission of The Royal Society of Chemistry.

2.4 Photoswitchable polymer actuators

In recent years, the range of applications for lab-on-a-chip systems has significantly increased due to several promising aspects, such as smaller sample and reagent volume consumption and less wastage produced, which is cost-effective and environmental friendly. Since it is possible to place many microfluidic architectures in a relatively small area, it enables complex sample processing operations with rapid analysis times to be performed, due to the large increase in the surface area to volume ratio associated with reduction in dimensions. Because of the numerous advantages offered by the microscaled channels, the concept of microfluidic "lab-on-a-chip" has triggered significant

effort in development of materials and their employment in miniaturised devices. In particular, switchable materials offer intriguing possibilities and the potential to integrate sophisticated functions in a simple overall design. Because of their relative ease of fabrication and simple control, stimuli responsive materials integrated with microfluidic manifolds could significantly advance the development of fully integrated microfluidic systems.

Smart engineering of analytical fluidic devices can generate improvements up to a limit, beyond which new, robust and smart materials are needed for further progress.[24] One of the most attractive strategies to implement fluid manipulation on integrated microfluidic platforms is light irradiation, which allows not only for non-contact operation but also independent and remote manipulation of multiple fluids. Photoresponsive polymer materials have been studied by many research groups, and many polymers and polymer gels functionalised with azobenzene,[25, 26, 27] leukochromophore,[28, 29] and spirobenzopyran[30, 31] have been examined. Valves can be controlled with IR,[32] blue[33, 34] or white light[24, 35].

2.4.1 IR-responsive materials

The performance of microvalves based on the volumetric change due to infrared (IR) light illumination was reported by Lo *et al.*[32] They presented an IR-light responsive hydrogel based on thermo-responsive pNIPAAm hydrogels incorporating glycidyl methacrylate functionalised graphene-oxide (GO–GMA). The valve operates in two states – closed, adopted when the IR source is turned off, and opened, adopted when the IR source is turned on, due to absorbance of the IR light by the GO–GMA sheets, which triggers the hydrogel to contract, allowing for fluidic flow. The performance of the hydrogel microvalve is shown in Fig. 2.8. When the infrared light is switched

off, the heat is dissipated to the surrounding environment, and the hydrogel absorbs water, expanding its volume and blocking the microchannel again.

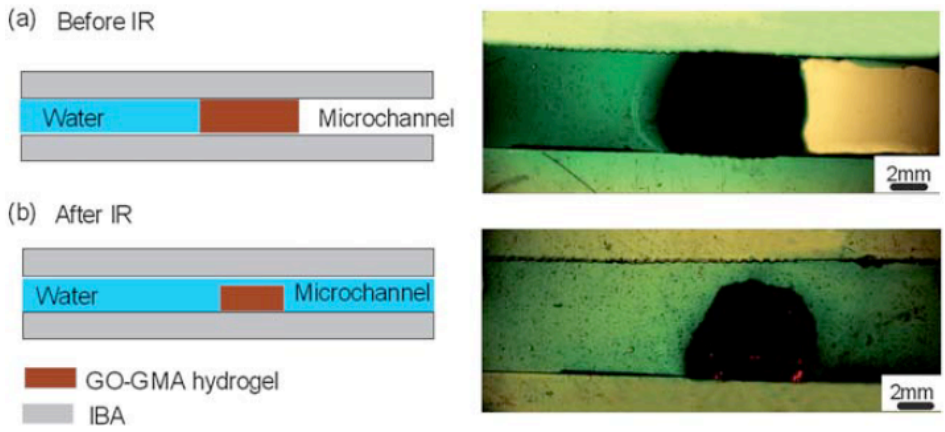

Figure 2.8. A microvalve made of GO–GMA IR-responsive hydrogel. Top views of the microvalve are on the left. Respective images taken under a microscope are on the right. (a) GO–GMA hydrogel microvalve before actuated by IR irradiation (*OFF* state) and (b) after exposure to IR light (*ON* state). Source: Reproduced from Lo *et al.* (2011) by permission of The Royal Society of Chemistry.

2.4.2 Spiropyran-based photocontrolled soft actuators

One of the first reports of a spiropyran monomer copolymerised with vinyl monomers to obtain a photoresponsive polymer was published by Smets *et al.*[36] in 1978. The author synthesised a crosslinker consisting of two connected spiropyran molecules each having one vinyl group attached. They showed that the spiropyran-crosslinked poly-bisphenol-A-pimelate or polyethyleneglycol tere/isophthalate rubbers contracted as the sample is irradiated with light, and the spiropyran opened into a merocyanine form. Furthermore, they showed that the opening of the spiropyran and consequential colour change was not directly linked with the polymer contraction. Fig. 2.9a shows that when the samples are exposed to light in the

range 290 nm $< \lambda <$ 400 nm the polymer does not contract significantly, but colouration appears. Illuminating the sample with the light above 472 nm wavelength produces a rapid contraction reaching a maximum when the light wavelength matches the merocyanine absorption wavelength (Fig. 2.9b).

Therefore, the authors claimed that:[36]

- The irradiation wavelength dependence of the contraction corresponds closely with the absorption spectrum of the merocyanine.
- The rates of ring opening/closure in the spiropyran ↔ merocyanine equilibrium do not control the rates of dilatation/contraction. The contribution of ring opening/closure is of secondary importance, except for the initial formation of the merocyanine.
- The isomerisation between different open merocyanine forms forces conformation changes in the neighbouring polymer units and this results in shrinkage.

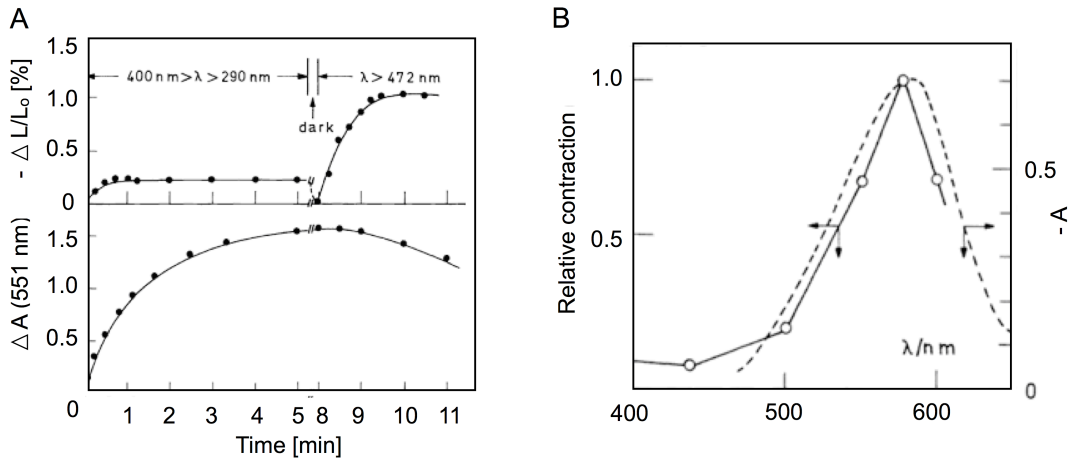

Figure 2.9. A) Colouration/contraction of spiropyran cross-linked rubbers under UV and visible light illumination. B) Contraction (—) and absorption (--) spectra of photochromic rubbers. Source: Reprinted from Smets *et al.* (1978). Copyright 1978 *Pure and Applied Chemistry.*

Another report from the same group claimed that the viscosity of solutions of poly(methylmethacrylate-co-1,3,3-trimethylindolino-6'-nitro-8'(methacryloxy)methyl]spirobenzopyran) can also be altered with light irradiation $\lambda > 310$ nm.[37] This is ascribed to the polar neighbouring methacrylate groups solvating the polar merocyanine form of the photochrome co-monomer. This effect decreases as the solvent polarity is increased and disappears in dichloromethane.

In more recent work, on spiropyran (3 mol %) copolymers of pNIPAM, by Sumaru *et al.*[38] presented an actuation mechanism based on the lower critical solubility temperature of poly(*N*-isopropylacrylamide)[17] and the fact that it changes depending on the chromophore state. Fig. 2.10 shows the copolymer used in this study, and the effect of switching. When the copolymer is immersed in an acidic (0.26 mM HCl) solution the spiropyran part of the polymer changes to the open merocyanine form, and becomes protonated. When this polymer is irradiated with light at 422 nm, which matches the absorbance of the protonated merocyanine form, the polymer chains collapse and the proton is released. A correlated change in both absorbance at 422 nm and ionic conductivity is observed.

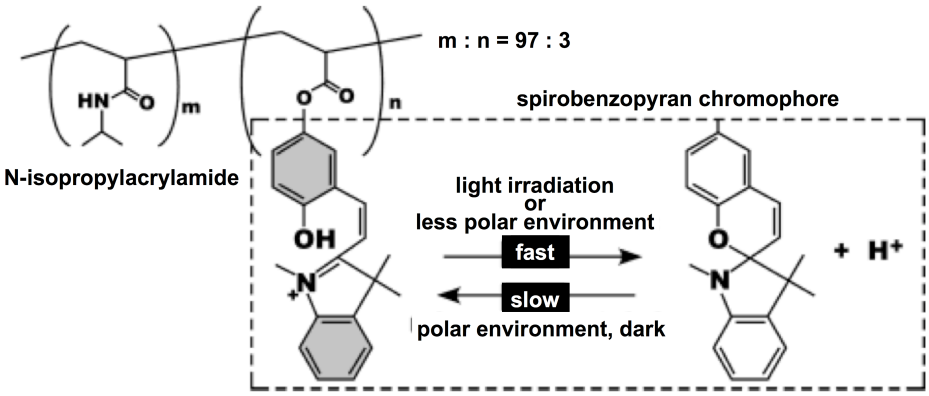

Figure 2.10. Chemical structure of p(SPNIPAAm) and characteristics of its components: pNIPAAm main chain and spirobenzopyran side chain. Source: Reprinted with permission from Sumaru *et al.* (2004). Copyright 2004

American Chemical Society.

In a parallel publication Sumaru *et al.*[39] investigated this system further. Solutions of p(SPNIPAAm) were analysed at acidic, basic and neutral pH with respect to the temperature and light induced precipitation of the polymer. The following observations were reported:

- The protonated merocyanine (MC-H^+) pNIPAM copolymer absorbs at 422 nm. The uncharged merocyanine copolymer absorbs strongly at 530nm and weakly around 370 nm.
- Without light irradiation the acidified pNIPAM solution becomes turbid around 32 °C however the turbidity increase is not significant due to the remaining protonated MC-H^+ chromophores that stabilise the polymer.
- With light irradiation at 422 nm (absorption band of MC-H^+) the acidified polymer solution becomes turbid at 29 °C and increases with increasing temperature. Also the absorption intensity at 422 nm is decreasing as the merocyanine chromophore reverts to the spiropyran form.
- A significant turbidity increase is also observed when the same sample is kept at 31.5 °C in the dark and then irradiated with 422 nm light.
- Little precipitation is observed when the pNIPAM solutions are neutral or basic due to the fact that at these conditions the chromophore is mostly in the spiropyran (SP) form.

These results suggest that the status of the SP ⇔ MC equilibrium in the copolymer chain, which is controlled by light irradiation, changes the hydrophobic-hydrophilic character of the whole polymer, leading to changes in the LCST. The system works best in acidic pH because under these conditions, the equilibrium predominantly favours the formation of MC. Based on this work of Sumaru, it seems that the LCST is lowered as the equilibrium shifts towards the closed-hydrophobic SP form. This implies that

the hydrophilic merocyanine form raises the entire copolymer's LCST. However it should be noted that the opposite effect has been reported by Ivanov *et al.*[40] In this case, a 10 °C downward swift of the LCST was reported when the sample was irradiated with UV light in deionised water, and the merocyanine absorption at 450 nm became apparent. However, Ivanov used a spiropyran molecule functionalised with a methacryloyl group through the indoline nitrogen linker, in contrast with Sumaru, who acrylated the spiropyran through the 6-hydroxybensopyran group.

Important claims in Sumaru's papers[38, 39] are as follows:

- No protonation at the tertiary amine of spirobenzopyrans with electron-withdrawing substituents in the closed-ring form was detectable by NMR even at acidic conditions.[38]
- The open merocyanine form of the chromophore used by Sumaru has a $pK_a \approx 6$ - 7 and is not strong enough base to remove protons from water molecules.[39]

Aditionally, Krüger *et al.*[41] showed that the LCST can be shifted as much as by 20 °C in acrylamide copolymerised with monomers containing azobenzenes.[41] Here, a similar explanation for the phenomena seen by Sumaru[38, 39] was also suggested.

To optimise the actuation of spiropyran functionalised pNIPAM polymers one needs to consider not only changes happening at the chromophore modified units, but also the contraction and swelling processes throughout the entire pNIPAM polymer. It is well known that pNIPAM collapses from an expanded coil to a compact globule form when heated above ~ 32 °C and the opposite happens when cooled down. Wang *et al.*[11] showed that there is a particle diameter-temperature hysteresis when pNIPAM is precipitated and left to reswell (Fig. 2.11a).

The authors claimed that the pNIPAM chains collapse above the LCST and form intrachain hydrogen bonds that make the resulting globule difficult to dissolve once the temperature decreases.[11] Moreover, according to Sun *et al.*[12], during heating the backbone chains collapse first, the side isopropyl groups react next and then water is expelled last. On the other hand, during cooling the globule swells once water becomes again a sufficiently good solvent for the polymer chains and diffuses in between the collapsed pNIPAM chains. After the water has diffused into the polymer network the intrachain hydrogen bonds break and the side chains reswell first and then the backbone follows.[11, 12]

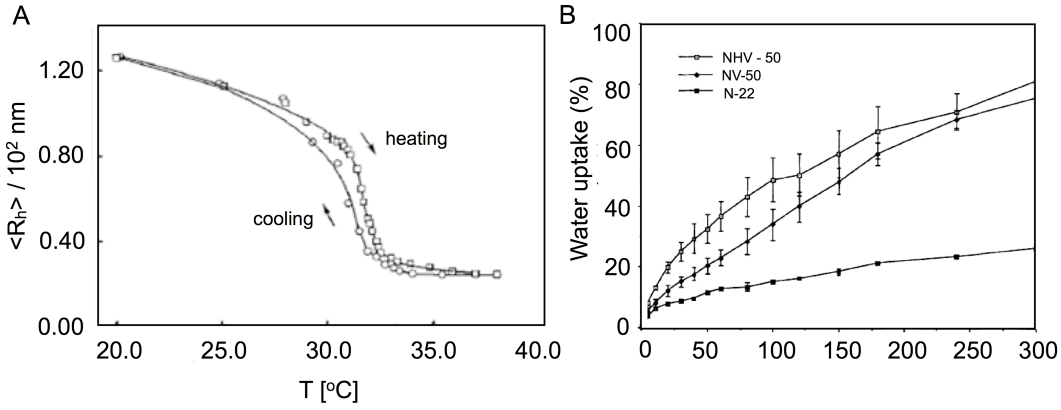

Figure 2.11. A) Temperature dependence of the average hydrodynamic radius ⟨Rh⟩ of the PNIPAM chains in the coil-to-globule (heating) and the globule-to-coil (cooling) transitions, respectively. B) Reswelling kinetics of macroporous and conventional pNIPAAm hydrogels. NHV-50 cellulose modified macroporous hydrogel, NV-50 macroporous hydrogel and N-22 standard hydrogel. Source: Reprinted with permission from Wu *et al.* (1992). Copyright 2003 Wiley.

On a macroscopic scale, one way to increase the speed of reswelling of pNIPAM hydrogels is to modify the morphology of the bulk material and increase the polymer surface area in contact with water. An effective way of using the inherent LCST pNIPAM property to make macroporous hydrogels

was developed by Wu *et al.*[42] In this work the NIPAM was polymerised and crosslinked above its LCST with and without hydroxypropyl cellulose. As a result NIPAM polymerised in its precipitated state and a porous network was formed in which swelling/deswelling ratio and rates were significantly higher than for the conventional hydrogel. The cellulose additive improved the gel performance even further (Fig. 2.11a).

Although all those approaches improved the characteristics of p(SPNIPAAm) system little has been done to optimise the fundamental phenomenon at the very core of the actuation process. Satoh *et al.*[43] prepared spiropyran monomers with different electron donating and electron withdrawing groups and demonstrated that the spiropyran opening in HCl can be drastically improved by certain substituents on the pyran-benzene ring (Fig. 2.12).

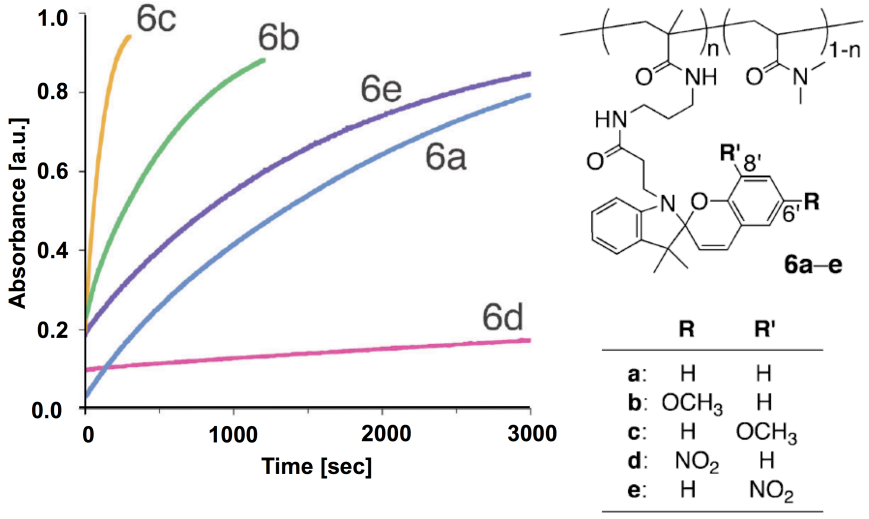

Figure 2.12. Left: Time course of the absorbance of the MC-H$^+$ in polymers 6a – 6e after stopping the light irradiation. The measurements were performed in 2 mM HCl at 25 °C. The values of the absorbance before the light irradiation were normalised to be 1.0 for comparison. Right: Substituents for different chromophore monomers prepared (a–e). Source: Reproduced from Satoh *et al.* (2011) by permission of the PCCP Owner Societies.

With this approach it was demonstrated that p(SPNIPAAm) hydrogels can collapse and reswell within 15 min.[44] However, the authors themselves admitted that the "fastest" hydrogels did not return to the original size. This was ascribed to photo-induced decomposition of the polymer. As for other systems mentioned above, the LCST driven collapse of the gel is rather fast but the reswelling of the gel is comparatively slow and problematic.[33] This is because the actuation of the p(SPNIPAAm) gel is a two-step process. For the shrinking the protonated merocyanine has to be first isomerised to the hydrophobic SP form. This increase in the hydrophobicity of the chain induces its collapse and water ejection.[33, 39] The reverse process is more difficult as after conversion of SP to the charged MC form, protonation occurs followed by diffusion of water into the collapsed polymer globules before the chains can reorder and swell.[11, 12] A manifold with microvalves made from such material was demonstrated by Sagiura *et al.*[33] (Fig. 2.13). The maximum pressure the p(SPNIPAAm) gel microvalves could withstand was determined to be 30 ± 6.6 kPa. At pressures in excess of this, the gels deformed and leakage occurred.

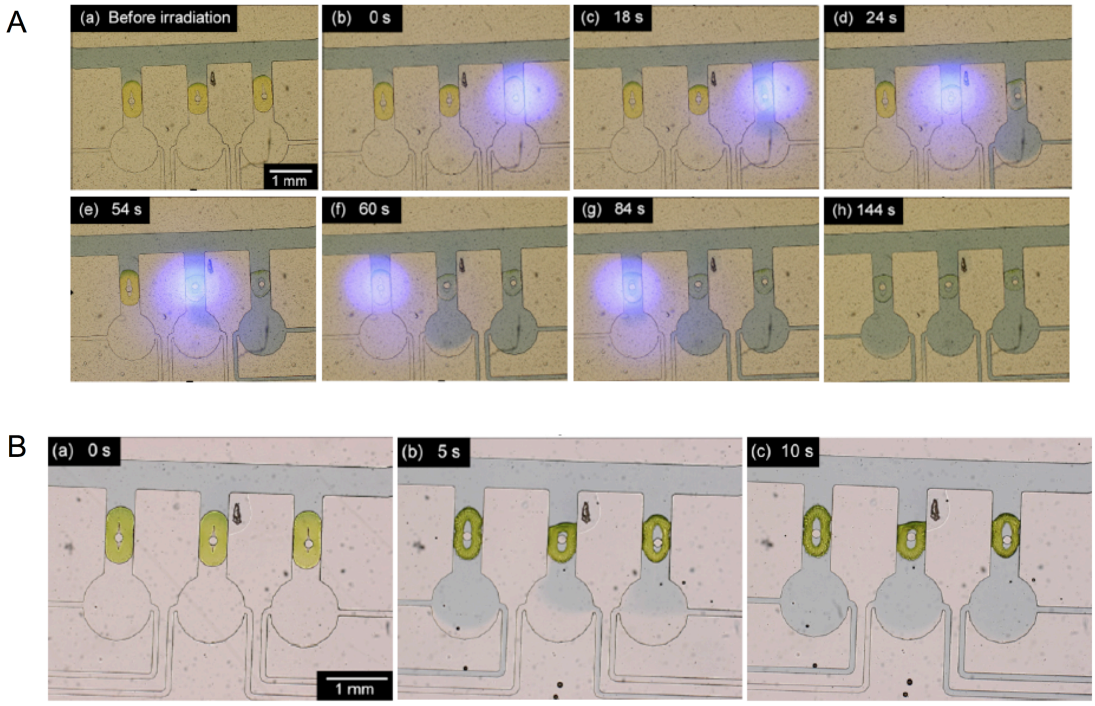

Figure 2.13. A) Independent control of multiple p(SPNIPAAm) gel microvalves by means of local light irradiation: (i) a solution containing blue dye was introduced into the main microchannel; (ii) blue light was locally irradiated to the right-side p(SPNIPAAm) gel microvalve; (iii) the right-side microvalve was opened after 18 s of blue light irradiation; (iv) blue light was locally irradiated to the centre microvalve; (v) the centre microvalve was opened after 30 s of blue light irradiation; (vi) blue light was locally irradiated to the left-side microvalve; (vii) the left-side microvalve was opened after 24 s of blue light irradiation and (viii) after light irradiation, the chambers were filled with the blue dye solution (for interpretation of the references to colour in this figure legend, the reader is referred to the web version of the article). B) Simultaneous control of multiple p(SPNIPAAm) gel microvalves by means of temperature change: (i) a solution containing blue dye was introduced into the main microchannel at 23 °C, (ii) temperature was raised by dipping the microchip into hot water. All of the microvalves were opened within 5 s after temperature rise to 46°C and (iii) 10 s after temperature rise. Source: Reprinted with permission from Sugiura *et al.* (2007). Copyright 2007 Elsevier.

A similar approach was presented by Benito-Lopez *et al.*[24, 35] However, in this case, an ionic liquid (IL) was incorporated within a poly(*N*-iso-propylacrylamide) polymer matrix copolymerised with acrylated spirobenzopyran. Using various IL components within the gels allows the

kinetics of valve actuation to be controlled, and the IL mediates the rate of protonation/deprotonation and movement of counter ions and solvent (water). Different ionogels were photopolymerised *in situ* in the channels of a poly(methyl methacrylate) (PMMA) microfluidic platform. After immersion for 2 h in 0.1 mM HCl aqueous solution, in which the ionogel exhibits a rapid swelling effect due to protonation of the polymer backbone, the rate of photo-induced shrinking due to dehydration of the ionogel was measured. The required light intensity is so low that low cost LEDs can be employed for successful valve actuation. Results showed that trihexyl-tetradecylphosphonium dicyanamide based ionogel produced the fastest valve-opening kinetics, opening 4 s after light irradiation (Fig. 2.14). Although it is possible to reuse the valves several times, the time to re-close the ionogel valve is relatively long (*ca.* 30 min) and requires re-immersion in an acidic solution.

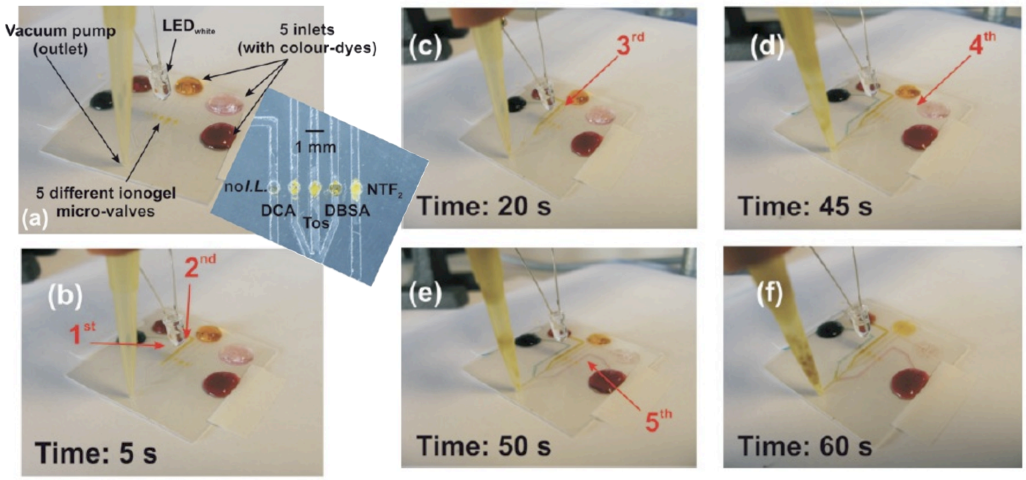

Figure 2.14. Performance of the ionogel microfluidic valves: (a) microvalves closed; the applied vacuum is unable to pull the dyes through the microchannels. (b) White light is applied for the time specified in each picture. (c) 'no I.L.' valve is first to actuate followed by ionogels incorporating dicyanamide [dca], (d) toluenesulfonate [tos], (e) dodecylbenzenesulphonate [dbsa], (f) bis(trifluoromethanesulfonyl)amide [NTf_2], all valves are open. Numbers and arrows indicate when the channel is filled with the dye because of microvalve actuation. Source: Reproduced from Benito-Lopez *et al.* (2010)

by permission of The Royal Society of Chemistry.

An innovative approach to microfluidics incorporating photoresponsive p(SPNIMAAm) hydrogels was described by Sugiura *et al.*[34] The group demonstrated on-demand formation of microchannels with arbitrary pathways using micropatterned light irradiation of (initially planar) hydrogel sheets. After light irradiation through an appropriately designed mask, a microchannel between adjacent inlet/outlet ports spontaneously formed under the irradiated area, allowing for fluid flow between a designated input and output and the channels rapidly became filled with reagent within a few minutes of illumination (Fig. 2.15). The effect was repeated for several channel configurations – straight, bent or serpentine. Furthermore, the authors demonstrated independent and parallel flow control in a polydimethylsiloxane (PDMS) microchannel network by micropatterned light irradiation of photoresponsive microvalves prepared from the same 200 μm thick hydrogel sheet. As a result of light irradiation, the gel in the irradiated area adjacent to the through-holes shrank, thus opening the valve within several minutes.

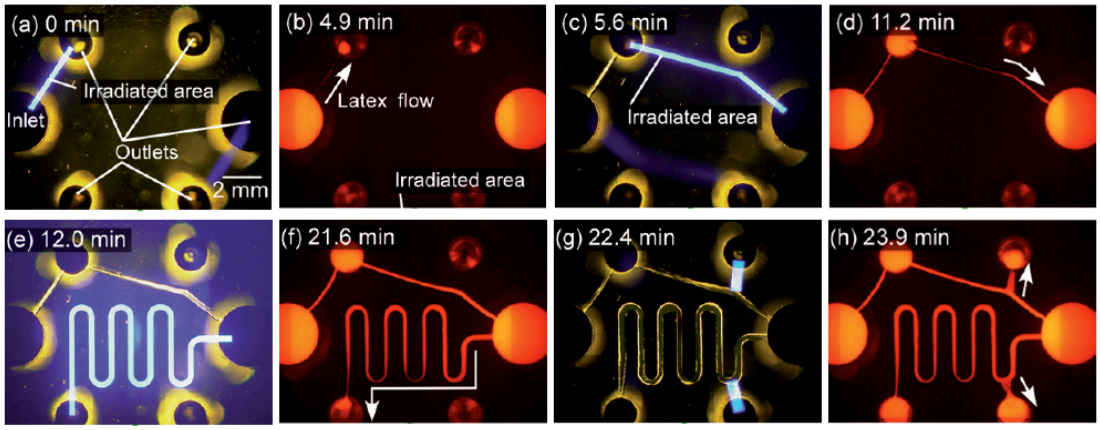

Figure 2.15. On-demand formation of microchannels with arbitrary pathways in the universal microfluidic system by micropatterned light irradiation. White arrows indicate the flow direction of a fluorescently labelled

latex bead suspension. (a) Microchannel formation by micropatterned light irradiation of the p(SPNIPAAm) hydrogel sheet. (b) Latex bead suspension flow through the microchannel after irradiation. Flow of the coloured latex bead suspension from the inlet to the upper- left-side outlet is slightly visible. (c)–(h) Three consecutive sequences of micropatterned light irradiation and microchannel formation. Source: Reproduced from Sugiura *et al.* (2009) by permission of The Royal Society of Chemistry.

2.4.3 Azobeznene based polymeric actuators

Another interesting class of photoactuated materials is based on azobenzenes.[27, 45, 46, 47, 48] These molecules are in a *trans* configuration in the ground state but when irradiated with UV light they isomerise to the *cis* orientation.[26, 27] The structural reorganisation of the molecule and the attached chains can have a significant macroscopic effect on the host material.[27] This phenomenon was greatly enhanced by D. Broer's group by incorporation of azobenzenes in liquid crystal structures.[25, 49] When the azobeznene molecule isomerises to the *cis* form under UV light there is an increase in disorder resulting in shrinkage along the direction of the liquid crystal structure and expansion in the perpendicular direction. When the white light is used the molecules and the polymer return to the initial state.[49] This shows a reversible and quick photoactuation of the polymeric material (Fig. 2.16).

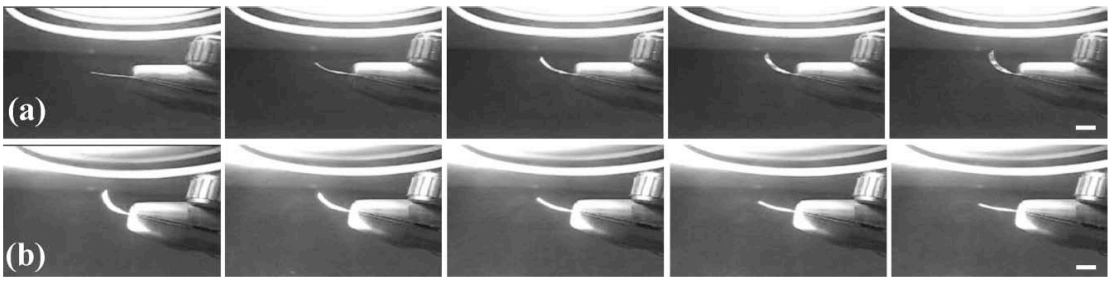

Figure 2.16. Bending of films under UV light 0, 8, 16, 24 and 32 s of UV exposure, respectively. (b) Return of the film to the original shape under white light shown after 0, 4, 8, 12 and 20 s, respectively. The white bar

corresponds to 5 mm in length. The UV intensity was roughly 10 mW cm^{-2}. Source: Reprinted with permission from Harris *et al.* (2005) by permission of The Royal Society of Chemistry.

The speed of actuation and strength of this material must be emphasised. The films reach 70 % of the maximum deformation within 7 s and take the same to return to the original shape while having over 1 GPa of elastic modulus. This material is therefore more suitable to generate mechanical work and displace fluids than considerably softer gels. Coupled with biomimetic approaches such as artificial *cilia*[25] these azobenzenes-ordered materials open new perspectives in microfluidic and lab-on-a-chip devices. The field of photomechanical actuators containing azobenzenes is covered in a review by Barrett *et al.*[27] Table 2.1. summarises the features of the presented classes of actuators.

Table 2.1. Approximate ranges for the characteristics of microvalves.

Actuator type	Energy requirement	Applied Pressure (kPa)	Actuation time	Generated deflection or volume change	Measured flow (μL min^{-1})	References
Pneumatic	0.04 – 0.5 W	20-230	< 25 s	3.5 -150 μm	$3{\cdot}10^{3}$ - $1{\cdot}10^{6}$	[50, 51, 52]
Magnetic gels	59.5 kA m^{-1}	NA	< 13 min	NA	0.2 - 100	[2, 53]
Chemically responsive gels	none	NA	12 s – 30 min	< 200 μm	10-150	[10, 13, 54]
Thermoresponsive gels	0.2 - 0.4 W	NA	1 - 9 s	< 30 %	1 - 50	[23, 55]
Spiropyran based photoactive gels	1 - 20 mW cm^{-2}	3.4-69	30 s -1 hr	< 60 %	30 ± 7	[33, 34, 35]
Azobenzene based photoactive polymers	10 mW cm^{-2}	-	< 15 s	100 m^{-1} (curvature)	-	[26]

2.5 Conclusions

There are many exciting developments happening in materials chemistry that one can only 'touch the surface' in a review chapter of this type. The potential range of stimuli responsive materials is virtually unlimited, and this, coupled with new deposition techniques that offer unsurpassed control of feature offer a tremendously rich research landscape for science to explore. The potential benefits to society emerging from this research are truly enormous. Perhaps the great issue of biofouling will finally be put to rest, opening up new opportunities in long-term implantable chem/bio-sensors that can monitor, report, and ultimately control the levels of key biomarkers. Similarly, reliable low cost sensors could open the way to environmental monitoring on a massive scale. Stimuli-responsive polymers could form the basis of new generations of biomimetic sensing based on polymer pumps and valves incorporated in microfluidic platforms much more reminiscent of our own circulation systems. The convergence of technologies that facilitate the control of micro/nano-structured surfaces coupled with these new materials is a powerful combination – materials chemistry now must be recognised as the core foundation underpinning these exciting possibilities.

2.6 Acknowledgements

This work was performed as part of the EU Framework 7 project "ATWARM" (Marie Curie ITN, No. 238273)". D. D. acknowledges funding from Science Foundation Ireland (SFI) under the CLARITY CSET award (Grant 07/CE/I1147).

2.7 References

1. Kovacs G., Microfluidic devices. In Micromachined Transducers - Sourcebook. McGraw-Hill Science/Engineering/Math, Boston, **1998**.
2. Satarkar, N. S.; Zhang, W.; Eitel, R. E.; Hilt, J. Z., Magnetic hydrogel nanocomposites as remote controlled microfluidic valves. *Lab on a Chip* **2009,** *9* (12), 1773-1779.
3. Ghosh, S.; Yang, C.; Cai, T.; Hu, Z. B.; Neogi, A., Oscillating magnetic field-actuated microvalves for micro- and nanofluidics. *Journal of Physics D: Applied Physiscs* **2009,** *42* (13), 135501-135509.
4. Zhang, W.; Lin, S.; Wang, C.; Hu, J.; Li, C.; Zhuang, Z.; Zhou, Y.; Mathies, R. A.; Yang, C. J., PMMA/PDMS valves and pumps for disposable microfluidics. *Lab on a Chip* **2009,** *9* (21), 3088-3094.
5. Go, J. S.; Shoji, S., A disposable, dead volume-free and leak-free in-plane PDMS microvalve. *Sensors and Actuators A: Physical* **2004,** *114* (2-3), 438-444.
6. Kaigala, G. V.; Hoang, V. N.; Backhouse, C. J., Electrically controlled microvalves to integrate microchip polymerase chain reaction and capillary electrophoresis. *Lab on a Chip* **2008,** *8* (7), 1071-1078.
7. Selvaganapathy, P.; Carlen, E. T.; Mastrangelo, C. H., Electrothermally actuated inline microfluidic valve. *Sensors and Actuators A: Physical* **2003,** *104* (3), 275-282.
8. Garcia-Cordero, J. L.; Kurzbuch, D.; Benito-Lopez, F.; Diamond, D.; Lee, L. P.; Ricco, A. J., Optically addressable single-use microfluidic valves by laser printer lithography. *Lab on a Chip* **2010,** *10* (20), 2680-2687.
9. Moorthy, J.; Beebe, D. J., Peer Reviewed: Organic and biomimetic designs for microfluidic systems. *Analytical Chemistry* **2003,** *75* (13), 292-301.
10. Beebe, D. J.; Moore, J. S.; Bauer, J. M.; Yu, Q.; Liu, R. H.; Devadoss, C.; Jo, B.-H., Functional hydrogel structures for autonomous flow control inside microfluidic channels. *Nature* **2000,** *404* (6778), 588-590.
11. Wang, X.; Qiu, X.; Wu, C., Comparison of the coil-to-globule and the globule-to-coil transitions of a single poly(*N*-isopropylacrylamide) homopolymer chain in water. *Macromolecules* **1998,** *31* (9), 2972-2976.
12. Sun, S.; Hu, J.; Tang, H.; Wu, P., Chain collapse and revival thermodynamics of poly(*N*-isopropylacrylamide) hydrogel. *The Journal of Physical Chemistry B* **2010,** *114* (30), 9761-9770.
13. Liu, R. H.; Qing, Y.; Beebe, D. J., Fabrication and characterization of hydrogel-based microvalves. *Journal of Microelectromechanical Systems,* **2002,** *11* (1), 45-53.

14. Beebe, D. J.; Moore, J. S.; Yu, Q., Liu, R. H.; Kraft, M. L,; Jo, B.-H.; Devadoss, C., Microfluidic tectonics: A comprehensive construction platform for microfluidic systems. *Proceedings of National Academy of Sciences of the United States of America* **2000,** *97* (25), 13488-13493.
15. Yu Q., Bauer J. M., Moore J. S., Beebe D. J., Responsive biomimetic hydrogel valve for microfluidics. *Applied Physics Letters* **2001,** *78 (17)*, 2589-2591.
16. Dusek K., Responsive gels, volume transition I and. II. In *Advances in Polymer Science*, **1993**; Springer, New York.
17. Schild, H. G., Poly (*N*-isopropylacrylamide) - experiment, theory and application. *Progress in Polymer Science* **1992,** *17* (2), 163-249.
18. Richter A., Kuckling D., Howitz S., Gehring T., Arndt K.-F., Electronically controllable microvalves based on smart hydrogels: magnitudes and potential applications. *Journal of Microelectromechanical Systems* **2003,** *12* (5), 748-753.
19. Yu C., Mutlu S., Selvaganapathy P., Mastrangelo C. H., F. Svec, J. M. J. Fréchet, Flow control valves for analytical microfluidic chips without mechanical parts based on thermally responsive monolithic polymers, Analytical Chemistry. *Analytical Chemistry* **2003,** *75* (8), 1958-1961.
20. Wang Y., Yang L., Electro-Hydro-Dynamic (EHD) Micropumps with electrode protection by parylene and gelatin. *Tamkang Journal of Science and Engineering* **2005,** *8* (3), 231-236.
21. Richter, A.; Klatt, S.; Paschew, G.; Klenke, C., Micropumps operated by swelling and shrinking of temperature-sensitive hydrogels. *Lab on a Chip* **2009,** *9* (4), 613-618.
22. Gerlach, G.; Guenther, M.; Sorber, J.; Suchaneck, G.; Arndt, K.-F., A. Richter, Chemical and pH sensors based on the swelling behavior of hydrogels. *Sensors and Actuators B* **2005,** 111-112, 555-561.
23. Luo, Q.; Mutlu, S.; Gianchandani, Y. B.; Svec, F.; Fréchet, J. M. J., Monolithic valves for microfluidic chips based on thermoresponsive polymer gels. *Electrophoresis* **2003,** *24* (21), 3694-3702.
24. Byrne, R.; Ventura, C.; Lopez, F. B.; Walther, A.; Heise, A.; Diamond, D., Characterisation and analytical potential of a photo-responsive polymeric material based on spiropyran. *Biosensensors and Bioelectronics* **2010,** *26* (4), 1392-1398.
25. van Oosten, C. L.; Bastiaansen, C. W. M.; Broer, D. J., Printed artificial cilia from liquid-crystal network actuators modularly driven by light. *Nature Materials* **2009,** *8* (8), 677-682.
26. Harris, K. D.; Cuypers, R.; Scheibe, P.; van Oosten, C. L.; Bastiaansen, C. W. M.; Lub, J.; Broer, D. J., Large amplitude light-induced motion in

high elastic modulus polymer actuators. *Journal of Materials Chemistry* **2005,** *15* (47), 5043-5048.

27. Barrett, C. J.; Mamiya, J.-i.; Yager, K. G.; Ikeda, T., Photo-mechanical effects in azobenzene-containing soft materials. *Soft Matter* **2007,** 3 (10), 1249-1261.
28. Irie, M.; Kanwatchakun, D., Photoresponsive polymers - Reversiblephoto-stimulated dilation of polyacrylamide gels having triphenylmethane leuco derivatives. *Macromolecules* **1986,** 19, 2476–2480.
29. Irie, M.; Hosoda, M., Photoresponsive polymers—reversible solution viscosity change of poly(*N,N*-dimethylacrylamide) with pendant triphenyl-methane leucohydroxide residues in methanol. *Makromolecular Rapid Communications* **1985,** 6 (8), 533–536.
30. Irie M., Menju, A.; Hayashi, K., Photoresponsive polymers. Reversible solution viscosity change of poly(methylmethacrylate) having spirobenzopyran side groups. *Macromolecules* **1979,** *12 (6)*, 1176–1180.
31. Menju, A.; Hayashi, K.; Irie, M., Photoresponsive polymers. 3. Reversible solution viscosity change of poly(methacrylic acid) having spirobenzopy-ran pendant groups in methano. *Macromolecules* **1981,** *14*, 755–758.
32. Lo, C.-W.; Zhu, D.; Jiang, H., An infrared-light responsive graphene-oxide incorporated poly(*N*-isopropylacrylamide) hydrogel nanocomposite. *Soft Matter* **2011,** *7* (12), 5604-5609.
33. Sugiura, S.; Sumaru, K.; Ohi, K.; Hiroki, K.; Takagi, T.; Kanamori, T., Photoresponsive polymer gel microvalves controlled by local light irradiation. *Sensors and Actuators A: Physical* **2007,** *140* (2), 176-184.
34. Sugiura, S.; Szilagyi, A.; Sumaru, K.; Hattori, K.; Takagi, T.; Filipcsei, G.; Zrinyi, M.; Kanamori, T., On-demand microfluidic control by micropatterned light irradiation of a photoresponsive hydrogel sheet. *Lab on a Chip* **2009,** *9* (2), 196-198.
35. Benito-Lopez, F.; Byrne, R.; Răduţă, A. M.; Vrana, N. E.; McGuinness, G.; Diamond, D., Ionogel-based light-actuated valves for controlling liquid flow in micro-fluidic manifolds. *Lab on a Chip* **2010,** *10* (2), 195-201.
36. Smets, G.; Braeken, J.; Irie, M., Photomechanical effects in photochromic systems. *Pure and Applied Chemistry* **1978,** *50* (8), 281-289..
37. Irie, M.; Menju, A.; Hayashi, K., Photoresponsive polymers. Reversible solution viscosity change of poly(methyl methacrylate) having spirobenzopyran side groups. *Macromolecules* **1979,** *12* (6), 1176-1180.
38. Sumaru, K.; Kameda, M.; Kanamori, T.; Shinbo, T., Reversible and efficient proton dissociation of spirobenzopyran-functionalized poly(*N*-isopropylacrylamide) in aqueous solution triggered by light irradiation and temporary temperature rise. *Macromolecules* **2004,** *37* (21), 7854-7856.

39. Sumaru, K.; Kameda, M.; Kanamori, T.; Shinbo, T., Characteristic phase transition of aqueous solution of poly(*N*-isopropylacrylamide) functionalized with spirobenzopyran. *Macromolecules* **2004,** *37* (13), 4949-4955.
40. Ivanov, A. E.; Eremeev, N. L.; Wahlund, P. O.; Galaev, I. Y.; Mattiasson, B., Photosensitive copolymer of *N*-isopropylacrylamide and methacryloyl derivative of spyrobenzopyran. *Polymer* **2002,** *43* (13), 3819-3823.
41. Kröger, R.; Menzel, H.; Hallensleben, M. L., Light controlled solubility change of polymers: Copolymers of *N,N*-dimethylacrylamide and 4-phenylazophenyl acrylate. *Macromolecular Chemistry and Physics* **1994,** *195* (7), 2291-2298.
42. Wu, X. S.; Hoffman, A. S.; Yager, P., Synthesis and characterization of thermally reversible macroporous poly(N-isopropylacrylamide) hydrogels. *Journal of Polymer Science Part A: Polymer Chemistry* **1992,** *30* (10), 2121-2129.
43. Satoh, T.; Sumaru, K.; Takagi, T.; Takai, K.; Kanamori, T., Isomerization of spirobenzopyrans bearing electron-donating and electron-withdrawing groups in acidic aqueous solutions. *Physical Chemistry Chemical Physics* **2011,** *13* (16), 7322-7329.
44. Satoh, T.; Sumaru, K.; Takagi, T.; Kanamori, T., Fast-reversible light-driven hydrogels consisting of spirobenzopyran-functionalized poly(*N*-isopropylacrylamide). *Soft Matter* **2011,** *7* (18), 8030-8034.
45. Long, K. N.; Scott, T. F.; Jerry Qi, H.; Bowman, C. N.; Dunn, M. L., Photomechanics of light-activated polymers. *Journal of the Mechanics and Physics of Solids* **2009,** *57* (7), 1103-1121.
46. Lee, K. M.; Koerner, H.; Vaia, R. A.; Bunning, T. J.; White, T. J., Relationship between the photomechanical response and the thermomechanical properties of azobenzene liquid crystalline polymer networks. *Macromolecules* **2010,** *43* (19), 8185-8190.
47. Wang, H.; Lee, K. M.; White, T. J.; Oates, W. S., trans–cis and trans–cis–trans microstructure evolution of azobenzene liquid-crystal polymer networks. *Macromolecular Theory and Simulations* **2011**, *21* (5), 285-301.
48. Lee, K. M.; Tabiryan, N. V.; Bunning, T. J.; White, T. J., Photomechanical mechanism and structure-property considerations in the generation of photomechanical work in glassy, azobenzene liquid crystal polymer networks. *Journal of Materials Chemistry* **2012,** *22* (2), 691-698.
49. van Oosten, C. L.; Corbett, D.; Davies, D.; Warner, M.; Bastiaansen, C. W. M.; Broer, D. J., Bending dynamics and directionality reversal in liquid crystal network photoactuators. *Macromolecules* **2008,** *41* (22), 8592-8596.

50. Yang, X.; Grosjean, C.; Tai, Y.-C.; Ho, C.-M., A MEMS thermopneumatic silicone rubber membrane valve. *Sensors and Actuators A: Physical* **1998,** *64* (1), 101-108.
51. Rich, C. A.; Wise, K. D., A high-flow thermopneumatic microvalve with improved efficiency and integrated state sensing. *Journal of Microelectromechanical Systems,* **2003,** *12* (2), 201-208.
52. Takao, H.; Miyamura, K.; Ebi, H.; Ashiki, M.; Sawada, K.; Ishida, M., A MEMS microvalve with PDMS diaphragm and two-chamber configuration of thermo-pneumatic actuator for integrated blood test system on silicon. *Sensors and Actuators A: Physical* **2005,** *119* (2), 468-475.
53. Santaneel, G.; Tong, C., Controlled actuation of alternating magnetic field-sensitive tunable hydrogels. *Journal of Physics D: Applied Physics* **2010,** *43* (41), 415504.
54. Baldi, A.; Yuandong, G.; Loftness, P. E.; Siegel, R. A.; Ziaie, B., A hydrogel-actuated environmentally sensitive microvalve for active flow control. *Journal of Microelectromechanical Systems,* **2003,** *12* (5), 613-621.
55. Richter, A.; Howitz, S.; Kuckling, D.; Arndt, K.-F., Influence of volume phase transition phenomena on the behavior of hydrogel-based valves. *Sensors and Actuators B: Chemical* **2004,** *99* (2-3), 451-458.

Chapter 3

Photopatterning and actuation behaviour of photoresponsive phosphonium-based ionogel microstructures

M. Czugala,[1] C. O'Connel,[1] C. Blin,[2] P. Fischer,[3] Kevin J. Fraser,[1] F. Benito-Lopez,[1, 4] D. Diamond[1]

Langmuir, 2013 (Under Review)

[1]CLARITY: Centre for Sensor Web Technologies, National Centre for Sensor Research, Dublin City University, Dublin 9, Ireland
[2]Fraunhofer Institute of Physical Measurement Techniques IPM, Freiburg, GERMANY
[3]Max Planck Institute for Intelligent Systems, Stuttgart, GERMANY
[4]CIC microGUNE, Arrasate-Mondragón, SPAIN

For Supplementary Information see Appendix A, pg. 219.

Abstract

A simple and inexpensive photolithographic set-up for the micropatterning of photoresponsive *N*-isopropylacrylamide ionogel microstructures is presented. The ionogels are synthesised using phosphonium based room temperature ionic liquids, together with the photochromic compound benzospiropyran. These stimuli responsive materials can be actuated using light irradiation, facilitating non-contact and non-invasive operation. For the first time, the characterisation of the swelling and shrinking behaviour of several photopatterned ionogel microstructures is presented and the influence of surface-area-to-volume ratio on the swelling kinetics is evaluated. It was found that the actuation behaviour of the ionogels is strongly dependent on the nature of the ionic liquid. In particular, the $[P_{6,6,6,14}][NTf_2]$ ionogel exhibits the greatest degree of swelling, reaching up to 180 % of its initial size, and the fastest shrinkage rate (k_{sh} = 29.3 ± 3.5 x 10^{-2} s^{-1}).

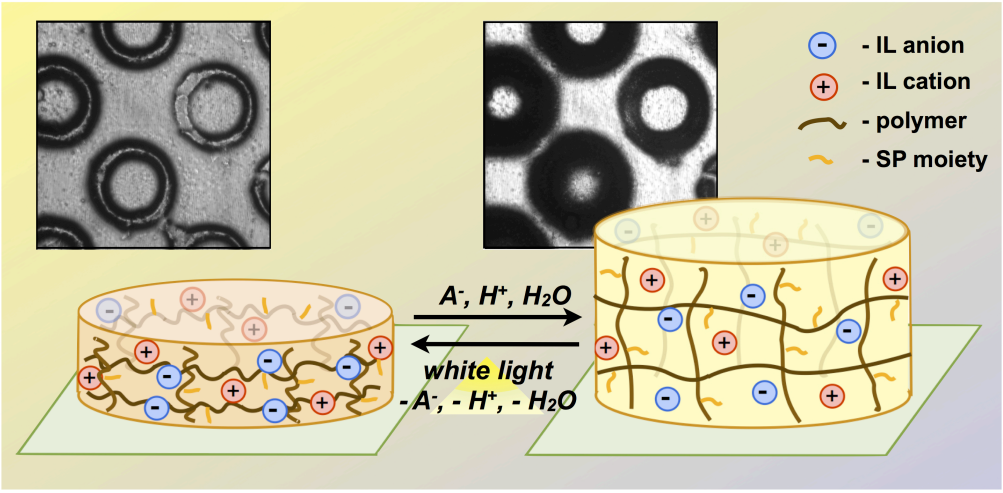

3.1 Introduction

Stimuli responsive materials, such as gels, have recently attracted widespread attention due to their highly attractive properties, including mechanical, optical, surface and permeability characteristics, which can be tuned in response to an externally applied stimulus. These materials are generally comprised of crosslinked monomer molecules that, in most cases, form porous macromolecular structures.[1] These pores can be filled with a solvent, often water (hydrogels) to provide a gel-like network arrangement.

The stimuli responsiveness of these materials is based on the existence of two metastable energy states associated with two structural forms (with different characteristics) that possess distinctly different energy minima. If the relative populations of molecules populating these energy states can be perturbed with an external stimulus, then the material is switchable, and can be transformed from one state to the other. These changes can be induced with different stimuli depending on the switchable functional group attached to the gel network, *e.g.* magnetic,[2] thermal,[3] light,[4] pH[5] or electrochemical stimuli.[6] Depending on the chemical composition of the gel and on the experimental conditions, the response of the gel to the external stimulus can be continuous, due to a gradual change of the environmental parameter, or discontinuous, for example in the form of an abrupt volume change when a critical threshold of a key response parameter (*e.g.* temperature) is crossed.[7]

In particular, *N*-isopropylacrylamide (NIPAAm) has been widely studied as a base material for stimuli responsive gels, due to the high degree of swelling at low temperatures, large volume change upon crossing the volume transition temperature, in this case, the lower critical solution temperature (LCST) which was found to be in the range 32-35 °C.[8] One of the most attractive approaches to polymer actuation is light irradiation,[9] as it

allows non-contact and non-invasive operation. This can be achieved by functionalising poly(*N*-isopropylacrylamide) gels p(NIPAAm) with spirobenzopyran chromophores (SP). Spirobenzopyrans are capable of interconversion between two thermodynamically stable states under light external stimulus. SP consists of two heterocyclic moieties in two orthogonal planes - the benzopyran part (B), which is the common structure to all spiropyran compounds, and the heterocyclic part (A), which is built upon a benzofused azaheterocycle. SP undergoes a heterocyclic ring cleavage at the C–O spiro bond that results in the formation of a planar, zwitterionic and highly conjugated merocyanine isomer (MC) which absorbs strongly in the visible region.[10]

Functionalising the p(NIPAAm) gels with SP produces hybrid materials (which we shall henceforth refer to as p(SPNIPAAm)), consisting of two stimuli responsive entities:

1. The thermoresponsive p(NIPAAm) gel which swells below its lower critical solution temperature (LCST);[11]
2. The photoresponsive spiropyran molecule, SP, that is able to open to the charged MC under UV-irradiation and revert to the uncharged SP isomer under white light irradiation. Switching from the MC to SP isomer triggers conformational rearrangements in the bulk p(NIPAAm) gel, changing it from a more hydrophilic (MC) to hydrophobic (SP) nature, which in turn induces water loss and contraction of the gel (and *vice versa*).[12, 13]

Normally the p(SPNIPAAm) gel is soaked in an aqueous solution of HCl (typically pH 3) to induce spontaneous isomerisation to the protonated merocyanine (MC-H^+) form, which has a yellow colour due to absorption in the visible spectrum by MC-H^+ (λ_{max} usually in the range 420 - 440 nm). The protons diffusing into the gel are accompanied by counter ions and water, causing the gel to swell and adopt a more hydrophilic conformation. Upon

irradiation with white light, the MC-H^+ reverts to the uncharged, colourless SP form, which triggers dehydration and shrinkage of the gel.[13]

The effects of ring-opening rates of spirobenzopyran derivatives on light-induced volume change behaviour of gels have been reported previously.[9] Several spirobenzopyran derivatives, having different ring-opening rates, were introduced into p(NIPAAm) hydrogels and the effects on volume changes of these gels were evaluated by Satoh *et al.*[14] It was found that the rates of the spontaneous re-swelling of the p(SPNIPAAm) gels from light-induced shrunken state increased with increasing ring-opening rates of the spirobenzopyran molecules in the gels. Furthermore, rod-like and sheet-like p(SPNIPAAm) gels were investigated as potential light-responsive soft actuators and micro-conveyors, respectively. Sugiura *et al.*,[13] for instance, presented the independent control of multiple p(SPNIPAAm) microvalves, which were fabricated by *in situ* photopolymerisation at desired positions within microchannels. Blue light irradiation of the microvalves induced shrinkage of the gels and caused the microvalves to open after 18 - 30 s irradiation.

Traditionally, organic solvents such as 1-butanol,[13] dimethyl sulfoxide,[15] 1,4-dioxane–water[14] and tetrahydrofuran/water[16] mixture solutions have been used for the preparation of p(SPNIPAAm) gels. A new approach is to incorporate ionic liquids (ILs) as solvents within polymer matrices to produce a new class of hybrid materials known as ionogels. Recently defined as "a solid interconnected network spreading throughout a liquid phase", the ionogel combines the physical properties of both the polymer gel and the physically entrapped IL.[17] Recent interesting reviews have examined the interaction and mobility of the IL within the polymer network[18] as well as the application of ionogels as functional materials for sensors and actuators.[17] The attractiveness of ionic liquids is based on the

possibility of tuning their properties through the choice of the cation-anion combination, which, given the wide range of available candidates, provides almost infinite possibilities for synthesising new materials. ILs generally offer excellent chemical and thermal stability, low vapour pressure, high ionic conductivity, and tuneable hydrophobicity and hydrophilicity depending on the particular cation/anion combination.[17] Recently it was reported that certain ionogels exhibit enhanced water uptake/release behaviour, and improved mechanical and viscoelastic properties compared to the equivalent hydrogel.[19] Diamond *et al.*[20, 21] recently published several papers on phosphonium-based ILs and their use in ionogels, and reported their application as valves based on SP copolymerised with poly(*N*-isopropylacrylamide) that can be photo-actuated using white light irradiation. Benito-Lopez *et al.*[22] successfully developed photo-actuating microvalves based on an IL incorporated within the pSPNIPAAm polymer matrix. It was demonstrated that by using different IL components within the gels, valve actuation kinetics could be controlled through IL mediation of the rate of protonation/deprotonation, and related movement of counter ions and solvent (water) in the ionogel matrix. As a consequence, ionogels containing different ILs were found to actuate at different times when exposed to a common light source. Further investigations showed that also the mechanical strength of the ionogels and their UV curing rates were noticeably different depending on the IL used.[23]

The adoption of stimuli responsive materials in practical macro-scale devices has been hindered by relatively slow response times, mainly due to the diffusion processes that govern polymer swelling/contraction mechanisms. Moving to microfluidic scaled devices should improve response times, due to improved surface-to-volume ratios of these actuators.[24] A number of microfabrication techniques have been developed for micropatterning of

polymeric structures with controlled sizes and shapes, including photolithography,[13, 25] molding,[26, 27] and hot-embossing.[27, 28] Photolithography is an extremely useful and popular technique that can be used to generate micrometer- to submicrometer-sized structures. Using this technique, it is possible to produce a pattern with high resolution, since the resolution is proportional to the exposure wavelength.[28] UV lithography is perhaps the most commonly used photolithography technique for fabrication of micropatterned gels.[24 13, 16] In some cases, a photomask is used to create well-defined patterns.[25, 29, 30] Although conventional photolithographic approaches show promise, expensive instrumentation is usually required for high quality photopatterning[13, 16] and the fabrication itself is relatively complex and complicated. Consequently, widespread use of this approach remains limited, and significant challenges still exist to transform photolithography in a low-cost and widely employed, non-specialist microfabrication technique. [31]

In this chapter, the synthesis of photoresponsive poly(*N*-isopropylacrylamide) ionogels functionalised with spiropyran chromophores is reported, and their ability to be photopatterned into complex microstructures using a simple and inexpensive photolithography set-up capable of generating 3D arrays of microstructures examined. The light-induced volume change of the ionogel microstructures has been fully characterised to examine the dependence of their swelling and shrinking behaviour on the dimensions of the photopatterned microstructures, and on the particular phosphonium based ionic liquid used. Such three-dimensional (3D) microstructures fabricated using this approach are believed to have a wide range of potential applications in micro-electromechanical systems (MEMS), sensors/actuators, optical devices and microfluidics.

3.2 Experimental

3.2.1 Ionogel materials

N-isopropylacrylamide, *N,N'*-methylene-bis(acrylamide) (MBAAm), 2,2-5 dimethoxy-2-phenyl acetophenone (DMPA) were used for ionogel preparation as purchased from Sigma-Aldrich®, Ireland. 1′, 3′, 3′-Trimethyl-6-hydroxyspiro(2H-1-benzopyran- 2, 2′-indoline) (Acros Organics, Geel, Belgium), 3-(Trimethoxysilyl) propyl methacrylate was purchased from Sigma-Aldrich®, Ireland. Trihexyltetradecyl-phosphonium dicyanoamide $[P_{6,6,6,14}][dca]$, trihexyltetradecyl-phosphonium bis(trifluoromethanesulfonyl)-amide $[P_{6,6,6,14}][NTf_2]$, trihexyltetradecyl-phosphonium chloride $[P_{6,6,6,14}][Cl]$ were obtained as compliments of Cytec® Industries, Ontario, Canada, Fig. 3.1A. Further purification was carried out as follows: 10 mL of IL decolourised by redissolution in 30 mL of acetone followed by treatment with activated charcoal (Darco-G60, Aldrich®) at 40 °C overnight. Carbon was removed by filtration through alumina (acidic, Brockmann I, Aldrich®) and the solvent removed under vacuum at 60 °C for 24 h at 0.1 Torr.

170 µm thick glass slides were purchased from Sigma-Aldrich®, Ireland. High power UV-365 nm light emitting diode was obtained from Electrolyte Corporation, USA.

3.2.2 Preparation of the ionogel prepolymer mixture

All the ionogels contain *N*-isopropylacrylamide (Fig. 3.1B, *y*), *N,N'*-methylene-bis(acrylamide) (Fig. 3.1B, *z*) and 1', 3', 3'-Trimethyl-6-acrylate(2H-1-benzopyran- 2,2'-indoline) (Fig. 3.1B, *x*) in the ratio of 100: 5: 1, respectively. The acrylated benzospiropyran was synthesised as described

elsewhere.[32] A liquid prepolymer mixture was prepared by dissolving the NIPAAm monomer (0.75 mmol), the MBAAm (0.04 mmol), acrylated spirobenzopyran monomer (0.01 mmol), and the photo-initiator DMPA (0.02 mmol) into the ionic liquid (0.52 mmol). Three types of phosphonium based ionic liquids were tested [$P_{6,6,6,14}$][dca], [$P_{6,6,6,14}$][Cl] and [$P_{6,6,6,14}$][NTf_2]. In order to dissolve the monomers, the solution was heated to 40 °C using an ultrasonic bath (Bennett Scientific Ltd.) for 15 min.

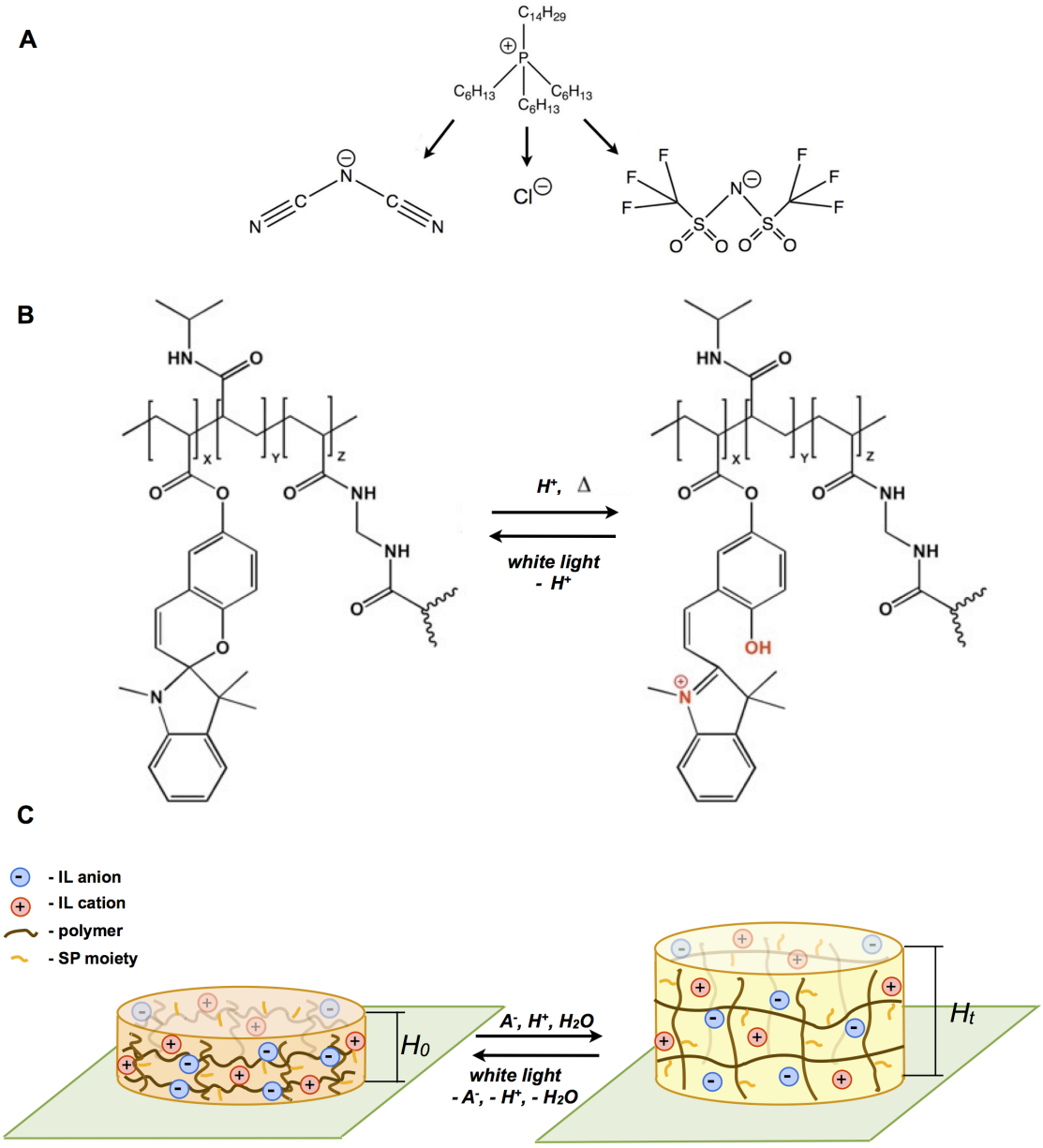

Figure 3.1. Chemical structure of A) the phosphonium cation and the anions

selected for the ionogel formulation - dicyanoamide $[dca]^-$ (left), chloride $[Cl]^-$ (middle) and bis(trifluoro-methanesulfonyl)-imide $[NTf_2]^-$ (right); B) the crosslinked pNIPAAm ionogel functionalised with acrylated spiropyran. C) Schematic illustration of the surface-attached polymer network reversibly swelling/contracting in one dimension away from the substrate due to movement of protons (H^+), counter ions (A^-) and water in/out of the gel.

3.2.3 Surface functionalisation

To facilitate homogeneous covalent bonding between the ionogel and the glass slide, the surface of the slide was chemically functionalised using method published previously by Hou *et al.*[29] After washing with acetone, methanol, ethanol (all from Brenntag UK & Ireland) and DI water, bare glass slides were incubated with 1 M sodium hydroxide (NaOH) (Sigma-Aldrich®, Ireland) for 10 min, flushed with DI water, and then purged by vacuum. A degassed 2:3:5 (v/v/v) mixture of 3-(trimethoxysilyl)-propyl methacrylate (MPTMS) (Sigma-Aldrich®, Ireland), glacial acetic acid (Merck KgaA, Germany), and DI water was then placed on the glass slides for silane monolayer formation. After 30 min incubation, the glass slides were rinsed for 10 min with methanol and DI water and dried under vacuum.

Contact angle measurements were performed using a FTA 200® dynamic contact angle analyser, using deionised water as the probing liquid. All measurements were undertaken under ambient humidity and temperature conditions. The values quoted are the averages of 4 individual measurements.

3.2.4 Photolithography set-up

The photopolymerisation of the microstructures was carried out using an *in house* designed and built optical set-up (Fig. 3.2). It consists of a 365 nm high power LED (Nichia NCSU033B, Japan), two N-BK7 Plano-Convex lenses (Thorlabs LA1027) to collimate the light beam, lens holder (Thorlabs)

to hold the substrate and an off axis angled mirror to prevent reflection as this can affect the polymerisation. All other optomechanical components (cage system construction rods, mounting adapters) were also purchased from Thorlabs, Germany. This UV wavelength was selected because of its compatibility with the DMPA photoinitiator. For the fabrication of the microstructures, different photolithography masks (transparency) designed using CleWin software were used (see Appendix A, Fig. A1). Since the liquid pre-polymer solution was viscous enough not to flow out of the surface of the glass slide, it was drop-cast onto the glass slide (upper side), which was then turned upside down and placed on the lens holder. The glass slide was then covered with the mask on the upper side. The UV source was placed 5 cm far from the glass slide/liquid prepolymer. Exposure of the liquid pre-polymer solution to UV light (intensity 2700 μW cm^{-2}) through a photomask for 30 min resulted in the crosslinking of the exposed regions. Development of the micropattern was achieved by rinsing the irradiated ionogel microstructures in deionised water, whereby the non-crosslinked, *i.e.*, the non-irradiated polymer segments, were dissolved. The photopatterned ionogels were dried at room temperature for 24 h. Finally, the ionogels were immersed for 2 h in 0.1 mM HCl aqueous solution.

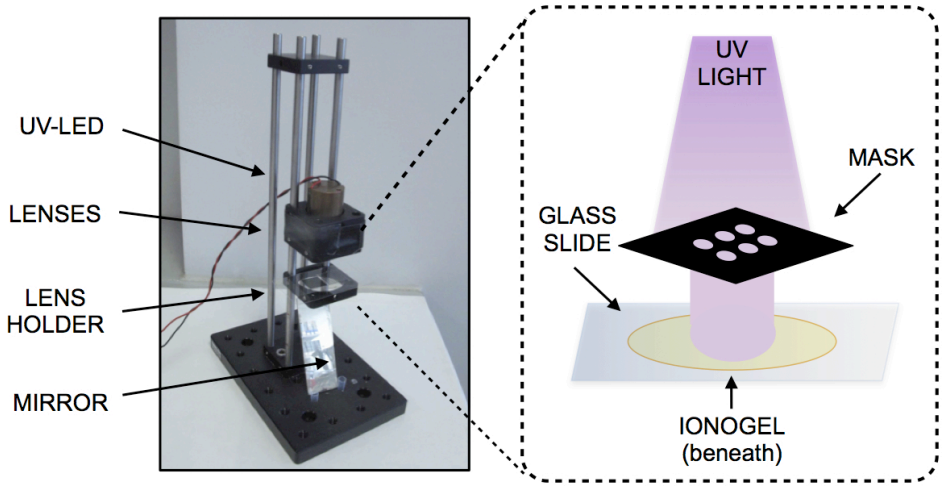

Figure 3.2. In house designed UV LED set-up for ionogel photopatterning.

3.2.5 Characterisation of the photoresponsive phosphonium-based ionogels

The volume phase-transition behaviour of the photoresponsive phosphonium-based ionogel microstructures was investigated using an Aigo Digital Microscope GE -5 and VHX-2000 3D Keyence Digital Microscope. The percent variation in ionogel microstructure height, $\%H$, is defined as

$$\%H = (H_t - H_0)/ H_0 \times 100 \quad (3.1)$$

where H_t is the height of the ionogel microstructure at time t and H_0 is the height before immersion in 1 mM HCl solution. The kinetics of swelling was investigated by placing the ionogel samples in a dark environment in 1 mM HCl aqueous solution, and taking digital images every 20 min for 140 min. A single exponential model (Eqn. 3.2)[33] was used to estimate the swelling rate constants:

$$\%H = a \times (1 - e^{-k_{sw}t}) + b \quad (3.2)$$

where $\%H$ is the percentage swelling, a is a scaling factor, k_{sw} is the first order rate constant (s^{-1}), b is the baseline offset and t is time (s).

The kinetics of the gel shrinking was evaluated by irradiating the disc-shaped ionogels with the white light coming from the Aigo Digital Microscope GE -5 for 30 min. Pictures were taken with the same microscope after 1, 3, 5, 10, 15, 20, 25 and 30 min of exposure. The shrinking rate constants were estimated using the following exponential decay model (Eqn. 3.3):

$$\%H = a \times e^{-k_{sh}t} + b \quad (3.3)$$

where $\%H$ is the percentage swelling (calculated in the same manner as for equation (1) above), a is a scaling factor, k_{sh} is the first order rate constant (s^{-1}), b is the baseline offset and t is time (s).

All measurements were carried out at 21 °C. In order to measure the height change of the microstructures while swelling and shrinking, the glass slide with photopatterned ionogels was placed perpendicularly to the lens. In order to get a sharp focus, the glass slides were cut as close to the microstructures as possible (*ca.* 500 μm).

SEM studies were performed using a Carl Zeiss EVOLS 15 Scanning Electron Microscopy system at an accelerating voltage of 26.11 kV. Gold sputtering of all ionogels was performed on a Polaron® SC7640 Auto/Manual High Resolution Sputter Coater. All ionogels were coated under the following conditions: voltage 1.5 kV, 15 mA for 2 min at a coating rate of 5 nm min^{-1}. The 10 nm gold coating proved capable of maintaining a hydrated ionogel for microscopy imaging.

3.3 Results and discussion

3.3.1 Substrate surface modification

Ionogel patterns were generated on silicon surfaces cleaned with methanol, ethanol, IPA and DI water, but in initial experiments, the surfaces were not modified to assist adhesion. Although the ionogel patterns were properly formed using this approach, the polymer array elements easily delaminated upon hydration due to swelling of the ionogel matrices and detachment of the microstructures from the slide surface. In order to prevent this delamination of the swollen ionogels from the substrate, the slide surfaces were treated with 3-(trimethoxysilyl)-propyl methacrylate, generating a

monolayer vinylised surface. The ionogel was then photopolymerised on the vinyl surface generating covalent bonds between the functionalised slide surface and the microstructures. By anchoring the ionogel network to the glass substrate in this manner, the mechanical stability of the ionogels microstructures is greatly increased.[34] The silanisation of glass substrates was carried out using MPTMS (see 3.2 Experimental) and the water contact angle values before and after each step of the treatment are shown in Table A1, Appendix A. The results demonstrate that the method provides a more hydrophobic surface than the bare glass. The final contact angle of the treated glass substrates was $72 \pm 4°$ ($n = 4$).

3.3.2 Fabrication of photopatterned ionogel microstructures

Arrays of microstructures were photopolymerised by free radical polymerisation using the *in-house* designed photolithography set-up described above. This approach allows the fabrication of ionogel microstructures of various dimensions and geometries simultaneously, from large (radius 500 μm) to small (radius 250 μm) discs, lines (width 500 μm) and rings (external radius 750 μm) (see Appendix A, Fig. A2). SEM images showed that the patterns were clear and well-defined (Fig. 3.3) and demonstrate good compatibility of the ionogels with the photopatterning technique. Improved photolithographic microstructures were obtained by reducing the distance between the liquid pre-polymer and the mask to the thickness of the cover glass (170 μm). Further improvement could be achieved by decreasing the thickness of the glass slide, thus decreasing the distance between the pre-polymer and the mask.

In comparison to the other photopatterning methods utilised by

Sugiura *et al.*[13, 16] and Hoffmann *et al.*,[24] this technique is simpler and inexpensive (*ca.* €150). The instrumentation presented in the aforementioned publications is costly (€40K), which significantly limits the range of potential applications, and the fabrication of the microstructures requires a sequence of many complicated steps. By reducing the infrastructure requirements, our photolithography set-up makes the generation of these microstructures accessible to non-specialists. The set-up presented here is not high-throughput but it is quick and easy-to-use, while still providing good microstructure resolution (Fig. 3.3).

It has been previously demonstrated that in the case of standard photo-curable materials, the dimensions of the resulting microstructures are sensitive to the UV exposure dose and the focal point of the light source.[35, 36] Our photolithography set-up takes advantage of these variables, and allows precise geometry control of the polymerised structures through control of the exposure time and the focal point of the light source (adjustable lens holder), thus users can easily define the dimensions and resolution of the structures according to their needs.

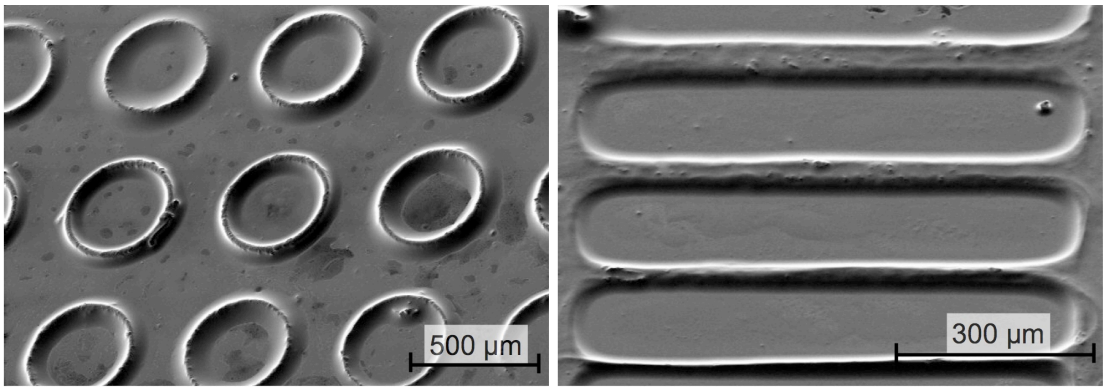

Figure 3.3. SEM pictures of the photoresponsive $[P_{6,6,6,14}][NTf_2]$ ionogel microstructures: rings (left) and lines (right).

3.3.3 Characterisation of the swelling behaviour of the ionogel microstructures

In this chapter, the swelling behaviour determines the microstructure performance, and therefore it is one of the basic properties that needs to be considered if it is to form the basis of a useful polymer actuator.[9] Due to the large surface-area-to-volume ratio of the photopatterned microstructures compared to bulk macro scaled gel structures, the rates of water diffusion into and out of the gel are highly accelerated. The swelling behaviour is determined by the balance between the expanding force induced by the osmotic pressure of polymer solvation and the restoring force of the chain segments between the crosslinks.[34] In addition, the polymer anchoring restricts movement of the gel along the surface of the substrate, and therefore swelling at the ionogel-glass substrate interface is inhibited, leading to highly anisotropic gel expansion primarily in the direction away from the surface.[34] A quasi one-dimensional swelling in the direction away from the substrate occurs, as illustrated in Fig. 3.1C.[34] Therefore, this Chapter focus on the height change measurements of the ionogel microstructures to investigate their swelling and shrinking behaviour. Moreover, for future applications of these materials as microvalves, due to the bonding with the bottom surface of the microchannel and their constriction within the microchannel walls, the change of the ionogel height will be crucial to determine the open-close state of the microvalve.

The two main parameters used to characterise the swelling process of the ionogel microstructures are the degree of swelling, which corresponds to the relative change of the ionogel height (in our case $\%H$) and the swelling time to reach the photostationary state (PSS).[34] The kinetics of the swelling process was monitored by immersing $[P_{6,6,6,14}][NTf_2]$, $[P_{6,6,6,14}][dca]$ and

$[P_{6,6,6,14}][Cl]$ ionogels (small discs, large discs, lines and rings microstructures) in a 0.1 mM HCl aqueous solution in the dark for 140 min at room temperature. The 3D visualisation of the height change upon swelling of $[P_{6,6,6,14}][dca]$ large disc ionogels is presented in Fig. A3, Appendix. Each ionogel was analysed in triplicate and the resulting kinetic curves for the large disc-shaped ionogels are presented in Fig. A4, Appendix. From the graphs it is evident that the swelling process is reproducible for each ionogel (see the Appendix A, Fig. A4) and microstructure (see the Appendix A, Table A2). The average $\%H$ of the large disc microstructures during immersion in 1 mM HCl solution *versus* time is plotted in Fig. 3.4A.

3.3.3.1. Swelling rates of the disc shaped phosphonium ionogels

First-order kinetic models were fitted (Microsoft Excel Solver)[33] to the experimental data (Fig. 3.4a) and the rate constants of the swelling process (k_{sw}) were estimated for each large disc-shaped ionogel using Eqn. 3.1. The swelling rate constant k_{sw} values obtained for all the ionogels fall into the same order of magnitude, Table 3.1. The value of k_{sw} for the $[NTf_2]^-$ based ionogel ($5.3 \pm 0.1 \times 10^{-2}$ s^{-1}) is *ca.* 1.2 times larger than k_{sw} of $[dca]^-$ ($4.5 \pm 0.3 \times 10^{-2}$ s^{-1}) and 1.4 times larger than k_{sw} of $[Cl]^-$ ($3.9 \pm 0.2 \times 10^{-2}$ s^{-1}).

Table 3.1. Rate constants of swelling and shrinking of pSPNIPAAm ionogels at 21 °C ($n = 3$).

IL used	***Average* k_{sw} (x 10^{-2}) [s^{-1}]**	***Average* k_{sh} (x 10^{-2}) [s^{-1}]**
$[P_{6,6,6,14}][NTf_2]$	5.3 ± 0.1	29.3 ± 3.5
$[P_{6,6,6,14}][dca]$	4.5 ± 0.3	8.3 ± 0.9
$[P_{6,6,6,14}][Cl]$	3.9 ± 0.2	9.1 ± 1.5

When exposed to an acidic environment, non-polar, colourless "spiro" form (SP) spontaneously converts to the coloured "merocyanine" form (MC-H^+). The formation of MC-H^+ leads to gel expansion in an acidic environment, however, for swelling to occur in the ionogels, the IL needs to be able to rearrange to accommodate not only water molecules but also the changing charged environment on the polymer (*i.e.* MC-H^+). We suggest that the charge delocalisation of the IL anion may contribute significantly to the hydrogen ion transport during the protonation process of SP to MC-H^+ and in turn to changing the ionogel environment from hydrophobic to more hydrophilic. The correlation between proton affinity and charge delocalisation of ionic liquid anions has been reported previously, whereby a greater degree of delocalisation lowers the proton affinity.[37] The swelling extent observed with these ionogels is in the order $[NTf_2]^- > [dca]^- > [Cl]^-$, (in terms of the anion of the IL) which is the opposite that might be predicted on the basis of water uptake capacity of the pure ILs, which was reported previously as 0.7 %, 3.1 %, 8.0 % w/w, respectively.[38] The reason for this difference in trend is not clear at this point, but it may lie in the way the ions interact with the gel polymer chains, and the impact of these interactions on IL nano-domain structure.[39, 40]

In $[P_{6,6,6,14}][Cl]$, the $[Cl]^-$ anions are very closely associated with the $[P_{6,6,6,14}]^+$ cations, to an extent wherein the charge is effectively shielded from the local environment, conveying a much more hydrophobic character to this ionic liquid than might be expected.[41] Consequently, the ionogels incorporating this IL do not swell to anything like the same extent as the gels incorporating $[P_{6,6,6,14}][NTf_2]$, and $[P_{6,6,6,14}][dca]$, as the ions in these latter ILs are less strongly associated, and therefore more free to exert their charged nature on their surrounding environment. Furthermore, in $[dca]^-$, the negative charge is extensively delocalised from the nitrogen across the whole molecule

through π conjugation, reducing its impact compared to $[NTf_2]^-$.[42, 43]

3.3.3.2. Percentage height change of ionogels upon swelling

The ionogels based on $[P_{6,6,6,14}][dca]$, $[P_{6,6,6,14}][NTf_2]$ and $[P_{6,6,6,14}][Cl]$ in the shape of large discs were kept in 1 mM HCl aqueous solution in the dark for 140 min at room temperature to study the time required to reach the PSS. All studied ionogels reached a steady-state swollen form after approximately 80 min and therefore, the shrinking behaviour was evaluated after soaking the ionogels microstructures in 1 mM HCl solution for 120 min, to be sure that they reached PSS, as explained before. As the ionogel is essentially anhydrous at the initial state, the chemical potential drive for water absorption into the IL is large, but despite this, there are significant differences in the degree of expansion between the phosphonium-based ionogels at the PSS. Values of *%H* for large disc ionogels microstructures at the PSS were 128 ± 8 %, 58 ± 2 % and 20 ± 3 % for $[NTf_2]^-$, $[dca]^-$ and $[Cl]^-$, respectively (Fig. 3.4A). As shown in Fig. 3.5 and Table A2, the same degree of swelling applies for all kinds of photopatterned microstructures. Depending on the shape of the microstructures, the *%H* of $[P_{6,6,6,14}][NTf_2]$, ionogels is in the range of 109 – 180 %, followed by $[P_{6,6,6,14}][dca]$ ionogels (40 – 58 %) and finally $[P_{6,6,6,14}][Cl]$ ionogels reaching just 20 - 27 %. Although $[P_{6,6,6,14}][NTf_2]$ is rather hydrophobic IL,[38] the $[NTf_2]^-$ anion can still re-arrange to accommodate a high amount of water within ionogel, thus resulting in the largest increase in *%H* (Fig. 3.4 and Fig. 3.5). The *%H* order again follows increasing charge delocalisation from $[Cl]^- < [dca]^- < [NTf_2]^-$. The weakly basic $[NTf_2]^-$ anion exhibits an extensive charge delocalisation within the S-N-S backbone $[NTf_2]^-$ anion,[44] and as a result it has a less affinity to nucleation sites in the p(SPNIPAAm) polymer backbone. As a consequence, the polar groups of the

polymer and the $[NTf_2]^-$ anions are more free to interact with water, and $[P_{6,6,6,14}][NTf_2]$ ionogels therefore draw a higher amount of water into the polymer matrix, resulting in the fastest and largest *%H.* In contrast, the $[Cl]^-$ anion charge is highly localised, and interaction with the polymer backbone is much stronger.[41] Consequently, the $[Cl]^-$ anions and the polar groups on the polymer backbone are less free to interact with water molecules, and therefore the smallest percentage change in *%H* therefore occurs with $[P_{6,6,6,14}][Cl]$ based ionogels. The charge delocalisation of $[dca]^-$ anion is intermediate between the $[NTf_2]^-$ and $[Cl]^-$ anions used in this study, which is reflected in the intermediate extent of swelling observed with the corresponding $[P_{6,6,6,14}][dca]$ ionogel.

The trend in the degree of swelling in the ionogels may also be related to the contrasting porosities as the preparation IL was varied. SEM micrographs of the $[P_{6,6,6,14}][NTF_2]$, $[P_{6,6,6,14}][dca]$ and $[P_{6,6,6,14}][Cl]$ ionogel surfaces clearly show that the type of IL has significant influence on the morphology of resulting material before and after hydration (see Appendix, Fig. A5). In its initial non-hydrated state, the $[P_{6,6,6,14}][NTf_2]$ ionogels display a highly porous structure, efficiently pre-disposed for water uptake (see the Appendix A, Fig. A5A, left). As the hydration process proceeds, the morphology changes, clearly showing a fully saturated exterior (see Appendix A, Fig. A5A, right). Interestingly, under equivalent conditions $[P_{6,6,6,14}][dca]$ ionogel exhibits a more compact surface, whilst still porous in places (see Appendix A, Fig A5B). In contrast, the ionogel based on $[P_{6,6,6,14}][Cl]$ presented a distinctly different morphology in the non-hydrated and hydrated states, forming compact surface without any visible pores (see Appendix A, Fig. A5C). Solvatomorphological effects have been found to correlate with the *%H* values at the PSS – the more porous matrix of the $[P_{6,6,6,14}][NTf_2]$ ionogel

provides more surface area per unit volume to accommodate water (higher $\%H$) in comparison to the $[P_{6,6,6,14}][dca]$ and $[P_{6,6,6,14}][Cl]$ ionogels, and this probably contributes to the more rapid kinetics of water uptake and release, and the greater extent of swelling (higher $\%H$).

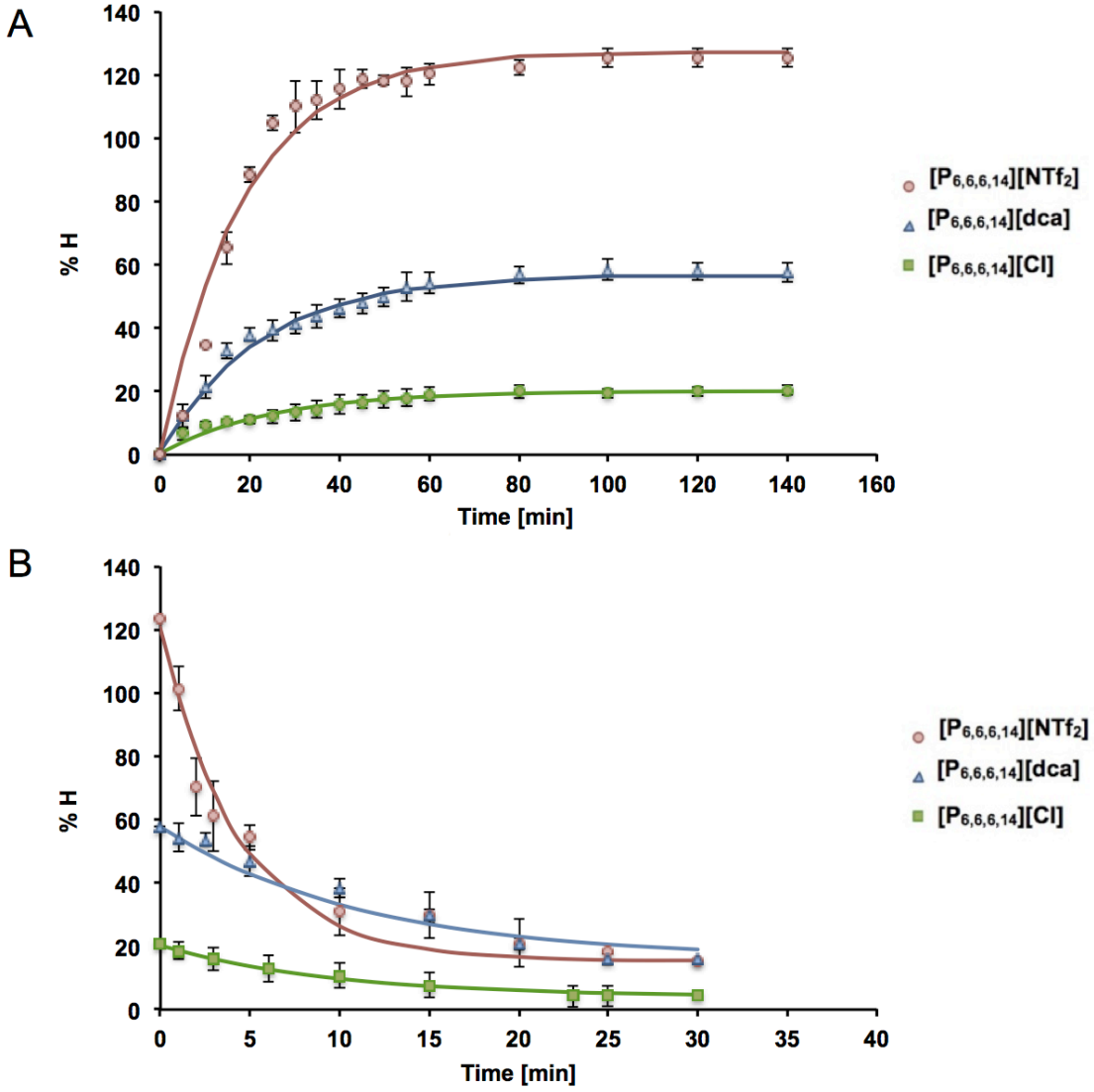

Figure 3.4. A) Swelling kinetics of p(SPNIPAAm) large disc ionogels in 1 mM HCl in the dark; and b) kinetics of shrinking induced by white light irradiation at 21 °C ($n = 3$).

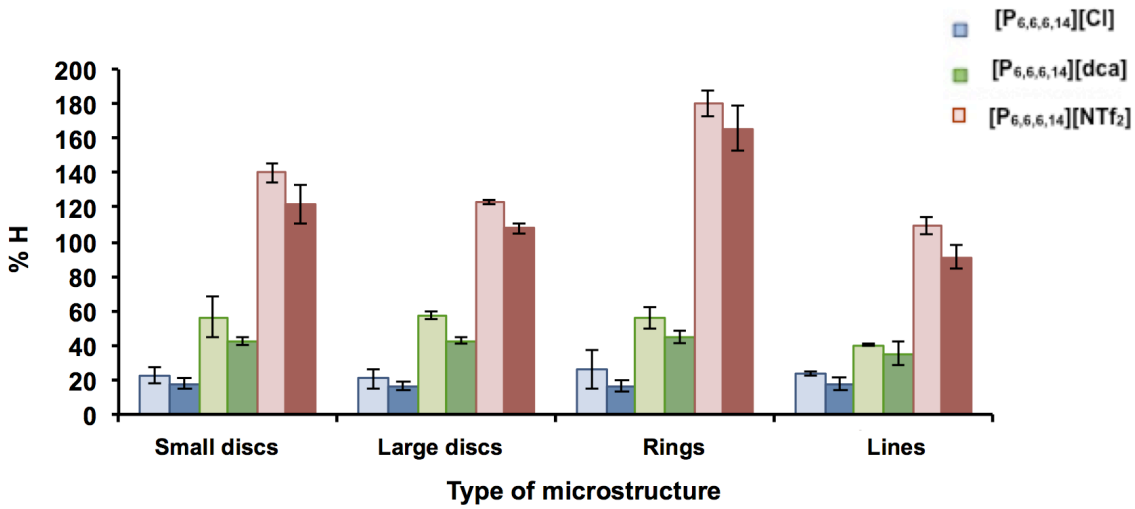

Figure 3.5. Swelling (after 120 min; bright colours) and shrinking after 30 min (dark colours) *%H* values for all the ionogel microstructures when using $[P_{6,6,6,14}][Cl]$ (blue), $[P_{6,6,6,14}][dca]$ (green) and $[P_{6,\ 6,6,14}][NTf_2]$ (red) ($n = 3$).

3.3.4 Influence of surface-area-to-volume ratio on the swelling rate of microstructures

For microvalve applications, a fast response is desirable, and as these materials undergo abrupt changes in volume in response to external stimuli, they may be suitable candidates for this type of application. The kinetics of swelling in ionogels is typically governed by diffusion-limited transport of the gel network in water,[45] and this is related to both the energy driving the process, and the surface area to volume ratio (SA/V). For example, when transforming between from a compact, contracted gel form to an open, swollen form, the polymer chains must physically migrate away from each other through the liquid phase (and vice versa). Therefore, miniaturisation of the gel features should yield an improvement in the rate of the swelling process[34] since the rate of diffusion is inversely proportional to the square of the dimension of the gel.[45, 46]

Therefore, the effect of SA/V of the microstructures on the swelling behaviour was investigated. Differently shaped $[P_{6,6,6,14}][NTf_2]$ ionogels were

photopolymerised as described before, and their SA/V values were estimated as follows: rings (SA/V = 0.0220 ± 0.0007), small discs (diameter = 250 μm, SA/V = 0.0150 ± 0.0003), large discs (diameter = 500 μm, SA/V = 0.0120 ± 0.0002) and lines (SA/V = 0.0090 ± 0.0006), as shown in Fig. A2 (see Appendix A) and Fig. 3.6. Each ionogel sample was immersed in 1 mM HCl aqueous solution in the dark at 21 °C and the $\%H$ value measured after 30 min. The results confirm that at a fixed time interval (t = 30 min) the higher the surface-area-to-volume ratio (SA/V), the greater $\%H$ for all the ionogel microstructures tested. Fig. 3.6 shows that the largest $\%H$ was observed for the rings, as these had the highest value of SA/V, while line shaped ionogels with the lowest SA/V ratio exhibited the smallest percentage of height change. The explanation for this behaviour lies in the swelling mechanism of the ionogel itself. If a structure is infinitesimally small (high SA/V ratio), then essentially everything is interfacial (surface) and there is no bulk. The swelling of such structures is described by a rate constant for interfacial transfer of water from the external solution into the interfacial polymer region, k_{int}. Therefore in the case of ionogel microstructures with high SA/V ratio values, *e.g.* rings, predominantly anisotropic water diffusion in the gel is very fast in all the gel matrix directions. Due to high surface-area-to-volume ratios at the microscale, mass transfer times and diffusion distances are shorter, facilitating faster actuation times,[47] in our case - swelling.

However, once a bulk region is introduced (microstructures with small SA/V ratio values), two processes emerge:

1. Transfer of the water from the external solution into the interfacial region (this will have the same rate constant as above, k_{int}).

2. Diffusion of water from the interfacial region into the bulk (the rate constant will be different from (1) – slower; $k_{bulk} < k_{int}$).

With the increase of the bulk region, a whole series of bulk layers is

envisaged with bulk-bulk water transfer rate constants, in which the transfer of water further into the bulk can only begin once water has reached the previous bulk layer. As a consequence, if the bulk region is made larger, the overall time for diffusion to establish a steady state throughout the entire structure becomes increasingly longer. Therefore, the 'effective rate constant' for the structure changes with the bulk-to-surface ratio, but the fundamental processes involved are the same. This phenomenon clearly supports our findings, that the fastest water diffusion dependent swelling process occurs for ring-shaped ionogels, followed by small disc, large disc and line microstructures, see Fig. 3.6.

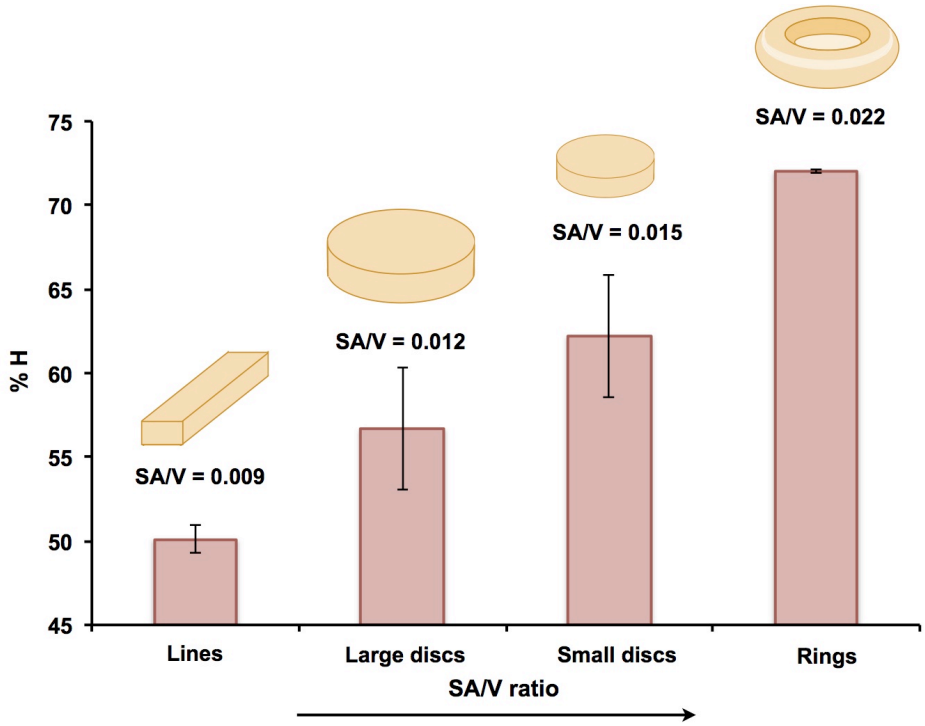

Figure 3.6. *%H* after 30 min as a function of surface-area-to-volume ratio for the $[P_{6,6,6,14}][NTf_2]$ microstructures in the dark, immersed in 1 mM HCl; error bars are standard deviations, $n = 3$.

3.3.5 Characterisation of the shrinking behaviour of the ionogel microstructures

After immersion in HCl aqueous solution, the p(SPNIPAAm) ionogels have a yellow color caused by the formation of the MC-H^+ species. Exposure to white light induces photoisomerisation of the MC-H^+ form to the closed spirobenzopyran chromophore SP, resulting in a change of the ionogel colour from strong yellow to bright yellowish. The hydrophobic SP isomer induces the dehydration of the polymer and thus the shrinkage of the ionogel due to restructuring of the polymer matrix.

3.3.5.1. Shrinking rates of ionogel microstructures

The kinetics of the shrinking behaviour of $[P_{6,6,6,14}][NTf_2]$, $[P_{6,6,6,14}][dca]$ and $[P_{6,6,6,14}][Cl]$ ionogels, monitored by white light irradiation for 30 min, shows that the IL plays an important role in the ionogel dehydration mechanism, similar to the swelling process. Fig. A6, Appendix, presents the kinetic curves of the large disc ionogel microstructures analysed in triplicate, showing that the shrinking process is reproducible for each ionogel and the related microstructures (see Appendix A, Table A2). Under constant white light irradiation, the $\%H$ values *vs.* time were obtained, and the average values fitted to exponential models (Eqn. 3.2), see Fig. 3.4B. Table 3.1 lists the shrinking rate constants of the ionogels. The largest shrinkage rate was observed for the $[P_{6,6,6,14}][NTf_2]$ ionogel microstructures with k_{sh} = 29.3 ± 3.5 x 10^{-2} s^{-1}, followed by $[Cl]^-$ (9.1 ± 1.5 x 10^{-2} s-1) and $[dca]^-$ (8.3 ± 0.9 x 10^{-2} s^{-1}) based ionogels. A video of the $[P_{6,6,6,14}][NTf_2]$ ring ionogel microstructures shrinking can be viewed at http://tinyurl.com/d5yvq6l (see Appendix A, Fig. A7).

Although stronger light irradiation may induce a faster isomerisation of

the protonated merocyanine to spiropyran, the dehydration of the polymer and subsequent ionogel shrinkage is not an immediate process since it requires a few minutes to reach ca. 50 % shrinkage of its initial swollen value. $[NTf_2]^-$ ionogels reached 50 % of their swollen height after 3 min, $[Cl]^-$ after 10 min and $[dca]^-$ after 15 min of irradiation, Fig. 3.4B. However, it is important to mention that when these materials are incorporated within microfluidic manifolds for microvalve applications, only a relatively small percentage of height change is required to open the valve. Therefore, valves based on these materials in microfluidic channels will typically occur at much shorter timescales (seconds).[22]

The *%H* of all the photopolymerised microstructures was measured after 30 min (Fig. 3.4B, Fig. 3.5) of white light irradiation following the same protocol described above. In all cases, the $[P_{6,6,6,14}][NTf_2]$ microstructures exhibit the greatest *%H* reduction, followed by $[P_{6,6,6,14}][dca]$ and $[P_{6,6,6,14}][Cl]$. There are several interesting outcomes arising from these experiments. For all the ionogels, the water release is clearly dependent on the IL encapsulated in the crosslinked p(SPNIPAAm) ionogel. As the ionogel shrinks, the water and ionic liquid interactions with the polymer backbone (*eg.* hydrogen bonding with pNIPAAm amide groups) are reduced in favour of increasingly strong polymer-polymer hydrogen bonding. In turn, the gel adopts more compact format, which also reduces the free volume available for water to occupy. This effect is more apparent in ionogels with more hydrophobic ionic liquids, such as $[P_{6,6,6,14}][NTf_2]$, leading to greater and faster shrinkage. The experiments presented in this chapter demonstrate that the ionogel k_{sh} increases with increasing hydrophobicity of the IL. Dehydration is more favourable for $[NTf_2]^-$ than for $[Cl]^-$ and $[dca]^-$, since $[NTf_2]^-$ presents six hydrophobic fluoride groups and consequently, exhibits larger tendency towards

dehydration.[38] The water release process is triggered by MC-H^+ – SP conversion, during which the polarity of the ionogel changes from hydrophilic to hydrophobic.[41] Therefore, the induced water expulsion will be promoted by more hydrophobic ILs, such as $[P_{6,6,6,14}][NTf_2]$, resulting in faster shrinking in comparison to more hydrophilic ionogels using ILs such as $[P_{6,6,6,14}]$[dca] or $[P_{6,6,6,14}]$[Cl]. The $[NTf_2]^-$ based ionogel shows the fastest actuation of the three ionogels, in agreement with previous published work,[10] that explains how $[NTf_2]^-$ anion does not interact with the MC form and therefore it does not inhibit the light induced thermal relaxation of MC to its ground non-zwitterionic state.

Another factor that can attribute to the shrinkage rates is the porosity of the ionogel structure, as this affects the SA/V ratio, and provides effective routes for water transport into and out of the bulk gel structure.[11] This is consistent with the behaviour of the $[NTf_2]^-$ ionogels compared to the other ionogels, as it exhibits a microporous structure (see Appendix A, Fig. A5) and has the fastest shrinking kinetics. The most probable reason for the rapid shrinking of the ionogels is the presence of large pores, and the open network mesh structure, which allows rapid collapse of the polymer chains.[48]

3.3.5.2. Height change of ionogels upon shrinking process

Fig. 3.4B and Fig. A8 (see Appendix A) show that after 30 min of white light irradiation, each ionogel microstructure exhibited various degrees of expulsion of absorbed water. $[NTf_2]^-$ disc ionogels exhibit a total of 108 % shrinkage, reaching *ca.* 15 % of the ionogel height in its swollen state (H_{sw}). In the case of $[dca]^-$ based microstructures, they exhibit 42 % shrinkage reaching also *ca.* 15 % of their H_{sw} for the same irradiation time. Finally, $[Cl]^-$ ionogels exhibit the smallest percentage shrinking (16 %). However, after 30 min of

irradiation they reached 4 % of H_{sw}, indicating that they almost reverted back to their initial size, prior to swelling.

These experimental results demonstrate that the swelling and shrinking behaviour of the ionogels are strongly influenced by the ionic liquid incorporated into the gel during photopolymerisation. Dramatic differences in swelling/shrinking behaviour of the ionogels can be seen if the ionic liquid is used alone or in a mixture with other organic solvents. In previous work, the order of actuation found with similar ionogels produced using 1:1 butanol IL v/v was different ($[P_{6,6,6,14}][dca]$ based ionogels were faster than ionogels incorporating $[P_{6,6,6,14}][NTf_2]$). The reason for this difference is not clear at present, but may lie in differing amounts of residual butanol remaining in the ionogels after formation, which affects the overall gel polarity and affinity for water. This opens the possibility of tuning the actuation of the microvalves by varying the solvent composition used for the synthesis of ionogel.

3.4 Conclusions

A simple and low cost photolithography set-up was developed and successfully applied for the photopolymerisation of ionogel microstructures and patterns. Although it has been applied specifically to ionogels, this method can be expanded to a variety of other materials. This technique also has a number of advantages over other patterning methods, the foremost being its simplicity and low cost. A variety of phosphonium based ionogel microstructures were fabricated, including discs, rings and lines, and their volume phase transition behaviour and swelling/shrinkage kinetics were investigated. Results show that the ionic liquids entrapped within the polymer matrix have a significant influence on the actuation of the ionogel microstructures. It was found that the p(SPNIPAm) swelling/shrinking

properties could be significantly altered by varying the anion of the phosphonium IL. $[P_{6,6,6,14}][NTf_2]$ ionogel microstructures undergo the largest volume expansion, up to 180 % of their initial size, and the fastest swelling and shrinking kinetics (k_{sw}= 5.3 ± 0.1 x 10^{-2} s^{-1} and k_{sh} = 29.3 ± 3.5 x 10^{-2} s^{-1}). It has been proved that each ionic liquid provides a specific and well defined degree of volume change ($\%H$) and photoresponse time of the microstructures. Therefore, this work presents the tremendous potential of using ionogels microstructures as microactuators with potential in microfluidic applications and set the basis for the work presented in the following chapters to develop photoswitchable ionogel microvalves within microfluidic manifolds.

3.5 Acknowledgements

M.C wishes to thank to the Marie Curie Initial Training Network funded by the EC FP7 People Program ATWARM (Advanced Technologies for Water Resource Management, Marie Curie ITN, No. 238273). K.J.F thanks Marie Curie Actions re-integration grant PIRG07-GA-2010-268365. D.D & F.B.L thank the Science Foundation Ireland under grant 07/CE/I1147. The authors are grateful to Dr. Al Robertson from Cytec® industries for the generous donation of phosphonium ILs. The authors would also like to thank Dr. Katya Izgorodina, Monash University, for useful discussion throughout and Larisa Florea for assistance in taking SEM micrographs.

3.6 References

1. Czugala, M.; Ziółkowski, B.; Byrne, R.; Diamond, D.; Benito-Lopez, F., Materials science: the key to revolutionary breakthroughs in micro-fluidic devices. *Proc. SPIE 8107, Nano-Opto-Mechanical Systems (NOMS)* **2011**, 81070C-81070C.

2. Xie, Z.-L.; Jelicic, A.; Wang, F.-P.; Rabu, P.; Friedrich, A.; Beuermann, S.; Taubert, A., Transparent, flexible, and paramagnetic ionogels based on PMMA and the iron-based ionic liquid 1-butyl-3-methylimidazolium tetrachloroferrate(III) [Bmim][$FeCl_4$]. *Journal of Materials Chemistry* **2010,** *20* (42), 9543-9549.
3. Suzuki, H., Stimulus-responsive gels: promising materials for the construction of micro actuators and sensors. *Journal of Intelligent Material Systems and Structures* **2006,** *17* (12), 1091-1097.
4. Lo, C.-W.; Zhu, D.; Jiang, H., An infrared-light responsive graphene-oxide incorporated poly(*N*-isopropylacrylamide) hydrogel nanocomposite. *Soft Matter* **2011,** *7* (12), 5604.
5. Orlov, M.; Tokarev, I.; Scholl, A.; Doran, A.; Minko, S., pH-responsive thin film membranes from poly(2-vinylpyridine): water vapor-induced formation of a microporous structure. *Macromolecules* **2007,** *40* (6), 2086-2091.
6. Liu, F.; Urban, M. W., Challenges and opportunities in stimuli-responsive polymeric materials. *Progres in Polymer Science* **2010,** *35* (3), 3-23.
7. Kuckling, D.; Richter, A.; Arndt, K.-F., Temperature and pH-dependent swelling behavior of poly(*N*-isopropylacrylamide) copolymer hydrogels and their use in flow control. *Macromolecular Materials and Engineering* **2003,** *288* (2), 144-151.
8. Inomata, H.; Goto, S.; Saito, S., Phase transition of *N*-substituted acrylamide gels. *Macromolecules* **1990,** *23* (22), 4887-4888.
9. Ziółkowski, B.; Czugala, M.; Diamond, D., Integrating stimulus responsive materials and microfluidics: The key to next-generation chemical sensors. *Journal of Intelligent Material Systems and Structures* **2012**, doi: 10.1177/1045389X12459591.
10. Byrne, R.; Fraser, K. J.; Izgorodina, E.; MacFarlane, D. R.; Forsyth, M.; Diamond, D., Photo- and solvatochromic properties of nitrobenzospiropyran in ionic liquids containing the $[NTf_2]^-$ anion. *Physical Chemistry Chemical Physics* **2008,** *10* (38), 5919-5924.
11. Wu, X. S.; Hoffman, A. S.; Yager, P., Synthesis and characterization of thermally reversible macroporous poly(*N*-isopropylacrylamide) hydrogels. *Journal of Polymer Science Part A: Polymer Chemistry* **1992,** *30* (10), 2121-2129.
12. Sumaru, K.; Kameda, M.; Kanamori, T.; Shinbo, T., Characteristic phase transition of aqueous solution of poly(*N*-isopropylacrylamide) functionalized with spirobenzopyran. *Macromolecules* **2004,** *37* (13), 4949-4955.

13. Sugiura, S.; Sumaru, K.; Ohi, K.; Hiroki, K.; Takagi, T.; Kanamori, T., Photoresponsive polymer gel microvalves controlled by local light irradiation. *Sensors and Actuators A: Physical* **2007,** *140* (2), 176-184.
14. Satoh, T.; Sumaru, K.; Takagi, T.; Kanamori, T., Fast-reversible light-driven hydrogels consisting of spirobenzopyran-functionalized poly(*N*-isopropylacrylamide). *Soft Matter* **2011,** *7* (18), 8030-8034.
15. Sumaru, K.; Ohi, K.; Takagi, T.; Kanamori, T.; Shinbo, T., Photoresponsive properties of poly(*N*-isopropylacrylamide) hydrogel partly modified with spirobenzopyran. *Langmuir* **2006,** *22* (9), 4353-4356.
16. Sugiura, S.; Szilagyi, A.; Sumaru, K.; Hattori, K.; Takagi, T.; Filipcsei, G.; Zrinyi, M.; Kanamori, T., On-demand microfluidic control by micropatterned light irradiation of a photoresponsive hydrogel sheet. *Lab on a Chip* **2009,** *9* (2), 196-198.
17. Kavanagh, A.; Byrne, R.; Diamond, D.; Fraser, K. J., Stimuli responsive ionogels for sensing applications—An overview. *Membranes* **2012,** *2* (1), 16-39.
18. Ueki, T.; Watanabe, M., Macromolecules in ionic liquids: Progress, challenges, and opportunities. *Macromolecules* **2008,** *41* (11), 3739-3749.
19. Gallagher, S.; Kavanagh, A.; Florea, L.; MacFarlane, D. R.; Fraser, K. J.; Diamond, D., Temperature and pH triggered release characteristics of water/fluorescein from 1-ethyl-3-methylimidazolium ethylsulfate based ionogels. *Chemical Communications* **2013,** *49* (41), 4613-4615.
20. F. Benito-Lopez; S. Coyle; R. Byrne; M. O'Toole; C. Barry; D.Diamond, Simple barcode system based on ionogels for real time pH-sweat monitoring. In *BSN 2010 - 7th International Workshop on Wearable and Implantable Body Sensor Network*, Singapore, **2010**, 291-296.
21. Kavanagh, A.; Byrne, R.; Diamond, D.; Radu, A., A two-component polymeric optode membrane based on a multifunctional ionic liquid. *Analyst* **2011,** *136* (2), 348-353.
22. Benito-Lopez, F.; Byrne, R.; Răduţă, A. M.; Vrana, N. E.; McGuinness, G.; Diamond, D., Ionogel-based light-actuated valves for controlling liquid flow in micro-fluidic manifolds. *Lab on a Chip* **2010,** *10* (2), 195-201.
23. Ziółkowski, B.; Ates, Z.; Gallagher, S.; Byrne, R.; Heise, A.; Fraser, K. J.; Diamond, D., Mechanical properties and UV curing behavior of poly(*N*-isopropylacrylamide) in phosphonium-based ionic liquids. *Macromolecular Chemistry and Physics* **2013,** *214*, 787-796.
24. Hoffmann, J.; Plotner, M.; Kuckling, D.; Fischer, W.-J., Photopatterning of thermally sensitive hydrogels useful for microactuators. *Sensors and Actuators A: Physical* **1999,** *77* (2), 139-144.

25. Liu, R. H.; Qing, Y.; Beebe, D. J., Fabrication and characterization of hydrogel-based microvalves. *Journal of Microelectromechanical Systems,* **2002,** *11* (1), 45-53.
26. Tang, M. D.; Golden, A. P.; Tien, J., Molding of three-dimensional microstructures of gels. *Journal of the American Chemical Society* **2003,** *125* (43), 12988-12989.
27. Wang, Z.; Hu, H.; Wang, Y.; Wu, Q.; Liu, L.; Chen, G., Fabrication of poly(3-hydroxybutyrate-co-3-hydroxyhexanoate) (PHBHHx) microstructures using soft lithography for scaffold applications. *Biomaterials* **2006,** *27* (12), 2550-2557.
28. Kobel, S.; Limacher, M.; Gobaa, S.; Laroche, T.; Lutolf, M. P., Micropatterning of hydrogels by soft embossing. *Langmuir* **2009,** *25* (15), 8774-8779.
29. Hou, C.; Herr A., Ultrashort separation length homogeneous electrophoretic immunoassays using on-chip discontinuous polyacrylamide gels. *Analytical Chemistry* **2010,** *82* (8), 3343-51.
30. Beebe, D. J.; Moore, J. S.; Bauer, J. M.; Yu, Q.; Liu, R. H.; Devadoss, C.; Jo, B.-H., Functional hydrogel structures for autonomous flow control inside microfluidic channels. *Nature* **2000,** *404* (6778), 588-590.
31. Yeom, J.; Shannon, M. A., Detachment lithography of photosensitive polymers: A route to fabricating three-dimensional structures. *Advanced Functional Materials* **2010,** *20* (2), 289-295.
32. Szilagyi, A.; Sumaru, K.; Sugiura, S., Takagi, T., Shinbo, T., Zrinyi, M.; Kanamori, T., Rewritable microrelief formation on photoresponsive hydrogel layers. *Chemistry of Materials* **2007,** *19*, 2730–2732.
33. Diamond, D.; Hanratty, V. C. A., Spreadsheet Applications for Chemistry Using Microsoft Excel. John Wiley and Sons: New York, 1997.
34. Mateescu, A.; Wang, Y.; Dostalek, J.; Jonas, U., Thin hydrogel films for optical biosensor applications. *Membranes* **2012,** *2* (1), 40-69.
35. Kavanagh, A.; Copperwhite, R.; Oubaha, M.; Owens, J.; McDonagh, C.; Diamond, D.; Byrne, R., Photo-patternable hybrid ionogels for electrochromic applications. *Journal of Materials Chemistry* **2011,** *21*, 8687-8693.
36. Narayan, R. J.; Doraiswamy, A.; Chrisey, D. B.; Chichkov, B. N., Medical prototyping using two photon polymerization. *Materials Today* **2010,** *13* (12), 42-48.
37. Izgorodina, E. I.; Forsyth, M.; MacFarlane, D. R., Towards a better understanding of delocalized charge in ionic liquid anions. *Australian Journal of Chemistry* **2007,** *60* (1), 15-20.
38. Forsyth, S. A.; Pringle, J. M.; MacFarlane, D. R., Ionic liquids - An overview. *Australian Journal of Chemistry* **2004,** *57* (2), 113-119.

39. Shimizu, K.; Padádua, A. A. H.; Canongia Lopes, J. N., Nanostructure of trialkylmethylammonium bistriflamide ionic liquids studied by molecular dynamics. *The Journal of Physical Chemistry B* **2010,** *114* (47), 15635-15641.
40. Coleman, S.; Byrne, R.; Minkovska, S.; Diamond, D., Investigating nanostructuring within imidazolium ionic liquids: A thermodynamic study using photochromic molecular probes. *The Journal of Physical Chemistry B* **2009,** *113* (47), 15589-15596.
41. Thompson, D.; Coleman, S.; Diamond, D.; Byrne, R., Electronic structure calculations and physicochemical experiments quantify the competitive liquid ion association and probe stabilisation effects for nitrobenzospiropyran in phosphonium-based ionic liquids. *Physical Chemistry Chemical Physics* **2011,** *13* (13), 6156-6168.
42. Deng, M.-J.; Chen, P.-Y.; Leong, T.-I.; Sun, I. W.; Chang, J.-K.; Tsai, W.-T., Dicyanamide anion based ionic liquids for electrodeposition of metals. *Electrochemistry Communications* **2008,** *10* (2), 213-216.
43. Illner, P.; Begel, S.; Kern, S.; Puchta, R.; van Eldik, R., Fast substitution reactions of Pt(II) in different ionic liquids. Reactivity control by anionic components, *Inorganic Chemistry* **2008,** *48* (2), 588-597.
44. Forsyth, C. M.; MacFarlane, D. R.; Golding, J. J.; Huang, J.; Sun, J.; Forsyth, M., Structural characterization of novel ionic materials incorporating the bis(trifluoromethanesulfonyl)amide anion. *Chemistry of Materials* **2002,** *14* (5), 2103-2108.
45. Yoshida, R.; Uchida, K.; Kaneko, Y.; Sakai, K.; Kikuchi, A.; Sakurai, Y.; Okano, T., Comb-type grafted hydrogels with rapid deswelling response to temperature changes. *Nature* **1995,** *374* (6519), 240-242.
46. Tanaka, T.; Sato, E.; Hirokawa, Y.; Hirotsu, S.; Peetermans, J., Critical kinetics of volume phase transition of gels. *Physical Review Letters* **1985,** *55* (22), 2455-2458.
47. Teh, S.-Y.; Lin, R.; Hung, L.-H.; Lee, A. P., Droplet microfluidics. *Lab on a Chip* **2008,** *8* (2), 198-220.
48. Li, X.; Wu, W.; Liu, W., Synthesis and properties of thermo-responsive guar gum/poly(*N*-isopropylacrylamide) interpenetrating polymer network hydrogels. *Carbohydrate Polymers* **2008,** *71* (3), 394-402.

Chapter 4

Portable integrated microfluidic analytical platform for the monitoring and detection of nitrite

M. Czugala,[1] C. Fay,[1] N. E. O'Connor,[1] B. Corcoran,[1] F. Benito-Lopez[1, 2, *]
Dermot Diamond[1]

Talanta, 2013, 997-1004
doi: 10.1016/j.talanta.2013.07.058

[1]CLARITY: Centre for Sensor Web Technologies, National Centre for Sensor Research, Dublin City University, Dublin 9, Ireland
[2]CIC microGUNE, Arrasate-Mondragón, SPAIN

For Supplementary Information see Appendix B, pg. 226.

Abstract

A wireless, portable, fully-integrated microfluidic analytical platform has been developed and applied to the monitoring and determination of nitrite anions in water, using the Griess method. The colour intensity of the Griess reagent nitrite complex is detected using a low cost Paired Emitter Detector Diode, while on-chip fluid manipulation is performed using a biomimetic photoresponsive ionogel microvalve, controlled by a white light LED. The microfluidic analytical platform exhibited very low limits of detection (34.0 ± 0.1 μg L^{-1} of NO_2^-). Results obtained with split freshwater samples showed good agreement between the microfluidic chip platform and a conventional UV-Vis spectrophotometer (R^2 = 0.98, RSD = 1.93 % and R^2 = 0.99, RSD = 1.57 %, respectively). The small size, low weight, and low cost of the proposed microfluidic platform coupled with integrated wireless communications capabilities make it ideal for *in-situ* environmental monitoring. The prototype device allows instrument operational parameters to be controlled and analytical data to be downloaded from remote locations. To our knowledge, this is the first demonstration of a fully functional microfluidic platform with integrated photo-based valving and photo-detection.

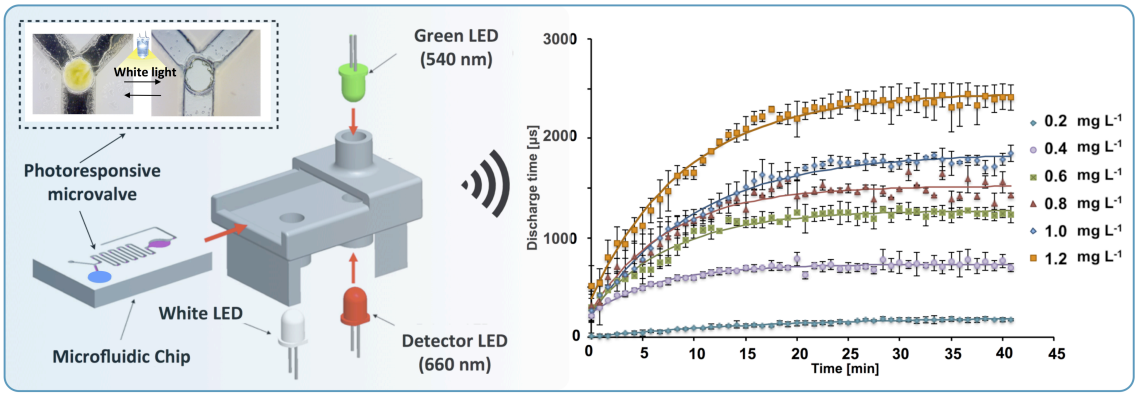

4.1 Introduction

Demand for environmental monitoring has grown substantially in recent years in response to increasing concerns over the contamination of natural, industrial, and urban areas with potentially harmful chemical agents. Environmental monitoring by regulatory agencies normally takes place on a manual basis, involving physical sampling and transportation of the samples to centralised facilities equipped with sophisticated instrumentation and analysed by highly trained personnel.[1] Advantages of employing this strategy include high precision and accuracy of the measurements, and adherence to regulatory methods for legal proceedings. However, because of the expense involved in maintaining these facilities and obtaining samples, there are inherent restrictions in terms of the degree of practical spatial and temporal monitoring.[2, 3] The use of recent technological breakthroughs may hold the key to addressing these issues. In both research and routine monitoring processes, *in-situ* chemical measurement offers substantial advantages relative to laboratory analysis. Prompt *in-situ* analysis, without human intervention, considerably reduces sample contamination possibilities, improves rates of sample throughput, and facilitates more rapid response to events. Furthermore, the use of autonomous sensor platforms opens opportunities for adaptive sampling of dynamic pollution events, either independently (*e.g.*, through automatic system control of sampling rates) or through human-directed responses (*e.g.,* surface-tethered control of sensor depth), in addition to ensuring substantial reductions in overall cost per measurement.

Characterisation of nutrient distribution within water bodies is critically important because, depending upon their concentrations, they have the potential to greatly disrupt the balance of an aquatic ecosystem. Natural and man-made environmental events can result in dramatic changes in

nutrient concentrations in aquatic waters, both in time and geographical distribution. The determination of nitrite (NO_2^-) levels in oceans, rivers, and drinking water is of importance for environmental monitoring agencies since nitrite is both a nutrient and an excretion product of phytoplankton, and it is important with respect to the global nitrogen and carbon cycles, with concomitant effects on climate.[4] The over-use of nitrogenous inorganic fertilisers, combined with the more general mismanagement of natural resources, have caused significant perturbation of both local and global nitrogen cycles.[5, 6] The high solubility and mobility of the nitrite and nitrate ions within soil and water have significantly contributed to the eutrophication of lakes and more recently coastal outfalls. This results in the generation of algal blooms that can wreak havoc with local ecological systems.[7] These problems have been widely recognised, and therefore monitoring the levels of nitrite is of major importance worldwide. Many lab-based analytical methods have been proposed for the determination of nitrite,[8, 9] but colorimetric methods are by far the most popular,[10] due to the excellent limits of detection, dynamic range, and cost efficiency. However, these characteristics can also form the basis of low-cost miniaturised sensors suitable for on-site analysis.

In particular, the spectrophotometric assay based on the Griess reagent has been very popular due to its high stability and sensitivity.[11] Early work in developing platforms for colorimetric sensing based on the Griess reaction was carried out by Greenway *et al.*[12] The system utilised electro-osmotic flow (EOF) for pumping and external optical components for absorbance measurements achieving a limit of detection (LOD) of 0.2 mM. Later, Sieben *et al.*[4] integrated a low cost optical illumination and detection method with a simple microfluidic system for nitrite detection using the Griess reaction with a limit of detection of 14 nM. Although there are commercial available

systems capable of measuring nitrite concentrations, their large physical size *(e.g.* 60 x 14 cm) and power consumption (typically greater than 100 W)[13] limit their practical use. Furthermore, due to the reactivity of the nitrite samples, deterioration can rapidly occur, and therefore a strong motivation also exists for the development of on-site measurement systems.[4]

An important aspect of environmental analysis is detection by optical methods. Unlike contact based sensors *e.g.* via electrochemical means, optical detection offers several advantages such as the necessity of a reference electrode required for electrochemical sensing, relative insensitivity to electrical interferences and the possibility of remote sensing. As a result, many environmental sensing systems have been reported based on a variety of light sensitive devices such as light dependant resistors,[14] photodiodes,[15] phototransistors,[16, 17] and imaging devices (cameras/scanners).[18, 19] However, the energy demands, reliability, and complexity of the sensor can be very significant limiting factors.[20] The paired emitter detector diode (PEDD) device allows overcoming these limitations because it possesses many advantages such as low cost, high resolution, increased sensitivity, ease of implementation, and a relatively low power demand. Recently it was shown that light emitting diodes (LEDs) based systems can be used for applications where high sensitivity is an absolute requirement.[21]

In recent years, advances in microfluidic techniques for environmental applications have opened opportunities for improvements in water quality monitoring.[4] However, the development of fully integrated microfluidic devices capable of performing complex functions requires the integration of microvalves with an appropriate performance, as they are essential tools for the control and manipulation of flows in microchannels.[22] The issue of liquid handling is a key factor inhibiting chemo-/biosensor network deployments for applications involving liquid-phase measurements such as water quality

monitoring, due to the cost and power demand of conventional valves, and their necessary use in off-chip configurations. Stimuli responsive materials, actuated by light irradiation, can significantly facilitate liquid movement within microfluidic devices. Several research groups have reported flow valves based on thermoresponsive poly(*N*-isopropylacrylamide) (pNIPAAm) polymer gels.[23,24] The fluid containing the block copolymer of poly(*N*-isopropylacrylamide-co-n-butyl methacrylate) and poly (ethylene glycol) was introduced into the microchannel, and the direction of the fluid was controlled by local sol–gel transformation of the polymer induced by infrared laser irradiation as strong as 650 mW. Fluid manipulation by ultraviolet (UV)[25] or 785 nm laser light[26] irradiation induced surface wettability change was also presented. Although the method is simple to manipulate fluids on microchips, once the channel is wetted with the fluid, it is difficult to stop the fluid. Sershern *et al.*[27] demonstrated light controlled nanocomposite hydrogel microvalves composed of pNIPAAm gels containing nanoparticles that have strong optical absorption. Optical energy from a laser light irradiation as strong as 1600–2700 mW cm^{-2} was transformed into heat by the nanoparticles, which induced shrinkage of the thermoresponsive pNIPAAm gels and the opening of microvalves. Although the fluid manipulation by light irradiation was successfully achieved, heat transfer between microvalves may well be a problem for controlling multiple integrated microvalves. Moreover, application of heat induced volume transition may not be suitable for the manipulation of fluids containing heat sensitive materials, such as proteins or cells. On the other hand, stimuli responsive microvalves based on pNIPAAM gels functionalised by spirobenzopyran chromophores (pSPNIPAAm) present an interesting option for fluid manipulation. Several groups have reported pSPNIPAAm gel microvalves, fabricated by *in-situ* photopolymerisation in the microchannel, and independently controlled by local light irradiation.[28, 29]

These photo-controlled microvalves provide non-contact, spatially independent and parallel fluid manipulation. Using ionogels rather than hydrogels, the physical robustness of the photoswitchable materials is increased. In contrast to conventional p(SPNIPAAm) hydrogels, which tend to physically collapse when dry, ionogels are protected from drying and cracking because of the negligible vapour pressure of the ionic liquid (IL) at room temperature. These polymer actuators can be integrated into microfluidic devices, providing a route to 'biomimetic' microfluidic systems that are inherently low power, and potentially more reliable in microchannels than equivalent conventional micro-engineered actuators.[2]

In this chapter, for the first time, the design, fabrication and testing of a wireless, portable, integrated microfluidic analytical platform for point-of-care monitoring and quantitative determination of nitrite in freshwater samples is reported. The miniaturised gold-standard Griess assay was implemented for detecting nitrite within a poly(methylmethacrylate) (PMMA) microfluidic device. The platform integrates optical fluid processing and detection, enabling monitoring of the kinetics of the Griess reaction and the detection of nutrient levels. For fluid control, the microfluidic device contains a biomimetic photo-switchable microvalve based on a phosphonium ionogel functionalised with spiropyran. The microvalve was simply actuated by illumination with a light emitting diode. In addition, the nitrite concentration was determined by a highly sensitive, low cost wireless PEDD detector, ensuring inexpensive fabrication and functioning of the whole platform.

4.2 Experimental

4.2.1 Chemicals and reagents

All solutions were prepared from analytical grade chemicals and

deionised water from a Millipore Milli-Q Q-GARD® 1 water purification system. Stock solutions were prepared freshly prior to use and stored in dark environment at room temperature for no longer than one week. The Griess reagent was prepared following this procedure: Firstly, a 5 % phosphoric acid solution was prepared by dissolving 5 g of phosphoric acid (H_3PO_4) in 100 mL of deionised water. Next, a 1 % sulfanilic acid solution was prepared by dissolving 1 g of sulfanilic acid in 100 mL of a 5 % phosphoric acid solution. A 0.1% *N*-(1-naphthyl)ethylenediamine dihydrochloride (NED) solution was prepared by dissolving 100 mg of NED in 100 mL of deionised water. Finally, 1 % sulfanilic acid solution and 0.1 % NED solution were mixed together forming a Griess reagent. A sodium nitrite ($NaNO_2$) stock solution was prepared by dissolving 0.3 g of $NaNO_2$ in 500 mL of deionised water. Nitrite standard solutions were diluted from a 200 mg L^{-1} $NaNO_2$ stock solution to the appropriate concentrations. Phosphoric acid, sulfanilic acid, *N*-(1-naphthyl)ethylenediamine dihydrochloride and sodium nitrite were purchased from Sigma-Aldrich®, Ireland and used without further purification.

For ionogel microvalve preparation *N*-isopropylacrylamide, *N*,*N*'-methylene-bis(acrylamide) (MBAAm), 2,2-5 dimethoxy-2-phenyl acetophenone (DMPA) were used and purchased from Sigma-Aldrich®, Ireland. 1′, 3′, 3′-Trimethyl-6-hydroxyspiro(2H-1-benzopyran- 2, 2′-indoline) (Acros Organics, Geel, Belgium), 3-(Trimethoxysilyl) propyl methacrylate was purchased from Sigma-Aldrich®, Ireland. Trihexyltetradecyl-phosphonium dicyanoamide $[P_{6,6,6,14}][dca]$ was obtained as compliments of Cytec® Industries, Ontario, Canada. Further purification was carried out as follows: 10 mL of IL decolourised by redissolution in 30 mL of acetone followed by treatment with activated charcoal (Darco-G60, Sigma-Aldrich®) at 40 °C overnight. Carbon was removed by filtration through alumina (acidic, Brockmann I, Sigma-Aldrich®) and the solvent removed under vacuum at 60 °C for 24 h at 0.1

Torr. A liquid prepolymer mixture was prepared by dissolving the NIPAAm monomer (0.75 mmol), the MBAAm (0.04 mmol), acrylated spirobenzopyran monomer (0.01 mmol) and the photo-initiator DMPA (0.02 mmol) into the ionic liquid (0.52 mmol).

4.2.2 Microfluidic device fabrication

The microfluidic device consists of a multi-layer structure made of poly(methyl methacrylate) and pressure-sensitive adhesive (PSA) sheets. Using a laser ablation system-excimer/CO_2 laser (Optec Laser Micromachining Systems, Belgium) reservoirs and microchannels were machined into the PMMA (PMMA, Radionics, Ireland) along with 50 μm and 86 μm thick double-sided, pressure-sensitive adhesive layers (PSA, Adhesives Research, Ireland). Once the appropriate pieces had been designed and machined, they were aligned and bonded using a thermal roller laminator (Titan-110, GBC Films, USA).

The ionogel microvalves were photopolymerised *in-situ* in a circular reservoir (500 μm radius; V_{IL} = 177 nL) for 25 min using a UV irradiation source (λ = 365 nm) placed 8 cm from the solution (UV intensity 10 mW cm^{-2}). When polymerisation was complete, the resulting ionogels were rinsed with deionised water to remove any un-polymerised monomer and excess of ionic liquid. The photopatterned ionogel microvalves were dried at room temperature for 24 h. Finally, the top PMMA layer was bonded to the microfluidic. Fig. 4.1A shows the microfluidic device fabrication procedure. After assembly the upper part of the microchannel (Y – branches) was then filled with 1 mM HCl aqueous solution and kept for 2 h at 21 °C for swelling of the p(SPNIPAAm) ionogels (closing of the microvalve).

The microfluidic device consisted of a small structure of 20 mm × 30 mm dimension, as shown in Fig. 4.1B. Round inlets for water sample (radius 2.25 mm) and for Griess reagent (radius 250 µm) are placed at the top of the Y-shaped channel. The junction of the collecting channels with the integrated microfluidic microvalve was followed by the mixing part of the channel which had a total length of 72 mm and was 1 mm wide. The detection chamber (radius 2.4 mm) was followed by a 1 mm wide channel to the outlet/waste area, which was connected with the back pressure system.

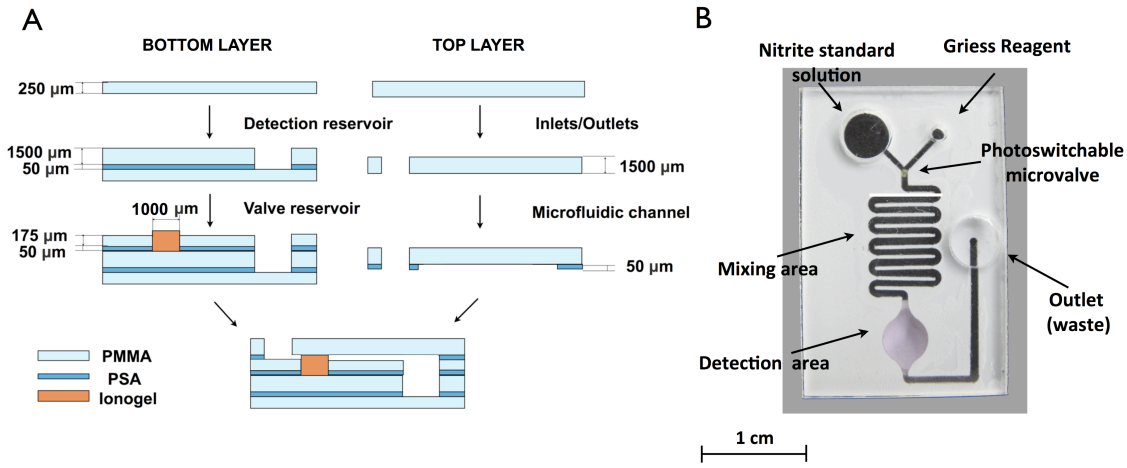

Figure 4.1. A) Schematic representation of the microfluidic device fabrication procedure. B) Picture of the microfluidic device fabricated in PMMA : PSA polymer by CO_2 laser ablation.

4.2.3 Portable, integrated microfluidic analytical platform fabrication

The control, communications, and detection system were designed to be compatible with the fabricated microfluidic device. A cradle was designed using 3D CAD software (Pro Engineer 4.0) to hold and restrain the microfluidic device during envisaged operational conditions. Fig. 4.2 presents the cradle consisting of three brackets to align the LEDs, with the locations of the microvalve and the detection area, see Fig. 4.1. The cradle parts were

manufactured using a rapid prototyping system (Dimension SST 768) using a black polymer formulation to reduce interference due to external light fluctuations or internal reflections.

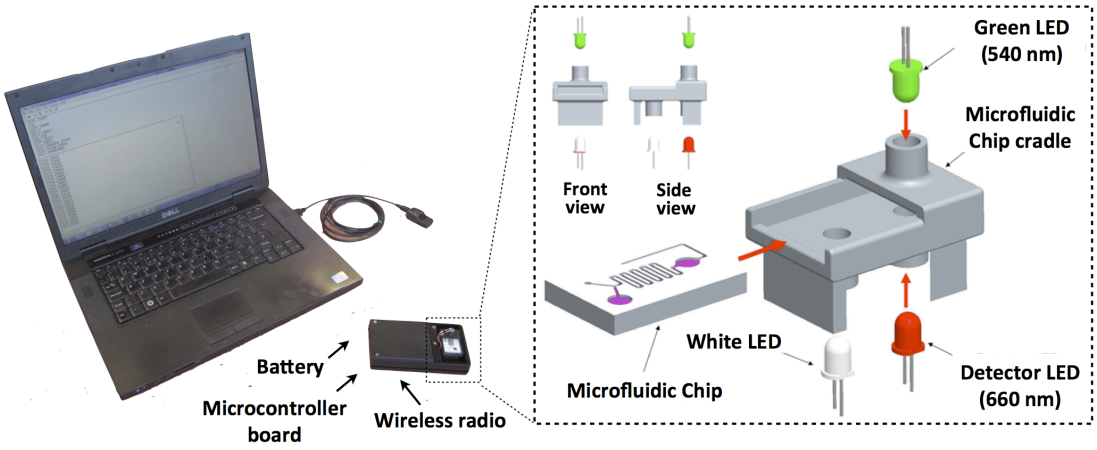

Figure 4.2. Computer with the wireless, portable, integrated microfluidic analytical platform (left) and CAD assembly model showing the microfluidic cradle (right), microfluidic device along with the white LED (actuate valve) and the PEDD detector LEDs (green-emitter and red-detector) positioning. Side and front views are also provided (right side, top left).

Fig. 4.3 shows the control and communication sub-systems responsible for operation of the device. A microcontroller board (with an MSP430 F449, Texas Instruments, at its core) was designed, created, and programmed in order to accept user commands (*e.g.*, turn on/off the LEDs), and to quantify the transmitted light through the reagent/sample mix (Fig. 4.3A). A 3.7 V lithium-ion battery (Panasonic PAL2) with a low form factor provided power to the portable unit and was regulated to a constant 3.3 V via an on-board, low noise, voltage regulator (LP2985, Texas Instruments), sourced from Farnell, Ireland. The 3.3 V source also supplied power to the white and green LEDs, which was important for maintaining constant illumination conditions.[30]

Communications between the operator and the microcontroller was achieved through two wireless radio transceivers (EZ-Radio ER900TRS, LPRS) with one located at the base station (connected to a PC/Laptop through a FDTI UB232R USB interface, Fig. 4.3B) and the other connected to the microcontroller *via* UART protocol.[31] Users/operators executed pre-programmed subroutines on the microcontroller *via* a command line interface, which was enabled through a terminal program on a PC/Laptop; Hyperterminal was used for this purpose. In addition, data harvested by the detector was wirelessly streamed to the PC/Laptop in real time where it was continuously saved to file for future analysis. Each data point was time stamped *via* a real time clock (32 KHz crystal, C-001R, Epson Toyocom). Schematic of the circuitry to actuate the power to the emitter LEDs and connection of the detector LED used in the platform is presented in Fig. 4.3C.

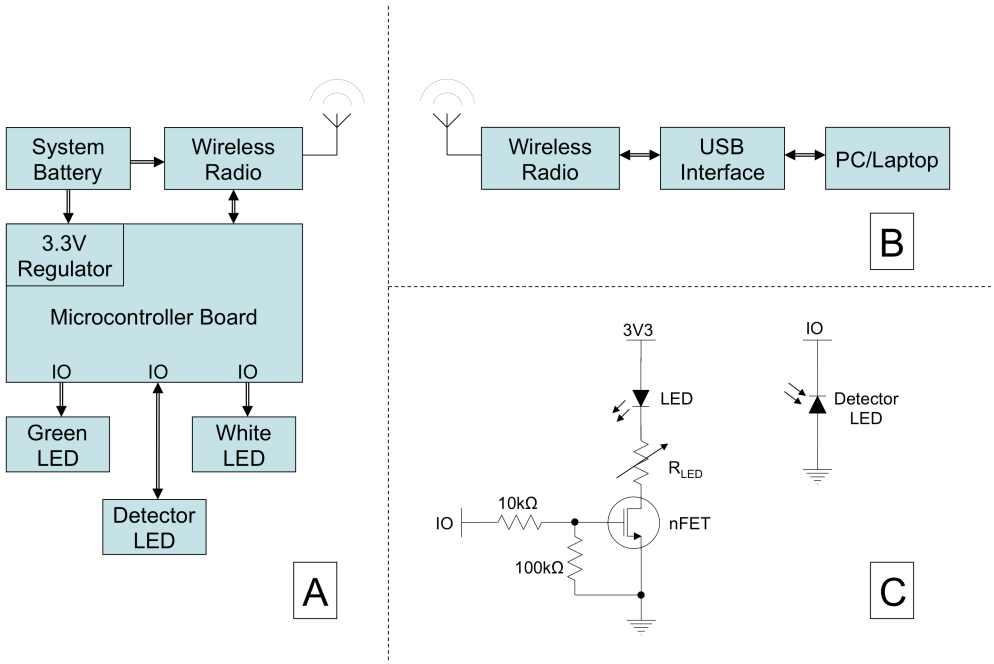

Figure 4.3. Device design. (A) Block diagram representation of the wireless analyser (B) Block diagram of the base station. (C) Schematic of the circuitry to actuate the power to the emitter LEDs (left) and connection of the detector LED (right).

Colorimetric detection was achieved through the use of the aforementioned LEDs, *i.e.* green (emitter, 540 nm, Radionics, Ireland) and red (detector, 660 nm, Radionics, Ireland), arranged in absorbance/transmission mode as shown in Fig. 4.2. Light generated by the emitter was partly absorbed by the Griess-nitrite complex, which absorbs strongly around 540 nm (λ_{max} = 547 nm).[32] Hence the photon flux reaching the reverse biased detector LED depends upon the concentration of nitrite within the sample. This in turn generates a photo current from the reverse biased detector diode,[33] which discharges a pre-set capacitance. The time taken to discharge the capacitance depends on the photocurrent generated by the detector LED, which in turn depends on the nitrite concentration in the sample, as described by Lau *et al.*[34] Accurate determination of the discharge time is achieved via a software counter within the microcontroller that accumulates the number of times the signal is above the I/O port's logic 0 (discharged) threshold over a fixed duration.[30] A time delay was implemented between each increment of the counter. This was determined experimentally by introducing the desired maximum and minimum concentrations into the microfluidic device in order to optimise the resolution for a 16-bit software counter *i.e.* in the range of 0 to 65535.

4.2.4 Measurement protocol

For conditioning the microvalve, 1mM HCl solution was introduced to the microfluidic channel allowing the ionogel to swell for 2 h in a dark environment. After microvalve actuation (contraction) triggered using the white light LED (Radionics, Ireland), nitrite detection was achieved via the Griess method.[35] The sample to reagent ratio adopted throughout all the experiments was 15: 1 v/v.[32] Measurements were obtained by introducing 34.5

μL nitrite standard/sample/water and 2.3 μL Griess reagent into their respective storage reservoirs on the microfluidic device, inlets (Fig. 4.1B). Using 25 mbar back pressure from a vacuum pipe connected to the microfluidic device *via* the outlet, the liquids were moved from the storage reservoirs and allowed to mix through the serpentine reaction microchannel as they moved towards the detection chamber (flow rate = 0.03 μL min^{-1}), wherein the concentration measurement took place. After the detection chamber was filled, see Fig. 4.1B, the intensity of the coloured solution was determined using the PEDD detector. The detector sampling rate under this protocol was set at 1 Hz.

For comparison, the calibration curve using UV-Vis spectrometer was carried out using the same nitrite standards/samples/water and Griess reagent mixtures pipetted into the cuvette. The development of the nitrite Griess reagent complex colour intensity was monitored, range 0.0 - 1.2 mg L^{-1} NO_2^-, using a Perkin-Elmer Lambda 900 spectrophotometer by taking an absorbance measurement at 540 nm for 40 min (T = 21 °C). Each experiment was carried out in triplicate.

4.3 Results and discussion

4.3.1 Volume phase transition of the photoswitchable ionogel microvalve

Fig. 4.4 shows the volume phase transition of a pSPNIPAAm ionogel disc induced by white light irradiation. From an initial height of 250 μm after photopolymerisation, the ionogels reached a height of 395 μm after swelling for 2 h in HCl (1 mM) solution, exhibiting an increase of ~ 58 % from its initial dimensions. Before white light irradiation, the swollen pSPNIPAAm ionogel had a strong yellow colour due to the protonated open-ring form of

the spirobenzopyran chromophore (MC-H^+), Appendix B, Fig. B1. Upon irradiation with white light, isomerisation to the closed-ring form (SP) was induced, and the yellow colour faded, followed by dehydration contraction of the pSPNIPAAm ionogel. It was found that the ionogel typically contracted by about 42 % of its initial swollen state after white light irradiation (30 min) in 1 mM HCl (pH = 3) at 21 °C.

In order to achieve effective fluid movement control, the photo-induced contraction of the ionogel must create an open channel (contracted gel) from a previously closed channel (swollen ionogel). To investigate this, 1 mm radius circular reservoirs with depths ranging from 200 to 300 μm were fabricated in the bottom layer of the microfluidic device (Fig. 4.1A), and then filled with the ionogel solution. The microvalves were photopolymerised with UV light, as described above, and their actuation in the microfluidic device investigated. It was found that microvalves prepared using 200 μm deep reservoirs were too small to block the channel after swelling, while microvalves prepared using 300 μm deep reservoirs were too large in their swollen state, and the microvalves did not open even after prolonged exposure (2 min) to white light irradiation. It was found that 1mm radius valves formed in 225 μm reservoirs (Fig. 4.1) gave a nice balance between effective blockage of the channel in the swollen state, and reasonably rapid opening of the channel when the valve was illuminated using the white light LED (see below).

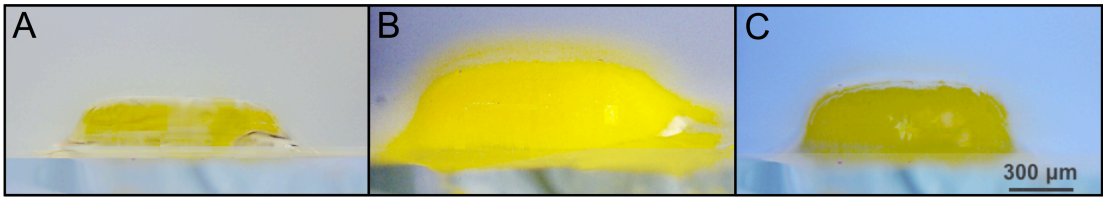

Figure 4.4. Photoswitchable ionogel after photopolymerisation (A), swelling in 1mM HCl for 2 h (B) and shrinking upon white light irradiation (C).

4.3.2 Fluidic control in the microfluidic device

Fig. 4.5 shows the basis arrangement for operation of the photoresponsive gel microvalve. Initially, the microvalve is in the closed (swollen) state, thus blocking the channel (Fig. 4.5, left). When the pSPNIPAAm ionogel is irradiated with white light from the LED (intensity 1 W cm^{-2}), photo-induced shrinkage occurs, and the microvalve opens after 30 ± 5 s (n = 3, Fig. 4.5, right). The microvalve was found to be unaffected by pressure up to 31 ± 4 mbar (n = 3) at which point they deformed and failed.

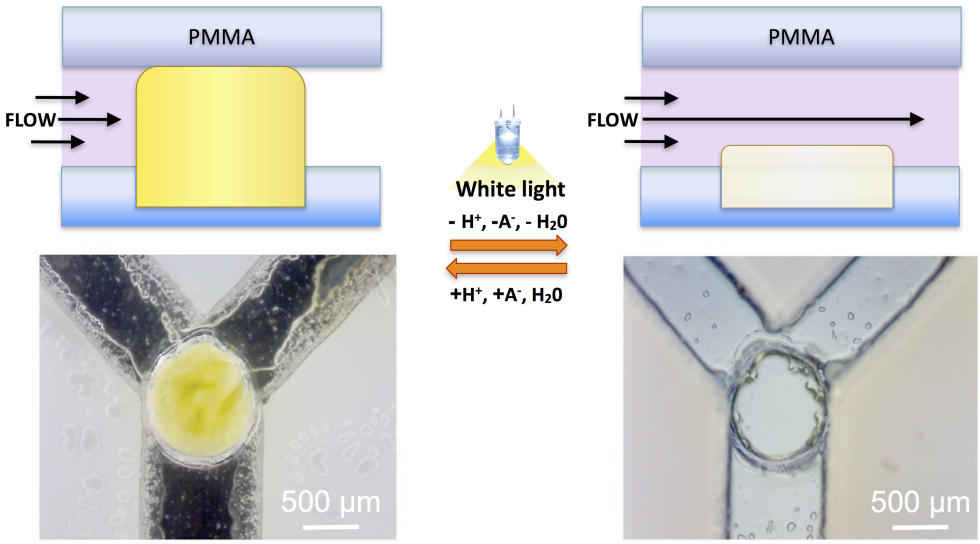

Figure 4.5. Schematic (top) and images (bottom) of the photoresponsive microvalve in closed (left) and opened (right) state.

After opening of the microvalve, the water sample and Griess reagent move from the reservoirs towards the serpentine mixing region. Preliminary experiments showed this design ensures efficient mixing of the sample and reagents. Appendix B, Fig. B2 demonstrates the effectiveness of the mixing process, which is essentially complete after *ca.* 10 mm (after the second channel loop). The sample then continues through the microfluidic device to the detector region where the absorbance of the LED radiation is measured at *ca.* 540 nm.

4.3.3 Portable, integrated microfluidic analytical platform characteristics

The microfluidic device presented in this study was integrated into a portable analytical platform that incorporated all the features necessary to actuate the microvalve, perform reagent/sample mixing, measure the colorimetric response, and transmit the harvested data wirelessly to a remote base station.

4.3.3.1 Reagent consumption

Typical flow injection analysis (FIA) systems employing the Griess method for nitrite detection consume relatively large amounts of reagent (approx. 5–20 mL per sample)[4] making the technique rather difficult to scale up. In contrast, the prototype platform only requires *ca.* 2.3 μL of Griess reagent per assay, resulting in significant reduction in costs associated with reagent purchase, servicing visits, platform size, power consumption and waste disposal.

4.3.3.2 Microvalve actuation

The photoswitchable ionogel microvalve is very low cost to produce in terms of materials, and its fabrication via *in-situ* photopolymerisation opens the possibility of creating complex microfluidic structures incorporating large numbers of valves. Furthermore, as it is actuated using light, no physical contact is required with the actuating stimulus, and therefore the microfluidic system can be completely sealed from the electronics, and the valve structures subsequently introduced. The white light intensity used to control the pSPNIPAAm ionogel microvalve in the current arrangement is *ca.* 1 mW cm^{-2}, which is substantially smaller than previously reported optically controlled

nanocomposite hydrogel microvalves (> 1600 mW cm^{-2}).[36] For comparison, the power consumption of typical miniature conventional solenoid valves (TX3P006, Sensor Technics; 600 mbar) is up to 500 mW. Moreover, the white LED used is a standard off-the-shelf component costing *ca.* €0.80 keeping the actuation at a low cost.

4.3.3.3 Detection system

As previously stated, the detection system was based on a paired emitter detector diode set-up. The emitter 540 nm LED wavelength was chosen to be compatible with the Griess reagent-nitrite azo dye absorption spectrum (λ_{max} = 547 nm), whereas the 660 nm LED was used as a detector because it was previously demonstrated that in the PEDD configuration, the reverse biased detector LED is sensitive to light of wavelength equal to or greater than the emission wavelength.[34] As the PEDD circuit generates a digital output from the counter (16-bits in this case, but can utilise 32-bits if required), which is greater resolution than a standard 10 or 12 bit ADC channel. In addition, the detector basically integrates the signal over a fixed time interval, noise is inherently supressed, and extremely low detection limits can be obtained.[32] Finally, the platform can be easily reconfigured for colorimetric detection at other spectral regions by changing the emitter LED.

Another significant advantage of this detection system is its low-cost feature. As LEDs are inexpensive and can be obtained off-the-shelf in a broad range of sizes and wavelengths,[37] this is an attractive detector strategy that can be implemented for a broad range of analytes.[34] In the context of colorimetric chemical detection a common implementation is based on photodiodes, for comparison. Photodiodes are by far one of the most commonly used detectors in optical sensing.[38] However, its implementation is

higher in cost and complexity as it requires Op Amps with additional components, an available analog to digital converter (ADC) on the microcontroller and a higher power requirement. A comparison of both approaches has already appeared in a study by O'Toole *et al.*,[39] who emphasised the low advantage of the PEDD implementation.

4.3.3.4 Communications

Many microcontroller devices using wireless modules are electing for the 2.4 GHz ISM band.[40] There are good reasons for this, one of which is the cost effective nature of device construction as this band has become increasing popular due to pervasive technologies such as Zigbee, WiFi, 3G, *etc.* However, it was decided to modularise this platform at the design stage to allow for ease of integration into other available networks, if required at future stages. However, for environmental applications the 900 MHz radio band offers the advantage over the 2.4 GHz band as it is capable of communicating around objects such as trees, or the landscape, *etc.*, all of which can be attenuated at 2.4 GHz.[41]

4.3.4 Portable, integrated microfluidic analytical platform performance

To demonstrate the utility of the portable integrated microfluidic analytical platform, the system was applied for the determination of nitrite levels in water samples. In colorimetric reagent based reactions, the reaction kinetics defines the time allowed for the sample to react with the reagent in the manifold. The kinetic curves obtained from the prototype platform are presented in Appendix B, Fig. B3. The signal (discharge time) *versus* time curves for the NO_2^- concentrations were modelled using a first order

exponential equation (Eqn. 4.1):

$$D_t = a \times (1 - e^{-kt}) + b \quad (4.1)$$

where D_t is the discharge time (μs) at the end of the reaction, a is a scaling factor, k is the first order rate constant (s^{-1}), t = time (s) and b is baseline offset.

First-order kinetic models were fitted (Microsoft Excel Solver)[42] to each of the curves and the rate constants were calculated over the concentration range 0.0 - 1.2 mg L^{-1} of NO_2^-. The average response (n = 3) and fitted models are presented in Fig. 4.6A. It was found that for nitrite concentrations higher than 0.4 mg L^{-1} and at a flow rate of flow rate of 0.03 μL min^{-1}, the reaction had already commenced by the time the data acquisition was initiated. This is due to the efficient mixing provided in the serpentine microchannel region, which caused the nitrite Griess reagent complex to rapidly form in the serpentine channel region at higher concentrations. This effect can be reduced by increasing the flow rate. When the reaction mixture reaches the detection chamber, signal acquisition is initiated. In Fig. 4.6 it can be seen that the colour formation increased rapidly at all concentrations until approximately 20 min after which a steady state signal was observed. Therefore this reaction time was adopted for all further experiments.

Calibration plots obtained with the prototype platform were found to be linear up to 1.2 mg L^{-1} of nitrite (R^2 = 0.98, RSD = 1.93 %, n = 3). The responses were plotted against the nitrite Griess reagent complex concentration using Eqn. 4.1 and the results are presented in Fig. 4.6B. The LOD, calculated as the concentration of nitrite which produced an analytical signal three times the standard deviation of the blank, was estimated as 34.0 ± 0.1 μg L^{-1} nitrite, and the limit of quantification (LOQ), calculated as the concentration of nitrite which produced an analytical signal ten times the

standard deviation of the blank, was 115.2 ± 3.1 μg L^{-1}.

For comparison, the absorbance of the same Griess reagent/nitrite solutions was measured using a UV-Vis spectrophotometer. As shown in Appendix B, Fig. B4, the absorbance at 540 nm plotted against nitrite Griess reagent complex concentration gave a linear range (R^2 = 0.99) of 0.0 - 1.2 mg L^{-1} with an RSD = 1.57 %, n = 3, LOD = 1.50 ± 0.02 μg L^{-1} and LOQ = 14.8 ± 0.23 μg L^{-1} (Table 4.1). The difference in LOD/sensitivity is primarily due to the much smaller path length of the microfluidic detection chamber (*ca.* 1.8 mm compared to the 10 mm pathlengths of standard cuvettes). According to the World Health Organisation the detection limits achievable by spectrometric standard procedures for drinking water are reported to be 0.005 – 0.010 mg L^{-1} for nitrite.[43] The levels obtained by the portable, integrated microfluidic analytical platform remain lower than the allowable limits, and are therefore useful for quantification as well as threshold testing.

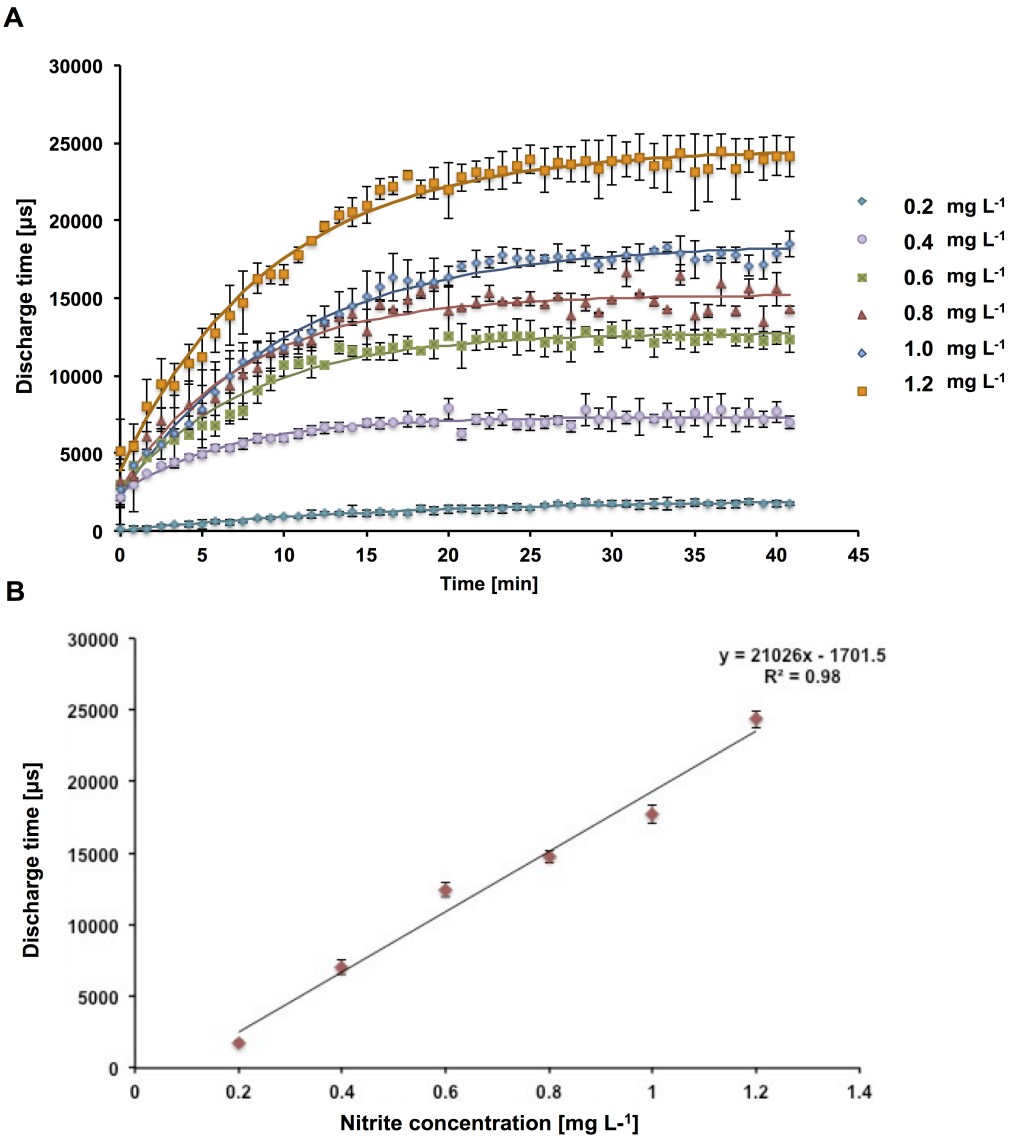

Figure 4.6. A) Kinetic study of colour formation using a 540 nm emitter LED for the nitrite Griess reagent complex formation (n = 3) and B) calibration plot from the same data taken at $t = 40$ min.

Table 4.1. Comparison of the data obtained for the detection of nitrite Griess reagent complex using both the portable, integrated microfluidic analytical platform and a UV-Vis spectrophotometer ($n = 3$).

	Microfluidic analytical platform (540 nm)	**UV-Vis spectrophotometer** (540 nm)
R^2	0.98	0.99
LOD	34.0 ± 0.1 μg L^{-1}	1.5 ± 0.02 μg L^{-1}
LOQ	115.2 ± 3.1 μg L^{-1}	14.8 ± 0.2 μg L^{-1}
RSD	1.93 %	1.57 %

The usefulness of the proposed portable integrated microfluidic analytical platform for the determination of traces of nitrite in freshwater samples obtained from Tolka River, Ireland, was evaluated using our system and UV-Vis spectrophotometer, for comparison. Table 4.2 shows that there is very good correlation between the bench top instrument and the portable platform.

Table 4.2. Analysis of freshwater samples for nitrite using the portable, integrated microfluidic analytical platform and the UV-Vis spectrophotometer ($n = 3$).

Water sample no.	**Microfluidic analytical platform [mg L^{-1}]**	**UV-Vis spectrophotometer [mg L^{-1}]**
1	0.010 ± 0.003	0.010 ± 0.001
2	0.400 ± 0.006	0.410 ± 0.004
3	0.410 ± 0.009	0.420 ± 0.003
4	0.310 ± 0.045	0.380 ± 0.025

4.4 Conclusions

It has been demonstrated through this study that a light actuated polymer gel microvalve can be operated successfully within a microfluidic channel to perform an assay, and the platform has been successfully applied to the analysis of water samples for nitrite. This could have important implications for the practical implementation of microfluidics, as it potentially opens the way towards the generation of low-cost, photo-controlled microflow systems in which the actuation stimuli can be totally separated from the chemistry, which can be contained within a physically separate and sealed fluidic chip. Full integration of the valve structures is possible, and the ability to create these structures *in-situ*, post-fabrication of the fluidic unit, could enable entire fluidic system components to be manufactured at very low cost.

However, in their current form, the pSPNIPAAm ionogel based valves require exposure to acidic solution in order to induce swelling. It should be noted that the shrinking mechanism of the gel results in the release of protons into the external solution around the gel. While this does not affect the chemistry presented in this work, it may affect other assays, for example, enzyme or antibody based methods, or the handling of cells and proteins, which typically require neutral pH. In such cases, the valves may have to be restricted to single use, with the acidic solution pushed through the microfluidic system in front of the assay reagents. Strategies to extend the functional pH range of the valve (currently restricted to around pH 3 for reswelling), and to improve the response time (by increasing the rate of water uptake and release, or increasing the surface area to bulk ratio of the valve structure) are currently being actively investigated. Finally, we have chosen nitrite as the target analyte for demonstrating the functionality of the prototype platform. This can easily be extended to include nitrate (through

incorporation of a reduction step), and the wide range of other important analytes for which effective colorimetric methods exist.

4.5 Acknowledgements

The authors wish to thank to the Marie Curie Initial Training Network funded by the EC FP7 People Programme under grant no. 238273, Science Foundation of Ireland under grant no. 07/CE/I1147. C.F. acknowledges the support of SFI under the same grant code. This work has been supported by the Science Foundation Ireland under grant no. 10/CE/B1821.

4.6 References

1. Lucey, J., Water Quality in Ireland 2007-2008: Key Indicators of the Aquatic Environment. *Environmental Protection Agency Website (Online)* **2009**.
2. Ramirez-Garcia, S.; Diamond, D., Internet-scale Sensing: Are Biomimetic Approaches the Answer? *Journal of Intelligent Material Systems and Structures* **2007,** *18* (2), 159-164.
3. Diamond, D.; Lau, K. T.; Brady, S.; Cleary, J., Integration of analytical measurements and wireless communications - Current issues and future strategies. *Talanta* **2008,** *75* (3), 606-612.
4. Sieben, V. J.; Floquet, C. F. A.; Ogilvie, I. R. G.; Mowlem, M. C.; Morgan, H., Microfluidic colorimetric chemical analysis system: Application to nitrite detection. *Analytical Methods* **2010,** *2* (5), 484-491.
5. United Nations Environment Programme, Global Environment Outlook 3. *Earthscan Publications*, London, **2002**.
6. Brimblecombe, P.; Stedman, D. H., Historical evidence for a dramatic increase in the nitrate component of acid rain. *Nature* **1982,** *298* (5873), 460-462.
7. Koupparis, M. A.; Walczak, K. M.; Malmstadt, H. V., Kinetic determination of nitrite in waters by using a stopped-flow analyser. *Analyst* **1982,** *107* (1280), 1309-1315.
8. Melanson, J. E.; Lucy, C. A., Ultra-rapid analysis of nitrate and nitrite by capillary electrophoresis. *Journal of Chromatography A* **2000,** *884* (1-2), 311-316.

9. Davis, J.; Moorcroft, M. J.; Wilkins, S. J.; Compton, R. G.; Cardosi, M. F., Electrochemical detection of nitrate and nitrite at a copper modified electrode. *Analyst* **2000,** *125* (4), 737-742.
10. Moorcroft, M. J.; Davis, J.; Compton, R. G., Detection and determination of nitrate and nitrite: a review. *Talanta* **2001,** *54* (5), 785-803.
11. Dutt, J.; Davis, J., Current strategies in nitrite detection and their application to field analysis. *Journal of Environmental Monitoring* **2002,** *4* (3), 465-471.
12. Petsul, P. H.; Greenway, G. M.; Haswell, S. J., The development of an on-chip micro-flow injection analysis of nitrate with a cadmium reductor. *Analytica Chimica Acta* **2001,** *428* (2), 155-161.
13. Hanson, A. K., A new in situ chemical analyzer for mapping coastal nutrient distributions in real time, OCEANS 2000 MTS/IEEE Conference and Exhibition **2000**; *3*, 1975-1982.
14. Sombatsompop, N.; Intawong, N. S.; Intawong, N. T., Design and construction of photo-conductive light pressure sensor for highly viscous fluids. *Sensors and Actuators A: Physical* **2002,** *102* (1-2), 76-82.
15. Schmidt, G. J.; Scott, R. P. W., Simple and sensitive ion chromatograph for trace-metal determination *Analyst* **1984,** *109* (8), 997-1002.
16. Feres, M. A.; Reis, B. F., A downsized flow set up based on multicommutation for the sequential photometric determination of iron(II)/iron(III) and nitrite/nitrate in surface water. *Talanta* **2005,** *68* (2), 422-428.
17. Betteridge, D.; Cheng, W. C.; Dagless, E. L.; David, P.; Goad, T. B.; Deans, D. R.; Newton, D. A.; Pierce, T. B., An automated viscometer based on high-precision flow-injection analysis. *Analyst* **1983,** *108* (1282), 1-16.
18. Curto, V. F.; Fay, C.; Coyle, S.; Byrne, R.; O'Toole, C.; Barry, C.; Hughes, S.; Moyna, N.; Diamond, D.; Benito-Lopez, F., Real-time sweat pH monitoring based on a wearable chemical barcode micro-fluidic platform incorporating ionic liquids. *Sensors and Actuators B: Chemical* **2012,** *171-172*, 1327 - 1334.
19. Fay, C.; Lau, K.-T.; Beirne, S.; Conaire, C.; McGuinness, K.; Corcoran, B.; O'Connor, N. E.; Diamond, D.; McGovern, S.; Coleman, G.; Shepherd, R.; Alici, G.; Spinks, G.; Wallace, G., Wireless aquatic navigator for detection and analysis (WANDA). *Sensors and Actuators B: Chemical* **2010,** *150* (1), 425-435.
20. Diamond, D.; Coyle, S.; Scarmagnani, S.; Hayes, J., Wireless sensor networks and chemo-/biosensing. *Chemical Reviews* **2008,** *108* (2), 652-679.

21. Czugala, M.; Gorkin III, R.; Phelan, T.; Gaughran, J.; Curto, V. F.; Ducrée, J.; Diamond, D.; Benito-Lopez, F., Optical sensing system based on wireless paired emitter detector diode device and ionogels for lab-on-a-disc water quality analysis. *Lab on a Chip* **2012,** *12*, 5069-5078.
22. Czugala, M.; Ziolkowski, B.; Byrne, R.; Diamond, D.; Benito-Lopez, F., Materials science: the key to revolutionary breakthroughs in micro-fluidic devices. *Proceedings SPIE 8107, Nano-Opto-Mechanical Systems (NOMS)* **2011**, 81070C-81070C.
23. Watabe, S.; Tatsuoka, M.; Shimomae, T.; Shirasaki, Y.; Mizuno, J.; Funatsu, T.; Shoji, S., Multi particles and biomolecules sorting system using thermoreversible gelation controlled by DMD [digital mirror device]. *Digest of Technical Papers.* The 13th International Conference on Solid-State Sensors, Actuators and Microsystems (Transducers) **2005**; *1*, 445-448.
24. Shirasaki, Y.; Tanaka, J.; Makazu, H.; Tashiro, K.; Shoji, S.; Tsukita, S.; Funatsu, T., On-chip cell sorting system using laser-induced heating of a thermoreversible gelation polymer to control flow. *Analytical Chemistry* **2005,** *78* (3), 695-701.
25. Nagai, H.; Takahashi, J.; Wakida, S., Micro optical switching valve system based on reversible wettability conversion, *Proceedings of the 7th International Conference on Miniaturized Systems for Chemistry and Life Sciences* (μTAS) **2003**, 927-930.
26. Liu, G. L.; Kim, J.; Lu, Y.; Lee, L. P., Optofluidic control using photothermal nanoparticles. *Nature Materials* **2006,** *5* (1), 27-32.
27. Sershen, S. R.; Mensing, G. A.; Ng, M.; Halas, N. J.; Beebe, D. J.; West, J. L., Independent optical control of microfluidic valves formed from optomechanically responsive nanocomposite hydrogels. *Advanced Materials* **2005,** *17* (11), 1366-1368.
28. Sugiura, S.; Sumaru, K.; Ohi, K.; Hiroki, K.; Takagi, T.; Kanamori, T., Photoresponsive polymer gel microvalves controlled by local light irradiation. *Sensors and Actuators A: Physical* **2007,** *140* (2), 176-184.
29. Satoh, T.; Sumaru, K.; Takagi, T.; Kanamori, T., Fast-reversible light-driven hydrogels consisting of spirobenzopyran-functionalized poly(*N*-isopropylacrylamide). *Soft Matter* **2011,** *7* (18), 8030-8034.
30. de Vargas-Sansalvador, I. M. P.; Fay, C.; Phelan, T.; Fernandez-Ramos, M. D.; Capitan-Vallvey, L. F.; Diamond, D.; Benito-Lopez, F., A new light emitting diode-light emitting diode portable carbon dioxide gas sensor based on an interchangeable membrane system for industrial applications. *Analytica Chimica Acta* **2011,** *699* (2), 216-222.
31. Fay, C.; Doherty, A. R.; Beirne, S.; Collins, F.; Foley, C.; Healy, J.; Kiernan, B. M.; Lee, H.; Maher, D.; Orpen, D.; Phelan, T.; Qiu, Z.;

Zhang, K.; Gurrin, C.; Corcoran, B.; O'Connor, N. E.; Smeaton, A. F.; Diamond, D., Remote real-time monitoring of subsurface landfill gas migration. *Sensors* **2011,** *11* (7), 6603-6628.

32. O' Toole, M.; Shepherd, R.; Lau, K. T.; Diamond, D., Detection of nitrite by flow injection analysis using a novel Paired Emitter-Detector Diode (PEDD) as a photometric Detector. *Proc. SPIE* **2007,** *6755,* 67550P.
33. Mims, M. F., How to monitor ultraviolet radiation from the sun. *Scientific American* **1990,** *263*, 106-109.
34. Lau, K. T.; Baldwin, S.; Shepherd, R. L.; Dietz, P. H.; Yerzunis, W. S.; Diamond, D., Novel fused-LEDs devices as optical sensors for colorimetric analysis. *Talanta* **2004,** *63* (1), 167-173.
35. MacFaddin, J., Nitrate/nitrite reduction tests, In: Biochemical tests for identification of medical bacteria. 3rd ed.; Lippincott Williams & Wilkins, Philadelphia, **2000**.
36. Sumaru, K.; Kameda, M.; Kanamori, T.; Shinbo, T., Characteristic phase transition of aqueous solution of poly(*N*-isopropylacrylamide) functionalized with spirobenzopyran. *Macromolecules* **2004,** *37* (13), 4949-4955.
37. O'Toole, M.; Diamond, D., Absorbance based light emitting diode optical sensors and sensing devices. *Sensors* **2008,** *8*, 2453-2479.
38. Dasgupta, P. K.; Eom, I.-Y.; Morris, K. J.; Li, J., Light emitting diode-based detectors: Absorbance, fluorescence and spectroelectrochemical measurements in a planar flow-through cell. *Analytica Chimica Acta* **2003,** *500* (1-2), 337-364.
39. O'Toole, M.;. Lau, K. T; Shepherd, R.; Slater, C.; Diamond, D., Determination of phosphate using a highly sensitive paired emitter-detector diode photometric detector. *Analytica Chimica Acta* **2007,** *597*, 290-294.
40. Brand, O., Microsensor integration into systems-on-chip. *Proceedings of the IEEE* **2006,** *94* (6), 1160-1176.
41. Tse, D.; Viswanath, P., Fundamentals of wireless communication. Cambridge University Press, Cambridge, **2005**.
42. Diamond, D.; Hanratty, V. C. A., Spreadsheet Applications for Chemistry Using Microsoft Excel. John Wiley and Sons, New York, **1997**.
43. World Health Organization, Guidelines for drinking-water quality [electronic resource]: incorporating 1st and 2nd addenda, vol. 1, Recommendations, Geneva, **2008**.

Chapter 5

A wireless paired emitter detector diode device as an optical sensor for lab-on-a-disc applications

R. Gorkin,[1] M. Czugala,[2] C. Rovira-Borras,[2] J. Ducrée,[1] D. Diamond[2] and F. Benito-Lopez[2]

16th International Conference on Solid-State Sensors, Actuators and Microsystems (Transducers), 2011
doi: 10.1109/TRANSDUCERS.2011.5969761

[1]School of Physical Sciences, Dublin City University, Dublin, IRELAND
[2]CLARITY: Centre for Sensor Web Technology
National Centre for Sensor Research
Dublin City University, Dublin, IRELAND

Abstract

This chapter reports on a novel optical sensing configuration for lab-on-a-disc colorimetric analysis applications. The system employs a wireless paired emitter detector diode device (PEDD), which consists of two light emitting diodes (LEDs). One LED, forward biased, serves as the light source whereas the other, in reverse bias mode, serves as the light detector. A simple timer circuit is used to measure the time taken for the photocurrent generated by the emitter LED to discharge the detector LED from 5 V (logic 1) to 1.7 V (logic 0) to give a digital output directly. The light dependent discharging process has been deployed in measurement of concentrations of colored solutions. The PEDD system was validated and showed close alignment and similar limits of detection *versus* standard UV-Vis spectroscopy.

5.1 Introduction

Over the last decade increased awareness of long term consequences of water contamination has taken the spotlight of the chemical sensing community, as water quality monitoring plays a crucial role in understanding and managing potential risk. This spurred the need of development of inexpensive optical sensors capable of wireless communication.[1, 2] The key requirements such as reproducibility, reliability, low power consumptions as well as sensitivity and selectivity are vital in the development of scale-up and mass productions of sensing devices, which allow for the widespread deployment.[3, 4] Availability of broadly applicable optical components like light emitting diodes (LEDs) or photodiodes opens the potential of sensors to be widely employed in platforms for wireless network systems (WSN).

Commonly, optical system configurations combine LEDs as a light source with a charge coupled device (CCD),[5, 6] a light wave multimeter[6] and a photodiode.[7, 8, 9] However, these systems cannot be incorporated into small devices or be scaled-up within WSN. For reference, the first configuration of optical sensing system using LED as a light detector was presented by Mims III *et al.*[10, 11] Diamond and co-workers further described the developments of PEDD based sensors with regard to configuration and application.[12, 13]

In general, a PEDD consists of two light emitting diodes (LEDs), one serving as the light source and the other, in reverse bias mode, as the light detector. Instead of the traditional way of measuring the photocurrent directly, a simple timer circuit is used to measure the time taken for the photocurrent generated by the emitter LED to discharge the detector LED. This system allows for the creation of a digital output directly without using an A/D converter or operation amplifier. The method achieves excellent sensitivity and signal-to-noise ratio (SNR) in comparison to the more

commonly employed method of coupling a LED to a photodiode. The low cost, small size, low power consumption, increasing spectral range coverage (247–1550 nm), intensity and efficiency, ease of fabrication and simplicity of the PEDD make it an ideal optical detector for colorimetric assays.[4]

This chapter describes the first use of wireless paired emitter detector diode (PEDD) as an optical sensor for colorimetric analysis for lab-on-a-disc applications. In particular, environmental water quality analysis has been reported using standard lab chip systems.[14] However the use of centrifugal discs (CDs) has several advantages in regards to portability in microfluidic systems. Principally CD technology allows for the elimination of large power supply and pumps along with the interconnections required to driving fluids in many traditional chips.[15] In terms of microfluidics, the non-contact PEDD detection scheme aligns perfectly with centrifugal Lab-on-a-disc systems, which can have difficulties in monitoring during rotation.[16] By employing centrifugal microfluidic technology, several individual experiments can be automated, allowing for parallel processing. In turn, this system has huge potential for point-of-care systems for environmental water quality analysis.

5.2 Experimental

5.2.1 Prototype system

The instrument consists of two Surface Mount LEDs (Surface Mount Technology), placed above and below the sensing area of a disc, with supporting electronics (Fig. 5.1). One LED acts as the light source while the other is reverse biased, acting as a detector. Both LEDs are controlled by a microcontroller (Arduino Fio). Briefly, the detector LED in output mode was charged up to 3.3 V for 100 μs using microcontroller's I/O in output mode which was then switched to high impedance input mode. Light from the

emitter LED generates a photocurrent in the reverse biased detector LED, resulting in discharge of the capacitance based voltage from an initial value of 3.3 V (logic 1) to a present value of 1.7 V (logic 0). In order to provide a stable +3.3 V source to drive the circuit and LEDs, a voltage regulator running from a battery was employed. After passing through the microfluidic device, the observed light intensity is related to the discharge time due to stray capacitance of the device.[17]

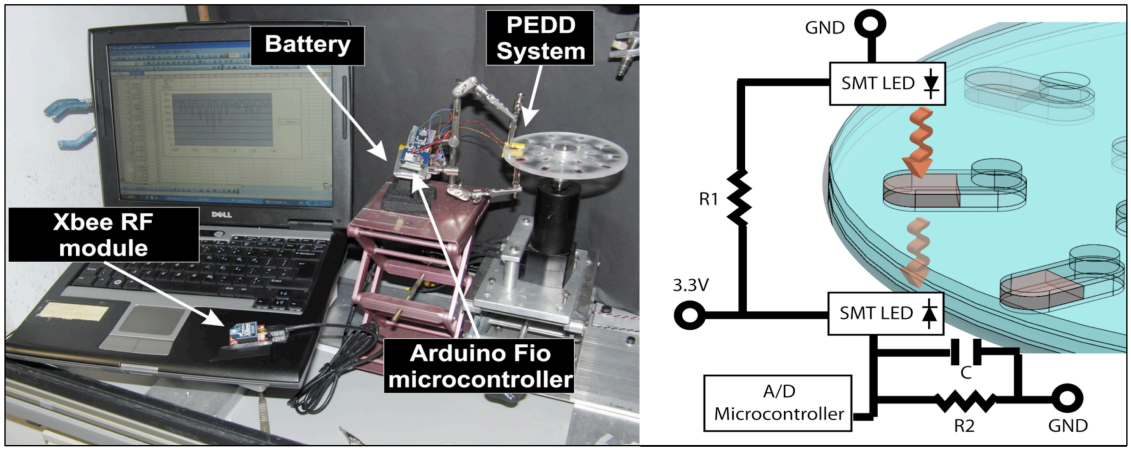

Figure 5.1. Prototype configuration of the PEDD system with a schematic of the used circuit.

Portability is sustained using a lithium polymer battery as the power source and includes a charge circuit over USB/XBee socket to record data to a laptop in real time via Bluetooth.

To fabricate the multilayer centrifugal disc devices, poly(methyl methacrylate) (PMMA, Radionics, Ireland) components were laser milled while double-sided, pressure sensitive adhesive (PSA, Adhesives Research, Ireland) were cut. After manufacturing the assembly was laminated together to create the final device. The colorimetric experiments utilised Bromocresol Purple pH dye, Vitamin B12 and Vitamin B2 analytical grade (Sigma-Aldrich®, Dublin, Ireland). All solutions were prepared using deionised water

(Milli-Q).

5.2.2 Calibration procedure

Preliminary characterisation of the device looked at the light intensity from three different colored dyes (red, blue and black) placed in sequential disc reservoirs (Fig. 5.2.). This work was followed by the calibration of the system using three biochemical analytes: vitamin B2 (Riboflavin), Bromocresol Purple (BCP) pH dye and Vitamin B12 (Cobalamin). The analytes were chosen for relevance for colorimetric sensing and the applications. Vitamin B2 (Riboflavin) was chosen to investigate the colour efficiency of the system. BCP was chosen because it is a good example of an analyte with chemical relevance as pH sensor dye in several processes. Vitamin B12 represents an important clinical analyte that ensures the smooth functioning of vital life processes of the human body (*e.g.* regulation of the formation of red blood cells in the body).

To provide references, concentration ranges of Vitamin B12 and BCP were measured using UV-Vis spectrometry (UV-Vis-NIR Perkin-Elmer Lambda 900 spectrometer) for control. A serie of dilutions (1.0×10^{-3} M to 2.5×10^{-6} M) for the three analytes were then examined with the PEDD system by placing 10 μL of the solutions in the disc reservoirs of the CD, while the rotor itself was placed on a spin stand with a motor. Spinning the CD allowed for proper loading of the fluids and for testing under spin conditions. The light dependence discharge time of detector LED was measured continuously for 30 s.

5.3 Results and discussion

Fig. 5.2 shows that the system was able to distinguish between the

chambers during rotation.

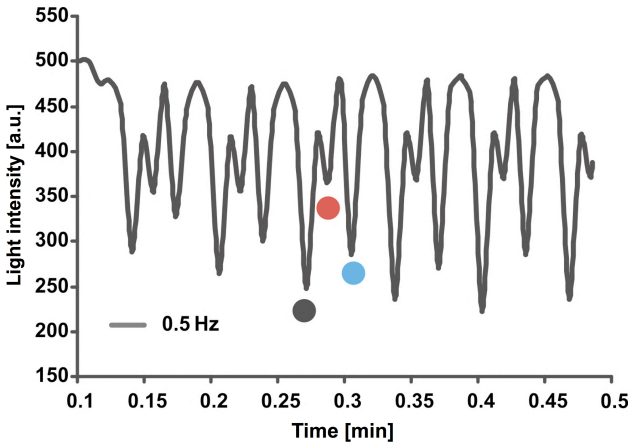

Figure 5.2. Detection of three different dyes (black, red and blue) during spinning of the disc at 0.5 Hz.

According to the UV-Vis spectra of vitamin B12 and Bromocresol Purple pH dye (Fig. 5.3 and Fig. 5.4, respectively), the linear relationship between absorbance and dye concentration was found to be in the concentration range from 2.5 x 10^{-6} to 5.0 x 10^{-5} M. It should be noted that higher concentrations were not accurately measured while lower concentrations were not detected.

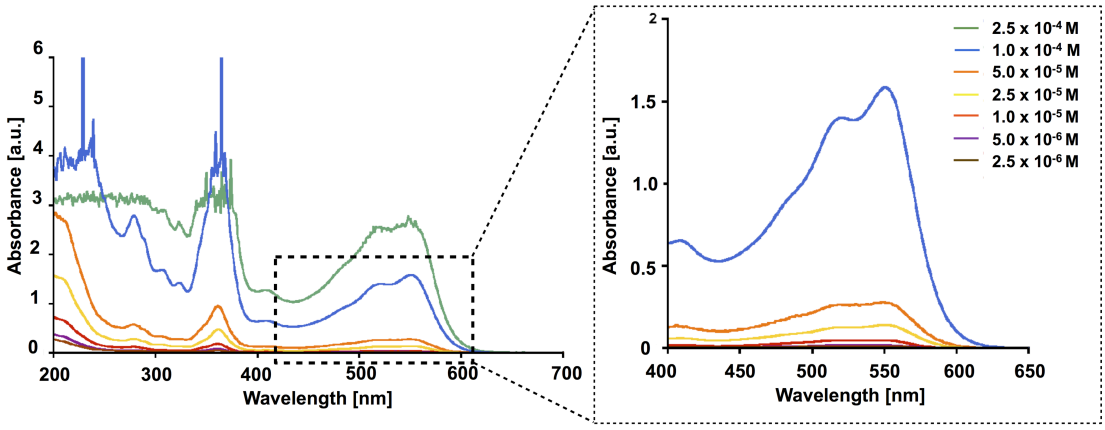

Figure 5.3. UV-Vis spectra of vitamin B12 at different concentrations. The spectra show that vitamin B12 is detected quantitatibly in the range from 2.5 x 10^{-6} till 5.0 x 10^{-5} M using a UV-Vis spectrometer, L = 1 cm.

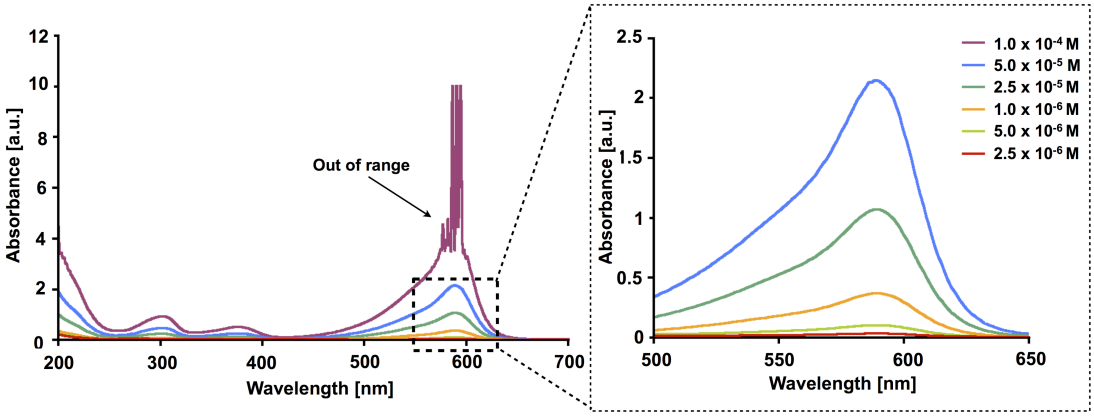

Figure 5.4. UV-Vis spectra a of Bromocresol Purple pH dye at different concentrations. The spectra show that BCP is detected quantitatively in the range from 2.5 x 10^{-6} till 5.0 x 10^{-5} M using a UV-Vis spectrometer, L = 1 cm.

The calibration curve of vitamin B12 and BCP pH dye are presented in Fig. 5.5. and Fig. 5.6. respectively, for both optical systems. Results showed close alignment between the PEDD system and standard UV-Vis spectrometry with similar limits of detection (LOD) (2.5 x 10^{-6} M). However, the PEDD system showed slight improvement with a linear trend over a wider range of concentrations.

The data obtained for vitamin B2 is illustrated in Fig. 5.7. Although small changes in the light intensity where observed when increasing the concentration of the analyte, the calibration was not successfully achieved. The LED is emitting in the same wavelength range of the maximum absorbance peak of vitamin B2 preventing colour variation determination by the detector.

Unlike other results within the thesis, which represent the light measurement directly as processor counts (discharge time), Figures in this chapter present the light measurements in terms of 'light intensity'. In this case, the light intensity is calculated by subtracting the count representing the measurements (of sample of certain solute concentration) by the maximum

processor count representing the situation when no light is passing through the sample (eg. for sample of very high solute concentration). By this approach, the light being measured is proportional to the light intensity and the resulting plots show an inverted trend.

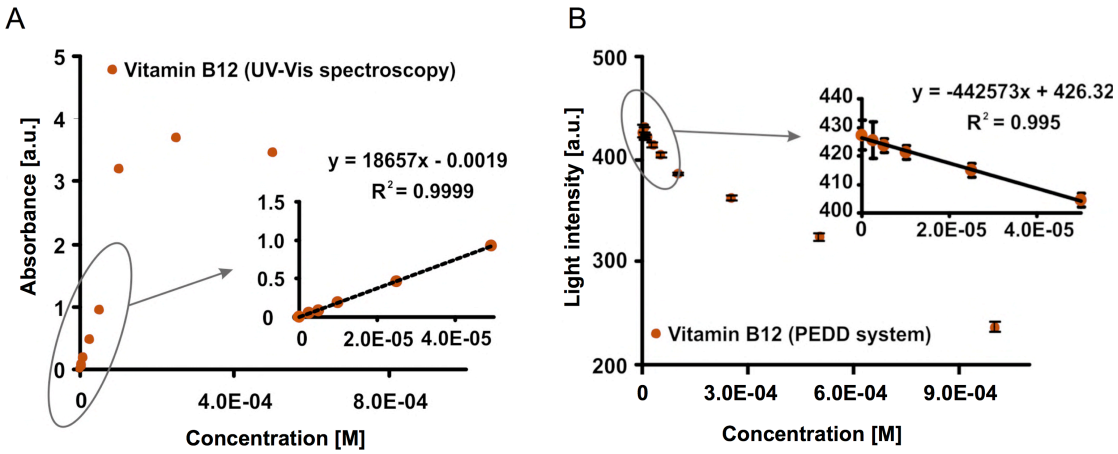

Figure 5.5. Calibration curves of vitamin B12 (Cobalamin) using a UV-Vis spectrometer (A) and the PEDD system (B), $L_{UV\text{-}Vis}$ = 1 cm, L_{PEDD} = 0.16 cm, $n = 4$.

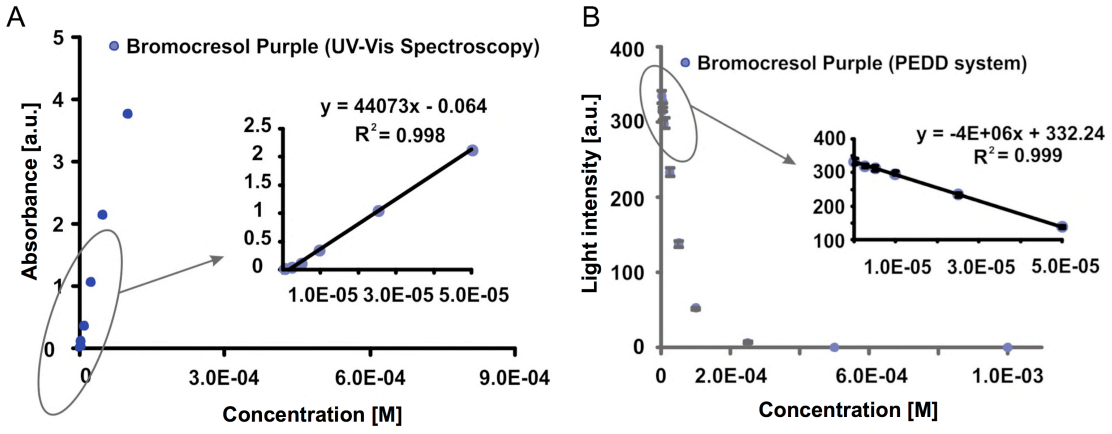

Figure 5.6. Calibration curves of Bromocresol Purple pH dye using a UV-Vis spectrometer (A) and the PEDD system (B), $L_{UV\text{-}Vis}$ = 1 cm, L_{PEDD} = 0.16 cm, $n = 6$.

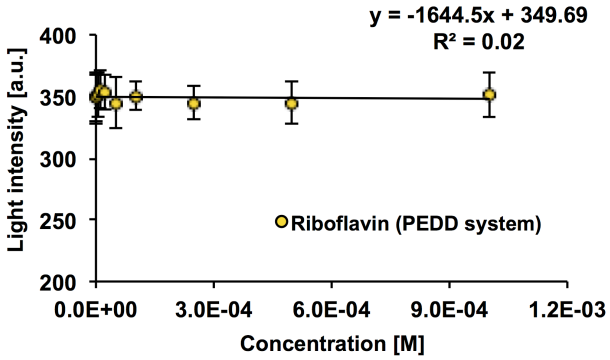

Figure 5.7. Calibration curve for vitamin B2 (Riboflavin) using the PEDD system, $L_{PEDD} = 0.16$ cm, $n = 4$.

5.4 Conclusions

A portable system for long-term colorimetric analysis in solution has been developed and will form the basis of the devices presented in the following chapters. This device incorporates low power detection coupled with wireless communication and power supply into Lab-on-a-disc system. Integration of a wireless communication device allows data acquisition according to individual needs. Similar limits of detection between PEDD system and standard UV-Vis spectrometer imply that the system is highly sensitive thus allowing for detection even low concentrations levels. In general, this shows potential for the PEDD system to be a cheap and versatile alternative optical detector for lab-on-a-disc applications. Further work on the system, Chapters 6 and 7, includes better packaging in order to improve the detection limit by reducing external light noise and more extensive experimentation with various analytes in point-of-care settings.

5.5 Acknowledgments

The authors wish to thank to the Marie Curie Initial Training Network funded by the EC FP7 People Programme under grant 238273 and Science

Foundation of Ireland under grant 07/CE/I1147.

5.6 References

1. Rogers, K. R.; Recent advances in biosensor techniques for environmental monitoring. *Analytica Chimica Acta* **2006**, *568* (1-2), 222-231.
2. Kim, P.; Albarella, J. D.; Carey, J. R. ; Placek, M. J.; Sen, A.; Wittrig, A. E. W.; McNamara III, B., Towards the development of a portable device for the monitoring of gaseous toxic industrial chemicals based on a chemical sensor array. *Sensors and Actuators B: Chemical* **2008**, *134* (1), 307-312.
3. Mabrook, M. F.; C. Pearson, M. C. Petty, An inkjet-printed chemical fuse, *Applied Physics Letters* **2005,** *86*, 0135071-0135073.
4. O'Toole, M., Shepherd, R.; Wallace, G. G.; Diamond, D.; Inkjet printed LED based pH chemical sensor for gas sensing, *Analytica Chimica Acta* **2009**, *652* (1-2), 308-314.
5. Carter, J. C.; Alvis, R. M.; Brown, S. B.; Langry, K. C.; Wilson, T. S.; McBride, M. T.; Myrick, M. L.; Cox, W. R.; Grove, M. E.; Colston, B. W., Fabricating optical fiber imaging sensors using inkjet printing technology: A pH sensor proof-of-concept. *Biosensors and Bioelectronics* **2006**, *21* (7), 1359-1364.
6. Weigl, B. H.; Wolfbeis, O. S.; Sensitivity studies on optical carbon dioxide sensors based on ion pairing. *Sensors and Actuators B: Chemical* **1995**, 28 (2), 151-156.
7. Crowley, K.; Pacquit, A.; Hayes, J.; Lau, K. T.; Diamond, D., A gas-phase colorimetric sensor for the detection of amine spoilage products in packaged fish. *IEEE Sensors Journal* **2005**, *2* (10), 754-757.
8. Pacquit, A.; Lau, K. T.; McLaughlin, H.; Frisby, J.; Quilty, B.; Diamond, D., Development of a volatile amine sensor for the monitoring of fish spoilage. *Talanta* **2006**, *69* (2), 515-520.
9. Pacquit, A.; Frisby, A.; Diamond, D.; Lau, K. T.; Farrell, A.; Quilty, B.; Diamond, D., Development of a smart packaging for the monitoring of fish spoilage. *Food Chemistry* **2007**, *102* (2), 466-470.
10. Mims III, F.M., Sun photometer with light emitting diode as spectrally selective detectors. *Applied Optics* **1992**, 31, 6965-6967.
11. Mims III, F.M., How to monitor ultraviolet radiation from the sun. *Scientific American* **1990**, *263*, 106-109.
12. O'Toole, M.; Lau, K.-T.; Diamond, D., Photometric detection in flow analysis systems using integrated PEDDs. *Talanta* **2005**, *66*, 1340-1344.

13. Lau, K.-T.; Shepherd, R.; Diamond, D., Solid state pH sensor based on light emitting diodes (LED) as detector platform. *Sensors* **2006**, *6* (8), 848-859.
14. Jang, A.; Zou, Z.; Lee, K. K.; Ahn, C. H.; Bishop, P. L., State-of-the-art lab chip sensors for environmental water monitoring. *Measurement Science and Technology* **2001**, *22* (3), 032001-032019.
15. Siegrist, J.; Gorkin, R.; Bastien, M.; Stewart, G.; Peytavi, R.; Kido, H., Validation of a centrifugal microfluidic sample lysis and homogenization platform for nucleic acid extraction with clinical samples. *Lab on a Chip* **2010**, *10* (3), 363-371.
16. Gorkin, R.; Park, J.; Siegrist, J.; Amasia, M.; Lee, B.; Park, J.; Kim, J.; Kim, H.; Madou, M., Y. Cho, Centrifugal microfluidics for biomedical applications. *Lab on a Chip* **2010**, *10* (14), 1758-1773.
17. Lau, K. T.; Baldwin, S.; Shepherd, R. L.; Dietz, P. H.; Yerzunis, W. S.; Diamond, D., Novel fused-LEDs devices as optical sensors for colorimetric analysis. *Talanta* **2004**, *63* (1), 167-173.

Chapter 6

Optical sensing system based on wireless paired emitter detector diode device and ionogels for lab-on-a-disc water quality analysis

M. Czugala,[1] R. Gorkin,[2] T. Phelan,[1] J. Gaughran,[2] V. F. Curto,[1] J. Ducrée,[2] D. Diamond[1] and F. Benito-Lopez,[1]

Lab on a Chip, 2012 (12), 5069-5078
doi: 10.1039/C2LC40781G

[1]CLARITY: Centre for Sensor Web Technologies, National Centre for Sensor Research, Dublin City University, Dublin 9, Ireland
[2]School of Physical Sciences, National Centre for Sensor Research, Dublin City University, Dublin 9, Ireland

For Supplementary Information see Appendix C, pg. 229.

Abstract

This chapter describes the first use of a wireless paired emitter detector diode device (PEDD) as an optical sensor for water quality monitoring in a lab-on-a-disc device, following the proof of concept device presented in Chapter 5. The microfluidic platform, based on an ionogel sensing area combined with a low-cost optical sensor is applied for pH (quantitative) and qualitative turbidity monitoring of water samples at the point-of-need. The autonomous capabilities of the PEDD system, combined with the portability and wireless communication of the full device, provide the flexibility needed for on-site water testing. Water samples from local fresh and brackish sources were successfully analysed using the device, showing very good correlation with standard bench-top systems.

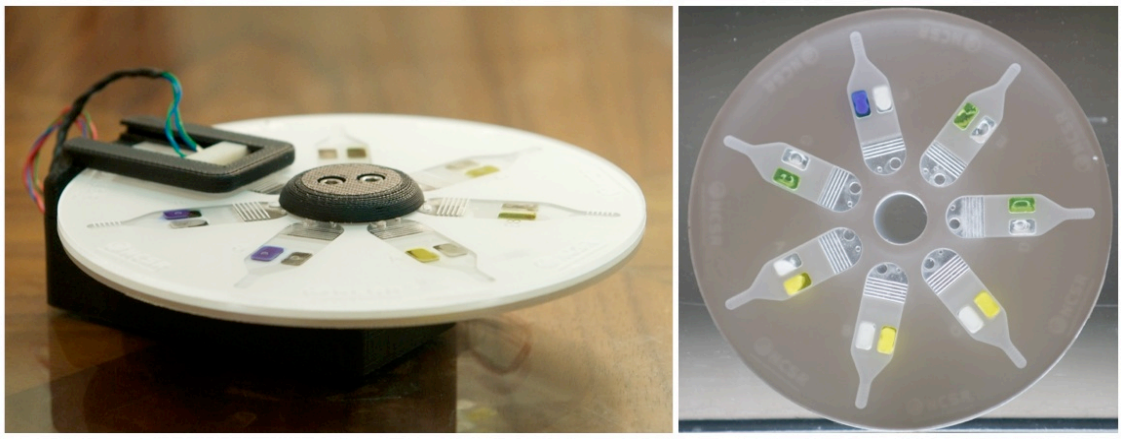

6.1 Introduction

Water is an essential resource for living systems, industrial processes, agricultural production and domestic use. The quality of the environment in which we live influences a range of sectors including the general economy, and personal health and well-being.[1] In spite of the significant efforts to improve water quality in recent years, more than one in six people worldwide – nearly 900 million – do not have access to safe drinking water.[2]

These problems highlight the importance of adequate water quality monitoring in order to trigger early warning of contamination of water supplies. The need for reliable water quality information has never been greater - to identify current and emerging problems of water pollution, and to assess long-term trends and environmental impact of housing developments, or changes in industrial/agricultural practices.

Traditional monitoring of water contamination is generally based upon manual in-situ 'grab' sampling followed by testing using lab-based methods. While this approach can provide some information regarding quality, it is not scalable in terms of the number of locations that can be sampled and the frequency of sampling. Consequently, even in developed countries, the vast majority of water bodies are monitored infrequently at a limited number of locations.[3] In contrast, *in-situ* measurements generated with autonomous instruments present a much more scalable model, enabling denser monitoring in terms of geographical locations and sampling frequency. This in turn can provide new information regarding natural processes governing the dynamics of chemical species behaviour.[4] In addition, various physical, chemical and biological processes can affect a sample from the time of collection to that of analysis, influencing its speciation, and causing significant uncertainty in the validity of aqueous speciation measurements.[5, 6, 7]

In view of the limitations of manual sample collection and subsequent laboratory analysis, there is great interest in *in-situ* water quality monitoring to ensure that aquatic areas are compliant with legislation. The challenge is to develop cheap and autonomous devices that can be used *in-situ*, with the capability to make the resulting data available remotely via web-databases, so that water quality can be monitored independently of location.[8, 9]

Miniaturisation of analytical devices through the advent of microfluidics is an important development for applications such as environmental monitoring as reflected in papers appearing in the literature. For example, Rohrlack *et al.*[10] developed an opto-fluidic lab-on-a-chip that functions as a compact robust tool for the fast screening, real-time monitoring, and initial classification of algae. Diamond and co-workers presented a microfluidic sensor for long-term monitoring of phosphate levels that incorporates sampling, reagent and waste storage, detection, and wireless communication into a compact and portable device.[11, 12, 13] An interesting approach to environmental monitoring was presented by Salazar *et al.,*[14] which developed a portable cell-based impedance sensor for toxicity testing of drinking water. In addition, Ahn *et al.*[15] presented an on-site water analyser capable of automatically performing long-term continuous sampling for heavy metals measurement using a continuous flow sensing method with an array of disposable polymer chips.

So far, on-chip water quality analysis have been mostly provided using standard lab-on-a-chip systems[16] and only a few examples have been reported in which centrifugal disc (CD) platforms have been used.[17, 18] For the last decade, such ‘‘Lab-on-a-disc’’ systems have been the focus of intense research, particularly for the development of diagnostic point-of-care devices[19] although some examples of applications for water quality analysis have begun to appear.[17] Centrifugal force has been used for sedimentation in numerous

applications, both micro- and macro-fluidic. Since environmental samples can contain large amounts of suspended particulate matter, generally samples are routinely filtered prior to analysis. Employment of sedimentation/filtering directly on the disc therefore eliminates at least one sample preparation step leading to faster, simpler analysis.

In comparison to standard micro-chip-based systems, the use of centrifugal discs has several advantages in regards to portability, which is a key issue for *in-situ* water monitoring systems. Generally speaking, CD technology removes the need for pumps along with the interconnections required to driving fluids in traditional chips,[20] which allow the complete fluidic network and the employed assay to be contained within a single disc. Typically, fluid-pumping rotation speeds range from 300 to 3000 revolutions per minute (rpm).[20] Additionally, by employing centrifugal microfluidic technology, multiple experiments can be automated, enabling parallel processing and integration towards sample-to-answer systems. In comparison to the electro-osmotic pumping, centrifugal control of fluid movement is not dependent on pH, ionic strength[21] or chemical composition (in contrast to alternating current AC and direct current DC electro-kinetic pumping).[22] Finally, centrifugal platform technology replaces complex fluidic handling equipment and complicated interconnects, which helps keep costs to a minimum.[22]

While the centrifugal microfluidic platform is amendable for fluid processing, a complete analysis instrument requires the integration of sensing devices. The increased importance of environmental monitoring has spurred the need of developing inexpensive optical sensors capable of being combined with wireless communication capabilities.[23] The availability of broadly applicable optical components like light emitting diodes (LEDs) or photodiodes opens the potential of sensors to be widely employed in platforms

for wireless network systems (WNSs). The key requirements such as reproducibility, reliability, low power consumptions as well as sensitivity and selectivity are vital for scale-up and mass production of sensing devices, opening the potential for more widespread deployment.[24]

Commonly, optical system configurations combine LEDs as a light source with a charge coupled device (CCD),[25] a light wave multimeter[25] or a photodiode.[26] Mims III *et al.* [27] demonstrated that a reverse-biased LED could also be employed as a very effective light detector. More recently, Diamond and co-workers have described the so-called, 'Paired Emitter-Detector Diode' (PEDD), optical sensor with regard to configuration and application.[28] Worsfold *et al.* have successfully employed LED based chemical sensors for *in-situ* monitoring of a variety of analytes with particular focus on phosphate[29] and nitrate/nitrite/ammonia.[30] An interesting approach to the photometric measurements based on PEDD for pH detection, enzymatic detection of urea, and evaluation of urease and alkaline phosphatase activities was presented by Koncki *et al.*[31] O'Toole *et al.*[28] applied a paired emitter-detector diode for the detection of phosphate using the malachite green spectrophotometric method.

In general, a PEDD consists of two light emitting diodes, one serving as the light source and the other, in reverse bias mode, as the light detector. The method achieves excellent sensitivity and signal-to-noise ratio (SNR) in comparison to the more commonly employed method of coupling a LED to a photodiode.[32] The low cost, small size, low power consumption, increasing spectral range coverage (247–1550 nm), intensity and efficiency, ease of fabrication and simplicity of the PEDD make it as an ideal optical detector for colorimetric assays.

The integration of low power, reliable wireless communications devices and *analytical* sensing (*e.g.* with chemo/biosensors) is an attractive proposition for the development of sensors working that can function

collaboratively to monitor specific target parameters. In recent years, our group has focused its investigations on the incorporation of ionic liquids (ILs) in polymer matrixes, resulting in materials called ionogels. ILs have been widely studied because of their potential applications in many different fields like electrochemistry[33, 34] biochemistry[35] and microfluidics,[36] due to their tunable hydrophobic and hydrophilic nature, chemical and thermal stability, low vapour pressure and high ionic conductivity properties.[37]

The incorporation of ILs into ionogels is a particularly attractive strategy in the field of sensing, since these materials, inherit all of the favourable IL properties whilst being in a solid, gel like structure.[38] For instance, Zhu *et al.*[39] used phosphonium based ionogels with a conventional chromoionophore for the detection of inorganic acids. Topal *et al.*[40] presented the increased selectivity of zinc phthalocyanines to pH when incorporated into imidazolium ionogels. Benito-Lopez *et al.*[41, 42] presented for the first time a wearable, flexible and disposable barcode system based on phosphonium ionogels for real time monitoring of the sweat pH. An optode membrane capable of simultaneous recognition of Cu^{2+} and Co^{2+} ions in a single measurement has also been realised.[43]

This chapter presents the fabrication, characterisation and performance of a low-cost, wireless optical sensor based on a PEDD system, combined with a portable, multi-channel lab-on-a-disc platform based on a dye-ionogel sensing area. The platform is applied to *in-situ* monitoring of the pH (quantitatively) and the degree of turbidity (qualitatively) of river water samples. In addition to the easy operation and robustness of the sensor, the obtained results can be downloaded in remote locations and displayed in *real time.* The water quality results obtained with the prototype platform are in good agreement with parallel reference measurements, which provides a degree of validation for the platform and the analytical method employed.

6.2 Experimental

6.2.1 Materials

N-Isopropylacrylamide (NIPAAm, Sigma-Aldrich®, Ireland), *N,N'*-methylene-bis(acrylamide) (MBAAm, Sigma-Aldrich®, Ireland), 2,2-5 dimethoxy-2-phenyl acetophenone (DMPA, Sigma-Aldrich®, Ireland), sodium dicyanamide (Sigma-Aldrich®, Ireland) and bromocresol purple (Sigma-Aldrich®, Ireland) were used for ionogel preparation. Tetrabutyl-phosphonium chloride $[P_{4,4,4,4}][Cl]$ ionic liquid was provided by Cytec Industries, Ontario Canada. The anion exchange reaction of $[P_{4,4,4,4}][Cl]$ with sodium dicyanamide was performed as described elsewhere,[44] in order to obtain tetrabutyl-phosphonium dicyanamide (abbreviated: $[P_{4,4,4,4}][dca]$). The IL was then purified thoroughly by column chromatography, dried under vacuum at 40 °C for 48 h, and stored under argon at 20 °C.

The colorimetric pH sensor utilised bromocresol purple pH dye (BCP) (Sigma-Aldrich®, Dublin, Ireland). Aqueous solutions were prepared using deionised water (Milli-Q). For the silanisation process acetic acid, methanol and 3-(trimethoxysilyl)propyl methacrylate were purchased from Sigma-Aldrich®, Ireland. Oxidation of the PMMA surfaces was carried out using a Harrick Plasma Cleaner oxygen plasma. PMMA sheets (1500 μm) were purchased from Radionics, Ireland and 50 μm and 86 μm double-sided Pressure Sensitive Adhesive film (AR8890) from Adhesives Research, Ireland.

Yellow (590 nm) Surface Mount LEDs were purchased from Radionics, Ireland. These were operated under a stabilised constant current of 25 mA generated by an in-house made power supply. Arduino microcontrollers and Xbee modules were purchased from Sparkfun Electronics, Boulder, Colorado, USA. The in-house designed case and disc holder of wired and wireless detectors were fabricated using a 3D printer (Stratasys, USA), in acrylonitrile

butadiene styrene co-polymer (ABS) plastic in order to protect the electronics and to minimise interferences from ambient light during the operation of the device. The printed parts were designed using ProEngineer CAD/CAM software package. The UV light source used for photopolymerisation was a BONDwand UV-365 nm obtained from Electrolyte Corporation, USA (800 $\mu W\ cm^{-2}$). UV-Vis spectra and the emission spectrum of the emitter LED were recorded on a UV-Vis-NIR Perkin-Elmer Lambda 900 spectrometer. The bench-top pH meter (SevenEasy™ pH S20) was obtained from VWR International, Inc.

6.2.2 Lab-on-a-disc fabrication

To fabricate the multilayer centrifugal disc devices, poly-(methyl methacrylate) (PMMA) components were laser milled while double-sided, pressure sensitive adhesive (PSA) was cut using a knife plotter machine (Graphtec, Japan). After manufacturing, the assembly was laminated together to create the final device (Fig. 1b). The fabrication of the microfluidic devices was carried out using a laser ablation system (Epilog Zing Laser Engraver, USA) and a cutter-plotter.

Design 1

In order to demonstrate the suitability of the PEDD device for integrated detection in a lab-on-a-disc, a first prototype was fabricated. The full characterisation of the integrated device was carried out using a five layer centrifugal disc with ten micro-channels (see Fig. C1, Appendix C). The upper chamber with inlet ports has an oval shape, with a length of 1.5 cm and a width 0.5 cm, whereas the bottom chamber, circle shaped, has a diameter of 0.5 cm. The length of the microchannel is 1 cm (1 mm wide), with a total

length of the microfluidic structure of 3.5 cm. The height of both chambers, which determines the light path length of the optical system, is 1.636 mm depth (PMMA layer and PSA thickness together).

Design 2

The multi-parameter water analysis study was carried out using a CD containing seven large chambers with several sub-compartments for performing various functions, Fig. 6.1a. A PMMA upper section of height 1.5 mm, restricted by the thin PSA, creates the chamber containing an inlet port and a hole which facilitates air expulsion during rotation (Fig. 6.1b, A). The sieve opens over the middle microfluidic part (Fig. 6.1b, B), fabricated using a 1.5 mm PMMA and 50 μm PSA layer, which contains two rectangular reservoirs (4.5 mm x 7 mm and 1.55 mm depth), with photopolymerised ionogels: the reference, and the sensor with a pH sensing dye, bromocresol purple. Finally, the microfluidic area tapers to a bottom chamber of height 86 μm (Fig. 6.1b, C). Both, the upper and bottom chambers, contain horizontal laser milled lines which aided in visual inspection of collected particulates.

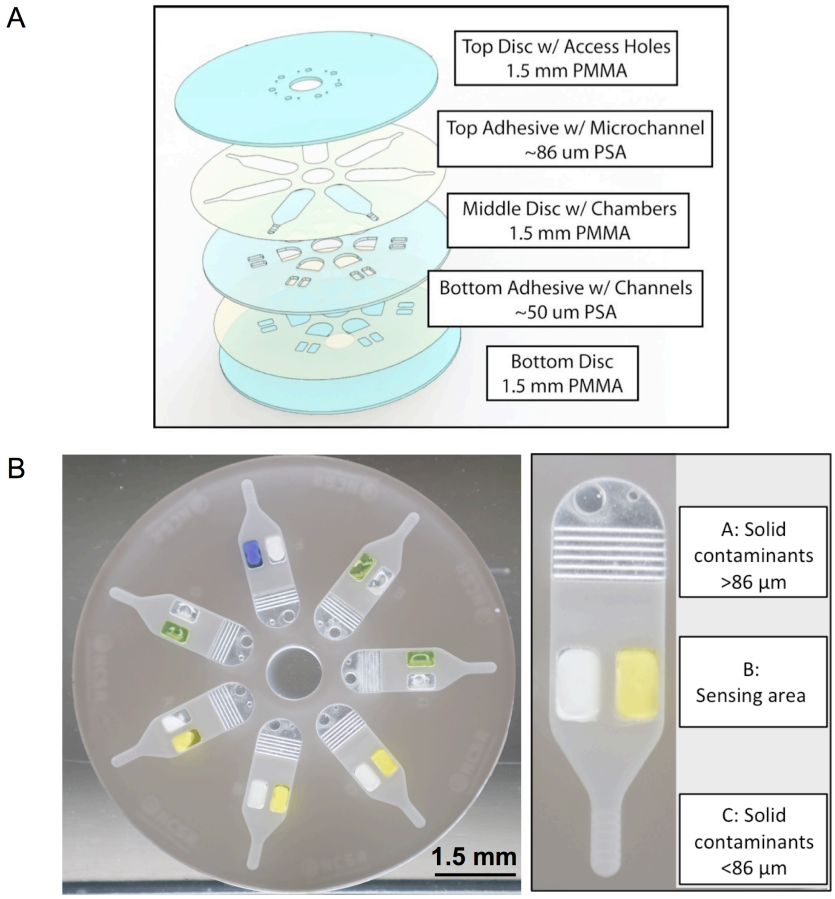

Figure 6.1. a) Scheme showing the assembly of the microfluidic CD consisting of poly(methyl methacrylate) and Pressure Sensitive Adhesive layers. The plastic layers contain the chambers, whereas the adhesive layers contain the fluidic channels, b) picture of the Lab-on-a-disc device with a zoom of the fluidic channel with the sensing area; white (reference region) and yellow (ionogel sensor).

6.2.3 Ionogel pH sensing area fabrication

The sensing areas are based on ionogels consisting of poly(*N*-isopropyl-acrylamide) [x] and *N,N'*-methylene-bis(acrylamide) [y] cross-linked polymer in the ratio 100 (x):5 (y) in which the ionic liquid $[P_{4,4,4,4}][dca]$ was entrapped into the polymer matrix.[45] Fig. 6.2 presents the chemical structure of the polymer, Fig. 6.2A, the ionic liquid, Fig. 6.2B, and the dye, Fig. 6.2C, used in this study when drop-casted and photopolymerised in the PMMA/PSA reservoirs.

To facilitate ionogel stability in the disc, the PMMA surface in the reservoirs was chemically treated to facilitate covalent bonding of the ionogel. Firstly, the surface was oxidised in an oxygen plasma chamber for 60 s, and then each reservoir was filled with 60 μL mixture of water at pH 3.5, methanol, and 3-(trimethoxysilyl)propyl methacrylate in the volume ratio 24 : 10 : 1. The silanisation step was adapted from a previously published protocol presented in the reference.[46] After 2 h, the reservoirs were rinsed with methanol and water several times and dried under nitrogen. The ionogel solution was prepared by adding the NIPAAm monomer, MBAAm crosslinker, and DMPA photo-initiator (molar ratio 100 : 5 : 3, respectively) to the ionic liquid (0.7 mL, 40 °C for 20 min). This mixture was used to prepare an unresponsive reference (ionogel without pH dye) version of the sensor. The pH sensitive ionogel was obtained using the same mixture but with BCP dye (concentration 6 x 10^{-3} M or 1 x 10^{-3} M) dissolved in the IL before the addition of monomers and photo-initiator. Polymerisation of the reference and pH sensitive films was performed using a UV irradiation source (λ = 365 nm) placed 8 cm from the solution for 40 min (UV intensity 10 mW cm^{-2}). When polymerisation was complete, the resulting ionogels were washed with water to remove any un-polymerised monomer and the excess ionic liquid.

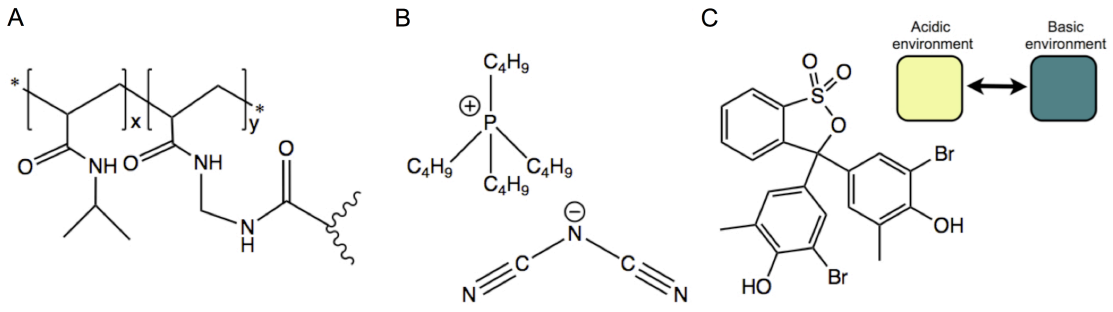

Figure 6.2. A) *N*-Isopropyl-acrylamide and *N,N'*-methylene-bis(acrylamide) crosslinked polymer in the ratio 100(x) : 5(y) B) ionic liquid tetrabutyl-

phosphonium dicyanoamide [$P_{4,4,4,4}$][dca], C) bromocresol purple dye showing typical colour changes in acidic and basic environments.

6.2.4 Concentration of the dye within the ionogel matrix

The effect of BCP concentration on the sensor response was studied by preparing two series of ionogels with BCP concentrations of 6 x 10^{-3} M and 1 x 10^{-3} M. Both ionogels were exposed to buffer solutions and the colour dependent discharge time was recorded for 15 minutes using the PEDD detector. The concentration of the dye that provided the faster detection time, 15 min, *i.e.* when the relative slope of the signal was found to be less than 2 % for 1 min, was 6 x 10^{-3} M. Therefore, 6 x 10^{-3} M of BCP dye was adopted throughout all remaining experiments. An interesting point is that the polymerisation time required for the ionogel formation was shorter in the formulation containing the lower BCP concentration, at 25 min for 1 x 10^{-3} M, and 40 min, for 6 x 10^{-3} M. Moreover, no significant photobleaching was observed after exposure to the UV source for 40 min.

6.2.5 PEDD optical detector system

The PEDD detector consists of two pairs of Surface Mount LEDs (for reference and sensing regions), placed above and below the sensing area of the disc (Fig. 6.3A). One LED in each pair acts as the light source while the other is reverse biased, acts as a detector, as previously reported.[47, 48] Briefly, the detector LED in output mode was charged up to 5 V for 100 μs and then switched to high impedance input mode. Light from the emitter LED generates a photocurrent in the reverse biased detector LED, resulting in discharge of the capacitance based voltage from an initial value of 5 V (logic 1) to a present value of 1.7 V (logic 0). In order to provide a stable +5 V

source to drive the circuit and LEDs, a voltage regulator running from a 9 V battery was employed. After passing through the microfluidic device, the observed light intensity is related to the discharge time of the acquired charge in the device.[49] The detector signal was captured using HyperTerminal software, saved as a text file and then analysed using MS Excel.

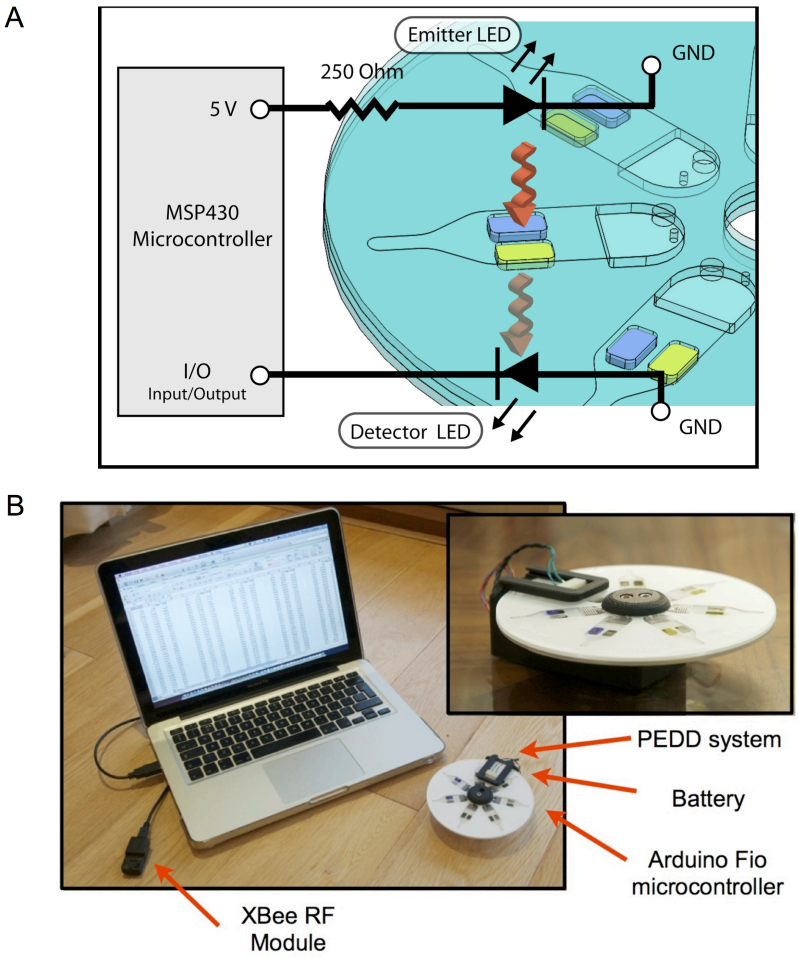

Figure 6.3. A) Scheme of circuit used for the PEDD system. B) Prototype of the PEDD centrifugal microfluidic system.

A lithium polymer battery serves as the prototype power source and a USB/XBee socket is available to transmit data wirelessly to a laptop in real time as shown in Fig. 6.3B. The PEDD system is integrated into an in-house generated 3D printed arm-like structure to ensure good alignment of the LED emitters and the LED detectors with the sensing and reference regions, Fig.

6.3B. Moreover, the PEDD detector can be slipped through the x-axis of the arm providing an extra degree of flexibility of the system. After spinning, the disc is transferred to a stand that provides free rotation and ensures that the PEDD detector addresses the sensing/reference regions in a reproducible manner.

6.2.6 Optical characterisation of the PEDD detector in the lab-on-a-disc platform

The design 1 of the microfluidic platform was used to characterise the PEDD detector using different concentrations of aqueous solutions of BCP at pH 6.5. For comparison, UV-Vis spectra of the same BCP solutions were also obtained. A series of dilutions (1.0×10^{-3} M to 2.5×10^{-6} M in water) of BCP were also examined with the PEDD system by placing 10 μL of the solutions in the sample reservoirs of the CD, and subsequently spinning to load the fluids into the testing regions. The resulting signal was measured continuously for 30 s. The sampling rate under this protocol is *ca.* 1 point per second.

6.2.7 Ionogel pH sensor calibration

To examine the behaviour of the pH-sensing ionogel, the pKa of the dye incorporated in the ionogel was determined. PH measurements of six buffer solutions with differing pH values (range 4-8) were carried out using the *design 2*. Solutions were placed sequentially in the sample reservoirs and spun at 1500 rpm for 5 min, in order to drive the liquid to the sensing area of the disc, where the photopolymerised ionogels were integrated as previously described. After 15 min the ionogel was fully hydrated and a stable and homogeneous colour was obtained.

6.2.8 Analysis of real samples

Water samples were collected from nine different locations on the Tolka River, Dublin, Ireland. 100 μL volumes of the samples were pipetted into the sampling ports the disc spun at 1500 rpm. Solids in the samples were retained in the upper chamber and/or accumulated in the bottom chamber according to their size, as mentioned before. The analytical measurement was carried out using the PEDD detection system in a dark environment, to reduce external light interference. The light dependence discharge time of detector LED was measured continuously for 30 s. The emitter LED was set to give 1 ms pulses of light as the light source for the absorption based measurements. The sampling rate under this protocol is *ca.* 1 point per second. In order to provide reference data, samples were also measured using a standard pH-meter, and turbidity was examined by UV-Vis spectrometry (% Transmittance).

6.3 Results and discussion

6.3.1 PEDD lab-on-a-disc device

A centrifugal microfluidic platform was chosen for water quality analysis and monitoring because fluid manipulation required a minimal amount of instrumentation. Additionally, multiple parallel fluidic assays can be integrated within one disc structure, enabling parallel processing of different samples, minimising costs and reagent consumption as explained in the introduction section.[22] The fabrication of the centrifugal platforms based on the milling of the PMMA layers and cutting of the adhesive layers, followed by the lamination step, was simple and straightforward. Moreover, the designed features could easily be adapted for mass production processes

such as injection moulding.

Colorimetric disc-based detection has been previously used for clinical applications to detect biochemical markers such as calcium, creatinine, glucose, electrolytes and various blood protein panels,[50] and also for analysis of chromium VI and nitrites in environmental water samples.[17] The integration of colorimetric detection using the PEDD system within the centrifugal platform presents significant advantages for lab-on-a-disc technology, as it can facilitate the integration of on-line, wireless and *in-situ* rapid measurements due to its inherent non-contact mode of operation. The autonomous capabilities of the system, combined with the portability and wireless communication, provide the flexibility needed for on-site water monitoring.

The present platform design enables simultaneous pH and turbidity measurements, which provides useful information on the management of the water during a treatment process and hence the quality of drinking water on the point-of-side. Although these parameters are not a risk to health, they indicate that corrective action and investigation is required before it becomes a potential risk. For example, elevated levels of turbidity have been shown to be associated with outbreaks of *Cryptosporidium* (Carlow, Ireland, in 2006 and Galway City, Ireland in 2007).[51]

6.3.2 PEDD detector characterisation

The wireless paired emitter detector diode device consists of two light emitting diodes (LEDs), as previously explained. This system allows for the creation of a digital output directly without using an A/D converter or operation amplifier. The system was chosen due to its excellent sensitivity and signal-to-noise ratio (SNR) as explained in the introduction,[32] in addition to

its universal and tunable properties,[24] which makes PEDD an ideal low-cost optical detector for many colorimetric assays.

A yellow LED (λ_{max} = 590 nm) was used as the emitter as the emission spectrum of the LED efficiently overlapped with the absorbance spectra of bromocresol purple dye (see Fig. C2, Appendix C). At this wavelength, the acid form of this dye has much lower absorbance than its basic form, which absorbs the LED light more efficiently and will give optimal sensitivity for this colorimetric measurement. In addition, a yellow LED was also employed as the detector.

In order to examine the efficiency of the wireless paired emitter detector diode device, series of dilutions of BCP were measured using UV-Vis spectrometry for control, and then with the PEDD system, employing the design 1 disc. According to the UV-Vis spectra of BCP (see Fig. C3, Appendix C), a linear relationship between absorbance and dye concentration was found over the concentration range from 2.5 x 10^{-6} to 5.0 x 10^{-5} M (pH = 6.5, basic form of the dye). It should be noticed that higher concentrations were not accurately measured while lower concentrations were not detected. The calibration curve of BCP pH dye is presented in Fig. 6.4, for both optical systems. Results showed close correlation between the PEDD system and standard UV-Vis spectrometry with similar limits of detection (LOD) (2.5 x 10^{-6} M). The results of the absorbance analysis of different concentrations of BCP dye water solutions using *design 1* platform showed the successful application of this system for colour and colour-based pH measurements and offered high sensitivity, enabling detection down to the sub micro-molar concentrations of the dye.

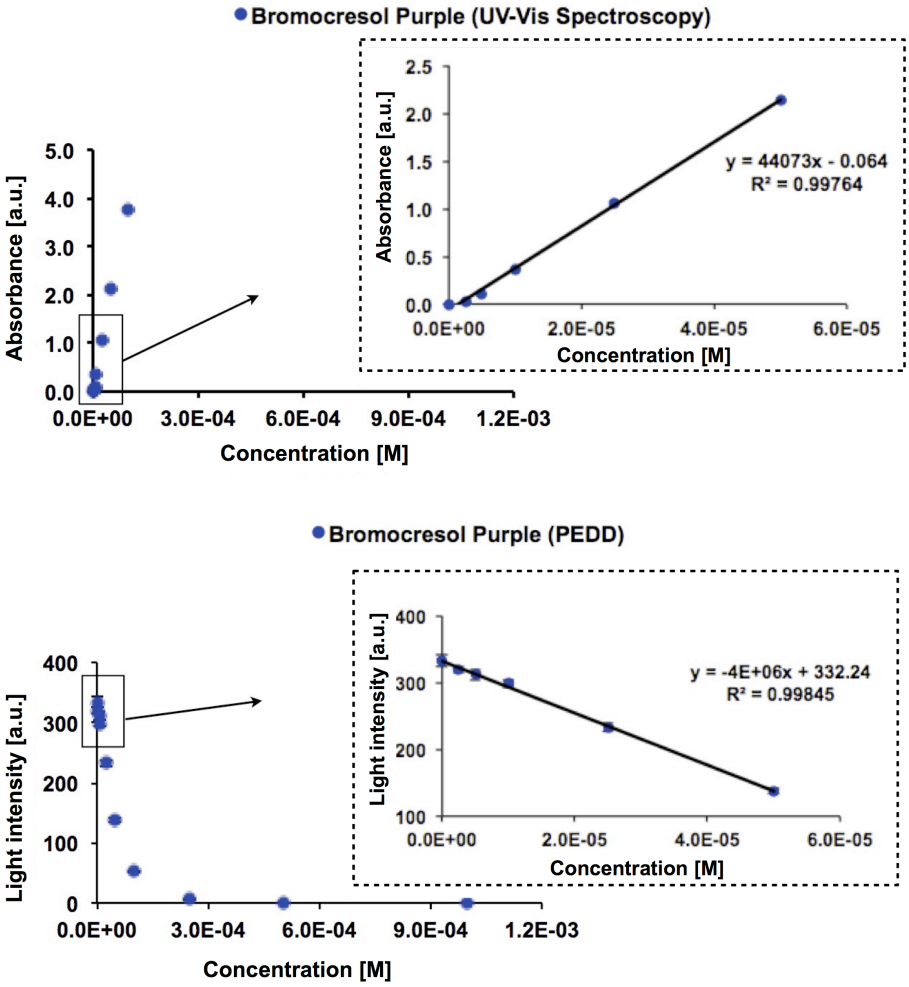

Figure 6.4. Calibration curves of bromocresol purple pH dye in solution, n = 6, using a UV-Vis spectrometer (top) and the PEDD system (bottom), $L_{UV\text{-}Vis}$ = 1 cm, L_{PEDD} = 0.16 cm.[52]

6.3.3 Ionogel optical calibration using the lab-on-a-disc with PEDD detection

The use of the paired emitter detector diode (PEDD) device for colour and pH measurements has been reported previously in static solutions[49] and for flow analysis.[53] Here, for the first time the performance of a custom designed PEDD device for lab-on-a-disc applications is presented. In the case of water pH analysis, the sensing function was provided by a pH indicator dye immobilised within an ionogel polymer matrix, which provides an excellent matrix for immobilising the dye (Fig. 6.1). As it was previously reported, due

to ion-pair interactions between the pH indicator and the ionic liquid that forms the ionogel structure, there is no leaching of the pH dye during experiments, thereby providing improvement in robustness of the pH sensor.[54] In addition, the stability of the ionogel under harsh conditions (pH ranging from 0 to 14)[45] ensures accurate water quality monitoring over a wide pH range can be carried out without degradation of the sensor matrix.

Further, a long-term sensor stability was achieved by ensuring covalent immobilisation of the ionogel to the surface of the PMMA substrate. This avoided the delamination of the swollen ionogel from the microfluidic device during sample analysis over time. The surface of the PMMA was treated with O_2 plasma and subsequently silanised using 3-(trimethoxysilyl)propyl methactylate. In this way, during the ionogel polymerisation, the monomers crosslinked with the free double bonds of the surface generating a covalent bond between the ionogel and the PMMA bottom channel surface.

6.3.4 Calibration of the chemical sensor

The pKa of BCP in the ionogel was determined using standard buffer solutions (Fig. 6.5A). Depending on the pH of the buffer solution, the initial bright green ionogel colour changed to yellowish in a more acidic environment (pH = 4.0) and to dark green in a more basic environment (pH = 8.4) as depicted in the picture of the disc in Fig. 6.5B. The PEDD optical sensor was able to detect the colour changes of the ionogel that occurs at different pH values. The data obtained follow a sigmoidal curve, which is expected for this acid-base dye chemistry. The first derivative showed a pK_a value of 6.6 for the solid-state pH sensor. This indicates that immobilisation of the pH indicator dye in the ionogel, results in a shifting of the dye pK_a up to 0.3 pH units, in comparison to a pK_a of 6.3 reported in literature.[55] It was previously

demonstrated that when pH indicator dyes are immobilised within solid gels, the micro-environment of the matrix shifts the pK_a of the dye slightly, on occasions by over 0.5 pH unit.[56] The observed pK_a value is also influenced by the thickness of the gel, due to the increased diffusion constraint of the protons concerned and a change in dielectric properties of the ionogel.[56] From the pictures of the centrifugal platform in Fig. 6.1B it can be seen that a strong colour change is obtained using the *ca.* 0.8 mm thick ionogel sensor layer as this facilitates more efficient bulk proton diffusion and faster detection times.

The stability of the chemical sensor was demonstrated by performing several calibrations using the centrifugal platform (*design 2*). Calibrations showed good repeatability with relative standard deviation (RSD) typically within 2.7 % (see errors in Fig. 6.5A). This indicated that the pH indicator dye is stable over time (no leaching is observed during the measurements), and that the results are reproducible for different discs. Moreover the dye acid/base character is maintained within the ionogel since the dye is fully reversible from acidic to basic pH changes.

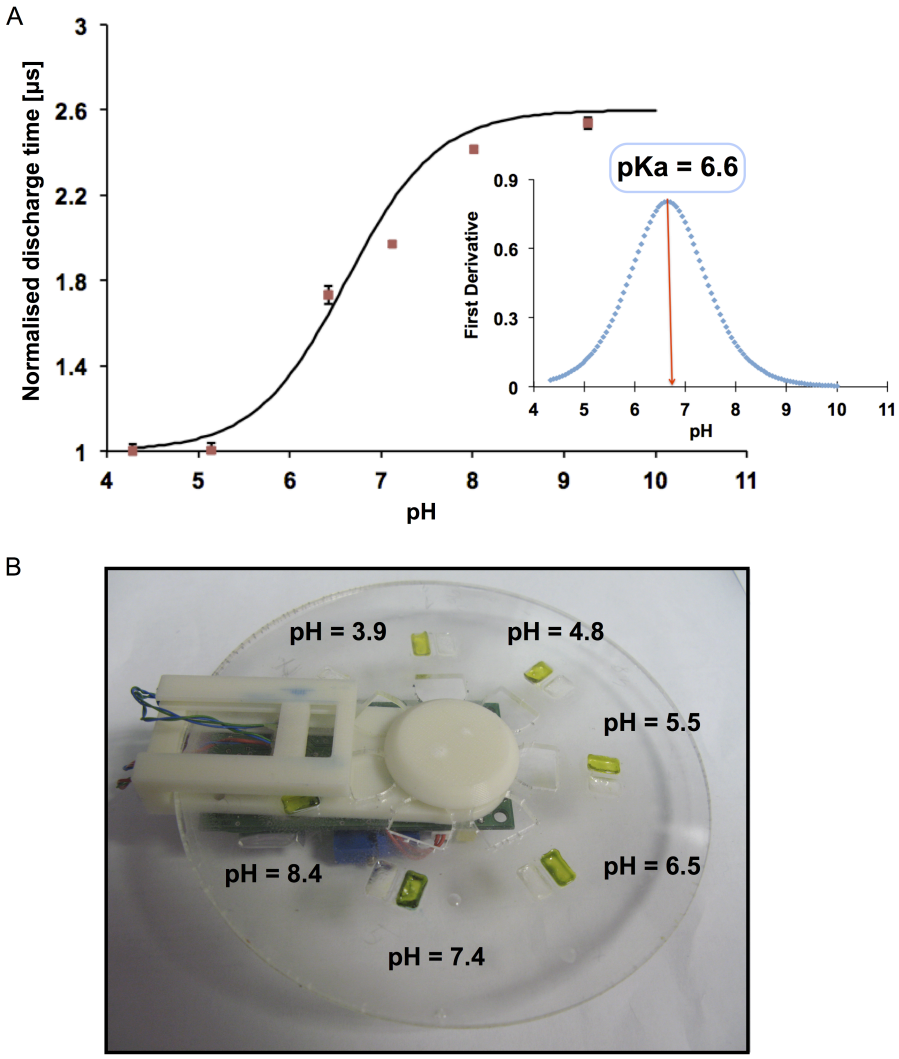

Figure 6.5. A) Calibration curve of the sensing area of the microfluidic device using pH buffer solutions. (n = 3, error represents the average of discharge time values during data collection), and the first derivative with presented pK_a = 6.6 for the solid-state pH sensor. The equation used for the curve fit is as follows: y = 2.6-1.6/(1+exp((x-6.62)/0.49); sum of square residuals (SSR) = 0.07. B) A CD platform with the ionogel/dye sensing area at different pH values, for calibration.

6.3.5 Application to environmental water analysis (pH and turbidity)

Water quality analysis of samples from seven different locations of the Tolka River were carried out using the centrifugal disc (*design 2*). This river was chosen due to the report published in 2005 on a poor quality discharge of

effluent and an associated fish mortality.[57] After collection, samples were loaded to the different upper chambers through the inlet ports of the disc. The disc was then placed on the motor stand and spun at 1500 rpm forcing the samples to the bottom chambers, covering the whole sensing area. The liquid and solid contaminants present in the water were transported through the microfluidic channel from the top to the bottom chamber during disc rotation (Fig. 6.6). After rotation, the sensing area that contains the ionogels/dye is fully covered with the sample and so the BCP pH dye changes colour according to the water pH.

6.3.5.1 Filtration

Light scattering of the solid suspended particles from the real samples results in an additional absorption in the detector. This problem can be solved by filtering the sample before detection, since it has been previously reported that the remaining particles lead to a large error during the colorimetric measurement if not filtered out.[58] Therefore, the *design 2* of the centrifugal platform employed a filtration step (Fig. 6.6, yellow square). Due to the constriction generated in the upper chamber by the decrease in height of the micro-channel from 1500 μm to 86 μm (more than 94 %), solid particles larger than about 86 μm are trapped in this upper chamber, enabling an efficient sample filtration process. As a consequence, optical measurements carried out in the lower parts of microfluidic system can be substantially independent of the particles content of the sample, allowing for higher accuracy and reliability of analysis.

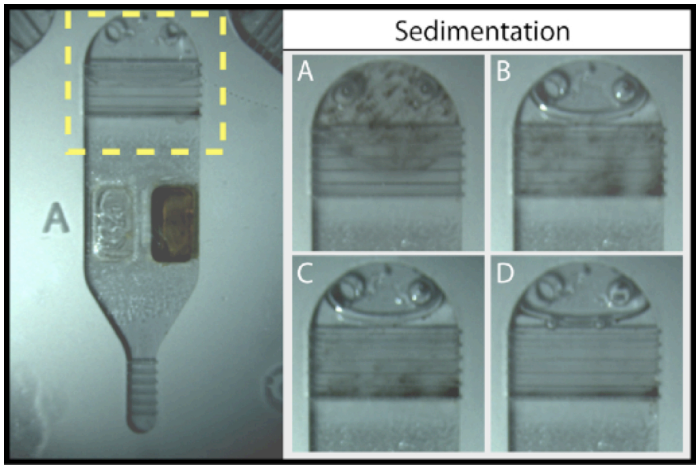

Figure 6.6. Images of a channel of the CD during centrifugation at 1500 rpm. A) the upper chamber is filled with sample, then the disc is spun for two minutes and all the liquid is transferred to the sensing area (B-D). Particles of a diameter greater than 86 µm are accumulated in the upper chamber during the spinning process (B-D).

6.3.5.2 Turbidity

The results obtained with samples from the River Tolka are shown in Figure 6.6 A-D and in Figure C4 in Appendix C. The larger particles (> 86 µm) were trapped in the upper chamber, whereas particles smaller than 86 µm were accumulated in the bottom chamber. Fig. 6.7 shows a comparison of quantitative UV-Vis measurements (transmittance), for two samples (Fig. 6.7A), and a picture of the same two samples after qualitative on-chip analysis, (Fig. 6.7B). The low transmittance of sample no. 3 obtained by the UV-Vis spectrophotometer at 600 nm (Fig. 6.7A) correlates with the high amount of solid contaminants trapped in the upper chamber of the microfluidic system (Fig. 6.7B). In contrast, sample no. 7, which was relatively clean in comparison to sample 3 shows higher UV-Vis transmittance and a smaller amount of solid material accumulated in the upper filter region.

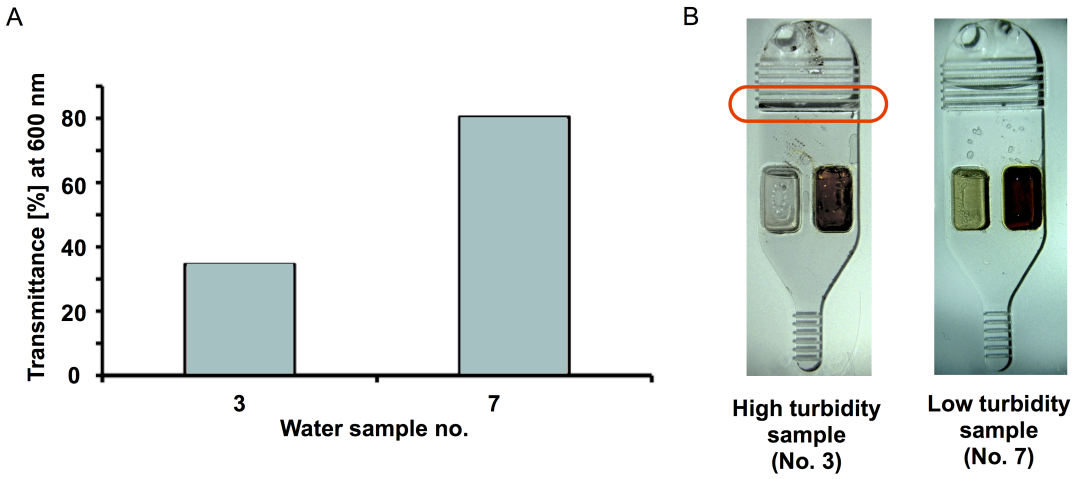

Figure 6.7. a) UV-Vis spectrometer transmittance measurements of samples 3 and 7; b) pictures of the channels containing sample 3 (left, with particles accumulated in the highlighted region) and 7 (lower amount of solid material accumulated, right).

6.3.5.3. PH measurements

In the *design 2* of the disc, the parallel microfluidic systems with pH dye/ionogel sensing areas are provided, allowing analysis of seven separate 100 μL samples. Measurements were carried out using the PEDD detector in a dark environment, to minimise external light effects, and the detector output monitored continuously for 30 seconds. As shown in the Fig. 6.8, an excellent correlation between pH results using the PEDD system and a standard pH-meter was obtained over the pH range 5-9. Our results also demonstrated that the ionic liquid anion $[dca]^-$, that is well known to behave like a Lewis base,[59] does not interfere with the response of the dye.

The results also indicate that the filtering step employed within the microfluidics allows for an accurate measurement even of turbid samples, thus making the colorimetric detection substantially independent of the particle content of the real samples.

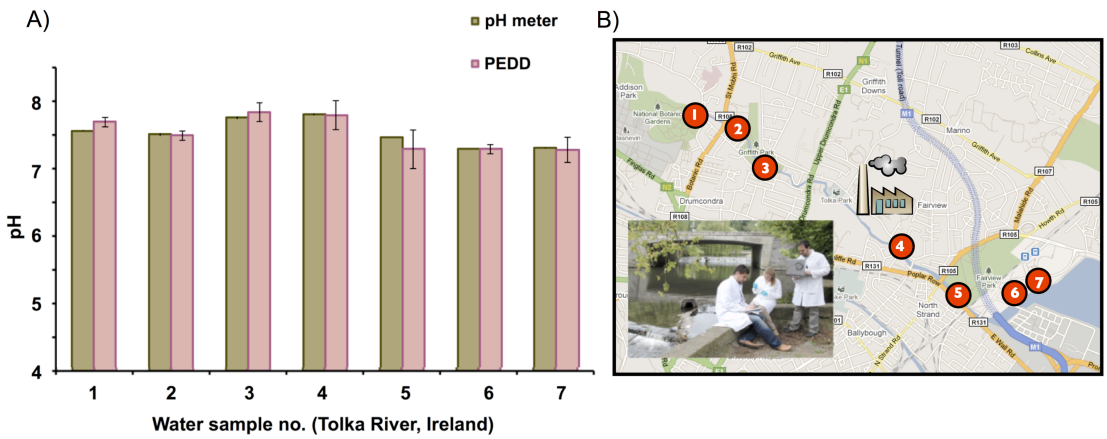

Figure 6.8. A) Water pH analysis using a commercially available pH-meter and the PEDD lab-on-a-disc device at different locations of the Tolka River (Dublin, Ireland) ($n = 3$). B) Google map picture of the different locations where samples were taken (right side picture).

Overall, the results obtained by the wireless, portable PEDD system demonstrate relatively good quality of the water samples, with regards to the turbidity and pH values. The results are within the range accepted by Environmental Protection Agency.[60] The data obtained with standard UV-Vis spectrometer, as well as those obtained with the lab-on-a-disc device, provide information on the improvement of the Tolka River water quality, which confirms the latest report showing significant reduction of the pollution levels.[61]

At the moment, the spinning of the disc is performed using the bench-top spin stand setup, and once the fluids have reached the sensing areas, the optical system is attached to the centrifugal platform thus the detection takes place. Therefore, the incorporation of a remotely controlled motor for *in-situ* spinning of the CD within the optical system, will be presented in Chapter 7. In addition, the on-chip turbidity measurement is performed through a simple visual inspection of the centrifugal platform, thus providing qualitative estimation of water turbidity. In order to improve the autonomous capabilities of the device, crucial for on-site water monitoring, our future work will also

focus on the incorporation of a quantitative turbidity measurement method based on the PEDD device.

6.4 Conclusions

A portable system for *in-situ* colorimetric water quality analysis has been developed. The device incorporates low-power detection coupled with wireless communication and power supply into lab-on-a-disc system. Integration of a wireless communication device allows data acquisition according to individual needs. Similar performance characteristics between the lab-on-a-disc device and standard UV-Vis spectrometer imply that the system provides accurate results and allows for for detection of several parameters at low concentration levels.

In general, this system shows the huge potential for the PEDD system to be a cheap and versatile alternative as point-of-care optical detector for lab-on-a-disc applications. This device will be of special interest in samples with a relatively high level of solid particles that could interfere with the optical analytical measurements.

6.5 Acknowledgements

The authors wish to thank to the Marie Curie Initial Training Network funded by the EC FP7 People Programme, Science Foundation of Ireland under grant 07/CE/I1147 and Cytec Canada Inc. for supplying the phosphonium salts. VFC thanks to the Research Career Start Programme 2010 fellowship from Dublin City University. This work was also supported in part by the Science Foundation Ireland under Grant No. 10/CE/B1821.

6.6 References

1. Environmental Protection Agency, A year in Review – highlights from 2011; Dublin, **2011**.
2. World Health Organization, The Global Annual Assessment on Sanitation and Drinking-Water (GLAAS) 2010; **2010**.
3. Diamond, D.; Coyle, S.; Scarmagnani, S.; Hayes, J., Wireless sensor networks and chemo-/biosensing. *Chemical Reviews* **2008,** *108* (2), 652-679.
4. Hanrahan, G.; Patil, D. G.; Wang, J., Electrochemical sensors for environmental monitoring: design, development and applications. *Journal of Environmental Monitoring* **2004,** *6* (8), 657-664.
5. Heninger, I.; Potin-Gautier, M.; de Gregori, I.; Pinochet, H., Storage of aqueous solutions of selenium for speciation at trace level. *Journal of Analytical Chemistry* **1997,** *357*, 600–610.
6. Polya, D. A.; Lythgoe, P. R.; Abou-Shakra, F.; Gault, A. G.; Brydie, J. R.; Webster, J. G.; Brown, K. L.; Nimfogpoulus, M. K.; Michailidis, K. M., IC-ICP-MS and IC-ICP-HEX-MS determination of arsenic speciation in surface and groundwaters: preservation and analytical issues. *Mineralogical Magazine* **2003,** *67* (2), 247–261.
7. Environmental Protection Agency, Sampling and analysis of waters, wastewaters, soils and wastes. Carlton, Australia, **2009. (**acessed on 10/07/2012)
8. McGraw, C. M.; Stitzel, S. E.; Cleary, J.; Slater, C.; Diamond, D., Autonomous microfluidic system for phosphate detection. *Talanta* **2007,** *71* (3), 1180-1185.
9. Rogers, K. R., Recent advances in biosensor techniques for environmental monitoring. *Analytica Chimica Acta* **2006,** *568* (1-2), 222-231.
10. Schaap, A.; Bellouard, Y.; Rohrlack, T., Optofluidic lab-on-a-chip for rapid algae population screening. *Biomedical Optics Express* **2011,** *2* (3), 658-664.
11. Cleary, J.; Slater, C.; McGraw, C.; Diamond, D., An Autonomous microfluidic sensor for phosphate: On-site analysis of treated wastewater. *IEEE Sensors Journal,* **2008,** *8* (5), 508-515.
12. Bowden, M.; Diamond, D., The determination of phosphorus in a microfluidic manifold demonstrating long-term reagent lifetime and chemical stability utilizing a colorimetric method. *Sensors and Actuators B* **2003,** *90* (1-3), 170-174.
13. Bowden, M.; Sequiera M.; Krog J. P.; Gravesen P.; Diamond, D., Analysis of river water samples utilizing a prototype industrial sensing system for

phosphorus based on micro-system technology. *Journal of Environmental Monitoring* **2002,** *4* (5), 767-771.

14. Curtis, T. M.; Widder, M. W.; Brennan, L. M.; S. J. Schwager, S. J.; van der Schalie, W.H.; Fey, J.; Salazar, N., A portable cell-based impedance sensor for toxicity testing of drinking water. *Lab on a Chip* **2009,** *9* (15), 2176-2183.
15. Zou, Z.; Jang, A.; MacKnight, E. T.; Wu, P.-M.; Do, J.; Shim, J. S.; Bishop, P. L.; Ahn, C. H., An on-site heavy metal analyzer with polymer lab-on-a-chips for continuous sampling and monitoring. *IEEE Sensors Journal* **2009,** *9* (5), 586-594.
16. Jang, A.; Zou, Z.; Lee, K. K.; Ahn, C. H.; Bishop, P. L., State-of-the-art lab chip sensors for environmental water monitoring. *Measurement Science and Technology* **2011,** *22* (3), 032001-032019.
17. LaCroix-Fralish, A.; Clare, J.; Skinner, C. D.; Salin, E. D., A centrifugal microanalysis system for the determination of nitrite and hexavalent chromium. *CORD Conference Proceedings* **2009,** *80* (2), 670-675.
18. Yongqing, X.; Templeton, E.J.; Salin, E. D., Rapid simultaneous determination of nitrate and nitrite on a centrifugal microfluidic device. *Talanta* **2010,** *82* (4), 1612-1615.
19. Steigert, J.; Grumann, M.; Dube, M.; Streule, W.; Riegger, L.; Brenner, T.; Koltay, P.; Mittmann, K.; Zengerle, R.; Ducrée, J., Direct hemoglobin measurement on a centrifugal microfluidic platform for point-of-care diagnostics. *Sensors and Actuators A: Physical* **2006,** *130-131*, 228-233.
20. Siegrist, J.; Gorkin, R.; Bastien, M.; Stewart, G.; Peytavi, R.; Kido, H.; Bergeron, M.; Madou, M., Validation of a centrifugal microfluidic sample lysis and homogenization platform for nucleic acid extraction with clinical samples. *Lab on a Chip* **2010,** *10* (3), 363-371.
21. Madou, M., *Fundamentals of Microfabrication.* CRC Press: Boca Raton, Florida, **2002**.
22. Madou, M.; Zoval, J.; Jia, G.; Kido, H.; Kim, J.; Kim, N., Lab on CD. *Annual Review of Biomedical Engineering* **2006,** *8*, 601-628.
23. Diamond, D.; Lau, K. T.; Brady, S.; Cleary, J., Integration of analytical measurements and wireless communications - Current issues and future strategies. *Talanta* **2008,** *75* (3), 606-612.
24. O'Toole, M.; Shepherd, R.; Wallace, G. G.; Diamond, D., Inkjet printed LED based pH chemical sensor for gas sensing. *Analytica Chimica Acta* **2009,** *652* (1-2), 308-314.
25. Weigl, B. H.; Wolfbeis, O. S., Sensitivity studies on optical carbon dioxide sensors based on ion pairing. *Sensors and Actuators B: Chemical* **1995,** *28* (2), 151-156.

26. Pacquit, A.; Lau, K. T.; McLaughlin, H.; Frisby, J.; Quilty, B.; Diamond, D., Development of a volatile amine sensor for the monitoring of fish spoilage. *Talanta* **2006,** *69* (2), 515-520.
27. Mims, M. F., How to monitor ultraviolet radiation from the sun. *Scientific American* **1990,** *263*, 106-109.
28. M. O'Toole; Diamond, D., Absorbance based light emitting diode optical sensors and sensing devices. *Sensors* **2008,** *8*, 2453-2479.
29. Worsfold, P. J.; Richard Clinch, J.; Casey, H., Spectrophotometric field monitor for water quality parameters : The determination of phosphate. *Analytica Chimica Acta* **1987,** *197*, 43-50.
30. Gardolinski, P. C. F. C.; David, A. R. J.; Worsfold, P. J., Miniature flow injection analyser for laboratory, shipboard and in situ monitoring of nitrate in estuarine and coastal waters. *Talanta* **2002,** *58* (6), 1015-1027.
31. Pokrzywnicka, M.; Koncki, R.; Tymecki, L., A very simple photometer based on paired-emitter-detector diodes. *Analytical Chemistry* **2009,** *54* (3), 427-435.
32. O'Toole, M.; Lau, K. T.; Shepherd, R.; Slater, C.; Diamond, D., Determination of phosphate using a highly sensitive paired emitter-detector diode photometric detector. *Analytica Chimica Acta* **2007,** *597* (2), 290-294.
33. Forsyth, S. A.; Fraser, K. J.; Howlett, P. C.; MacFarlane, D. R.; Forsyth, M., N-methyl-N-alkylpyrrolidinium nonafluoro-1-butanesulfonate salts: Ionic liquid properties and plastic crystal behaviour. *Green Chemistry* **2006,** *8* (3), 256-261.
34. Kavanagh, A.; Byrne, R.; Diamond, D.; Fraser, K. J., Stimuli responsive ionogels for sensing applications - An overview. *Membranes* **2012,** *2* (1), 16-39.
35. Khodagholy, D.; Curto, V. F.; Fraser, K. J.; Gurfinkel, M.; Byrne, R.; Diamond, D.; Malliaras, G. G.; Benito-Lopez, F.; Owens, R. M., Organic electrochemical transistor incorporating an ionogel as a solid state electrolyte for lactate sensing. *Journal of Materials Chemistry* **2012,** *22* (10), 4440-4443.
36. Benito-Lopez, F.; Byrne, R.; Răduţă, A. M.; Vrana, N. E.; McGuinness, G.; Diamond, D., Ionogel-based light-actuated valves for controlling liquid flow in micro-fluidic manifolds. *Lab on a Chip* **2010,** *10* (2), 195-201.
37. Fraser, K. J.; Izgorodina, E. I.; Forsyth, M.; Scott, J. L.; MacFarlane, D. R., Liquids intermediate between "molecular" and "ionic" liquids: Liquid ion pairs? *Chemical Communications* **2007,** (37), 3817-3819.
38. Torimoto, T.; Tsuda, T.; Okazaki, K.-i.; Kuwabata, S., New Frontiers in materials science opened by ionic liquids. *Advanced Materials* **2010,** *22* (11), 1196-1221.

39. Zhu, J. W.; Zhai, J. Y.; Li, X.; Qin, Y., Applications of hydrophobic room temperature ionic liquids in ion-selective optodes. *Sensors and Actuators B-Chemical* **2011,** *159* (1), 256-260.
40. Topal, S. Z.; Ertekin, K.; Gurek, A. G.; Yenigul, B.; Ahsen, V., Tuning pH sensitivities of zinc phthalocyanines in ionic liquid modified matrices. *Sensors and Actuators B: Chemical* **2011,** *156* (1), 236-244.
41. Benito-Lopez, F.; Coyle, S.; Byrne, R.; O'Toole, C.; Barry, C.; Diamond, D., Simple barcode system based on ionogels for real time pH-sweat monitoring. In *BSN 2010 - 7th International Workshop on Wearable and Implantable Body Sensor Network*, Singapore, **2010**, 291-296.
42. Curto, V. F.; Fay, C.; Coyle, S.; Byrne, R.; O'Toole, C.; Barry, C.; Hughes, S.; Moyna, N.; Diamond, D.; Benito-Lopez, F., Real-time sweat pH monitoring based on a wearable chemical barcode micro-fluidic platform incorporating ionic liquids. *Sensors and Actuators B: Chemical* **2012,** *171-172* , 1327-1334.
43. Kavanagh, A.; Byrne, R.; Diamond, D.; Radu, A., A two-component polymeric optode membrane based on a multifunctional ionic liquid. *Analyst* **2011,** *136* (2), 348-353.
44. Tsunashima, K.; Kodama, S.; Sugiya, M.; Kunugi, Y., Physical and electrochemical properties of room-temperature dicyanamide ionic liquids based on quaternary phosphonium cations. *Electrochimica Acta* **2010,** *56* (2), 762-766.
45. Benito-Lopez, F.; Coyle, S.; Byrne, R.; O'Toole, C.; Barry, C.; Diamond, D., Simple barcode system based on inonogels for real time pH-sweat monitoring. In *Proceedings of the 2010 International Conference on Body Sensor Networks*, IEEE Computer Society, **2010**, 291-296.
46. Zangmeister, R. A.; Tarlov, M. J., UV graft polymerization of polyacrylamide hydrogel plugs in microfluidic channels. *Langmuir* **2003,** *19* (17), 6901-6904.
47. de Vargas-Sansalvador, I. M. P.; Fay, C.; Phelan, T.; Fernandez-Ramos, M. D.; Capitan-Vallvey, L. F.; Diamond, D.; Benito-Lopez, F., A new light emitting diode-light emitting diode portable carbon dioxide gas sensor based on an interchangeable membrane system for industrial applications. *Analytica Chimica Acta* **2011,** *699* (2), 216-222.
48. O' Toole, M.; Shepherd, R.; Lau, K. T.; Diamond, D., Detection of nitrite by flow injection analysis using a novel Paired Emitter-Detector Diode (PEDD) as a photometric Detector. *Proceedings SPIE* **2007,** *6755, 67550P.*
49. Lau, K. T.; Baldwin, S.; Shepherd, R. L.; Dietz, P. H.; Yerzunis, W. S.; Diamond, D., Novel fused-LEDs devices as optical sensors for colorimetric analysis. *Talanta* **2004,** *63* (1), 167-173.

50. Gorkin, R.; Park, J.; Siegrist, J.; Amasia, M.; Lee, B. S.; Park, J.-M.; Kim, J.; Kim, H.; Madou, M.; Cho, Y.-K., Centrifugal microfluidics for biomedical applications. *Lab on a Chip* **2010,** *10* (14), 1758-1773.
51. Environmental Protection Agency, The Provision and Quality of Drinking Water in Ireland. A Report for the Years 2008 – 2009. Wexford, Ireland, **2011**.
52. Gorkin, R.; Czugala, M.; Rovira-Borras, C.; Ducrée, J.; Diamond, D.; Benito-Lopez, F., A wireless paired emitter detector diode device as an optical sensor for lab-on-a-disc applications. The 17th International Conference on Solid-State Sensors, Actuators and Microsystems (Transducers) **2011**, 2526-2529.
53. O' Toole, M.; Lau, K. T.; Diamond, D., Photometric detection in flow analysis using PEDD. *Talanta* **2005,** *66*, 1340-1344.
54. O'Neill, S.; Conway, S.; Twellmeyer, J.; Egan, O.; Nolan, K.; Diamond, D., Ion-selective optode membranes using 9-(4-diethylamino-2-octadecanoatestyryl)-acridine acidochromic dye. *Analytica Chimica Acta* **1999,** *398* (1), 1-11.
55. El-Ashgar, N. M.; El-Basioni, A. I.; El-Nahhal, I. M.; Zourob, S. M.; El-Agez, T. M.; Taya, S. A., Sol-gel thin films immobilized with bromocresol purple pH-sensitive indicator in presence of surfactants. *ISRN Analytical Chemistry* **2012,** 11.
56. Lau, K. T.; Shepherd, R. ; Diamond, D., Solid state pH sensor based on light emitting diodes (LED) as detector platform. *Sensors* **2006,** *6* (8), 848-859.
57. Eastern Regional Fisheries Board, Summary Report on pollution of the Tolka River near Clonee, Co. Dublin. Dublin, **2005**.
58. Ingo, F.; Mark, J., Non-contact, scattering-independent water absorption measurement using a falling stream and integrating sphere. *Measurement Science and Technology* **1999,** *10* (7), 612-617.
59. MacFarlane, D. R.; Pringle, J. M.; Johansson, K. M.; Forsyth, S. A.; Forsyth, M., Lewis base ionic liquids. *Chemical Communications* **2006,** (18), 1905-1917.
60. Environmental Protection Agency, Water Framework Directive: Proposed Quality Standards for Surface Water Classification. Dublin, **2007**.
61. A "New" Salmon River in Ireland. http://www.fisheriesireland.ie/Press-releases/a-new-salmon-river-in-ireland.html (accessed on 4/07/2012).

Chapter 7

CMAS: fully integrated portable Centrifugal Microfluidic Analysis System for on-site colorimetric analysis

M. Czugala,[1] D. Maher,[1] F. Collins,[1] R. Burger,[2] F. Hopfgartner,[1] Y. Yang,[1] J. Zhaou,[1] J. Ducrée,[2] A. Smeaton,[1] K. J. Fraser,[1] F. Benito-Lopez[1, 2] and D. Diamond[1]

RSC Advances, 2013 (3), 15928-15938
doi: 10.1039/C3RA42975J

[1]CLARITY: Centre for Sensor Web Technology, National Centre for Sensor Research
Dublin City University, Dublin, IRELAND
[2]Biomedical Diagnostics Institute, National Centre for Sensor Research,
Dublin City University, Dublin, IRELAND
[3]CIC microGUNE, Arrasate-Mondragón, SPAIN

For Supplementary Information see Appendix D, pg. 232.

Abstract

A portable, wireless system capable of *in-situ* reagent-based colorimetric analysis is demonstrated. The system is based on a reconfigurable low cost optical detection method employing a paired emitter detector diode device, which allows a wide range of centrifugal microfluidic layouts to be implemented. Due to the wireless communication, acquisition parameters can be controlled remotely and results can be downloaded in distant locations and displayed in real time. The stand-alone capabilities of the system, combined with the portability and wireless communication, provide the flexibility crucial for on-site water monitoring.

The centrifugal microfluidic disc presented here is designed for nitrite detection in water samples, as a proof of principle. A limit of detection of 9.31 ppb, along with similar coefficient of correlation and precision, were obtained from the Centrifugal Microfluidic Analysis System compared with the same parameters measured using a UV-Vis spectrophotometer (R^2 = 0.994, RSD = 1.02 % and R^2 = 0.993, RSD = 1.57 %, respectively).

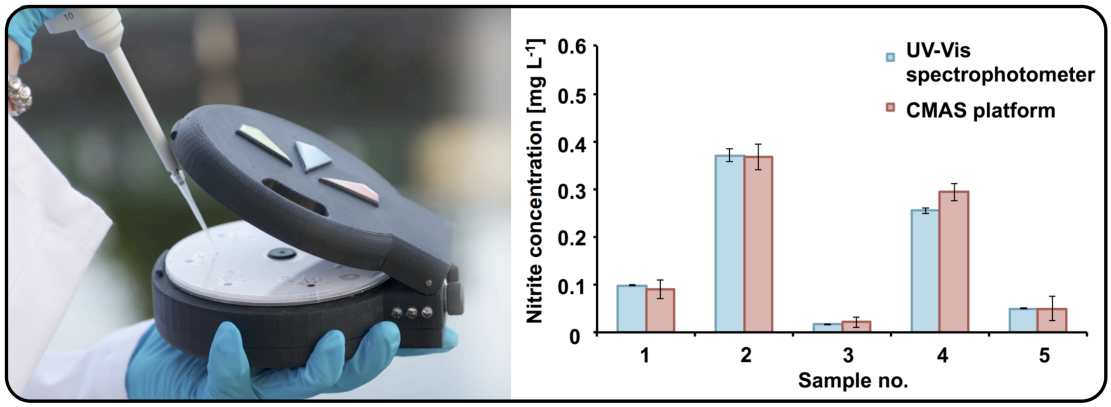

7.1. Introduction

Currently, water quality monitoring is still largely based on manual sample collection and subsequent laboratory testing, despite the very costly and time-consuming nature of this approach. Therefore the development of fast, accurate and robust *in-situ* monitoring techniques, which can provide the required analytical information at a much lower cost, would be of great benefit.[1] The availability of easy to use and low cost analytical measurements is the key to future scalability in terms of the number of locations that can be sampled and the sampling frequency, thus facilitating the emergence of higher resolution temporal and spatial monitoring strategies.

There is a wide range of commercially available portable devices that can provide rapid indication of water quality parameters. Some techniques are relatively cheap ($<$ \$100), but they do not possess data logging capabilities and allow for only one spot test (*e.g.* Hanna instruments nitrite ULR Checker (HI 764),[2] and API® test kits).[3] Conversely, more sophisticated probes allow multi-parameter measurements with integrated wireless data transmission, but their application is quite limited due to the high cost of hardware and maintenance (Hach® Hydrolab DS5[4] and YSI® V2 Multiparameter Water Quality Sondes,[5] costs typically \$20K or greater).

Micro total analysis systems (μTAS) provide a route for the generation of micro-dimensioned analytical instruments that can be operated in remote locations, enabling *in-situ* water analysis to become a reality.[6] It has been previously described that there are clear advantages of using microfluidic devices in the integration of sample processing in order to meet the increasing needs of modern environmental monitoring.[7] The small amounts of sample and reagents typically required, the ability to generate results rapidly and the use of a single motor to control complex fluidic transport make "lab-on-a-disc"

based platforms attractive options for generating fully integrated μTAS platforms.[8, 9] Several implementations of centrifugal discs for environmental monitoring have been reported;[10] Salin *et al.* developed discs for the detection of aqueous sulfide,[11] nitrate, nitrite[12] and chromium VI[10] employing centrifugal microanalysis. More recently, Hwang *et al.*[13] published a microfluidic centrifugal disc that is capable of simultaneous determination of several nutrients in water samples (nitrite, nitrate, ammonium, orthophosphate, and silicate). However, in these cases a bench-top fiber-based optics/spectrophotometer system was employed for the optical detection.[11, 13] Therefore, while these platforms did demonstrate the excellent use of centrifugal discs for implementing environmental assays, the devices were not suitable for *in-situ* remote water quality monitoring.

While many individual analysis steps and functions for centrifugal discs have been demonstrated, there are relatively few examples of fully integrated sample-to-answer centrifugal systems for environmental analysis. One challenge to overcome is the complex and expensive hardware platform required for complete analysis[8] where motor control, analysis instrumentation, optical systems and other equipment must be integrated in a cost effective way. In centrifugal microfluidics, optical detection remains the preferred technique for quantitative analysis as CD platforms are manufactured with high optical quality plastics that enable absorbance and fluorescence to be employed. Due to the rapid reduction in the cost of quality optoelectronic components like laser diodes, photodiodes, CCD cameras and light emitting diodes (LEDs), optical detection is becoming more practical for point-of-care (POC) diagnostics. Specifically, the advancement in LED sources and photodetector technologies provides a solution to all these issues. In particular, due to their small size, low cost, increasing spectral range coverage (247–1550 nm), low power consumption, efficiency and ease of fabrication,

paired emitter detector diode (PEDD) based systems provide an excellent solution to the incorporation of colorimetric and fluorescence analytical detection into remotely deployable devices.[6, 14]

Despite the advances described above, few successful integrated systems employ centrifugal discs. Several of these integrated systems have been published for point-of-care biomedical diagnostics[15, 16] applications and only a few functioning systems are available in the market. For instance, the Piccolo clinical blood analyser system from Abaxis can process whole blood samples, and is one of the first examples of a disc-based sample-to-answer systems.[16] The colorimetric absorbance measurements are performed using an off-disc spectrophotometer. In addition, calibration is carried out simultaneously as the reference solutions are read from the disc reference cuvettes. Ducrée *et al.* [17, 18] have also shown the successful integration of blood-plasma separation and colorimetric-based analyte detection systems.[17, 18] They demonstrated a bench-top device for a fully integrated processing and read-out of the hemoglobin assay, which comprises a PC-controlled actuation unit, a synchronised free-droplet dispenser unit to load the reagents, a low-cost laser and a spectrophotometer as components for the optical detection. The use of a spectrophotometer ensures a flexible read-out of additional colorimetric assays or even fluorescence immunoassays (FIA),[19] allowing different types of assays to be run on the same disc, either simultaneously or sequentially. Also techniques for on-board-storage and release of liquid reagents have been successfully integrated in the meantime.[20, 21]

The nitrite and nitrate ions are ubiquitous within environmental, industrial, food and physiological systems.[22] Excessive levels can lead to detrimental human health effects and marine life degradation.[23, 24] Current techniques for the detection of nitrite are electrochemical, capillary/column, biosensing, however spectrophotometric methods are the most popular by

far,[22] due to the excellent limits of detection (as low as sub-nanomolar), dynamic range and cost efficiency. In particular, the spectrophotometric assay based on the Griess reagent has been very popular for over a century.[23] This assay is well-known for its sensitivity, stability and robustness, but existing flow injection analysis systems tend to consume large volumes of reagent (mL per sample),[25] and are thus unsuitable for *in-situ* and remote deployment. Recently Xi *et al.*[26] determined nitrite/nitrate concentrations in water samples using the Griess reagent method on a centrifugal microfluidic disc. The authors concluded that use of powdered reagents was compatible with the centrifugal disc format and suitable for field use.

Currently, commercially available systems for water analysis have limited on site usage capabilities, mainly due to their large size,[27] high power consumption (typically 10-150 W),[28] and excessive reagent usage (mL per sample).[27] Therefore a stand-alone, compact and low power environmental sensor that requires minimal reagent could have significant impact. In this chapter, we present the design and the development of a fully integrated portable centrifugal microfluidic analysis system (CMAS) for on-site lab-on-a-disc colorimetric analysis. CMAS is coupled via Bluetooth to an Android tablet for data collection, geotagging and Cloud sharing. Unlike the first generation system (Chapter 6),[29] CMAS employs not only colorimetric chemical detection, but also centrifugal disc spinning, enabling on site sample manipulation analysis. CMAS has a modular design with easily interchangeable optical detection units, which allow any colorimetric reagent based assay to be implemented. As a proof of concept, the analysis of nitrite from environmental water samples is carried out in the system and compared to results obtained with a standard bench-instrument.

7.2 Experimental

7.2.1 Chemicals and reagents

All solutions were prepared from analytical grade chemicals and deionised water from a Millipore Milli-Q Q-GARD® 1 water purification system. Stock solutions were prepared freshly prior use and stored in dark environment at room temperature for no longer than one week. The Griess reagent was prepared following previously published procedures.[30] Phosphoric acid (H_3PO_4), sulfanilic acid, *N*-(1-naphthyl)ethylenediamine dihydrochloride (NED) and sodium nitrite ($NaNO_2$) were purchased from Sigma Aldrich, Ireland and used without further purification. Nitrite standard solutions were diluted from a 200 mg L^{-1} $NaNO_2$ stock solution to the appropriate concentrations.

7.2.2 Centrifugal microfluidic fabrication

The centrifugal disc presented here consists of a multi-layer structure made of poly(methyl methacrylate) (PMMA) plastic and double-sided, pressure-sensitive adhesive (PSA). Using a CO_2 laser ablation system (Epilog Zing Laser Engraver, USA) fluid reservoirs were machined into 1.5 mm PMMA plastic (Radionics, Ireland). A cutter-plotter (Graphtec, Japan-Graphtec) was used to cut channels of 1 mm width in a 86 μm thick pressure sensitive adhesive layer (PSA, AR8890, Adhesives Research, Ireland). Once the appropriate pieces had been designed and machined, they were aligned centrally as well as azimuthally and bonded using the PSA layers. The CD consists of 5 layers: (1) top PMMA disc with laser-machined sample and reagent loadings and air venting hole, (2) pressure-sensitive adhesive with reservoirs features cut using a plotter, (3) middle PMMA disc with sample

and reagent reservoirs (radius 2.25 mm and 0.5 mm, respectively), and detection chamber (radius 2.2 mm), (4) pressure-sensitive adhesive with microchannel features cut using a plotter, (5) solid PMMA disc to seal off the channels (Fig. 7.1A). When assembled, the centrifugal disc allows complex 3D fluidics through the use of multiple layers. Fig. 7.1B shows a fully assembled CD for the determination of nitrite consisting of seven microfluidic structures and the detailed microfluidic layout and functions, Fig. 7.1C.

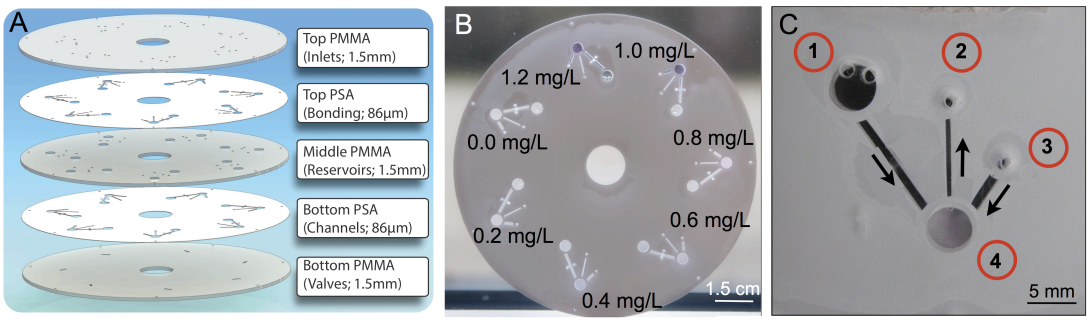

Figure 7.1. A) Schematic showing the assembly of the centrifugal disc, B) fully assembled centrifugal disc for determination of nitrite with seven microfluidic structures filled with different concentrations of nitrite and C) image showing the detailed microfluidic layout and functions: 1 - inlet for sample, 2 – air vent, 3 – inlet for the reagent, 4 – mixing/detection chamber.

7.2.3 Instrumentation

7.2.3.1 CMAS hardware

CMAS incorporates wireless communication and is powered *via* two 9 V lithium polymer batteries. A Pololu Wixel-based general-purpose programmable module based on a TI CC2511F32 microcontroller controls the entire system operation. System control and data acquisition are wirelessly enabled in real time by the use of Bluetooth communication (BlueSMiRF RN-42) with a custom designed interface on an Android tablet. A pulse-width modulation (PWM) controlled motor (Mabuchi Motor RF-500TB) enables spinning of the disc, thus allowing for the loading of the samples to the

detection chambers. CD speed is calculated using an optical switch (Optek OPB830L51) and rotating interrupter.

The in-house designed CMAS case was fabricated using a 3D printer (Stratasys, USA) in acetonitrile butadiene styrene co-polymer (ABS) plastic in order to protect the electronics and to minimise interferences from ambient light during the operation of the device. The printed parts were designed using ProEngineer CAD/CAM software package, 3D rendered pictures are presented below. Appendix D, Fig. D1A presents a schematic of the bottom side of CMAS, wherein the two batteries, motor and the other electronic components are integrated. In Appendix D, Fig. D1B the side view of the CMAS with loaded centrifugal disc is shown, whereas Fig. D1C presents an exploded view of the system with specified components such as the LED board, LED detector intensity knob, printed circuit board (PCB), motor and batteries.

7.2.3.2 **CMAS software**

To enhance user experience and maintain true portability of the system, several software requirements were needed; these included:

- Wireless connection with CMAS via Bluetooth;
- Real time display of the results;
- Internal data storage,
- Data connectivity to the Cloud, either *via* mobile network or WiFi.

A commonly available Android Tablet PC was used to implement these requirements (Samsung Galaxy Tab with 7-inch screen). The tablet runs Android Honey comb (v3.2) to provide Internet connectivity via a WiFi 802.11 a/b/g/n chip and has Bluetooth 3.0 connectivity, a GPS chip and a 3.0 MP rear camera. Data can be stored on an external SD card and the reported

battery duration in normal use is 30 h. Data synchronisation with the Cloud can either happen on start up if an Internet connection is available, or if the user presses on the Cloud icon in the CMAS application. Among various remote hard drive services available, Dropbox (http://www.dropbox.com) was chosen since it allows easy data sharing with other users. Fig. 7.2A shows CMAS with the Android tablet controller base station. See Appendix D, Fig. D2 – D9 for more detail on the software and user interface.

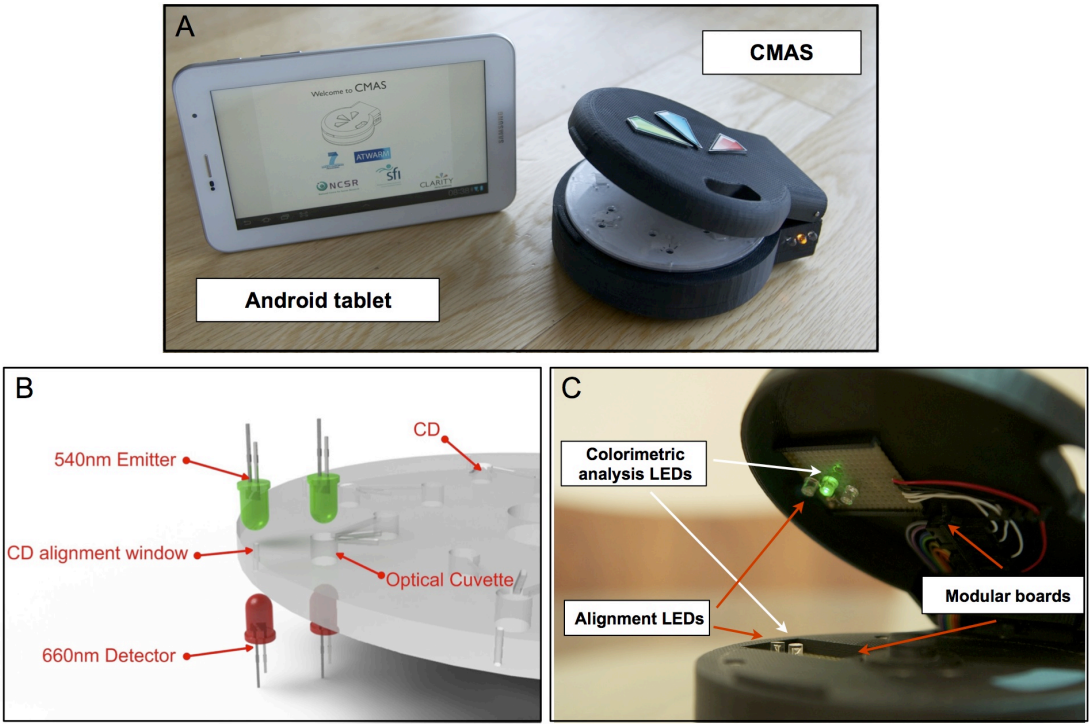

Figure 7.2. A) Portable Android controller and CMAS, B) schematic representation of the alignment/emitter/detector LEDs and C) CMAS LED configuration specific to the nitrite CD (bottom right).

7.2.3.3 **CMAS detection system**

The colorimetric detection and disc alignment systems are based on a low cost paired emitter detector diode (PEDD). The PEDD device consists of two 5 mm light emitting diodes, one serving as the light source and the other, in reverse bias mode, as the light detector (Fig. 7.2B).[30, 31] The detector LED

(660 nm) in output mode was firstly charged up to 5 V for 100 μs and then switched to input mode. Light from the emitter LED (540 nm) generates a photocurrent in the reverse biased detector LED, resulting in discharge of the capacitance based voltage from an initial value of 5 V (logic 1) to a pre-set value of 1.7 V (logic 0). In order to provide a stable +5 V source to drive the circuit and LEDs, a voltage regulator running from a 9 V battery was employed. After passing through the microfluidic device, the observed light intensity is related to the discharge time of the acquired charge in the device.[32] The discharge time of the detector LED, thus the output signal, is dependent on the colour intensity of the solution.

The alignment system is based on the second PEDD device and a CD alignment window fabricated in the CD adjacent to each microfluidic structure. The alignment of the optical cuvette with the respective PEDD detector (Fig. 7.2A) is achieved by the user manually when rotating the disc with the finger through the window in the top lid (Fig. 7.2C), using as a reference the alignment system explained above. Once the CD is correctly positioned (*i.e.*, the PEDD diodes are aligned with the CD alignment window, resulting in the lowest discharge time of the detector LED) a green light appears on the screen of the tablet. In order to optimise the sensitivity of the detector, the emitter LED intensity can be controlled by the potentiometer accessible on the side of the system (Appendix D, Fig. D1C).

The analytical measurement is based on the following theoretical model which has been derived by Lau *et al.*[33]

$$Log\ (t) = \varepsilon Cl + Log\ (t_0) \qquad (7.1)$$

where l is the optical path length through the solution (cm), ε the molar extinction coefficient, C the concentration of the absorbing species (mol L^{-1}),

t_0 a constant that represents discharge time in the absence of the coloured species in solution (μs) and t is the discharge time in the presence of the coloured species in solution (μs). In the presented centrifugal disc the optical path length is 1.59 mm.

The emission spectrum of the emitter LED was obtained by using an Ocean Optics spectrometer (OOIBase 32TM, Ocean Optics, Inc., Dunedin, USA).

7.2.4 Experimental protocol for nitrite detection

In order to conduct a routine experiment on CMAS, the operator simply needs to open the system and place the disc inside. The disc used for the analysis and the PEDD board have to match for the assay (in this case nitrite detection). After that, the water sample and the reagents are introduced (micropipetting) in the storage reservoirs of the disc (Fig. 7.3A).

Fluid distribution occurs *via* the centrifugal field generated through the spinning process (Fig. 7.3B). Rotation at 1000 rpm for 90 s forces the liquids from the more central sample/reagent addition location outwards towards the detection chamber, where mixing (by diffusion) and the readout take place. The centrifugal forces applied causes sedimentation of solid interferences suspended in the water sample. Therefore filtration of the sample prior to introduction into the microfluidic device was not necessary.[29] After stopping the CD and manual alignment of the LEDs (Fig. 7.3C), the intensity of the coloured solution, filling the detection chamber, was determined using the PEDD system of CMAS (Fig. 7.3D). A video of CMAS can be viewed at http://tinyurl.com/dyoumds.

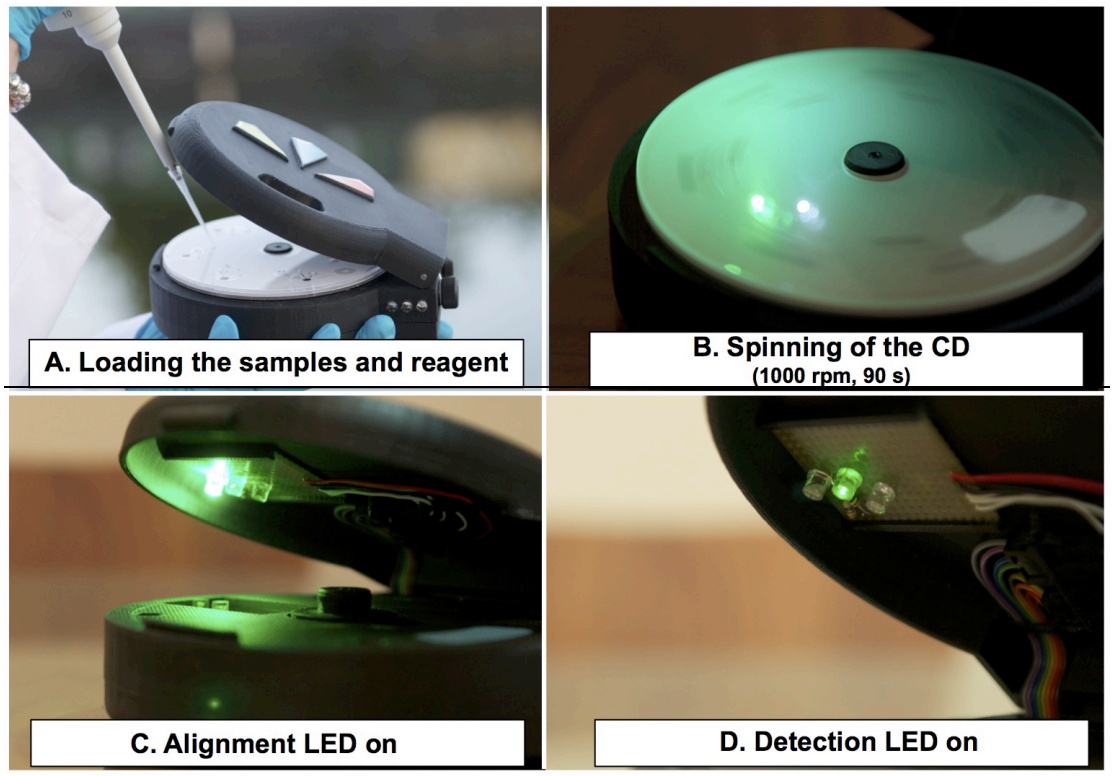

Figure 7.3. Photographs of CMAS during nitrite detection: A) loading of freshwater samples, B) spinning of the CD at 1000 rpm for 90 s, C) on completion of spinning, the CD is manually aligned for PEDD detection (CMAS lid opened for clarity) and D) PEDD detection (CMAS lid opened for clarity). A video of the system can be found at http://tinyurl.com/dyoumds.

7.2.5 Repeatability measurements

The repeatability of the PEDD optical detector was determined by injecting a 1.0 mg L^{-1} nitrite standard solution premixed with the Griess reagent to the same microfluidic structure followed by monitoring of the detector steady-state signal for 60 s (3 data points per second, n = 10). After each measurement, the microfluidic structure was washed three times with DI water and dried with N_2.

The repeatability of the measurements within one single CD was investigated by filling the seven microfluidic structures with an intensely coloured food dye solution (Goodall's, Ireland; λ_{max} = 505 nm; n = 3) and

monitoring the detector steady-state signal for 60 s (3 data points per second; $n = 3$).

Next, the difference in output signals across three separate centrifugal discs (CD1, CD2, CD3) was determined. One microfluidic structure on each CD was filled with the coloured food dye solution and the steady-state signal of the detector monitored for 60 s (3 data points per second; $n = 3$). After each measurement, the microfluidic structure was washed three times with DI water and dried with N_2.

7.2.6 Nitrite assay calibration

Nitrite detection was carried out employing the Griess reaction method, which is based on the conversion of sulfanilic acid (Reagent A) to a diazonium salt by reaction with nitrite in acidic solution.[34] The diazonium salt is then coupled to *N*-(1-naphthyl)ethylenediamine (NED) (Reagent B), forming an azo dye, of which the intensity is directly related to nitrite concentration. The dye can be spectrophotometrically quantified/detected based on its absorbance at *ca.* 547 nm (Appendix D, Fig. D10). It was previously reported that the reagent volume which provided the most intense colour was determined as 0.2 : 3 v/v reagent to sample ratio and this was the ratio adopted throughout all the experiments.[30]

To demonstrate the utility of the system, a study of the colour formation between NO_2^- and Griess reagent was performed using CMAS and a commercially available UV-Vis spectrophotometer (Perkin-Elmer Lambda 900) as reference. The microfluidic colorimetric assay testing was carried out using various standard solutions containing a nitrite concentration from 0.0 - 1.2 mg L^{-1}. The development of the nitrite Griess reagent complex colour intensity was monitored for 30 min. The sampling rate under this protocol

was *ca.* 3 points per second.

7.2.7 Analysis of freshwater samples

Freshwater samples were collected from five different inland waters in Ireland. The colorimetric reagent (2.1 μL) and the filtered water sample (31.5 μL) were loaded to the disc, and spun as previously described. Next, the solution was left to stand for 30 min for colorimetric development. The absorbance of the solution was measured at 540 nm using the PEDD system in CMAS and a UV-Vis spectrophotometer for reference (540 nm every 1 s for 30 min, cuvette = 1 cm). The resulting signal was measured continuously for 60 s. The sampling rate under this protocol was *ca.* 1 point per second.

7.3 Results and discussion

CMAS presented several significant advances over the previously reported first generation system.[29] For example, spinning of the CD no longer has to be performed using a separate bench-top motor stand, which required manual transfer of the CD to the PEDD device for analytical measurements. In addition, sample testing had to be carried out in the dark to reduce the impact of ambient light noise, which affects the accuracy and precision of the measurements. In contrast, CMAS incorporates a stepper motor that allows fully integrated fluid manipulation and detection at point-of-need, and therefore enables true *in-situ* water analysis (Appendix D, Fig. D11).

7.3.1 Centrifugal disc performance

The CD was designed, in this particular case, for water analysis in terms of nitrite *via* seven parallel microfluidics structures, allowing for

sequential testing of multiple samples. Each of the microfluidic structures contained two inlet reservoirs for the uptake of the sample and the reagent, connected to a detection chamber ($V_{chamber}$ = 34 μL) *via* the microchannels. These microchannels form a kind of capillary valve, which develops when the liquid encounters a transition from a small microchannel into a larger chamber. The burst frequency of the valve, *i.e.* the speed at which the surface tension force is overcome and the fluid continues to flow, was tested by spinning the disc at an increasing speed using increments of 2 rpm. The liquid movement to the detection chamber commenced in the region of *ca.* 250 rpm. A rotational speed of 1000 rpm was found to be sufficient to force the sample and the reagent towards the detection chamber, where mixing and detection occurred. Colour development was very rapid and kinetic measurements could be started in as little as for nitrite detection 90 s (see experimental protocol).

As previously reported,[10] the presence of bubbles in the detection chamber during analysis adversely affects the measured transmittance, and causes slightly degraded precision. Therefore an air vent that connected with the detection chamber was implemented, reducing substantially this problem and thereby improving the overall analytical performance (Fig. 7.1C).

The nitrite ion was chosen as the target analyte for demonstrating the functionality of the prototype platform, however, the microfluidic structure can be easily redesigned to split the sample flow into parallel channels, one of which including a reduction step. There, the relatively inert nitrate ion would be chemically reduced to the more reactive nitrite, before initiating the detection sequence. In this way, the determination of nitrite by a two step process would provide information on the "total" amount of nitrate and nitrite. Similar approach has been presented by Xi *et al.*[26]

7.3.2 Centrifugal Microfluidic Analysis System

The portable device presented here provides many unique fluidic implementations for rapid and robust sample analysis. The system has been designed from the ground up specifically for integration with further downstream steps (*e.g.* automated alignment). The extremely compact footprint of the centrifugal disc provides extensive free space for integrating additional fluidics, in order to facilitate multi-parameter assays in future designs, *e.g.* nitrate, pH, turbidity, among others.

A unique function of CMAS is the modular PEDD alignment/detection configuration wherein the electronic boards, along with the PEDD devices, are easily interchangeable, thus allowing a wide range of centrifugal microfluidic layouts to be implemented using this system. Moreover, the modular board design can incorporate any low cost optical detector, including photodiodes, providing freedom of choice depending on the application. Another unique function of CMAS is that it allows for *in-situ* universal colorimetric analysis for centrifugal platforms, since the light emitting diodes used as an optical detector cover a broad spectral range (LEDs in the spectral range *ca.* 247-1550 nm are commercially available).[35, 36] At the same time, increased lifetime, low cost and reduced power consumption of the LEDs help keep the overall cost of the device low, making it more accessible for a broad range of potential applications.

The device supports any centrifugal disc design up to a thickness of 4.8 mm, which encompasses most of the centrifugal platforms presented in the literature. The motor enables rotational speed to be controlled over the range 500 – 4000 rpm. As previously reported,[37] the PEDD Device output can be continuously monitored during spinning of the disc at 0.5 Hz (30 rpm) and therefore the PEDD system is able to distinguish between chambers filled

with solutions of different colours, during rotation. This implies that many samples can be analysed simultaneously during a single run, eliminating the need for start/stop detection, and manual alignment of the PEDD detector with the sample reservoir. Due to the wireless communication, method parameters can be controlled remotely and results can be downloaded in remote locations and displayed in *real time*. These capabilities, together with an adequate battery power supply (20 h of continuous operation) provide great flexibility for on-site water monitoring at remote locations.

7.3.3 Optimatisation of the PEDD parameters

The optimum wavelength (λ_{max}) to monitor the nitrite Griess reaction complex is in the range *ca.* 526 - 563 nm.[38, 39, 40, 41] Under our experimental conditions (20.0 ± 0.5 ^{o}C, NO_2^- concentration range 0.2 – 1.2 mg L^{-1}) we found the λ_{max} to be 531 nm (Appendix D, Fig. D12). Therefore, an emitter LED with a λ_{max} of 525 nm (Appendix D, Fig. D13) was employed as the light source, and a LED with a λ_{max} 660 nm that had a slightly smaller bandgap employed as the detector. The maximum absorbance of the nitrite Griess reaction complex therefore efficiently overlaps with the emission spectrum of the emitter green LED and will therefore allow high sensitivity.

7.3.4 Repeatability of the PEDD measurements

The repeatability of the optical detector was determined by injecting a 1.0 mg L^{-1} nitrite standard solution premixed with the Griess reagent as explained in the experimental section. An average discharge time was then calculated upon subtraction the output signal of blank (DI water). As shown in Appendix D, Fig. D14, excellent repeatability was achieved with a relative standard deviation (RSD) of 0.24 % between all measurements and an average

signal (detector discharge time) of 12917 ± 29 μs (n = 10). The raw data is presented in Table D1 (Appendix D).

7.3.5 Repeatability of intra- and inter-centrifugal discs measurements

The average discharge times for the measurement of a coloured dye solution in seven microfluidic structures within one CD are presented in Fig. 7.4. Each value has been subtracted from the same average baseline generated with deionised water. The measurement of the coloured dye solution was repeated three times for each microfluidic structure with a RSD of typically *ca.* 1 % or less for each structure. The raw data is presented in Appendix D Table D2. The average discharge time of the coloured dye solution for the 21 runs for all the microfluidic structures was 16873 ± 693 μs (RSD = 4.11 %). The results demonstrate that an event such as a colour intensity can be measured using the PEDD within CMAS (Fig. 7.4A) with reasonably good reproducibility, considering the fabrication of the structures within the discs is manual in nature. The expanded view of the graph shows that to a considerable extent, measurement variations within a disc are not random, but are consistently different from structure to structure (Fig. 7.4B). These inconsistencies in discharge times can be attributed to the manual fabrication of the CD's and exemplifies the fact that our results are strongly influenced by the manual fabrication of the microfluidic structures on each CD. Clearly, therefore, one can predict a substantial improvement in the platform performance will be achieved through adoption of automated techniques associated with mass production/manufacturing of the microfluidic structures.

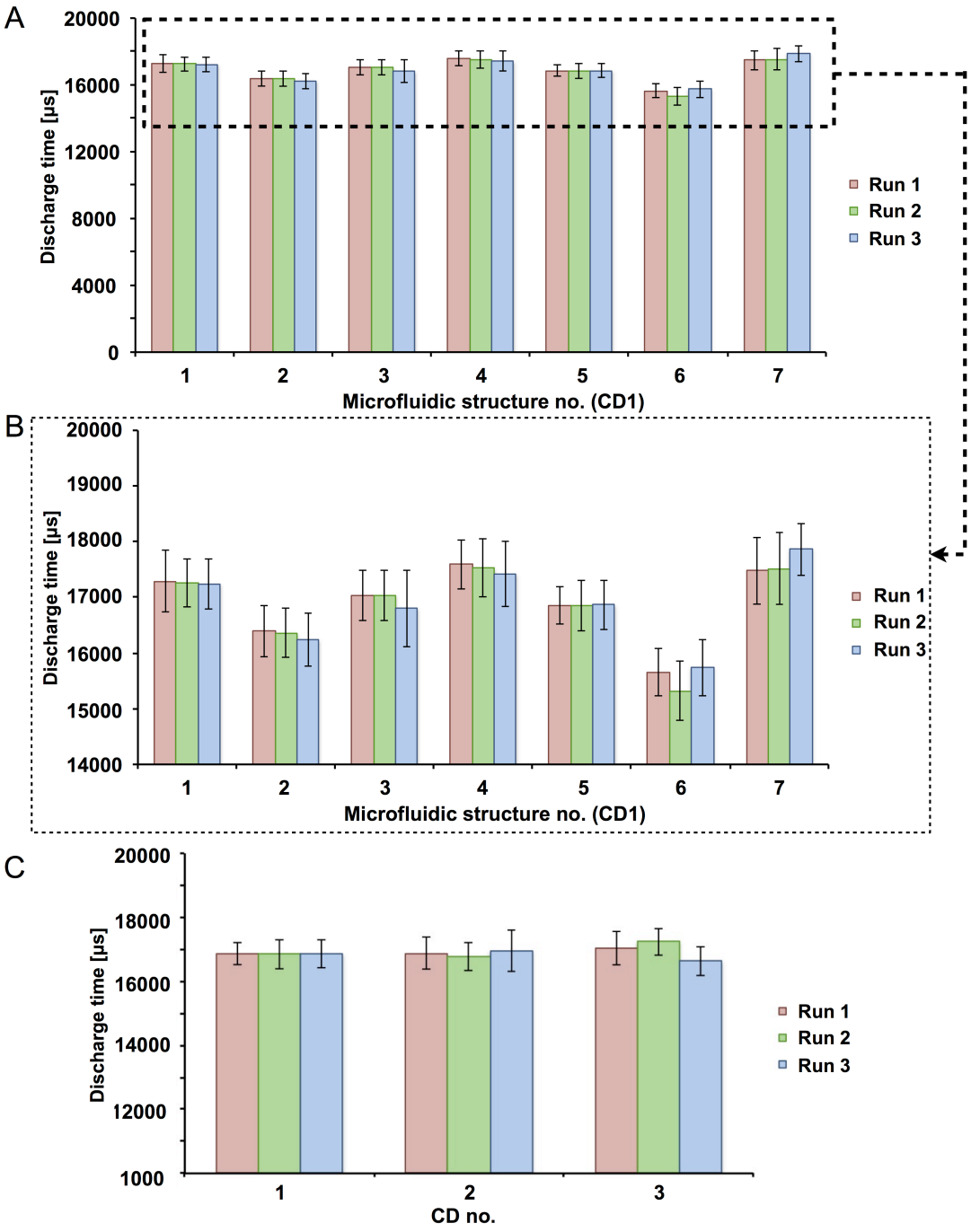

Figure 7.4. A-B) Repeatability of the microfluidic structures within a single CD and C) between three separate CDs ($n = 3$).

Next, the repeatability experiments were carried out to compare the difference in output signals across three centrifugal discs (CD1, CD2, CD3) as explained in the experimental section. Each average value has been then subtracted from the same average baseline obtained with deionised water. The

results are presented in Fig. 7.4C and the raw data can be found in Table D3 (Appendix D).

An average discharge time of 16858 ± 8 μs (R.S.D. = 0.049 %; n = 3) was obtained for CD1, 16867 ± 100 μs (R.S.D. = 0.59 %, n = 3) for CD2 and 16966 ± 3134 μs (R.S.D. = 1.85 %, n = 3) for CD3. This resulted in an average discharge time of 16897 ± 173 μs (R.S.D. = 1.02 %, n = 9) for the detection of the dye solution using three separate CDs (fabricated manually). The results indicate that CMAS measurements can be carried out using different centrifugal discs with very good repeatability. These results demonstrate that there is good within-disc and between-disc repeatability for the overall analytical approach based on CMAS, despite the manual fabrication of the discs and microfluidic structures.

7.3.6 CMAS sensitivity

To determine the limit of detection and limit of quantitation, we used the following approach. The LOD was estimated as three times standard deviation of blank response and LOQ was calculated as ten times standard deviation of blank response.[42] Based upon these formulations,[42] the LOD and LOQ for NO_2^- using the Greiss method on CMAS were estimated to be 9.31 ± 0.09 μg L^{-1} and 89 ± 11 μg L^{-1} (n = 3), respectively. As outlined in Table 7.1, these values are higher than the LOD and LOQ of the UV-Vis spectrophotometer (1.50 ± 0.02 μg L^{-1} and 14.8 ± 0.2 μg L^{-1}, respectively). However, CMAS is portable, can be operated at point-of-use, is relatively low cost to produce, and can process large numbers of samples *in-situ* relatively quickly. Furthermore, the incorporation of wireless communications on CMAS means that data can be automatically transmitted to a remote cloud-based database. CMAS demonstrates slightly higher value of coefficient of

correlation ($R^2 = 0.994$) than the UV-Vis spectrophotometer ($R^2 = 0.993$) and an improved precision (RSD = 1.02 %) in comparison to the results calculated from the bench top instrument (RSD = 1.57 %), see Table 7.1.

Table. 7.1. A comparative summary of the data obtained for the detection of nitrite Griess reagent complex using both CMAS and a UV-Vis spectrophotometer ($n = 3$).

	CMAS (λ_{max} = 540 nm)	**UV-Vis spectrophotometer** (λ_{max} = 540 nm)
R^2	0.994	0.993
LoD	9.31 ± 0.09 μg L^{-1}	1.50 ± 0.02 μg L^{-1}
LoQ	89 μg L^{-1} ± 11 μg L^{-1}	14.8 ± 0.2 μg L^{-1}
RSD	1.02 %	1.57 %

The detection limits for nitrite achievable by this spectrometric standard procedures have been reported as typically being in the range 5 - 10 μg L^{-1}, according to the World Health Organisation (WHO).[43] The detection limits achieved by CMAS fall into this region, which demonstrates the appropriate performance of the device. The results are particularly interesting because of the relatively small path length (1.59 mm), which according to the Beer-Lambert law has a significant influence on transmittance measurement. Therefore, the results obtained with CMAS are useful not only for threshold testing, but also for both qualitative and quantitative measurements.

7.3.7 Kinetics of colour development on the CMAS

The kinetics of the colour development for the detection of nitrite ion via the Griess method was monitored using six standard solutions 0.0 – 1.2

mg L^{-1} of $NaNO_2$ using CMAS (on-chip) at 540 nm for 30 min. This procedure was also performed using UV-Vis spectrophotometer (off-chip) by taking an absorbance measurements over a similar time period per sample. Each standard solution was analysed in triplicate and the resulting kinetic curves for CMAS and UV-Vis spectrophotometer are presented in Appendix D, Fig. D15a-b. From the graphs it is evident that the room temperature analysis yielded three reproducible kinetic curves for each standard solution. First-order kinetic models were fitted (Microsoft Excel Solver)[44] to each curve and the rate constants were calculated over the concentration range 0.0 – 1.2 mg L^{-1} NO_2^-. The average response and fitted models are presented in Fig. 7.5a for CMAS and in Appendix D, Fig. D16a for the UV-Vis spectrophotometer. As shown in Table 7.2 and the Table D4a-b (Appendix D), the results obtained with CMAS and the UV-Vis spectrophotometer are equivalent, with negligible difference, which further demonstrates similar performance of the portable CMAS, compared to a standard bench-top UV-Vis instrument.

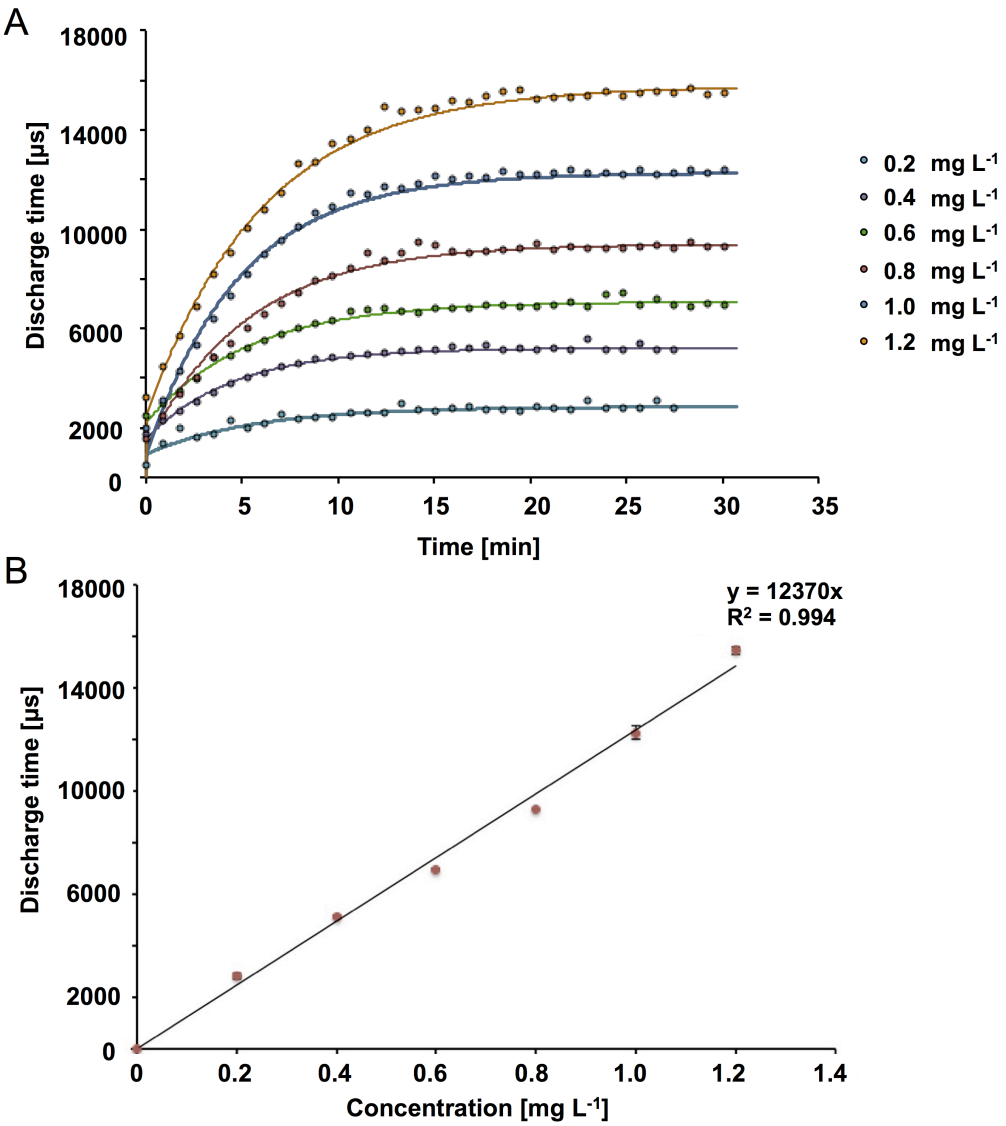

Figure 7.5. A) Kinetic study of the colour formation between NO_2^- and the Griess reagent at 540 nm (20.0 ± 0.5 °C), and fitted to the first order model and B) discharge time *versus* nitrite Griess reagent complex concentration for CMAS ($n = 3$).

Table 7.2. Comparison of average rate constants obtained with CMAS and the benchtop UV-Vis spectrophotometer for colour formation using NO_2^- samples with the Griess method (20.0 ± 0.5 °C; $n = 3$).

Sample no.	**Nitrite concentration [mg L^{-1}]**	**CMAS *Average k* (x 10^{-3}; s^{-1})**	**UV – Vis spectrophotometer *Average k* (x 10^{-3}; s^{-1})**
1	**0.2**	1.03 ± 0.04	1.8 ± 0.2
2	**0.4**	1.27 ± 0.08	1.7 ± 0.3
3	**0.6**	1.09 ± 0.08	1.8 ± 0.2
4	**0.8**	1.04 ± 0.06	1.8 ± 0.2
5	**1.0**	1.2 ± 0.2	1.9 ± 0.4
6	**1.2**	1.0 ± 0.1	1.7 ± 0.3

7.3.8 Calibration of the system for nitrite detection

The discharge time (detector signal) as a function of nitrite ion concentration is presented in Fig. 7.5B. The discharge time values for each concentration were calculated by subtracting the baseline signal obtained with deionsed water from the discharge time value at steady state (an average of 50 data points was used; 3 data points per second) obtained with each standard. A R^2 value of 0.994 (RSD: 1.45 %) was calculated indicating a good linear response over the range 0 - 1.2 mg L^{-1}. The calibration curve obtained with UV-Vis spectrophotometer is presented in Appendix D, Fig. D16b. Absorbance values were calculated from an average of 17 data points (1 data point per second). Discharge times and absorbance values related to each NO_2^- standard are presented in the Table D5a-b (Appendix D), respectively. The results demonstrate that the relative standard deviations for the three runs for each standard solution obtained with CMAS are lower than those obtained with UV-Vis spectrophotometer (1.61 % compared to 2.96 %). These

results imply that CMAS provided slightly more reproducible data compared to the UV-Vis bench-top instrument.

7.3.9 Nitrite detection in environmental water samples

Once the calibration method had been validated, CMAS was then used to measure nitrite in freshwater samples from five different locations around Ireland. The concentration of nitrite ions measured using Griess reaction was reported within 30 min. As it is presented in Fig. 7.6 and Table D6 (Appendix D), the results obtained using CMAS are within error to that of the UV-Vis spectrophotometer, which validate the utility of this device.

In comparison to the bench top microanalysis instrumentation based on the centrifugal platform presented by Salin *et al.*,[10, 12] our technique provides comparable results of nitrite detection with a portability which in turn allows for on-site water analysis.

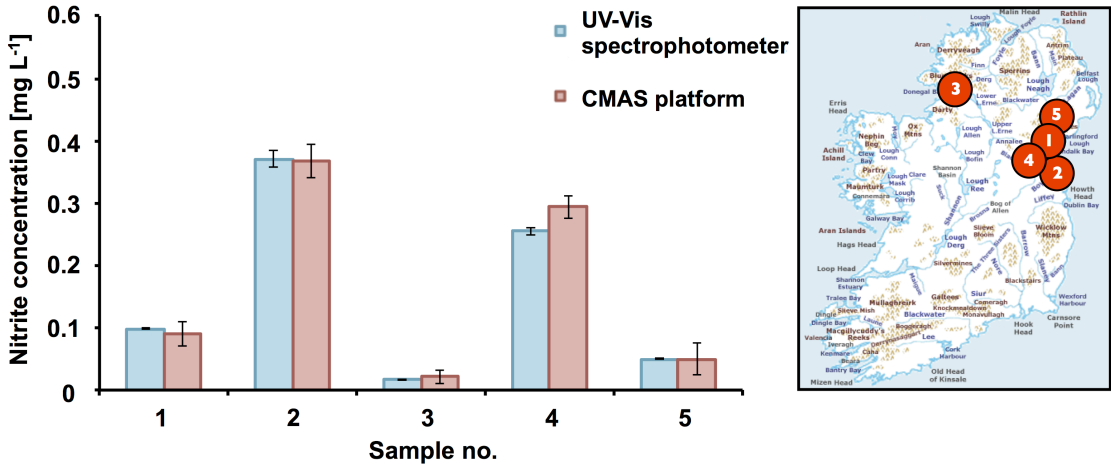

Figure 7.6. Water nitrite analysis using a bench-top UV-Vis spectrophotometer (blue) and CMAS (red) and a map of the sampling locations[45] ($n = 3$).

7.3.10 Practicality of CMAS for on-site water analysis

It is worth discussing some of the practical implications and limitations of this system at this stage of its development. The disposables required for the centrifugal platforms have been kept low cost, at < 7 € per CD, translating to a low cost per test of only 1€; which could be further reduced in a mass-manufacturing setting. As discussed, operation of the system is simple, requiring only metering of the specimen and reagent, followed by software operation. Automation of the system translates to less user-introduced error and contamination, thus reducing the percentage of false positives. Furthermore, automation has obvious cost advantages in terms of reduction in labor. The cost of CMAS in comparison to commercially available probes is relatively low; which a can be reduced if mass production processes are used during fabrication. A cost breakdown of CMAS components is presented in Appendix D, Fig. D17. The system presented is not a high-throughput system, but it is rapid and easy-to-use point of need device. As mentioned, the centrifugal platform has been designed to be part of a sample-to-answer system for water analysis, and not to replace larger, higher-throughput methods. While this system was tested and validated using water samples, it should be noted that CMAS has further potential applications beyond those of environmental monitoring, such as for the analysis of food samples for bacterial contamination and perhaps clinical diagnostics.

The varieties of architectures that can be constructed on centrifugal discs provide a great deal of versatility in developing dedicated variants of CMAS for a range of specific applications. The size and architecture of the disc reservoirs govern the number of microfluidic units that can be placed on a single disc. Therefore, further miniaturisation and changes in the

architectural design could easily allow for a greater number of assays per platform. While the case of nitrite ion detection is demonstrated as an exemplar, clearly the platform can be readily adopted for the wide array of water parameters for which colorimetric methods exist, such as those presented by Hwang *et al.*[13] Future work will focus on the design of such architectures so that multiple analytes can be detected on a single disc, including pH and turbidity which have already been implemented within a centrifugal disc by our group.[29]

7.4 Conclusions

In addition to easy operation, robustness, CMAS is an stand-alone, portable and compact device fully suitable for point-of-use analysis; it fulfills and indeed exceeds the requirements identified by Madou *et al.*[8] Analysed parameters can be adjusted according to individual needs; results can be downloaded in remote locations and displayed in *real time,* and stored on web-databases for location independent access, which will make CMAS an ideal choice for many applications, be it environmental or point-of-care diagnostics. The stand-alone capabilities of the system, combined with the portability and wireless communication, provide the flexibility needed for on-site monitoring, which in this example was nitrite detection in freshwater samples across Ireland. The LOD of CMAS (9.31 ± 0.09 μg L^{-1}) for nitrite is comparable to the detection limits achievable by the spectrometric standard procedures and is within the range required for industrial and environmental applications. When compared to the UV-Vis spectrophotometer, the same value of coefficient of correlation ($R^2 = 0.99$) was achieved with slightly improved RSD (1.02 % compared to 1.57 %), which indicates the good performance of CMAS. Due to all of the above-mentioned advantages, this

system represents significant progress towards the realisation of truly stand-alone microfluidic platforms with the potential to change the way many important environmental and health related measurements are performed.

7.5 Acknowledgements

The authors wish to thank to the Marie Curie Initial Training Network funded by the EC FP7 People Programme, Science Foundation of Ireland under grant 07/CE/I1147. K.J.F acknowledges the European Commission for financial support through Marie Curie Actions International Reintegration Grant (IRG) (PIRG07-GA-2010-268365) and the Irish Research Council. This work has been supported by the Science Foundation Ireland under Grant No. 10/CE/B1821. MC thanks Mr. Brendan Heery for freshwater samples.

7.6 References

1. Rogers, K. R., Recent advances in biosensor techniques for environmental monitoring. *Analytical Chimica Acta* **2006,** *568* (1-2), 222-231.
2. Hanna Instruments: http://www.hannainst.com/usa/prods2.cfm?id=045001&ProdCode=HI764. (accessed March 18, 2013).
3. API Test kits: http://www.apifishcare.co.uk/product.php?sectionid=1&catid=4&subcatid=0&id=82. (accessed March 18, 2013).
4. Hach: http://www.hachhydromet.com/web/ott_hach.nsf/id/pa_ds5-multiparameter-sonde.html. (accessed March 18, 2013).
5. YSI: http://www.ysi.com/productsdetail.php?6920-V2-3. (accessed March 18, 2013).
6. Sequeira, M.; Diamond, D.; Daridon, A.; Lichtenberg, J.; Verpoorte, S.; Rooij, N. F. d., Progress in the realisation of an autonomous environmental monitoring device for ammonia. *TrAC Trends in Analytical Chemistry* **2002,** *21* (12), 816-827.

7. Duford, D. A.; Peng, D. D.; Salin, E. D., Magnetically driven solid sample preparation for centrifugal microfluidic devices. *Analytical Chemistry* **2009,** *81* (11), 4581-4584.
8. Gorkin, R.; Park, J.; Siegrist, J.; Amasia, M.; Lee, B. S.; Park, J.-M.; Kim, J.; Kim, H.; Madou, M.; Cho, Y.-K., Centrifugal microfluidics for biomedical applications. *Lab on a Chip* **2010,** *10* (14), 1758-1773.
9. Watts, A. S.; Urbas, A. A.; Moschou, E.; Gavalas, V. G.; Zoval, J. V.; Madou, M.; Bachas, L. G., Centrifugal microfluidics with integrated sensing microdome optodes for multiion detection. *Analytical Chemistry* **2007,** *79* (21), 8046-8054.
10. LaCroix-Fralish, A.; Clare, J.; Skinner, C. D.; Salin, E. D., A centrifugal microanalysis system for the determination of nitrite and hexavalent chromium. *CORD Conference Proceedings* **2009,** *80* (2), 670-675.
11. Kong, M. C.; Salin, E. D., Spectrophotometric determination of queous Sulfide on a pneumatically enhanced centrifugal microfluidic platform. *Analytical Chemistry* **2012,** *84* (22), 10038-10043.
12. Yongqing, X.; Templeton, E.J.; Salin, E. D., Rapid simultaneous determination of nitrate and nitrite on a centrifugal microfluidic device. *Talanta* **2010,** *82*, 1612-1615.
13. Hwang, H.; Kim, Y.; Cho, J.; Lee, J.-y.; Choi, M.-S.; Cho, Y.-K., Lab-on-a-disc for simultaneous etermination of nutrients in water. *Analytical Chemistry* **2013,** *85* (5), 2954-2960.
14. Diamond, D., Peer Reviewed: Internet-scale sensing. *Analytical Chemistry* **2004,** *76* (15), 278 A-286 A.
15. Lee, B. S.; Lee, J.-N.; Park, J.-M.; Lee, J.-G.; Kim, S.; Cho, Y.-K.; Ko, C., A fully automated immunoassay from whole blood on a disc. *Lab on a Chip* **2009,** *9* (11), 1548-1555.
16. Schembri, G. T.; Burd, T. L.; Kopf-Sill, A. R.; Shea, L. R.; Braynin, R., Piccolo, ABAXIS. *Journal of Automated Methods and Management in Autom. Methods Manage. Chem.* **1995,** *17*, 99–104.
17. Grumann, M.; Steigert, J.; Riegger, L.; Moser, I.; Enderle, B.; Riebeseel, K.; Urban, G.; Zengerle, R.; Ducrée, J., Sensitivity enhancement for colorimetric glucose assays on whole blood by on-chip beam-guidance. *Biomedical Microdevices* **2006,** *8* (3), 1387-2176.
18. Steigert, J.; Grumann, M.; Dube, M.; Streule, W.; Riegger, L.; Brenner, T.; Koltay, P.; Mittmann, K.; Zengerle, R.; Ducrée, J., Direct hemoglobin measurement on a centrifugal microfluidic platform for point-of-care diagnostics. *Sensors and Actuators A: Physical* **2006,** *130-131*, 228-233.
19. Grumann, M.; Riegger, L.; Pastewka, L.; Brenner, T.; Zengerle, R.; Ducrée, J.; Nann, T.; Riegler, J.; Ehlert, O.; Mittenbuhler, K.; Urban, G. In: Parallelization of chip-based fluorescence immuno-assays with

quantum-dot labeled beads. The 13th International Conference on Solid-State Sensors, Actuators and Microsystems Conference (Transducers) **2005**, *2*, 1114-1117.

20. Godino, N.; Gorkin III, R.; Linares, A. V.; Burger, R.; Ducrée, J., Comprehensive integration of homogeneous bioassays via centrifugo-pneumatic cascading. *Lab on a Chip* **2013,** *13*, 685-694.
21. Gorkin III, R.; Nwankire, C. E.; Gaughran, J.; Zhang, X.; Donohoe, G. G.; Rook, M.; O'Kennedy, R.; Ducrée, J., Centrifugo-pneumatic valving utilizing dissolvable films. *Lab on a Chip* **2012,** *12* (16), 2894-2902.
22. Moorcroft, M. J.; Davis, J.; Compton, R. G., Detection and determination of nitrate and nitrite: a review. *Talanta* **2001,** *54* (5), 785-803.
23. Dutt, J.; Davis, J., Current strategies in nitrite detection and their application to field analysis. *Journal of Environmental Monitoring* **2002,** *4* (3), 465-471.
24. Al-Okab, R. A.; Syed, A. A., Novel reactions for simple and sensitive spectrophotometric determination of nitrite. *Talanta* **2007,** *72* (4), 1239-1247.
25. Patey, M. D.; Rijkenberg, M. J. A.; Statham, P. J.; Stinchcombe, M. C.; Achterberg, E. P.; Mowlem, M., Determination of nitrate and phosphate in seawater at nanomolar concentrations. *TrAC Trends in Analytical Chemistry* **2008,** *27* (2), 169-182.
26. Xi, Y.; Templeton, E. J.; Salin, E. D., Rapid simultaneous determination of nitrate and nitrite on a centrifugal microfluidic device. *Talanta* **2010,** *82* (4), 1612-1615.
27. Johnson, K. S.; Coletti, L. J., In situ ultraviolet spectrophotometry for high resolution and long-term monitoring of nitrate, bromide and bisulfide in the ocean. *Deep Sea Research Part I: Oceanographic Research Papers* **2002,** *49* (7), 1291-1305.
28. Hanson, A. K. In *A new in situ chemical analyzer for mapping coastal nutrient distributions in real time*, OCEANS 2000 MTS/IEEE Conference and Exhibition, **2000**, *3*, 1975-1982.
29. Czugala, M.; Gorkin III, R.; Phelan, T.; Gaughran, J.; Curto, V. F.; Ducrée, J.; Diamond, D.; Benito-Lopez, F., Optical sensing system based on wireless paired emitter detector diode device and ionogels for lab-on-a-disc water quality analysis. *Lab on a Chip* **2012,** *12*, 5069-5078.
30. O'Toole, M.; Shepherd, R.; Lau, K. T.; Diamond, D., Detection of nitrite by flow injection analysis using a novel Paired Emitter-Detector Diode (PEDD) as a photometric Detector. *Procee SPIE* **2007,** *6755, 67550P.*
31. de Vargas-Sansalvador, I. M. P.; Fay, C.; Phelan, T.; Fernandez-Ramos, M. D.; Capitan-Vallvey, L. F.; Diamond, D.; Benito-Lopez, F., A new light emitting diode-light emitting diode portable carbon dioxide gas

sensor based on an interchangeable membrane system for industrial applications. *Analytica Chimica Acta* **2011,** *699* (2), 216-222.

32. Lau, K. T.; Baldwin, S.; Shepherd, R. L.; Dietz, P. H.; Yerzunis, W. S.; Diamond, D., Novel fused-LEDs devices as optical sensors for colorimetric analysis. *Talanta* **2004,** *63* (1), 167-173.
33. Lau, K.-T.; Baldwin, S.; O'Toole, M.; Shepherd, R.; Yerazunis, W.; Izuo, S.; Ueyama, S.; Diamond, D., A low-cost optical sensing device based on paired emitter-detector light emitting diodes. *Analytica Chimica Acta* **2005,** *557*, 111-116.
34. MacFaddin, J., Nitrate/nitrite reduction tests, In: Biochemical tests for identification of medical bacteria. 3rd ed.; Lippincott Williams & Wilkins: Philadelphia, **2000**.
35. O'Toole, M.; Diamond, D., Absorbance based light emitting diode optical sensors and sensing devices. *Sensors* **2008,** *8*, 2453-2479.
36. Žukauskas, A.; Shur, M. S.; Gaska, R., Introduction to solid-state Lighting. John Wiley & Sons, Inc., **2002**.
37. Gorkin, R.; Czugala, M.; Rovira-Borras, C.; Ducrée, J.; Diamond, D.; Benito-Lopez, F., A wireless paired emitter detector diode device as an optical sensor for lab-on-a-disc applications. The 17th International Conference on Solid-State Sensors, Actuators and Microsystems Conference (Transducers) **2011**, 2526-2529.
38. Hauser, P. C.; Rupasinghe, T. W. T.; Cates, N. E., A multi-wavelength photometer based on light-emitting diodes. *Talanta* **1995,** *42* (4), 605-612.
39. Rocha, F. R. P.; Reis, B. F., A flow system exploiting multicommutation for speciation of inorganic nitrogen in waters. *Analytica Chimica Acta* **2000,** *409* (1-2), 227-235.
40. Frenzel, W.; Schulz-Brussel, J.; Zinvirt, B., Characterisation of a gas-diffusion membrane-based optical flow-through sensor exemplified by the determination of nitrite. *Talanta* **2004,** *64* (2), 278-282.
41. Steimle, E. T.; Kaltenbacher, E. A.; Byrne, R. H., In situ nitrite measurements using a compact spectrophotometric analysis system. *Marine Chemistry* **2002,** *77* (4), 255-262.
42. Shrivastava, A.; Gupta, V., Methods for the determination of limit of detection and limit of quantitation of the analytical methods. *Chronicles of Young Scientists* **2011,** *2* (1), 21-25.
43. World Health Organization, Guidelines for drinking-water quality [electronic resource]: incorporating 1st and 2nd addenda, vol. 1, Recommendations. Geneva, **2008**.
44. Diamond, D.; Hanratty, V. C. A., Spreadsheet Applications for Chemistry Using Microsoft Excel. John Wiley and Sona, New York, **1997**.

45. http://en.wikipedia.org/wiki/File:Ireland_physical_large.png (accessed 15/04/ 2012).

Chapter 8

Summary, conclusions and future perspectives

8.1 Overall summary and conclusions

The work presented in this thesis investigates several novel microfluidic based platforms for water quality analysis. Furthermore, several stimuli responsive materials have been charaterised and applied within these platforms as sensors and actuators, allowing for facile and low-cost operation of the systems.

In Chapter 2, a comprehensive review of stimuli-responsive materials for sensors and actuator applications in microfluidics has been presented. Special attention has been paid to the physical basics of photoresponsive gels behavior.

Chapter 3 introduced photoresponsive *N*-isopropylacrylamide phosphonium-based ionogels functionalised with the photochromic compound benzospiropyran. Microstructures were fabricated using a simple to use and inexpensive in-house designed photolithographic set-up. The characterisation of the swelling and shrinking behaviour the microstructures was presented in addition to the evaluation of the influence of the surface-area-to-volume ratio on the swelling kinetics. It was found that the actuation behaviour of the ionogels is strongly dependent on the nature of the ionic liquid encapsulated in the polymer matrix.

Chapters 4 – 7 discussed several microfluidic-based platforms for colorimetric analysis, with integrated wireless communication devices allowing for data acquisition according to individual needs. A portable, microfluidic analytical platform applied to the monitoring and determination of nitrite anions in water using the Griess method was presented (Chapter 4). The colour intensity of the Griess reagent nitrite complex was detected using a low cost paired emitter detector diode (PEDD). On-chip fluid manipulation was performed using a biomimetic photoswitchable $[P_{6,6,6,14}][dca]$ ionogel

microvalve, described in the previous chapters, controlled by a white light LED. Chapter 5 introduced a portable optical sensing configuration for lab-on-a-disc colorimetric analysis applications. The system employed a wireless PEDD, similar to the one employed in Chapter 4. The light dependent discharging process was used to measure concentrations of coloured solutions. Similar limits of detection between the PEDD system and a standard UV-Vis spectrophotometer were obtained. The results demonstrated that the system was able to detect low concentrations of analytes on the centrifugal microfluidic platform. In general, this showed potential for the PEDD system to be a cheap and versatile alternative optical detector for lab-on-a-disc applications. Chapter 6 described the first use of the PEDD system as an optical sensor for water quality monitoring in a lab-on-a-disc device. The design and development of the centrifugal microfluidic platform is based on an ionogel sensing area, Chapter 3, and applied for pH (quantitative) and turbidity (qualitative) monitoring of water samples at the point-of-need. The sensing area was based on phosphonium ionogels with incorporated pH dye, which change of colour can be quantified using the PEDD method to obtain pH value of analysed sample.

Finally, a portable, wireless system capable of *in-situ* reagent-based colorimetric analysis was demonstrated in Chapter 7. The Centrifugal Microfluidic Analysis System (CMAS) incorporated an easily reconfigurable detector board, which allows a wide range of centrifugal microfluidic layouts to be implemented. The stand-alone capabilities of the system, combined with the portability and wireless communication provided the flexibility crucial for on-site water monitoring. The centrifugal disc was designed for nitrite detection in water samples, as a proof of principle.

8.2 Possible future applications and limitations

Considering all the knowledge gained during the generation of this thesis there are several strands/research paths which should be further explored:

8.2.1. Nitrite and nitrate determination in a microfluidic platform

Within the work presented in Chapter 4 and Chapter 7, the nitrite ion was chosen, as proof of concept, as the target analyte for demonstrating the functionality of the prototype platforms. It would be advantageous to investigate nitrate ions analysis as well, within the microfluidic platform. The idea would be to incorporate a reduction step on-chip in a reservoir with pre-loaded powder (NitriVer, Hach), where the relatively inert nitrate ion would be chemically reduced to the more reactive nitrite before initiating the detection sequence. This approach has been presented by Xi *et al.*[1] The determination of nitrite by a two-step process provides information on the "total" amount of nitrate and nitrite. Nitrite quantification could then be made in a parallel assay, as the ones presented in Chapter 4 or 7, wherein the samples would not be reduced prior to the colorimetric assay. Actual nitrate levels could be then calculated by the subtraction of nitrite levels from the "total" nitrogen.

8.2.2 Multiparameter platform for pH and turbidity

The centrifugal disc for pH and turbidity analysis presented in Chapter 6 allows for analysis of 7 water samples in parallel (Fig. 8.1, GEN I). It would

also be worth investigating the possibility to further miniaturise and change the architectural design of the microfluidic structures, which would easily allow for a greater number of analyses per platform. The re-design of the CD has already been done, resulting in 12 structures on a single CD (see Fig. 8.1, GEN II). In this configuration, the volume of the required water sample was reduced compared to GEN I (50 μL instead of 100 μL), and the volume of the ionogel premixture required for photopolymerisation of sensing area was 53 % smaller than in GEN I (20 μL instead of 42 μL). By decreasing the amount of polymer for the sensing area the cost of a single sample analysis is reduced. Fresh water samples were relatively clean, therefore the preliminary results obtained with the new configuration (GEN II) did not provide sufficient qualitative data on the amount of solid contaminants (turbidity) since the filtration chamber of the chips was too big for that particular application. Therefore, by reducing the size of the upper chamber, which resulted in the GEN III of CD (Fig. 8.1, GEN III), it will be possible to determine the amount of solid contaminants and therefore the turbidity of relatively clean samples.

Figure 8.1. Development of the centrifugal microfluidic platform for water pH analysis; the green rulers represent 2 cm and the black rulers represent 0.5 cm.

8.2.3 Industrial validation of CMAS

The CMAS platform presented in Chapter 7 has great potential for commercialisation so the validation of the platform against the gold standard instrumentation used for water analysis in accredited laboratories is required. Therefore, initial experiments have been carried out in TELlab (http://www.tellab.ie/companyinformation.php) in order to further validate the system. The determination of nitrite in freshwater samples was carried out using Hach Portable Datalogging Spectrophotomer DR/2010 Ion Chromatograph and CMAS. Preliminary results of water analysis obtained with CMAS fall between the ones obtained using the portable Hach Spectrophotometer and Ion Chromatographer (Table 8.1). It is important to mention that the Hach Spectrophotometer Low Range (LR) method is able to reproducibly detect the nitrite levels up to ~ 1.5 mg L^{-1}, similarly to the assay based on Griess reagent used in CMAS (nevertheless, higher levels can be detected after dilution of the sample). In case of Ion Chromatography (IC), the low limit of detection of nitrites is 0.2 mg L^{-1}, which is much higher than the LOD of CMAS – 0.009 mg L^{-1}.

Table 8.1. Results of nitrite determination using Hach Spectrophotometer, IC and CMAS.

Sample No.	Hach Spectrophotometer [mg L^{-1}]				IC [mg L^{1}]	CMAS [mg L^{-1}]			
	Run 1	Run 2	Run 3	Avg.		Run 1	Run 2	Run 3	Avg.
1	1.532	1.472	1.406	**1.47**	**1.7**	1.58	1.65	1.60	**1.61**
2	0.010	0.019	0.017	**0.015**	**Not detected**	0.14	0.16	0.14	**0.15**
3	0.015	0.010	0.014	**0.013**	**Not detected**	0.08	0.10	0.10	**0.09**
4	0.028	0.021	0.019	**0.023**	**Not detected**	0.09	0.06	0.07	**0.08**
5	0.864	1.030	0.941	**0.945**	**1.35**	1.21	1.22	1.23	**1.22**

8.2.4 Centrifugal disc for multiparameter water analysis

While the simplest case of nitrite ions detection is demonstrated in Chapter 7, CMAS also can be configured as a single platform devoted to multiple analyte measurements covering an array of important water parameters, such as those presented by Hwang *et al.*[2] It will be certainly advantageous at this stage, to design new CDs so that multiple analytes could be detected on a single disc, such as phosphate, ammonia pH and turbidity, the latter two being already implemented within a CD (see Chapter 6), Fig. 8.2. The integration of a filtration step similar to that described in Chapter 6 would enable fully integrated and automated multi-step water analysis on a CD. This technique establishes a sequence of laboratory unit operations comprising water filtration, metering, mixing/incubation, and liquid reagent release from on-board reservoirs for detection by mere control of the rotational frequency using CMAS.

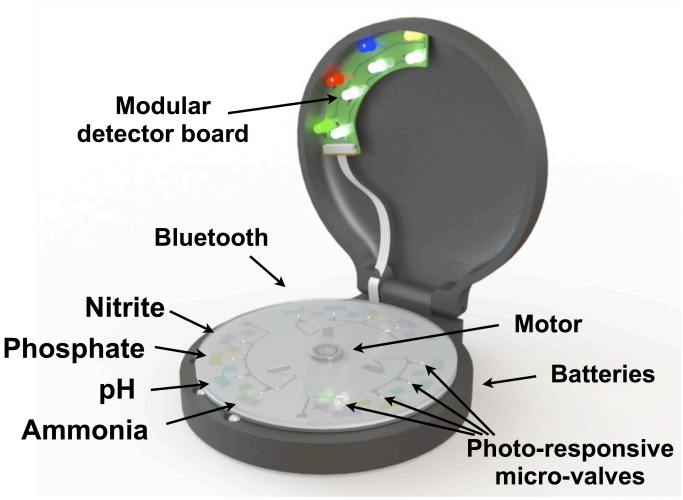

Figure 8.2. Proposed centrifugal disc that allows for the analysis of multiple analytes, with incorporated photoresponsive microvalves and the second generation of CMAS capable of measuring several parameters in parallel.

8.2.5 Versatility of CMAS

CMAS could also be configured for biomedical point-of-care diagnostics as the PEDD detection system can be used for any colorimetric assay. The easily interchangeable PEDD boards allow a wide range of centrifugal microfluidic layouts to be implemented. In collaboration with Dr. Charles Nwankire and Prof. Jens Ducrée from the Biomedical Diagnostics Institute (DCU), it has been demonstrated that CMAS can be used as a biomedical point-of-care device. A 5-parameter enzymatic liver assay panel on CD with colorimetric end-point (albumin (ALB), alkaline phosphatase (ALP) and total (TBIL) bilirubin) and kinetic detection (glutamyl transferase (GGT), Fig. 8.3 was developed and tested.

Figure 8.3. Image showing loading of blood sample on the portable CMAS interfacing with an Android tablet. A custom made program was used to control the spinning of the disc and also for wireless real time data extraction.

Medical reports suggest that a mortality from 2 % to 28 % could be linked with medication-induced liver damage, for example HIV, tuberculosis and cancer patients.[3] This has prompted local governments to fund routine monitoring of liver function protocols in centralised laboratories; however, in lack of transport logistics, accessibility of such centralised labs remains a significant challenge for the majority of patients. The CD presented above combined with CMAS could allow for autonomous, sample-to-answer operation by untrained staff at local community health centers. Starting with single-step pipetting of finger prick blood, the CD platform controlled multi-stage sample preparation and flow distribution into six outer reaction chambers by an array of dissolvable film (DF) valves.[4] Fig. 8.4 shows the multi-layered CD platform, designed by Dr. Nwankire, comprising two fluidically independent sections – one for calibration and one for running the assay panel.

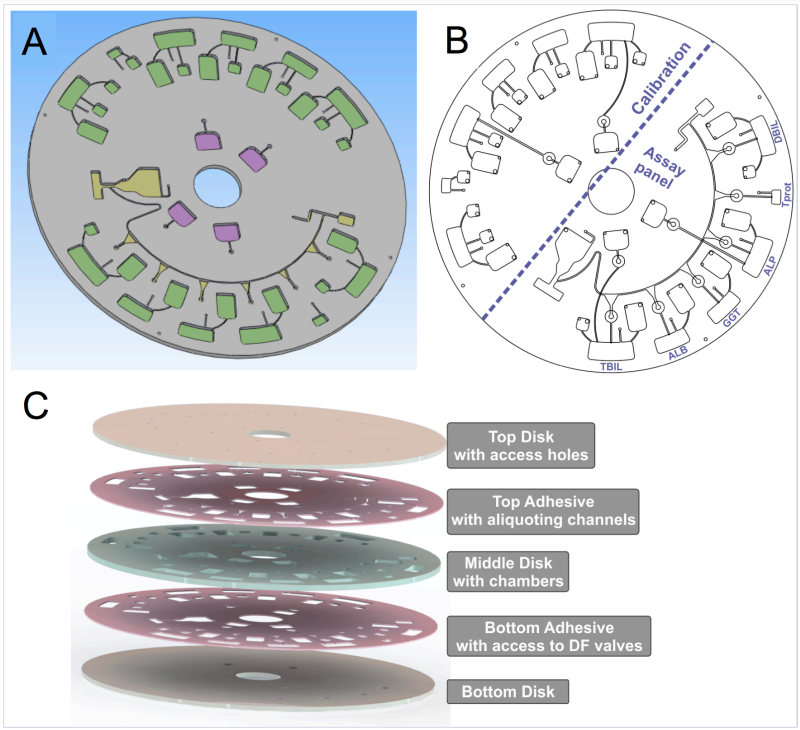

Figure 8.4. A-B) 3D representation and design of CD platform for both, system calibration and the liver assay panel (LAP) and C) 5-layer CD platform.

The corresponding calibration curves obtained from this system are shown in Fig. 8.5. The test results were benchmarked with a benchtop plate-well reader from Tecan and on intravenous blood samples sent the same day to a hospital laboratory. The results (Table 8.2) show very good correlation with an average standard deviation of 7.9 % across the full range of assays. The future plans focus on the extension of the range of clinically relevant assay panels, test formats and detection schemes.

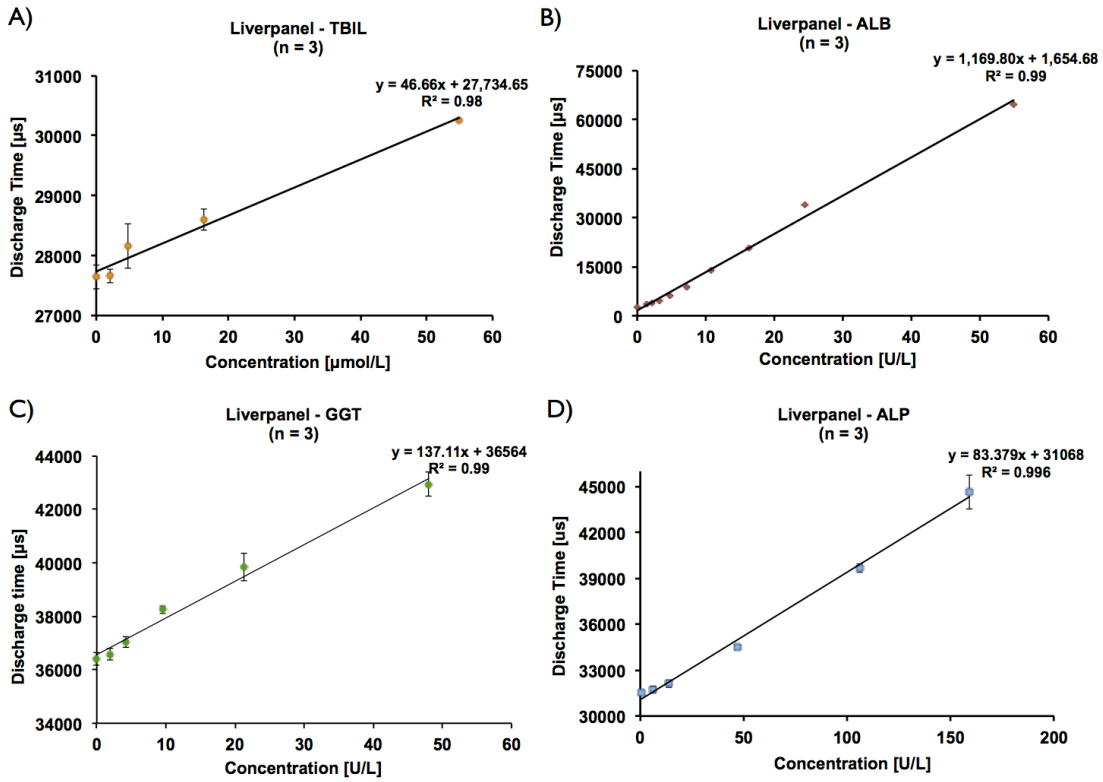

Figure 8.5. Calibration curves of TBIL, ALB, GGT and ALP obtained using the CD platform ($n = 3$).

Table 8.2. Comparison of hospital, benchtop and CMAS results of the Liver assay panel.

Liver assay	**Hospital clinic data**	**Tecan plate reader ($n = 3$)**	**CMAS ($n = 3$)**	**Normal clinical range**
ALB [g/l]	41	44.3 ± 2.0	45.8 ± 1.2	35 – 50
TBIL [µmol/l]	19	17.0 ± 2.1	22.1 ± 2.5	5 – 24
ALP [I.U./l]	83	84.9 ± 2.7	81.2 ± 2.0	30 – 130
GGT [I.U./l]	18	16.9 ± 3.1	20.8 ± 3.7	11 - 67

8.2.6 Photoswitchable microvalve for centrifugal disc application

In order to achieve automated analysis on CD, photoswitchable ionogel microvalves would play a crucial role. During storage and at rest (stop flow) the swollen photoswitchable microvalves provide permanent liquid barriers (as proven in Chapter 4). Therefore, preliminary experiments have been carried out on the incorporation of such microvalves in CD platforms. The ionogel microvalve (diameter 500 μm) was photopolymerised *in-situ* in a microchannel cavity, which connects the sample chamber with the bottom detection chamber. The microvalve is also connected to a perpendicular engraved microchannel, with an inlet and outlet for acidic solution, allowing for reswelling (closure of the microchannel) of the microvalve (Fig. 8.6, left). In this way, the main microchannel with sample and assay reagents was protected from the influence of the acid.

The microvalve was successfully controlled by simply applying white light irradiation from a LED source that had been integrated into CMAS (Fig. 8.6, right). Apart from the low-power actuation system, integrated wireless communications in CMAS allowed the microvalves to be controlled remotely *via* the Android tablet. Food dye solution was loaded in the upper chamber, and rotation at 600 rpm drove the sample towards the bottom chamber. When in the closed state, the microvalve prevented the sample from moving along the microchannel (Fig. 8.7A). Upon white light irradiation, the valve shrunk, opening the microchannel, and the fluid could move to the bottom chamber (Fig. 8.7B-D). The burst threshold of the microvalve was *ca.* 800 rpm, so at rotational speeds below this, the valve provided a stable physical barrier. The video of the microvalve operation can be viewed at http://db.tt/PMV7eKlF.

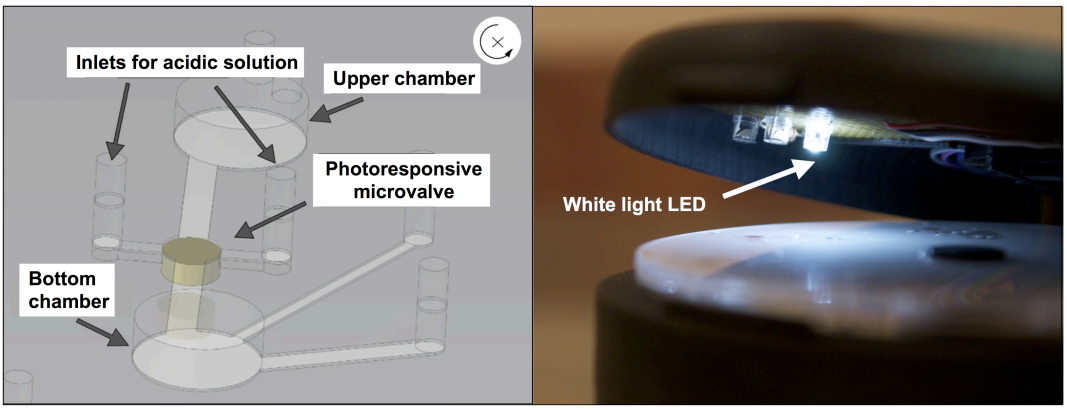

Figure 8.6. Design of the photoresponsive ionogel microvalve incorporated within a centrifugal microfluidic platform (left) and actuation set-up of the microvalve using a low cost light emitting diode (cost $< 1€$) in CMAS (the lid is opened for clarity) (right).

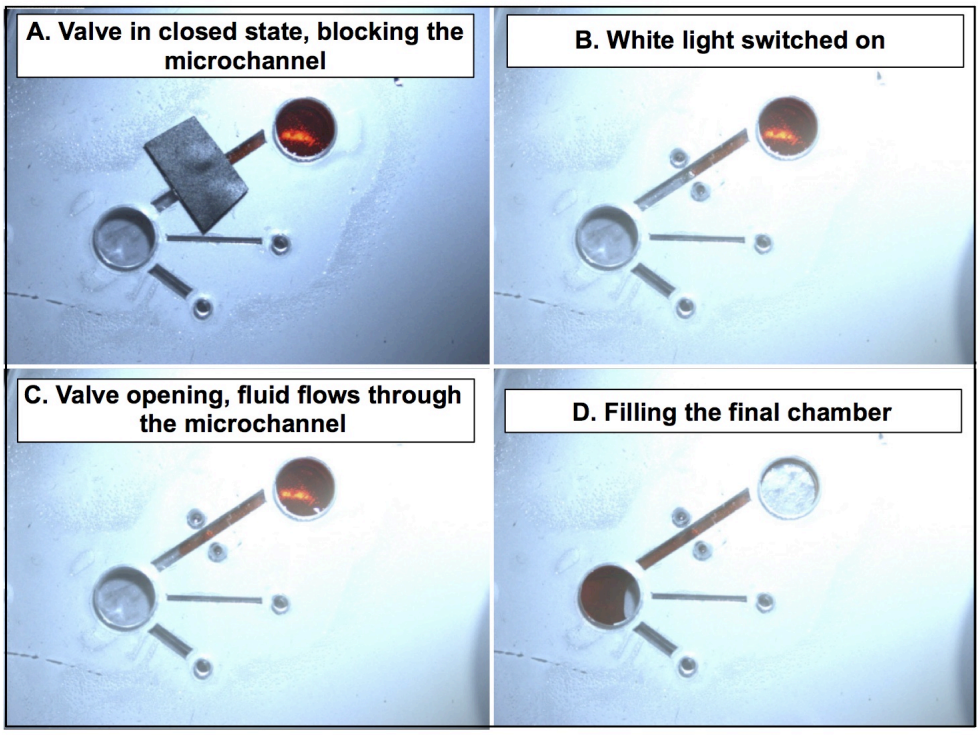

Figure 8.7. Series of images showing the actuation of the ionogel microvalve during spinning the CD at 600 rpm.

The integration of smart functional materials in microfluidic platforms has some drawbacks and limitations. The major ones observed during the progress of this thesis could be summarised as follows:

1. The p(SPNIPAAm) ionogel based microvalves require exposure to acidic solution (pH 3) in order to induce swelling, whereas the shrinking mechanism results in the release of protons into the external solution around the ionogel, as explained in detail in Chapter 3. It may affect some assays performance, like these handling with cells and proteins, which typically require neutral pH. In such cases, the microvalves will need to be isolated from the main microchannel containing the assay reagents by means of a flexible and non-permeable membrane. Strategies to extend the functional pH range of the microvalves and to improve the response time of the microvalves are currently under investigation in our laboratories. These are being tackled in a two prong approach - firstly by increasing the rate of water uptake and release, and secondly, by increasing the surface-area-to-bulk ratio of the microvalve structure, as presented in Chapter 3. Moreover, our group has recently addressed the issue discussed above by incorporating acrylic acid (AA) co-monomer into the structure of the p(SPNIPAAm) hydrogels. In this way, an internal source of protons for self spiropyran protonation was provided, resulting in spontaneous swelling of the gels when placed in deionised water.

2. The platform for nitrite analysis presented in Chapter 4 required the use of 25 mbar back pressure from a vacuum pipe connected to the microfluidic device *via* the outlet to move the liquids from the storage reservoirs towards the detection chamber. Although the presented system was a proof-of-concept, this method for fluid propulsion limits the possibilities of *in-situ* colorimetric analysis. In order to achieve stand-alone capabilities finger

pump[5] or the generation of inbound capillary flow[6] by surface modification of the microchannel inner walls could be employed for fluid propulsion.

3. The determination of the pH of water samples using Lab-on-a-Disc platform presented in Chapter 6 is relatively long (15 min). There are several possibilities to improve the time of the analysis: (1) decrease of the size of the sensing area to allow faster water diffusion within the ionogel; (2) functionalise the PMMA sensing area with adaptive materials based on polynailine. This coating has the potential for pH sensing of liquid giving the results within few minutes (2 min).[7]

4. At the moment, the alignment of the optical cuvette with the respective PEDD detector in the CMAS platform described in Chapter 7, is achieved manually when rotating the disc with the finger through the window in the top lid. The addition of an automatic alignment of the CD would be of huge benefit, eliminating possible errors in the alignment process and facilitating operation. This can be achieved by further development of the software interaction between the stepper motor and the alignment LED. Since the motor operates under pulse-width modulation, the angle of rotation is determined by the duration of the applied pulses. With the motor running at a low rate (500 rpm), the readings from the alignment LED indicates the relationship between the angle of rotation between each sample location and the pulse to be applied to the motor by the microcontroller; thus, the automated alignment is self-calibrating to account for the number of sample locations on the disc.

In summary there is huge potential in these materials and platforms for various applications in environmental research and point-of-care clinical analysis. I have no doubt that CMAS will continue to be developed for these and other as yet unrealised analytical applications.

8.3 References

1. Yongqing, X.; Templeton, E. J.; Salin, E. D., Rapid simultaneous determination of nitrate and nitrite on a centrifugal microfluidic device. *Talanta* **2010,** *82*, 1612-1615.
2. Hwang, H.; Kim, Y.; Cho, J.; Lee, J.-y.; Choi, M.-S.; Cho, Y.-K., Lab-on-a-disc for simultaneous determination of nutrients in water. *Analytical Chemistry* **2013,** *85* (5), 2954-2960.
3. Vella, S. J.; Beattie, P.; Cademartiri, R.; Laromaine, A.; Martinez, A. W.; Phillips, S. T.; Mirica, K. A.; Whitesides, G. M., Measuring markers of liver function sing a micropatterned paper evice designed for blood from a Fingerstick. *Analytical Chemistry* **2012,** *84* (6), 2883-2891.
4. Gorkin III, R.; Nwankire, C. E.; Gaughran, J.; Zhang, X.; Donohoe, G. G.; Rook, M.; O'Kennedy, R.; Ducrée, J., Centrifugo-pneumatic valving utilizing dissolvable films. *Lab on a Chip* **2012,** *12* (16), 2894-2902.
5. Li, W.; Chen, T.; Chen, Z.; Fei, P.; Yu, Z.; Pang, Y.; Huang, Y., Squeeze-chip: a finger-controlled microfluidic flow network device and its application to biochemical assays. *Lab on a Chip* **2012,** *12* (9), 1587-1590.
6. Zhu, Y.; Petkovic-Duran, K., Capillary flow in microchannels. *Microfluidics and Nanofluidics* **2010,** *8* (2), 275-282.
7. Florea, L.; Fay, C.; Lahiff, E.; Phelan, T.; O'Connor, N. E.; Corcoran, B.; Diamond, D.; Benito-Lopez, F., Dynamic pH mapping in microfluidic devices by integrating adaptive coatings based on polyaniline with colorimetric imaging techniques. *Lab on a Chip* **2013**, 13, 1079-1085.

Appendix A

Supplementary Information

Photopatterning and actuation behaviour of photoresponsive phosphonium-based ionogel microstructures

M. Czugala,[1] C. O'Connel,[1] C. Blin,[2] P. Fischer,[3] Kevin J. Fraser,[1] F. Benito-Lopez,[1, 4] D. Diamond[1]

Langmuir, 2013 (Under Review)

[1]CLARITY: Centre for Sensor Web Technologies, National Centre for Sensor Research, Dublin City University, Dublin 9, Ireland
[2]Fraunhofer Institute of Physical Measurement Techniques IPM, Freiburg, GERMANY
[3]Max Planck Institute for Intelligent Systems, Stuttgart, GERMANY
[4]CIC microGUNE, Arrasate-Mondragón, SPAIN

A1. Photomask for fabrication of ionogel microstructures

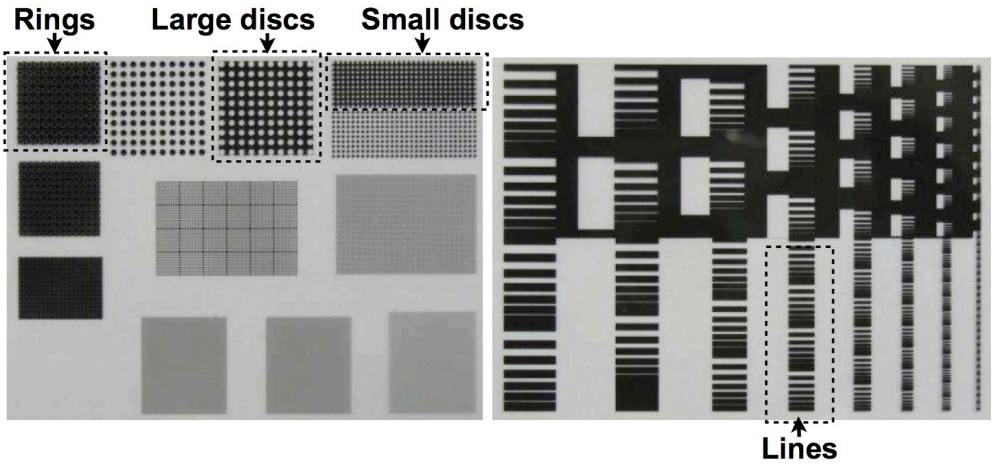

Figure A1. Pictures of the photomasks used for the photolithographic micropatterning of the ionogels.

A2. Contact angle results

Table A1. Contact angle values of the functionalised glass slide surfaces ($n = 4$).

After cleaning	I NaOH	II MPTMS
61 ± 3 °	52 ± 1 °	72 ± 4 °

A3. Ionogel microstructures

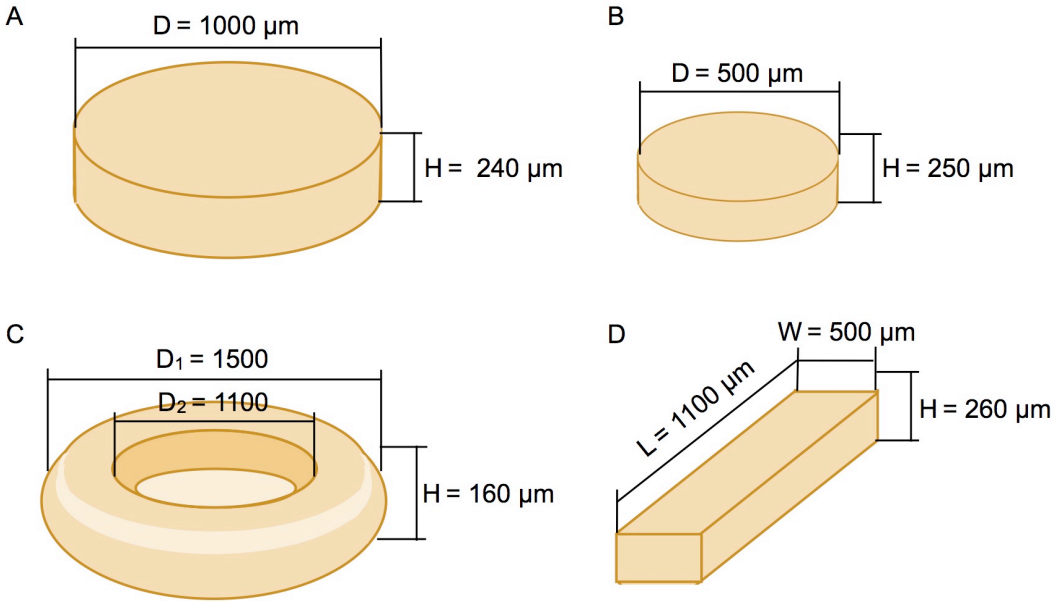

Figure A2. Schematic representation of the photopolymerised ionogel microstructures and dimensions: a) large disc, b) small disc, c) ring and d) line.

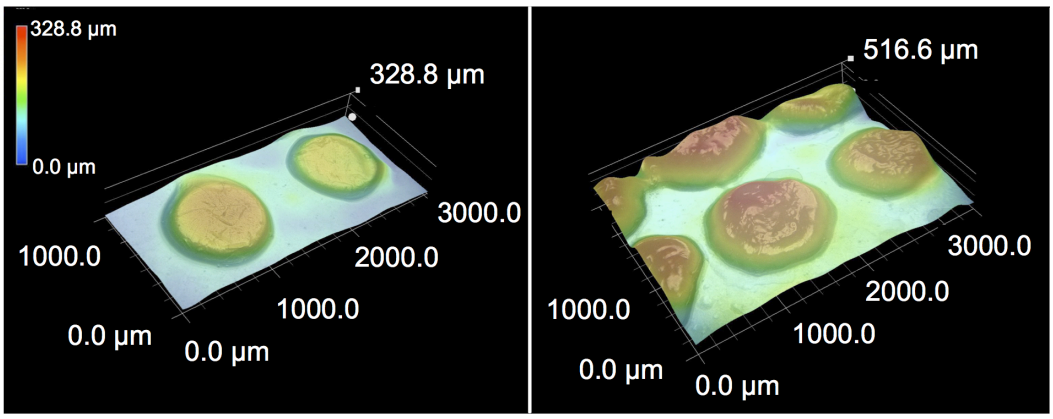

Figure A3. 3D images of photoswitchable $[P_{6,6,6,14}][dca]$ ionogel discs in the initial state (left) and the swollen (right) state taken with a 3D Keyence Microscope.

A4. Kinetic studies of ionogel swelling

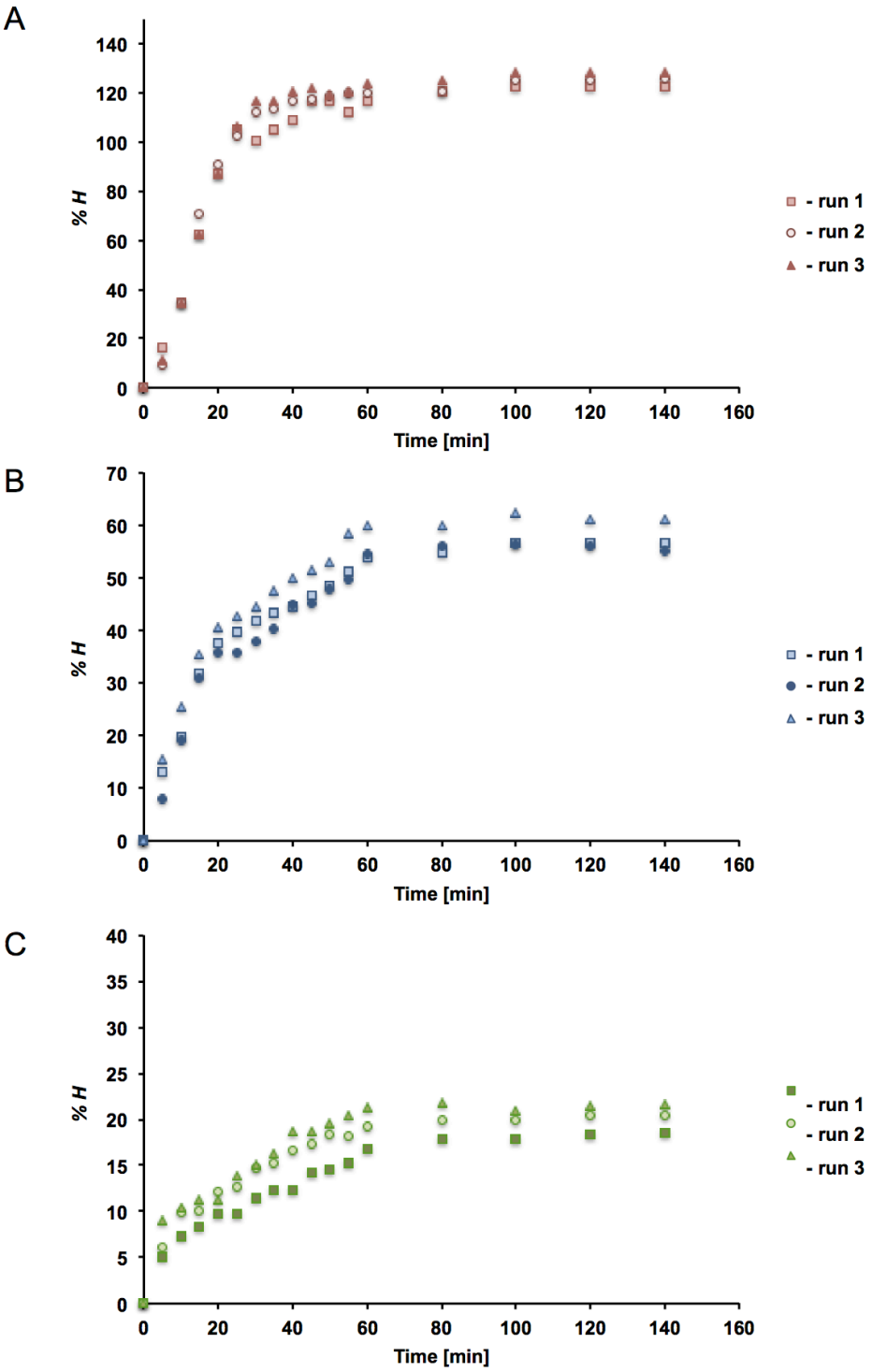

Figure A4. Swelling kinetics of pSPNIPAAm large disc ionogels based on a) $[P_{6,6,6,14}][NTf_2]$, b) $[P_{6,6,6,14}][dca]$ and c) $[P_{6,6,6,14}][Cl]$ in 1mM HCl in a dark environment at 21 °C over time.

Table A2. Percentage change height *(%H)* of the ionogel microstructures during the swelling and shrinking process ($n = 3$).

IL used for ionogel synthesis	Small discs		Large discs		Rings		Lines	
	Swelling [%]	Shrinking [%]	Swelling [%]	Shrinking [%]	Swelling [%]	Shrinking [%]	Swelling [%]	Shrinking [%]
$[P_{6,6,6,14}][NTf_2]$	140 ± 6	122 ± 11	123 ± 2	108 ± 3	80 ± 8	166 ± 14	109 ± 5	91 ± 7
$[P_{6,6,6,14}][dca]$	56 ± 8	42 ± 2	58 ± 2	42 ± 2	56 ± 6	44 ± 3	40 ± 1	35 ± 7
$[P_{6,6,6,14}][Cl]$	23 ± 5	18 ± 3	20 ± 5	16 ± 2	26 ± 8	16 ± 3	24 ± 1	17 ± 3

A5. Porosity of ionogels

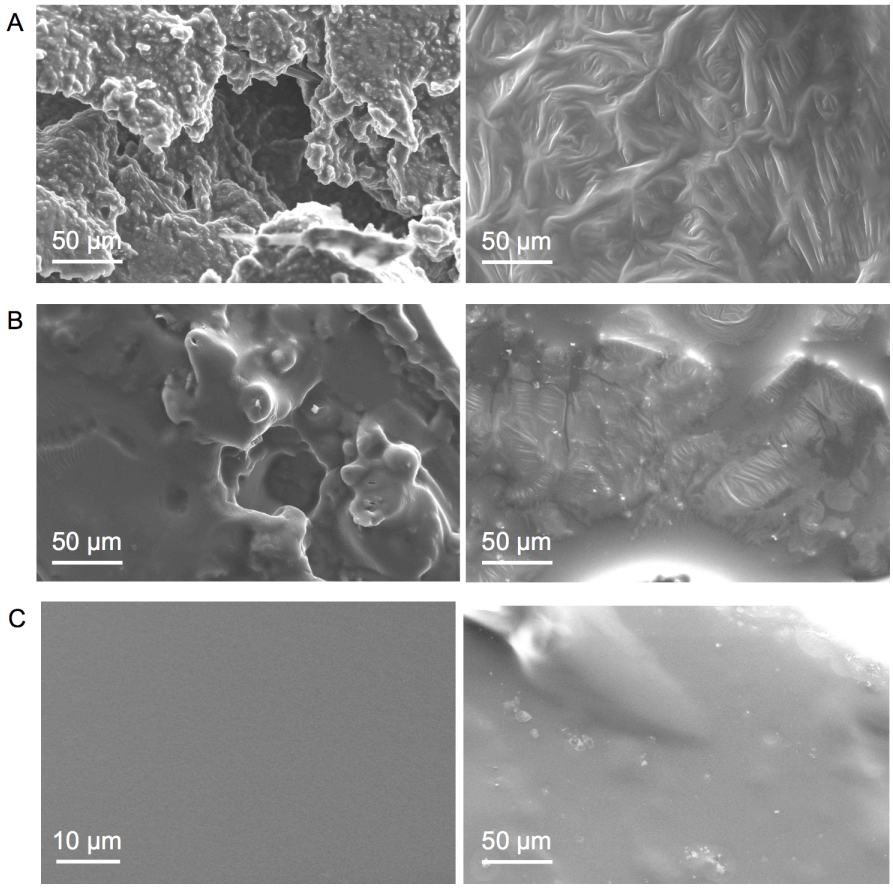

Figure A5. SEM images of a) $[P_{6,6,6,14}][NTf_2]$, b) $[P_{6,6,6,14}][dca]$ and c) $[P_{6,6,6,14}][Cl]$ ionogels after photopolymerisation (left) (non-hydrated) and (b) after hydration in de-ionised water for 24 h.

A6. Kinetic studies of ionogel shrinking

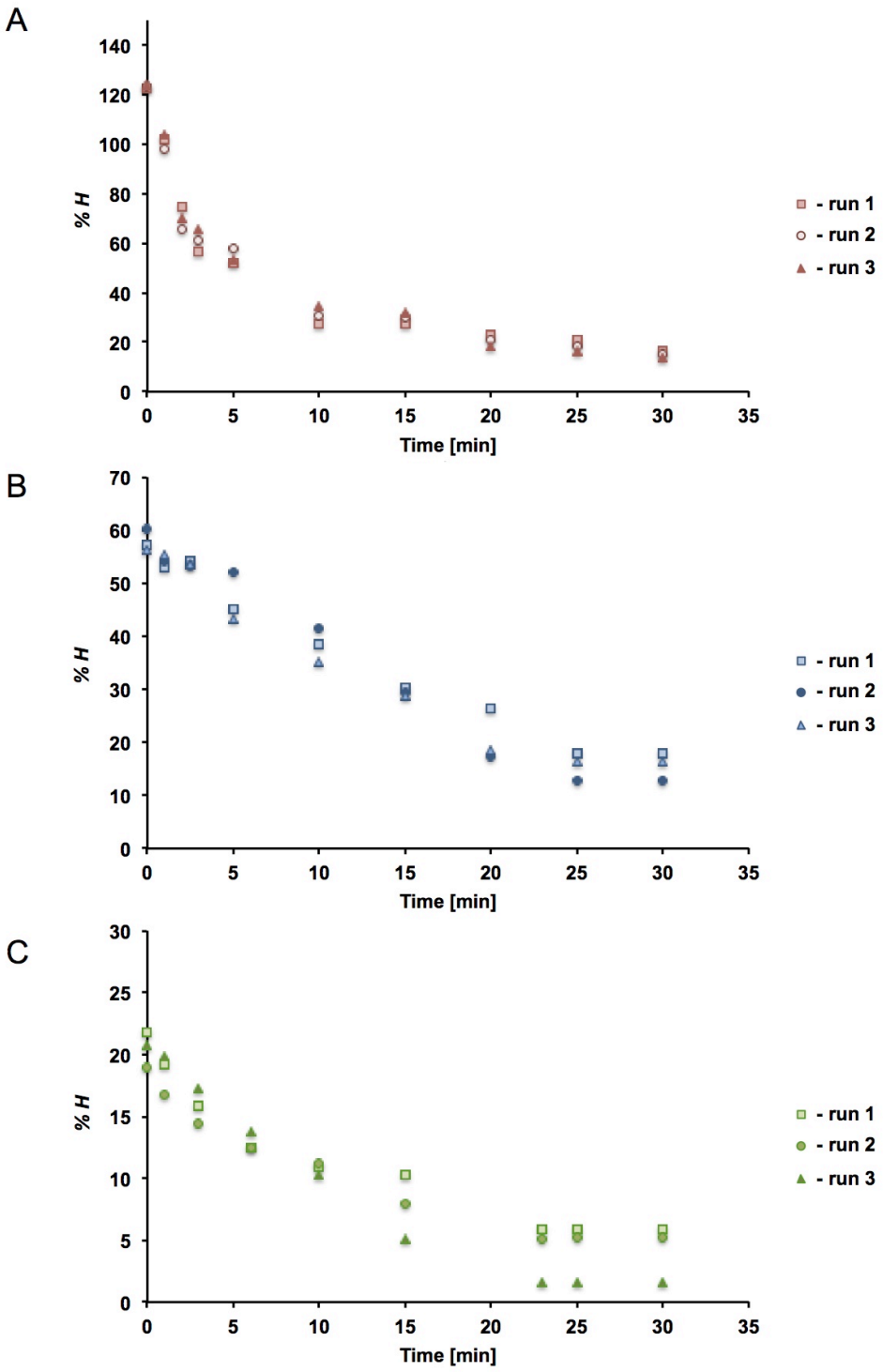

Figure A6. Shrinking kinetics of pSPNIPAAm large disc ionogel microstructures based on a) $[P_{6,6,6,14}][NTf_2]$, b) $[P_{6,6,6,14}][dca]$ and c) $[P_{6,6,6,14}][Cl]$ induced by white light irradiation at 21 °C over time.

A7. Images of ionogel microstructures

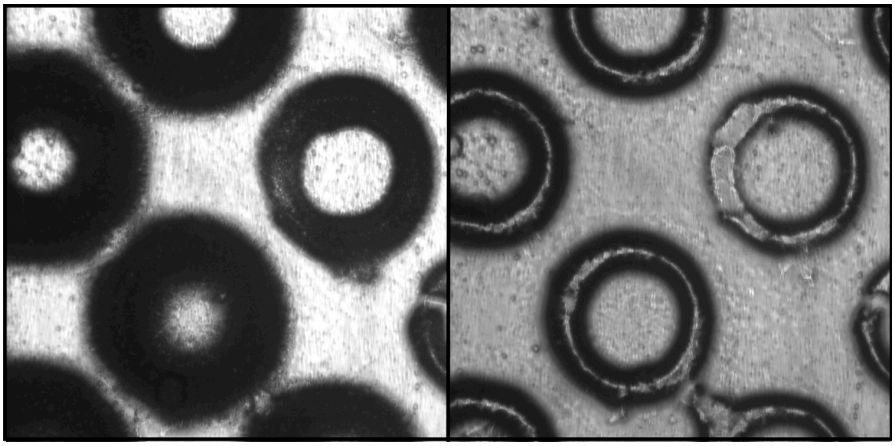

Figure A7. Ionogel $[P_{6,6,6,14}][NTf_2]$ rings after swelling in 1 mM HCl solution for 2 h (left) and shrinking upon white light irradiation (right). A video of the microstructures actuation is available on http://tinyurl.com/d5yvq6l.

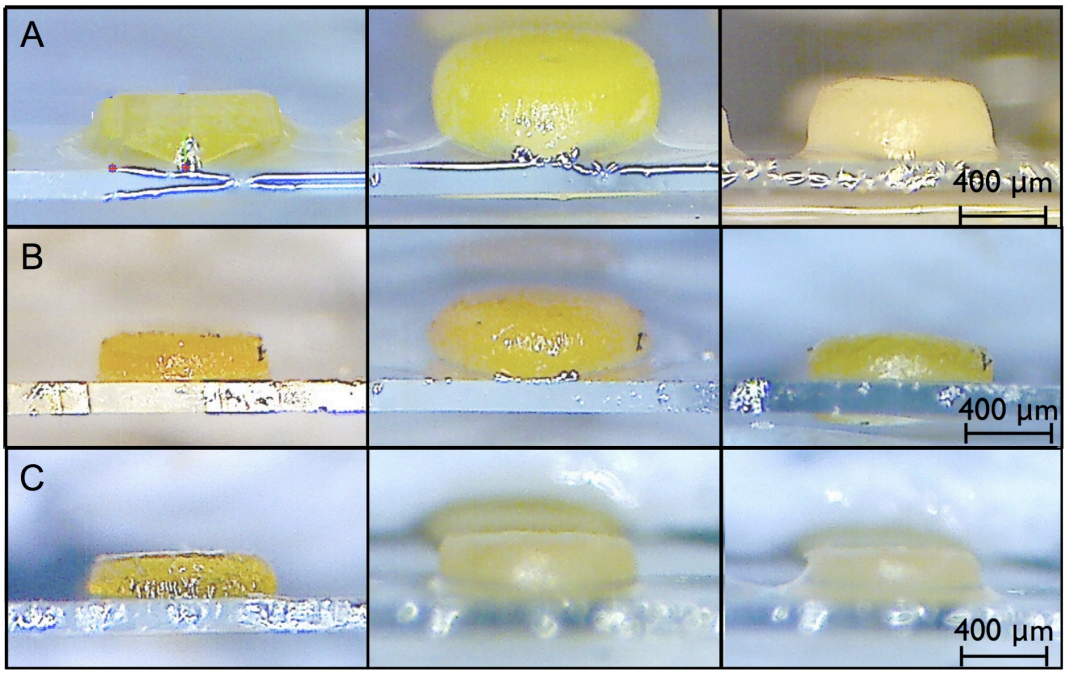

Figure A8. Ionogel small discs: (a) $[P_{6,6,6,14}][NTf_2]$, (b) $[P_{6,6,6,14}][dca]$ and (c) $[P_{6,6,6,14}][Cl]$ after photopolymerisation (left); swelling in 1 mM HCl solution for 2 h (middle) and shrinking upon white light irradiation (right).

Appendix B

Supplementary Information

Portable integrated microfluidic analytical platform for the monitoring and detection of nitrite

M. Czugala,[1] C. Fay,[1] N. E. O'Connor,[1] B. Corcoran,[1] F. Benito-Lopez[1, 2, *] Dermot Diamond[1]

Talanta, 2013, 997-1004
doi: 10.1016/j.talanta.2013.07.058

[1]CLARITY: Centre for Sensor Web Technologies, National Centre for Sensor Research, Dublin City University, Dublin 9, Ireland
[2]CIC microGUNE, Arrasate-Mondragón, SPAIN

B1. Isomerisation of spiropyran

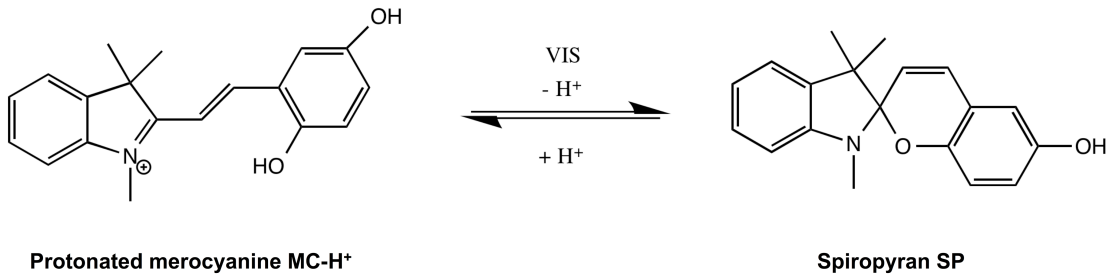

Figure B1. Photo-isomerisation of the protonated isomer ($MC{-}H^{+}$) into spiropyran (SP).

B2. Performance of the microfluidic mixing area

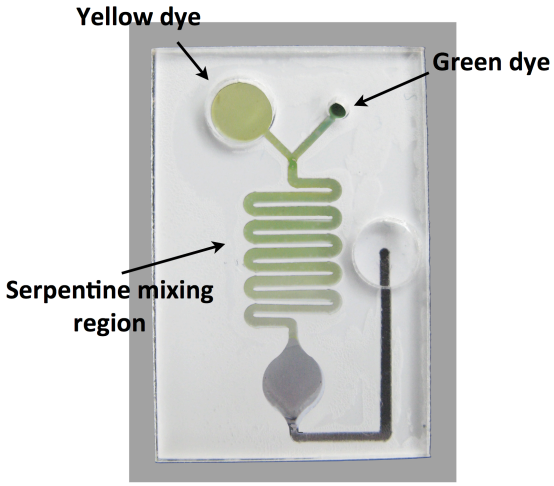

Figure B2. Image presenting the performance of the microfluidic mixing area.

B3. Kinetic studies of Griess reaction

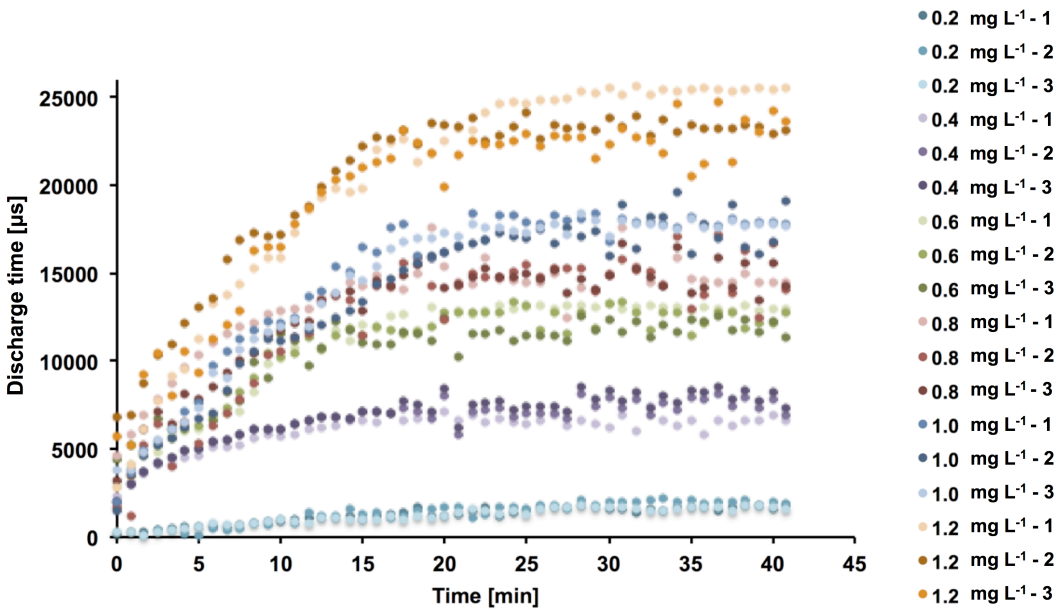

Figure B3. Kinetic study of the colour formation monitored at λ_{max} 540 nm for the nitrite Griess reagent complex using the portable, integrated microfluidic analytical platform at 21 °C.

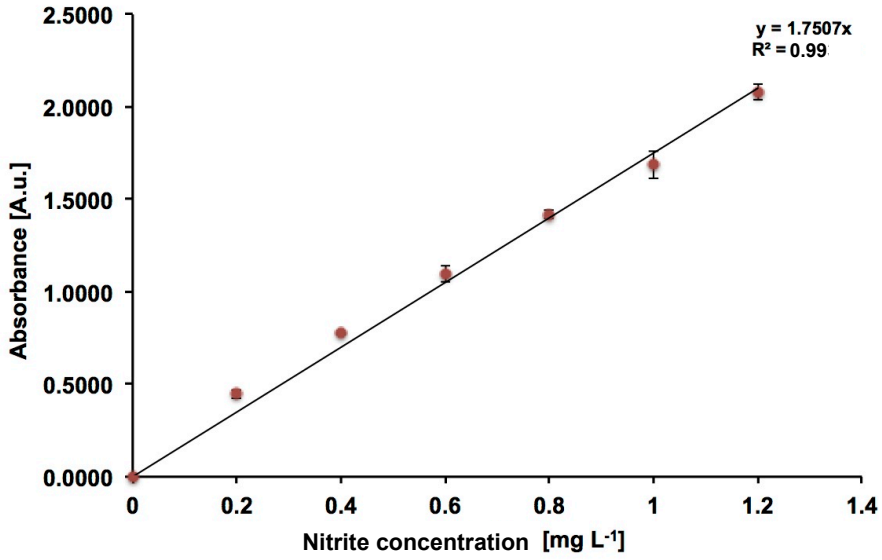

Figure B4. Absorbance *versus* nitrite concentration measured at 540 nm (nitrite Griess reagent complex) using a bench-top UV-Vis spectrophotometer ($n = 3$).

Appendix C

Supplementary Information

Optical sensing system based on wireless paired emitter detector diode device and ionogels for lab-on-a-disc water quality analysis

M. Czugala,[1] R. Gorkin,[2] T. Phelan,[1] J. Gaughran,[2] V. F. Curto,[1] J. Ducrée,[2] D. Diamond[1] and F. Benito-Lopez,[1]

Lab on a Chip, 2012 (12) 5069-5078
doi: 10.1039/C2LC40781G

[1]CLARITY: Centre for Sensor Web Technologies, National Centre for Sensor Research, Dublin City University, Dublin 9, Ireland
[2]School of Physical Sciences, National Centre for Sensor Research, Dublin City University, Dublin 9, Ireland

C1. Centrifugal disc for characterisation of PEDD

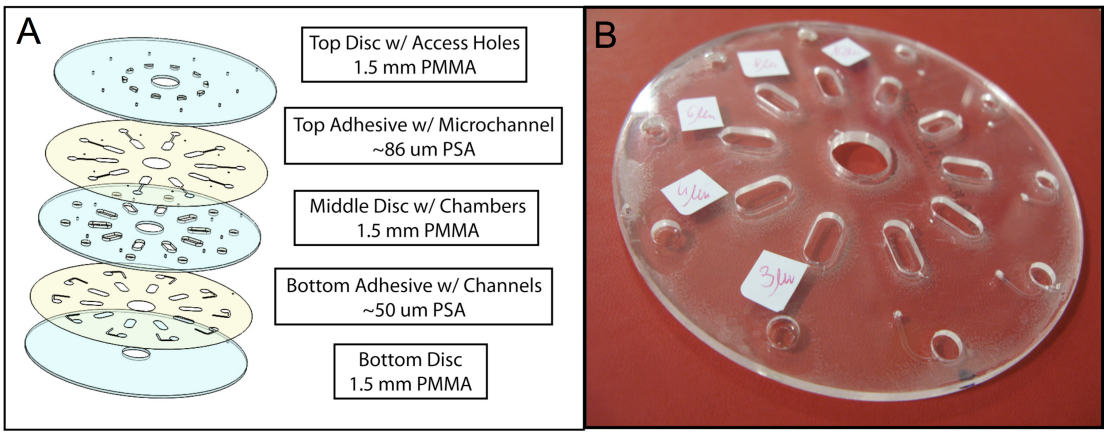

Figure C1. a) Scheme showing the assembly of the centrifugal disc used for the characterisation of the PEDD optical system; b) picture of the disc with milled microfluidics.

C2. Absorbance spectra of LED and ionogel

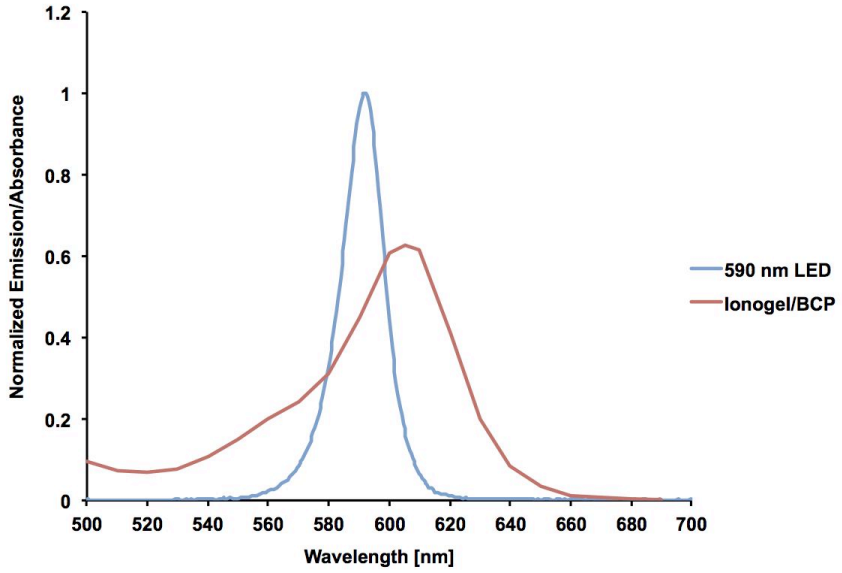

Figure C2. Emission spectrum (blue line) of the emitter LED (λ_{max} 590 nm) and the absorption spectrum of Bromocresol Purple (red line) in a basic environment.

C3. UV-Vis spectra of bromocresol purple solutions

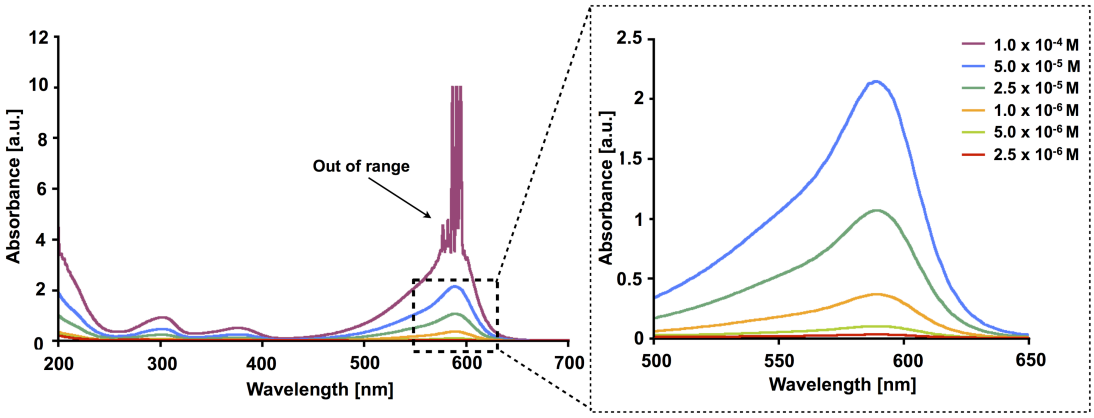

Figure C3. UV-Vis spectra of bromocresol purple pH dye, at different concentrations. The spectra show that bromocresol purple is quantitatively detected in the range 2.5 x 10^{-6} - 5.0 x 10^{-5} M using a UV-Vis spectrometer, L = 1cm.

C4. Turbidity of water samples

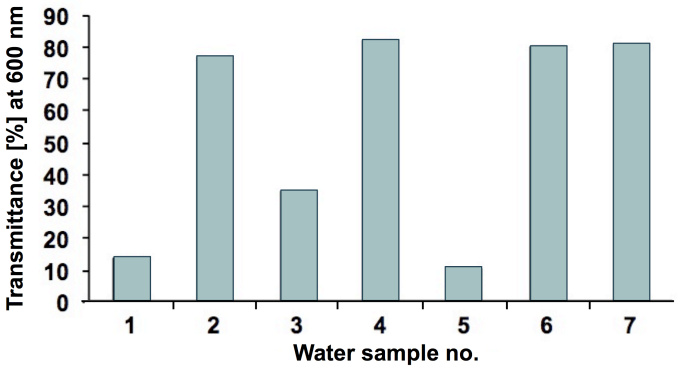

Figure C4. Quantitative turbidity measurements using a UV-Vis spectrometer (transmittance).

Appendix D

Supplement Information

CMAS: fully integrated portable Centrifugal Microfluidic Analysis System for on-site colorimetric analysis

M. Czugala,[1] D. Maher,[1] F. Collins,[1] R. Burger,[2] F. Hopfgartner,[1] Y. Yang,[1] J. Zhaou,[1] J. Ducrée,[2] A. Smeaton,[1] K. J. Fraser,[1] F. Benito-Lopez[1,2] and D. Diamond[1]

RSC Advances, 2013 (3), 15928-15938
doi: 10.1039/C3RA42975J

[1]CLARITY: Centre for Sensor Web Technology, National Centre for Sensor Research
Dublin City University, Dublin, IRELAND
[2]Biomedical Diagnostics Institute, National Centre for Sensor Research,
Dublin City University, Dublin, IRELAND
[3]CIC microGUNE, Arrasate-Mondragón, SPAIN

D1. Scheme of CMAS components

Figure D1. a) Bottom side view of CMAS with the components in place, b) CMAS with loaded CD and c) exploded view of CMAS and components.

D2. CMAS graphical user interface

The following section is a guide to the graphical user interface of CMAS application designed for an Android tablet. A brief description of each screen is provided in the figure caption.

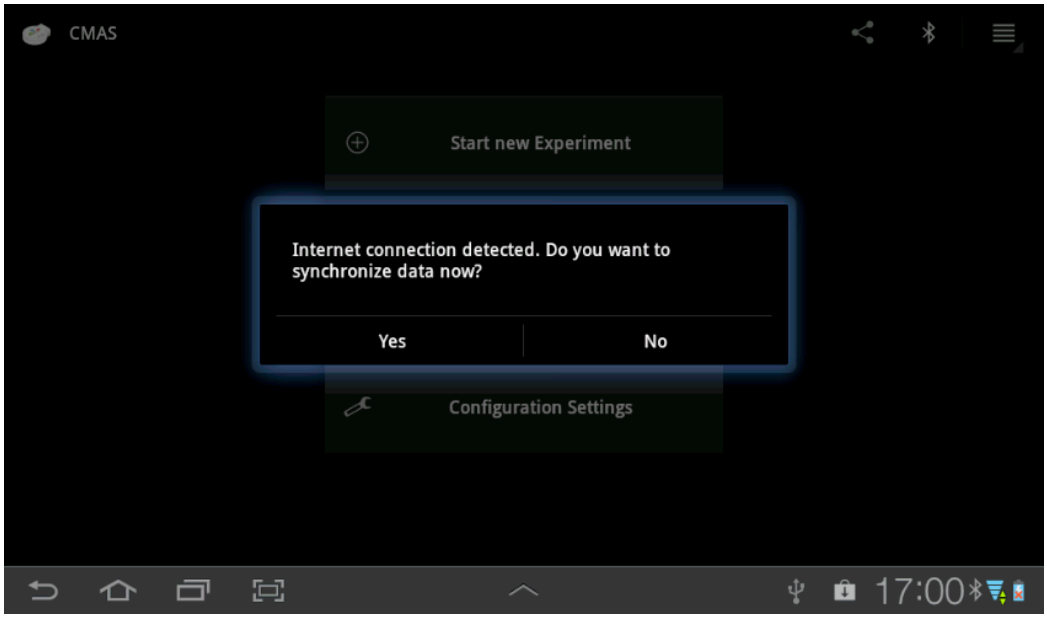

Figure D2. Upon startup the user has the option to upload previous collected data to the cloud (in this instance dropbox) if an Internet connection is available.

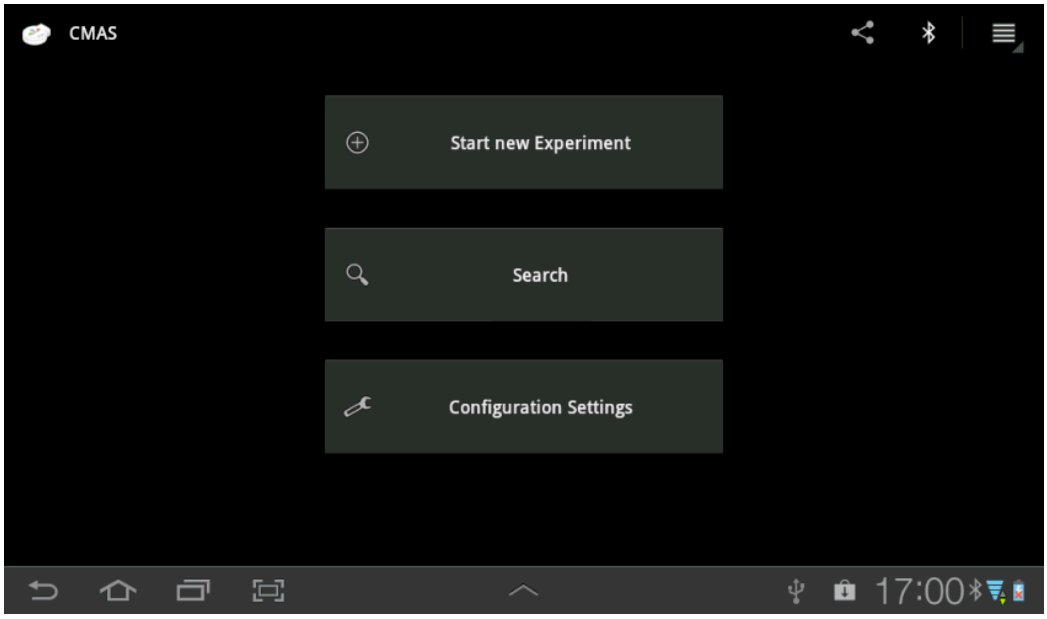

Figure D3. Homescreen of CMAS. The user can a) start a new experiment, b) search previous collected data locally on the tablet device or on the cloud and c) configure the settings of CMAS.

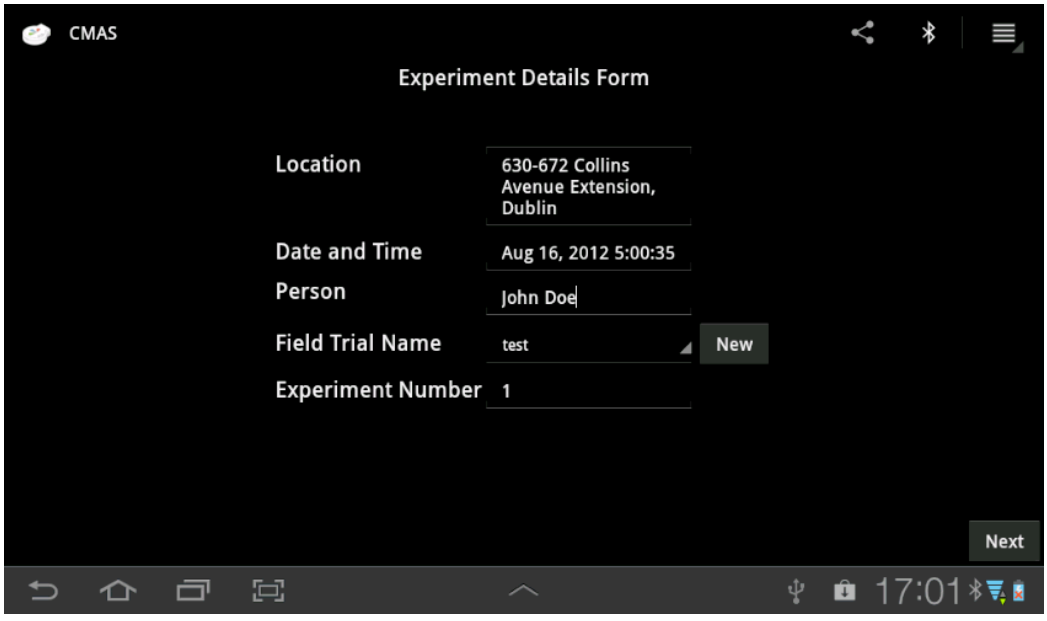

Figure D4. If the user selects to start a new experiment, certain information such as the current location, date and time are determined automatically. If an Internet connection is available, the GPS location is mapped to the associated geo name using the Google API. This information is used to provide additional information about the experiment, *i.e.*, it is the metadata.

In addition, the user can manually enter the name of the researcher. Once this information is provided, the user has to choose whether the planned experiment is part of an already existing trial or if it is the first experiment of a new trial.

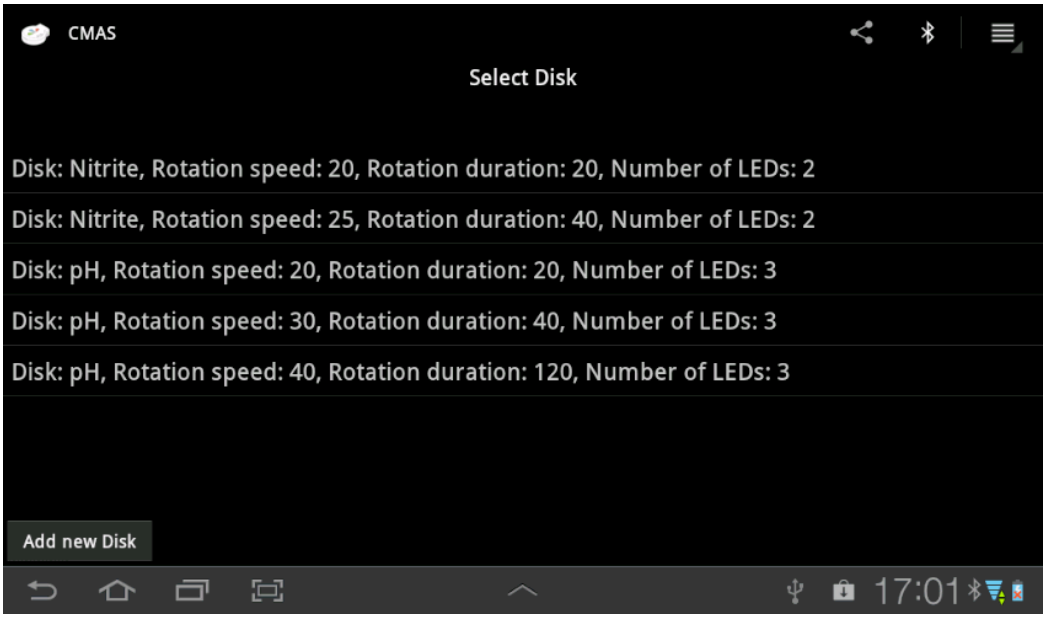

Figure D5. Further, the user has to register the disk that will be used within this experiment. The interface allows them to either select pre-defined disks or to enter a new disk into the system. In this case, the user is asked to define a disk ID, the number of LEDs that are required for the new disk and to set the disk speed that is required in the initial spinning task.

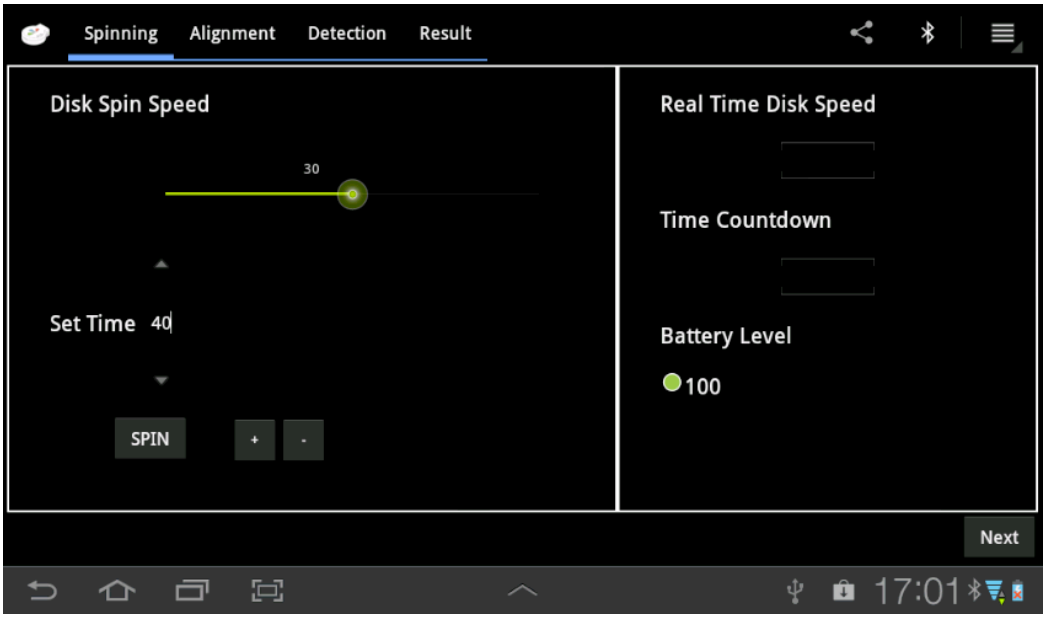

Figure D6. After providing all required information, the first step of the experiment, the spinning of the disk, can begin. Here, a screenshot of the spinning interface is shown. As can be seen, the users can trigger the disk spinning by tapping on the SPIN button. On the top right side of the interface, the real time disk speed is displayed. The spinning speed can be modified using the spinning controller. Once the disk reaches the requested speed, a count down starts. At the end of the count down, the spinning task is completed and the user can start the second task by clicking on the 'Next' button on the bottom right corner of the screen.

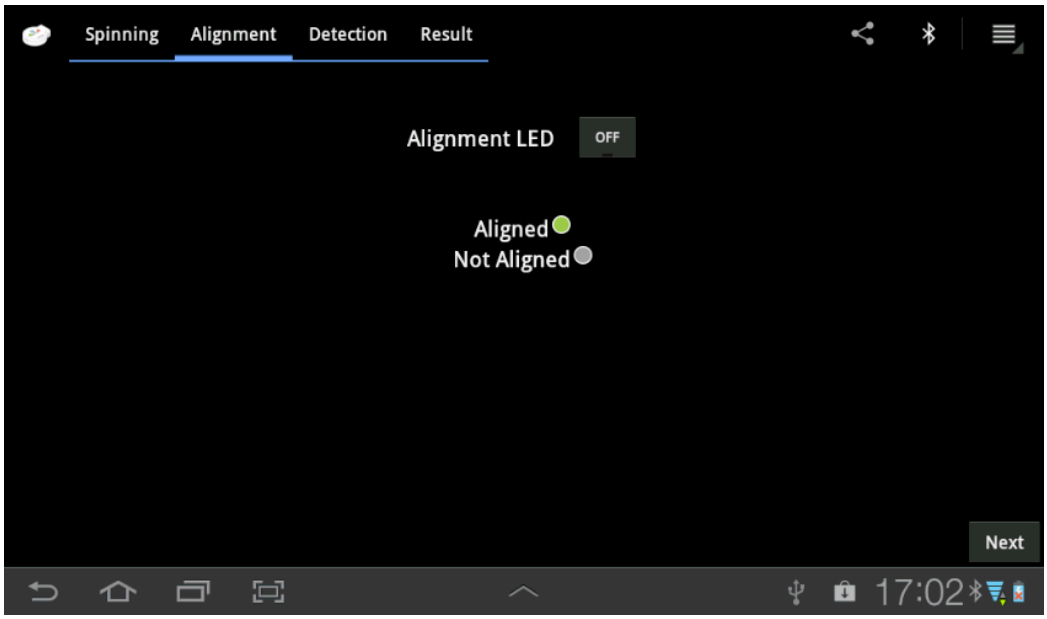

Figure D7. The next task is the correct alignment of the disk, *i.e.*, the correct positioning of the disk so that the LEDs can be used to measure the sample. The alignment LED can be activated by using a switch button on the interface, the actual alignment has to be performed manually by moving the disk in CMAS. The alignment status is indicated on the interface with a red or green light, respectively. Once the disk is properly aligned, the user can reach the detection screen by clicking on the 'Next' button in the bottom right corner of the interface.

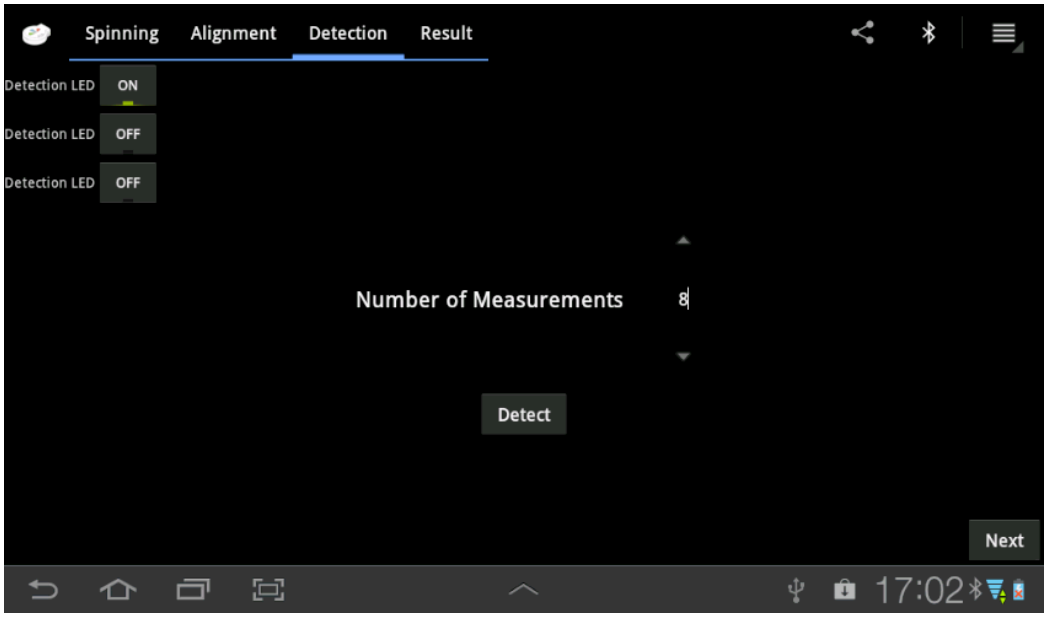

Figure D8. Before the user can start the detection, they can activate the LEDs and the number of measurements that are required during this experiment. The detection will start after the user then clicks the 'Detect' button. During the experiment, the readings from CMAS will be displayed in real time in a graph on the display. If more readings from other experiments during this trial that have been performed with this device, they will be displayed as well in the same graph. This allows the user a direct comparison with different experiments.

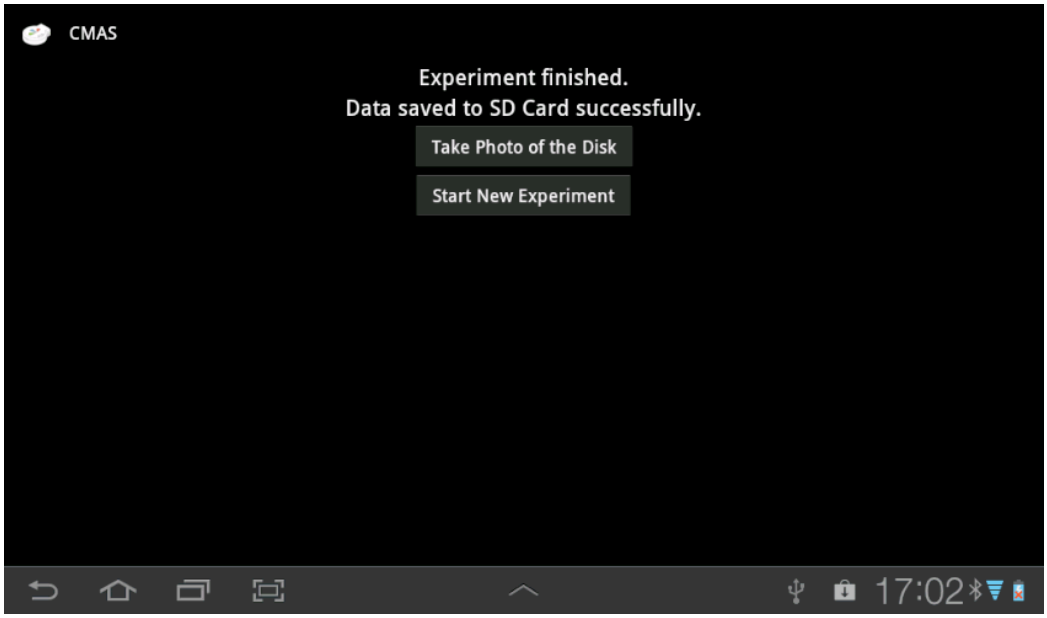

Figure D9. At the end of the experiment, the interface provides the option to take a picture of the disk, which will be stored on the SD card of the

device. As mentioned above, the user can inspect the results of previous trials by selecting the corresponding option on the main screen. This will open a new screen where all locally stored trials and experiments are listed. Further, small icons indicate whether a picture of the experiment is available and whether the results have already been uploaded to the cloud. Data synchronisation with the could will either happen on start up if an internet connection is available, or if the user presses on the cloud icon. Various generous online hard drive services are available. In our system, we opted for the service provided by Dropbox since it allows easy sharing with other users.

D3. Griess reaction scheme

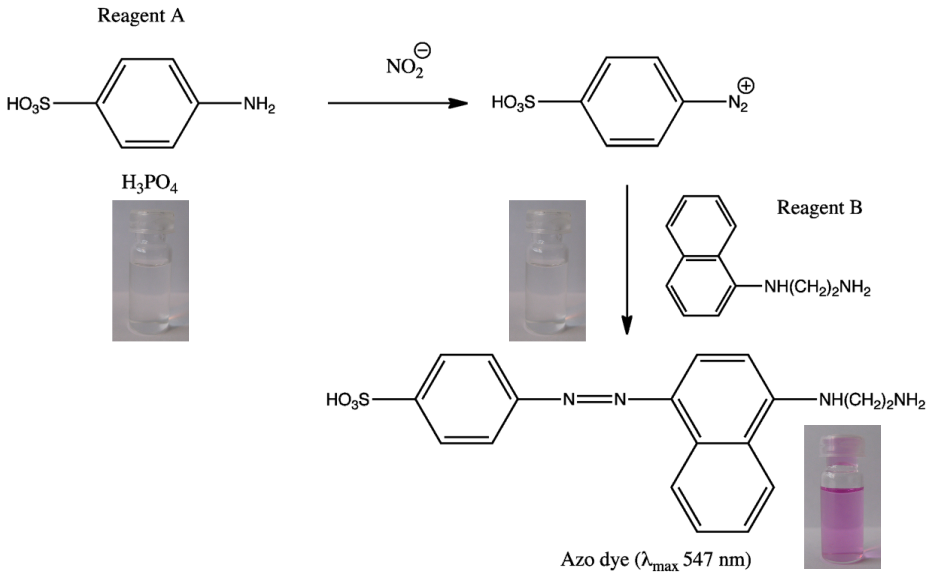

Figure D10. Mechanism of the nitrite detection employing the Griess reaction method.[1]

D4. First generation PEDD system *versus* CMAS

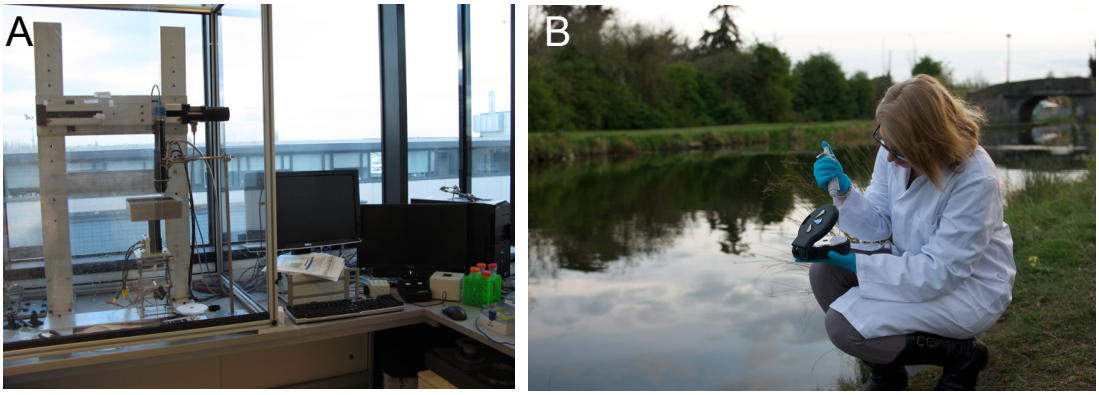

Figure D11. A) Motor stand used for fluid manipulation for the first generation PEDD device as reported by Czugala *et al.*[2] After fluid manipulation the sample was measured in a dark room. B) Second generation PEDD device, CMAS, being used in the field for freshwater analysis. A video of the system can be found at http://tinyurl.com/dyoumds.

D5. UV-Vis spectra

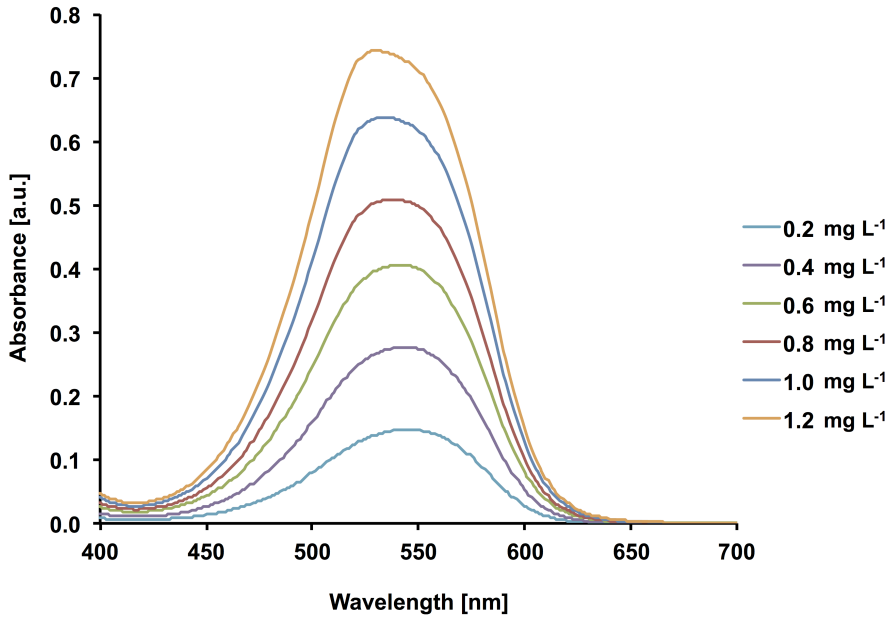

Figure D12. Absorbance spectra of nitrite Griess reagent complex at different concentrations of nitrite (λ_{max} = 537 nm).

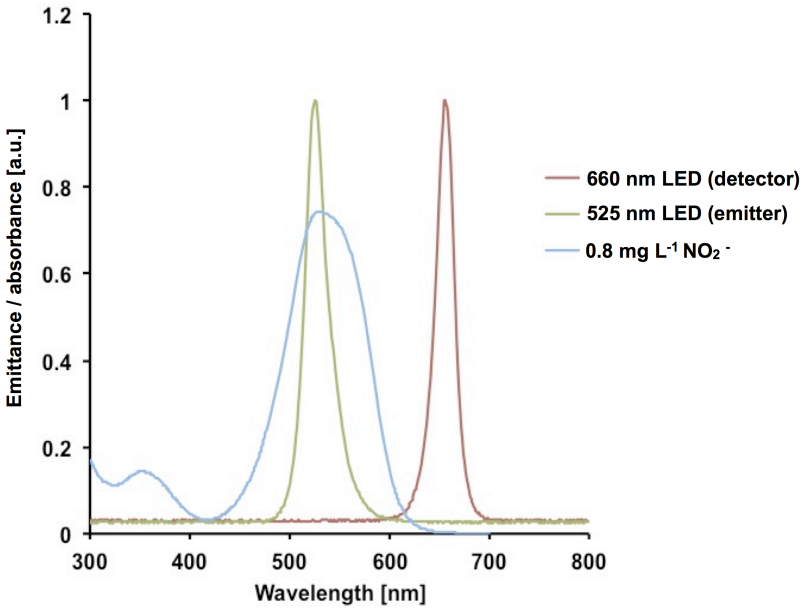

Figure D13. Emission spectrum (λ_{max} = 525 nm) of the emitter LED (green line) and the detector LED (red line) used in the integrated CMAS, absorption spectrum (λ_{max} = 537 nm) of 0.8 mg L^{-1} NO_2^- and Griess reagent (blue line).

D6. Repeatability of PEDD measurements

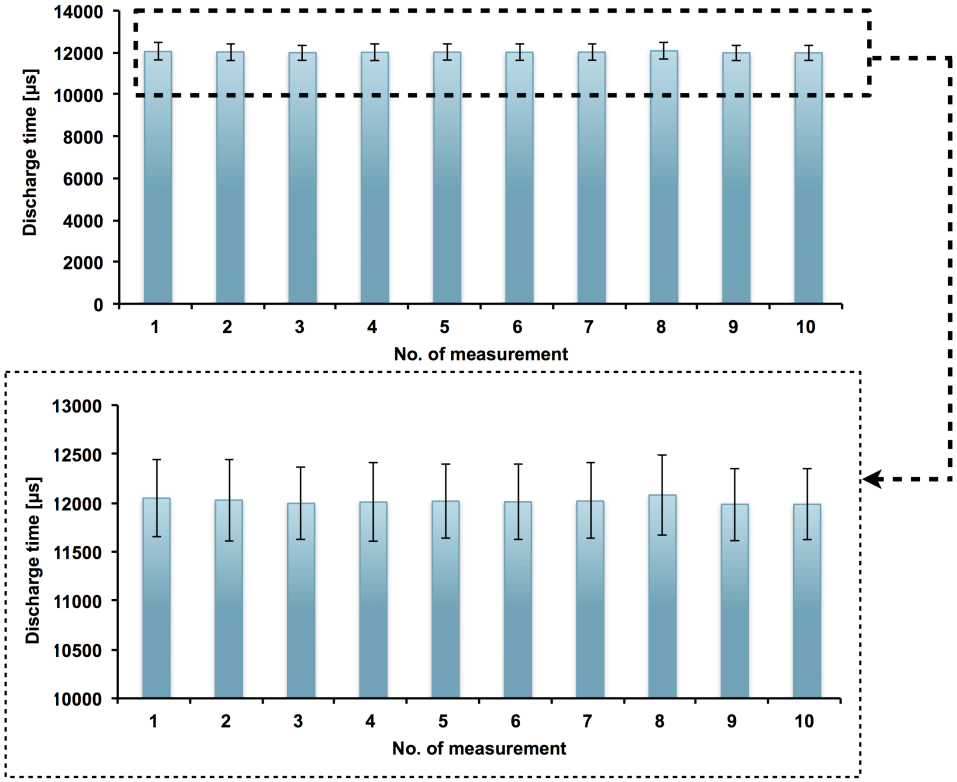

Figure D14. Determination of the PEDD repeatability for the detection of 1.0 mg L^{-1} NO_2^- Griess reagent complex ($n = 10$).

Table D1. Repeatability of the PEDD measurements by detection of discharge time of 1.0 mg L^{-1} nitrite standard solution premixed with Griess reagent loaded to the same microfluidic structure for 60 s (3 data points per second, $n = 10$).

Masurement no.	Discharge time [μs]	Std. Dev.	% RSD
1	12047	401	3.32
2	12028	418	3.48
3	11995	369	3.07
4	12008	403	3.35
5	12017	378	3.15
6	12011	385	3.20
7	12019	387	3.22
8	12080	410	3.39
9	11985	372	3.10
10	11985	361	3.01
Average between 10 measurements	12018	29	0.24

Table D2. Study of the repeatability of the microfluidic structures within one CD using a coloured dye solution ($n = 3$).

Microfluidic structure no.	Discharge time [μs] – red food dye			Avg. discharge time [μs]	Std. Dev.	% RSD
	Run 1	Run 2	Run 3			
1	17291	17256	17240	17262	26	0.15
2	16388	16359	16237	16328	80	0.49
3	17035	17035	16805	16958	133	0.78
4	17592	17525	17420	17512	87	0.50
5	16858	16849	16866	16858	8	0.05
6	15658	15314	15742	15571	227	1.45
7	17476	17519	17862	17619	212	1.20
Average between 21 measurements				16873	693	4.11

Table D3. Study of the repeatability of the output signal across three different CDs using a coloured dye solution ($n = 3$).

CD no.	Discharge time [μs] – red food dye			Avg. discharge time [μs]	Std. Dev.	% RSD
	Run 1	Run 2	Run 3			
CD 1	16858	16849	16866	16858	8	0.05
CD 2	16875	16763	16963	16867	100	0.59
CD 3	17033	17240	16624	16966	314	1.85
Average between 21 neasurements				16897	173	1.02

D7. Kinetic study

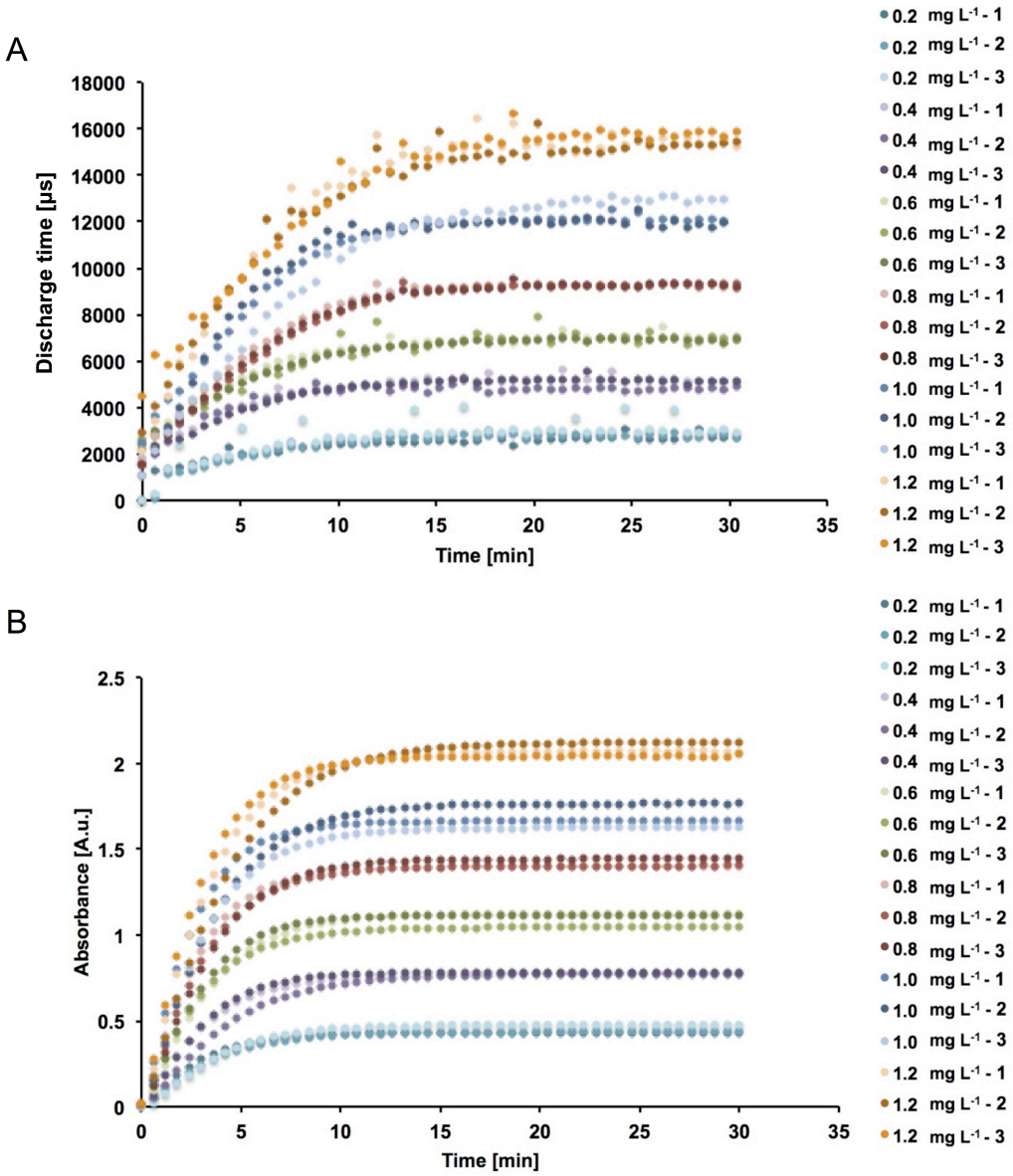

Figure D15. Kinetic study of the colour formation between NO_2^- and Griess reagent (20.0 ± 0.5 °C, at 540 nm) using a) CMAS (each 10^{th} point; total: 50 points) and b) UV-Vis spectrophotometer (each 36^{th} point; total: 50 points).

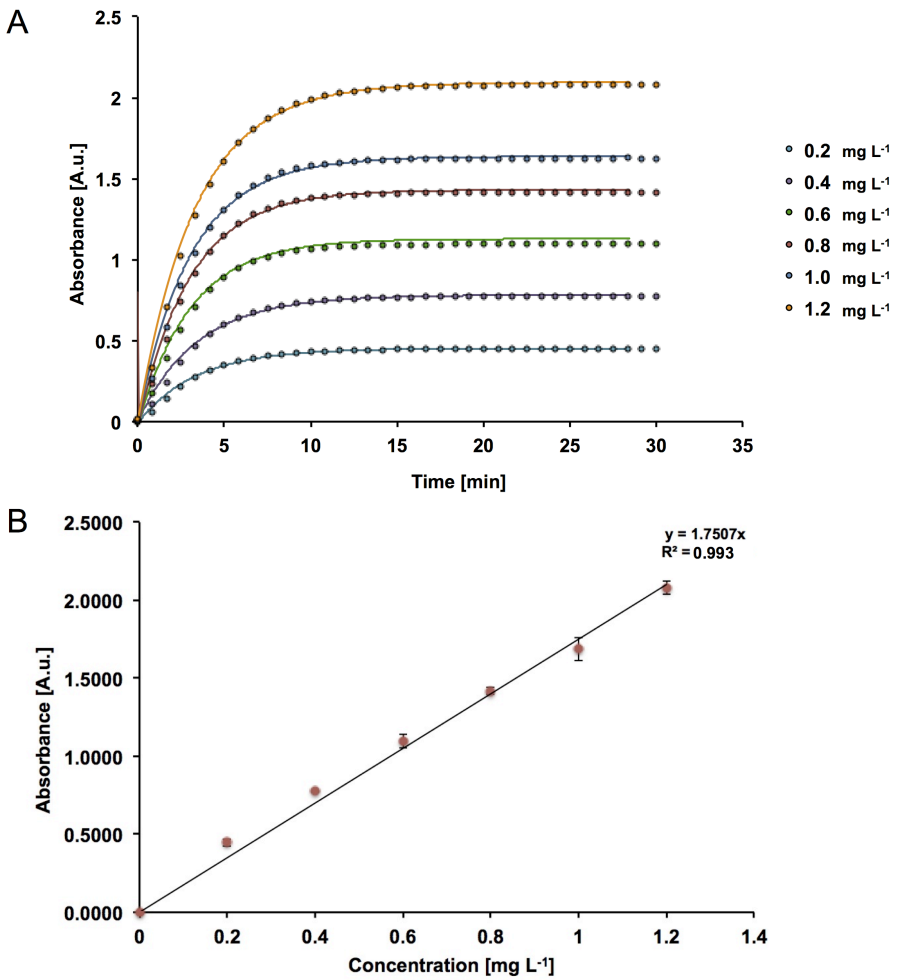

Figure D16. A) Kinetic study of the colour formation between NO_2^- and Griess reagent (20.0 ± 0.5 °C, at 540 nm) and (b) absorbance at 540 nm *versus* nitrite Griess reagent complex concentration using a UV-Vis spectrophotometer ($n = 3$).

Table. D4. Kinetic rate constants calculated for triplicate at 540 nm for (a) CMAS platform, (b) UV-Vis spectrophotometer (20.0 ± 0.5 °C, 540 nm).

a)

Sample no.	Nitrite concentration [mg L^{-1}]	CMAS – Kinetic Rates (x 10^{-3}) k_1 [s^{-1}]	k_1 [s^{-1}]	k_3 [s^{-1}]	Avg. k [s^{-1}] (x 10^{-3})	Std. Dev. (x 10^{-3})
1	**0.2**	0.97	1.05	1.05	1.03	0.04
2	**0.4**	1.31	1.31	1.18	1.27	0.08
3	**0.6**	1.18	1.02	1.06	1.09	0.08
4	**0.8**	1.10	0.99	1.02	1.04	0.06
5	**1.0**	1.10	1.37	1.06	1.2	0.2
6	**1.2**	1.07	0.99	0.79	1.0	0.1

b)

Sample no.	Nitrite concentration [mg L^{-1}]	UV-Vis – Kinetic Rates (x 10^{-3}) k_1 [s^{-1}]	k_1 [s^{-1}]	k_3 [s^{-1}]	Avg. k [s^{-1}] (x 10^{-3})	Std. Dev. (x 10^{-3})
1	**0.2**	2.00	1.64	1.63	1.8	0.2
2	**0.4**	1.83	1.34	1.86	1.7	0.3
3	**0.6**	1.70	1.70	1.96	1.8	0.2
4	**0.8**	2.10	1.71	1.71	1.8	0.2
5	**1.0**	2.35	1.62	1.69	1.9	0.4
6	**1.2**	1.76	1.40	2.06	1.7	0.3

Table. D5. Repeat absorbance measurements for the determination of NO_2^- over the concentration range 0.0 - 1.2 mg L^{-1} of NO_2^- with (a) CMAS platform, (b) UV-Vis spectrometer at a working wavelength of 540 nm (20.0 ± 0.5 °C).

a)

Sample no.	Nitrite concentration [mg L^{-1}]	CMAS –Discharge time [μs]			Avg. Discharge time [μs]	Std. Dev.	%RSD
		Run 1	Run 2	Run 3			
1	**0.2**	2704.05	2822.46	2946.69	2824	121	4.29
2	**0.4**	5154.54	5077.95	5157.54	5130	45	0.88
3	**0.6**	6993.28	6919.41	6984.10	6966	40	0.58
4	**0.8**	92.99.70	9294.10	9297.54	9297	3	0.03
5	**1.0**	12098.54	12126.63	12740.05	12322	364	2.94
6	**1.2**	15394.59	15334.29	15613.98	15448	147	0.95

b)

Sample no.	Nitrite concentration [mg L^{-1}]	UV-Vis spectrometer – Absorbance [au]			Avg. Abs. [au]	Std. Dev.	%RSD
		Run 1	Run 2	Run 3			
1	**0.2**	0.4337	0.4356	0.4752	0.45	0.02	5.22
2	**0.4**	0.7691	0.7746	0.7815	0.775	0.006	0.80
3	**0.6**	1.1249	1.0476	1.1164	1.10	0.04	3.87
4	**0.8**	1.4025	1.4042	1.4433	1.42	0.02	1.63
5	**1.0**	1.6665	1.7667	1.6255	1.69	0.07	4.31
6	**1.2**	2.0694	2.1240	2.0448	2.08	0.04	1.99

Table. D6. Water nitrite analysis using the CMAS platform and bench-top UV-Vis spectrophotometer.

Sample no.	CMAS platform [mg L^{-1}]		UV-Vis spectrometer [mg L^{-1}]	
	Average	Std. Dev.	Average	Std. Dev.
1	0.09	0.02	0.1000	0.0005
2	0.37	0.03	0.370	0.010
3	0.02	0.01	0.0200	0.0002
4	0.29	0.02	0.260	0.006
5	0.05	0.03	0.0500	0.0004

D8. CMAS cost breakdown

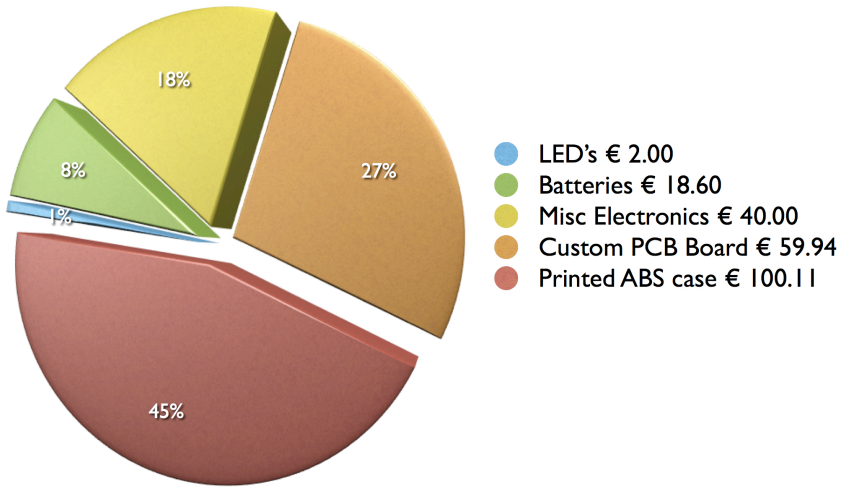

Figure. D17. Cost breakdown of CMAS components.

D9. References

1. J. MacFaddin, Nitrate/nitrite reduction tests, In: Biochemical tests for identification of medical bacteria, 3rd edn., Lippincott Williams & Wilkins, Philadelphia, **2000**.

2. M. Czugala, R. Gorkin III, T. Phelan, J. Gaughran, V. F. Curto, J. Ducrée, D. Diamond and F. Benito-Lopez, Optical sensing system based

on wireless paired emitter detector diode device and ionogels for lab-on-a-disc water quality analysis, *Lab on a Chip*, **2012**, 12, 5069-5078.